Influence of Tundra Vegetation on Radiation Fluxes

Dissertation

zur

Erlangung der naturwissenschaftlichen Doktorwürde
(Dr. sc. nat.)

vorgelegt der

Mathematisch-naturwissenschaftlichen Fakultät

der

Universität Zürich

von

Inge Juszak

aus

Deutschland

Promotionskomitee

Prof. Dr. Michael E. Schaepman (Vorsitz)
Dr. Gabriela Schaepman-Strub (Leitung der Dissertation)
Prof. Dr. Bernhard Schmid
Prof. Dr. Werner Eugster

Zürich, 2016

Influence of Tundra Vegetation on Radiation Fluxes

Published and distributed by:
Department of Evolutionary Biology and Environmental Studies
University of Zurich
Winterthurerstrasse 190
CH-8057 Zürich
Switzerland
http://www.ieu.uzh.ch

Abstract

Vegetation plays an important part in the climate system. Species composition and canopy structure do not only respond to climate conditions but also feed back to climate by changing the surface energy budget. As climate warming is about twice as strong in the Arctic as compared to the global mean, vegetation changes such as shrub expansion have been observed in many tundra regions. On one hand, shrub expansion is associated with an albedo decrease resulting in a positive feedback to climate warming. On the other hand, shrubs can shade the soil and reduce permafrost thaw. A second major consequence of climate change is a variation in lake and wetland extent, which also feeds back to vegetation and climate.

Extensive field measurements over two years provided insights in the radiation budget, soil heat flux, and canopy characteristics of two common tundra vegetation types in the Kytalyk study area, northeast Siberia (70.8 °N, 147.5 °E). Time series measurements of two study species, dwarf shrubs (*Betula nana*) and wet sedges (*Eriophorum angustifolium*), were taken in addition to canopy height, plant area index, and active layer thickness. We found that growing season albedo of dwarf shrubs is 0.02 ± 0.01 lower than that of wet sedges while transmittance is 0.08 ± 0.03 higher below dwarf shrubs. Despite lower albedo and less soil shading, soil heat flux is much smaller below dwarf shrubs as compared to wet sedges resulting in an on average 17 cm shallower active layer thickness. The elevated soil heat flux below wet sedges is mainly attributed to the soil properties. The water saturated soil below wet sedges has a five times higher thermal conductivity than the peat top soil below dwarf shrubs.

We used a 3D radiative transfer model (DART) and manipulated shrub densities to extend the field observations to altered shrub canopies. Furthermore, the model, which was parametrised with the above field data, provided insights on the characteristics of dwarf shrub (*Betula nana*) canopies which were most important for the radiation budget. The most important parts of the dwarf shrub canopy are the woody components, absorbing up to 2.4 times more shortwave radiation than green leaves. While canopy albedo remains relatively insensitive to changes in total plant area, it strongly depends on the ratio between leaf and wood area. Canopy absorption depends on both, but more strongly on the total plant area than on the ratio between leaves and wood.

Using additional field data on vegetation properties and drone imagery, we mapped vegetation types and parametrised the DART model for all major types present in

the study area. We quantified the influence of vegetation type and canopy properties on the shortwave radiation budget at landscape scale and assessed the importance of patch size and spatial arrangement of vegetation. Tundra albedo is most strongly influenced by the fraction of water surfaces, while plant area index is the primary driver of radiation absorbed by the canopy. Although the spatial distribution of vegetation has little influence on the shortwave radiation flux at the landscape scale, it considerably contributes to variation of albedo, canopy transmittance, and absorptance at local scale.

We found considerable variation between the radiation budget and soil heat flux of different tundra vegetation types. The three most important influencing factors are (I) the cover of water surfaces including waterlogged sedges, (II) the total plant area including wood and standing dead leaves, and (III) soil water content and soil properties. These variables are key controls of the feedback between vegetation, climate, and permafrost thaw.

As we currently lack spatially resolved data sets of these characteristics, more effort is needed to combine field measurements with upscaling methods based on satellite data and thus provide accurate input for large scale modelling of land–atmosphere interactions.

Zusammenfassung

Die Vegetation spielt eine wichtige Rolle im Klimasystem. Die Artenzusammensetzung und die Struktur der Pflanzendecke reagieren nicht nur auf die Klimabedingungen, sondern beeinflussen auch das Klima, indem sie die Energiebilanz der Erdoberfläche ändern. Da die Klimaerwärmung in der Arktis etwa doppelt so stark ist wie im globalen Mittel, wurden schon in vielen Tundraregionen Vegetationsveränderungen beobachtet, vor allem die Ausbreitung von Sträuchern. Einerseits bedingt die Ausbreitung von Sträuchern eine Verringerung der Albedo und damit eine positive Rückkoppelung mit der Klimaerwärmung, andererseits beschatten Sträucher den Boden und vermindern so das Auftauen des Permafrostes. Die zweite wichtige Folge des Klimawandels ist eine Änderung der Fläche von Seen und Feuchtgebieten, was wiederum die Vegetation und das Klima beeinflusst.

Umfangreiche Feldmessungen während zweier Jahre ergaben einen Einblick in die Strahlungsbilanz, den Bodenwärmestrom und Vegetationseigenschaften von zwei häufigen Tundravegetationstypen in Kytalyk, Nordostsibirien (70.8 °N, 147.5 °E). Zusätzlich zu den Zeitreihenmessungen bei beiden Vegetationstypen, Zwergsträuchern (*Betula nana*) und Seggen an Feuchtstandorten (*Eriophorum angustifolium*), maßen wir die Vegetationshöhe, die Pflanzenfläche und die Dicke der Auftauschicht. Unsere Messungen ergaben, dass die Albedo der Zwergsträucher in der Wachstumsperiode um 0.02 ± 0.01 geringer ist als die Albedo der Seggen. Die Strahlungstransmission ist dagegen unter Sträuchern um 0.08 ± 0.03 höher als unter Seggen. Trotz geringerer Albedo und Beschattung ist der Bodenwärmestrom unter Zwergsträuchern deutlich kleiner als unter Seggen, was zu einer um durchschnittlich 17 cm dünneren Auftauschicht führt. Der erhöhte Bodenwärmestrom unter Seggen wird hauptsächlich auf die Bodeneigenschaften zurückgeführt. Der wassergesättigte Boden der Seggen hat eine fünfmal höhere Wärmeleitfähigkeit als die Torfschicht unter den Zwergsträuchern.

Ein 3D Strahlungstransfermodell (DART) und manipulierte Strauchdichten ermöglichten es uns, die Ergebnisse der Feldmessungen auf veränderte Zwergstrauchdichten auszuweiten. Zudem konnten wir mit Hilfe des mit Felddaten parameterisierten Modells bestimmen, welche Eigenschaften der Zwergsträucher (*Betula nana*) für die Strahlungsbilanz besonders wichtig sind. Die wichtigsten Komponenten der Zwergstrauchvegetation sind die Äste, da sie bis zu 2,4 mal so viel kurzwellige Strahlung absorbieren wie die grünen Blätter. Während die Vegetationsalbedo kaum von der gesamten Pflanzenfläche abhängt, wird sie stark vom Verhältnis zwischen Blatt-

und Astfläche beeinflusst. Wie viel Strahlung die Vegetation insgesamt absorbiert hängt von beiden Faktoren ab, allerdings stärker von der gesamten Pflanzenfläche als von dem Verhältnis zwischen Blatt- und Astfläche.

Mit Hilfe von weiteren Felddaten zu Vegetationseigenschaften und Dronenbildern kartierten wir die Vegetation und parametrisierten das DART Modell für alle an der Feldstation häufigen Vegetationstypen. Wir quantifizierten den Einfluss von Vegetationstyp und -eigenschaften auf die kurzwellige Strahlungsbilanz auf Landschaftsebene und untersuchten die Bedeutung von Vegetationsmustern. Die Tundraalbedo hängt am stärksten vom Anteil der Wasserflächen ab. Der Anteil der Strahlung, die von der Vegetation absorbiert wird, wird dagegen hauptsächlich von der Pflanzenfläche bestimmt. Während die räumliche Verteilung der Vegetation nur wenig Einfluss auf die kurzwellige Strahlungsbilanz auf Landschaftsebene hat, trägt sie deutlich zur kleinskaligen räumlichen Variabilität von Albedo, Lichtdurchlässigkeit und -absorption der Vegetation bei.

Wir haben deutliche Unterschiede zwischen der Strahlungsbilanz und den Bodenwärmeflüssen von verschiedenen Tundravegetationstypen beobachtet. Die wichtigsten drei Einflussfaktoren waren dabei (I) der Anteil offener oder zerstreut bewachsener Wasserflächen, (II) die gesamte Pflanzenfläche, inklusive Äste und stehendes Streu, sowie (III) die Bodenfeuchte und Bodeneigenschaften. Diese Variablen bestimmen die Rückkopplungen zwischen Vegetation, Klima und tauendem Permafrost maßgeblich.

Da es zur Zeit keine räumlich aufgelösten Daten dieser Eigenschaften gibt, sind verstärkte Anstrengungen nötig, die Feldmessungen mit Hochskalierungsmethoden basierend auf Satellitendaten verbinden. Auf diese Weise können Eingangsgrößen für die Modellierung der Interaktion von Landoberfläche und Atmosphäre großer Gebiete erzeugt werden.

Contents

1 Introduction

Climate warming is about twice as strong in the Arctic as compared to the global mean (IPCC, 2013). Therefore, questions of how this change impacts vegetation, and how vegetation in turn alters regional climate and permafrost conditions arise (*Chapin et al.*, 2005). Two major vegetation–climate feedback mechanisms have been suggested. First, greenhouse gas emissions in tundra regions are influenced by vegetation type (*Walker et al.*, 1998; *Cahoon et al.*, 2012). Methane (CH_4) emissions are enhanced in wet areas with sedge vegetation, while shrubs are associated with low emissions (*van Huissteden et al.*, 2005). On the other hand, permafrost soils store large amounts of carbon (*Hugelius et al.*, 2014), a reservoir which may be released in case of permafrost thaw. That leads to the second vegetation–climate feedback, which is the effect of vegetation on the radiation budget and thus, indirectly, on the energy which is available for permafrost thaw. While greenhouse gas emissions are the subject of many recent studies (e.g. *Lafleur and Humphreys*, 2008; *McGuire et al.*, 2009; *Parmentier et al.*, 2011a; *Budishchev et al.*, 2014), the tundra radiation budget receives less attention and little field data are available to shed light on the controversy of whether shrubs contribute to soil warming through reducing the albedo (*Thompson et al.*, 2004; *Loranty et al.*, 2011), or rather cool the soil through shading (*Benninghoff*, 1952; *Briggs et al.*, 2014). Furthermore, few studies bridge the scaling gap between coarse satellite data and the small scale variability of canopy–radiation interaction. However, the effects of vegetation, and particularly shrubs, on the surface radiation budget are key to predict the future climate as changes in vegetation communities and shrub encroachment have been observed in many Arctic regions (*Myers-Smith et al.*, 2011; *McManus et al.*, 2012; *Frost and Epstein*, 2014).

1.1 Climate change in the Arctic

Increasing temperatures have been observed at many Arctic locations in recent years (*Hinzman et al.*, 2013). The projected warming until 2100 is also strongest in the Arctic (IPCC, 2013). The projections for northeast Siberia, for example, show an average temperature increase of 2–9 °C until 2100, depending on the greenhouse gas emission scenario (IPCC, 2013). The accelerated warming, as compared to other regions of the world, is partly due to a decreasing sea ice extent. For example, the East Siberian Sea has seen a rapid sea ice decline and strong summer warming

(*Serreze et al.*, 2000; *Bhatt et al.*, 2010). However, climate change does not only imply warming, but also changes in cloud cover (*Chapin et al.*, 2005; *Wang and Key*, 2005a; *Vavrus et al.*, 2009) and precipitation (*Serreze et al.*, 2000; *Hinzman et al.*, 2005; *Zhang et al.*, 2007). In conjunction with elevated ocean temperatures, higher evapotranspiration elevates atmospheric water content and increases cloud cover and precipitation in Arctic areas, including northeast Siberia (IPCC, 2013).

However, despite higher precipitation, climate warming can reduce the available water if the evapotranspiration increases more than precipitation (*Smol and Douglas*, 2007). The evaporative demand is especially relevant in the Arctic, where wetlands exist even though the annual precipitation is very low (*Hinzman et al.*, 2005; *Nauta et al.*, 2015). Thus climate warming and associated changes in the moisture regime are likely to affect Arctic land cover.

1.2 Landscape change in the Arctic

Arctic landscapes are strongly influenced by climate, which provides an important boundary condition for the permafrost, the hydrological cycle, and plant growth. As a result of climate change, landscape changes have been observed in many Arctic regions. At large scale, changes in lake area and wetland extent drive habitat changes. While lakes and wetlands expand in some tundra areas with continuous permafrost, lake area decreases in others. These conflicting observations indicate the complexity of pan-arctic landscape change.

On one hand, climate warming leads to a higher water vapour pressure deficit in the air and thus increases evapotranspiration from plants and moist surfaces. This process can lead to drought effects in the tundra (*Oechel et al.*, 2000; *Smol and Douglas*, 2007; *Carroll et al.*, 2011; *Jones et al.*, 2011; *Lin et al.*, 2012). Surface drying may be further enhanced by increasing transpiration if the canopy leaf area increases in warmer conditions. Furthermore, warming can trigger abrupt permafrost collapse which facilitates drainage of lakes and wetlands (*Schuur et al.*, 2015). Consequently, decreasing lake areas have been observed in the American Arctic (*Carroll et al.*, 2011; *Jones et al.*, 2011; *Lin et al.*, 2012).

On the other hand, lakes and wetlands may expand as climate warming can be coupled with increased precipitation (IPCC, 2013). Even with constant precipitation, more water can be kept in the plant–soil system if shrubs trap the snow and thus reduce the sublimation from blowing snow (*Pomeroy et al.*, 2006). Another process that can drive lake or wetland expansion is permafrost thaw. In ice-rich permafrost areas, thawing provides a continuous water source which can lead to ponding on the surface. As water absorbs sunlight very efficiently, ponds warm the surrounding permafrost leading to further thaw, ponding water, and subsidence. Thus lakes can expand if no drainage develops (*Smith et al.*, 2005; *Jorgenson et al.*,

2006; *Lin et al.*, 2012; *Schuur et al.*, 2015).

Besides soil moisture, soil temperature, air temperature, and nutrient availability control plant growth at the local scale. Soil warming can potentially increase nutrient availability as it accelerates decomposition (*Sturm et al.*, 2001a; *Mack et al.*, 2004; *Xue et al.*, 2016). However, short term warming experiments did not reveal increased soil nutrient availability (*Myers-Smith and Hik*, 2013; *DeMarco et al.*, 2014).

In some Arctic areas also anthropogenic influence alters the landscape and thus plant habitats. An important factor is grazing, which generally decreases shrub abundance and facilitates expansion of grasses (*Rees et al.*, 2003; *Olofsson et al.*, 2009; *Pajunen et al.*, 2011). Furthermore, resource exploitation from mining, oil industry, and gas fields affect ecosystems (*Convey et al.*, 2012).

The overall effect of climate change and anthropogenic influence on the tundra landscape is a combination of the processes described above. These processes work at different spatial and temporal scales and the net effect depends on local conditions such as topography, permafrost temperature, ice content, and the intensity of disturbances and pollution. While differences in net changes of lake and wetland extent have been observed among Arctic regions (*Lin et al.*, 2012), some patterns of vegetation change became apparent in multiple Arctic regions.

1.3 Tundra vegetation response to change

Vegetation responds in two ways to climate change. On one hand, vegetation composition can change, meaning that some species profit more than others from the new conditions and become more dominant (*van Wijk et al.*, 2003). Other species may get locally extinct if the environmental conditions are not suitable any more or other species outcompete them for resources. On the other hand, the same species may change in plant traits, such as plant height, leaf properties, and root depth. Both possible changes, in community composition as well as in plant traits, have already been observed in tundra areas using observational and experimental studies (*Schuur et al.*, 2007; *Hudson et al.*, 2011; *Elmendorf et al.*, 2012a).

Shrubs profit more than other tundra vegetation types from air and soil warming (*Wahren et al.*, 2005; *Myers-Smith et al.*, 2015). Additionally, several studies showed experimentally that under current conditions tundra shrubs are limited by nutrients. In case of nutrient addition, dwarf shrub leaf area and biomass increased strongly (*Bret-Harte et al.*, 2001; *Shaver et al.*, 2001; *Street et al.*, 2007). Higher future temperatures may increase nutrient availability (*Xue et al.*, 2016), which would favour shrubs, especially as compared to cryptogams (*Shaver et al.*, 2001; *van Wijk et al.*, 2003; *Walker et al.*, 2006). Shrub expansion and biomass increase, the so-called shrubification, consequently has been observed in many Arctic regions (*Tape et al.*, 2006; *Myers-Smith et al.*, 2011; *Sturm et al.*, 2001b; *McManus et al.*, 2012;

Lantz et al., 2013; *Frost and Epstein*, 2014). The shrub species that profits most from warming and nutrient addition is *Betula nana* (*Bret-Harte et al.*, 2001; *Walker et al.*, 2003a; *Hobbie et al.*, 2005; *Wahren et al.*, 2005). It is a common species in many tundra regions (*de Groot et al.*, 1997) and thus in a good position to expand further.

Increase in wetland extent can promote wet sedge expansion. Wet sedge species also increase biomass when nutrients are added (*Shaver et al.*, 1998; *Street et al.*, 2007). *Eriophorum angustifolium* (common cottongrass) is a widespread wet sedge species (*Phillips*, 1954) which can profit from disturbance (*Chapin and Shaver*, 1981). *Eriophorum angustifolium* can colonise shrub patches once they become more moist (*Myers-Smith et al.*, 2011; *Nauta et al.*, 2015).

Cryptogams are important components of tundra vegetation. Relative to vascular plants, cryptogams are more abundant at high latitudes where they can reach 100% cover (*Russell*, 1990). Under less extreme conditions, in northern Sweden subarctic tundra, cryptogams make up for 70% of the species (*Molau and Alatalo*, 1998) and 75% of the plant biomass (*Sonesson and Bergman*, 1980). However, cryptogam abundance decreases when tundra shrubs grow well (*Chapin et al.*, 1995; *van Wijk et al.*, 2003; *Walker et al.*, 2006). Thus, the widely observed shrub expansion affects cryptogam cover, which feeds back to climate and permafrost thaw (*Beringer et al.*, 2001). Mosses insulate the soil from air temperature (*Beringer et al.*, 2001; *Blok et al.*, 2011a), modify the drainage and moisture conditions of the soil (*Gornall et al.*, 2007), and facilitate seedling establishment (*Ohlson et al.*, 2001; *Stuiver et al.*, 2014).

1.4 Climate forcing by tundra vegetation

Vegetation does not only react to climate change, it also affects climate in multiple ways. In this thesis, the focus is on the effect of tundra vegetation on the energy rather than the carbon budget, which is discussed in detail in a number of studies (e.g. *Lafleur and Humphreys*, 2008; *McGuire et al.*, 2009; *Parmentier et al.*, 2011a; *Budishchev et al.*, 2014). The energy budget of the Earth's surface can be defined as

$$S\downarrow - S\uparrow + L\downarrow - L\uparrow = \lambda E + H + G \tag{1.1}$$

(*Oke*, 1987; *Eugster et al.*, 2000; *Eaton et al.*, 2001; *Liang et al.*, 2010). The left side of Equation 1.1 is the radiation budget (Figure 1.1). Incoming shortwave radiation ($S\downarrow$) is the direct solar energy which reaches the Earth's surface as electromagnetic radiation in a wavelength range of 300–4000 nm (*Liang et al.*, 2010). At noon on a clear day it can reach 600 W m^{-2} in northeast Siberia (Chapter 2). Parts of the incoming shortwave radiation are reflected back ($S\uparrow$). The ratio of $S\uparrow$ to $S\downarrow$ is defined as albedo (*Oke*, 1987). Typical tundra vegetation reflects about 15% to

20% of the incoming radiation, thus the albedo is 0.15–0.2 (*Eugster et al.*, 2000; *Thompson et al.*, 2004).

In addition to $S\downarrow$, incoming longwave radiation ($L\downarrow$) with wavelengths of 3–100 µm transports energy to the plant–soil system (*Oke*, 1987). This is the thermal radiation emitted by atmospheric gasses, aerosols, and clouds and arriving at the Earth's surface. Unlike solar radiation, this energy source acts day and night. In high latitudes it can be a larger energy source than the solar radiation, in particular in winter (*Ohmura*, 2001; *Sicart et al.*, 2006; *Langer et al.*, 2011a). A typical summer value would be 330 W m^{-2} in northeast Siberia (Chapter 2). $L\downarrow$ is balanced by the outgoing longwave radiation ($L\uparrow$) which is the thermal radiation emitted by the land surface. On average, it is larger than $L\downarrow$ as the surface heats up additionally due to solar radiation. 370 W m^{-2} is a typical summer value (Chapter 2). As $L\uparrow$ depends to a power of four on the surface temperature, it is smaller in winter.

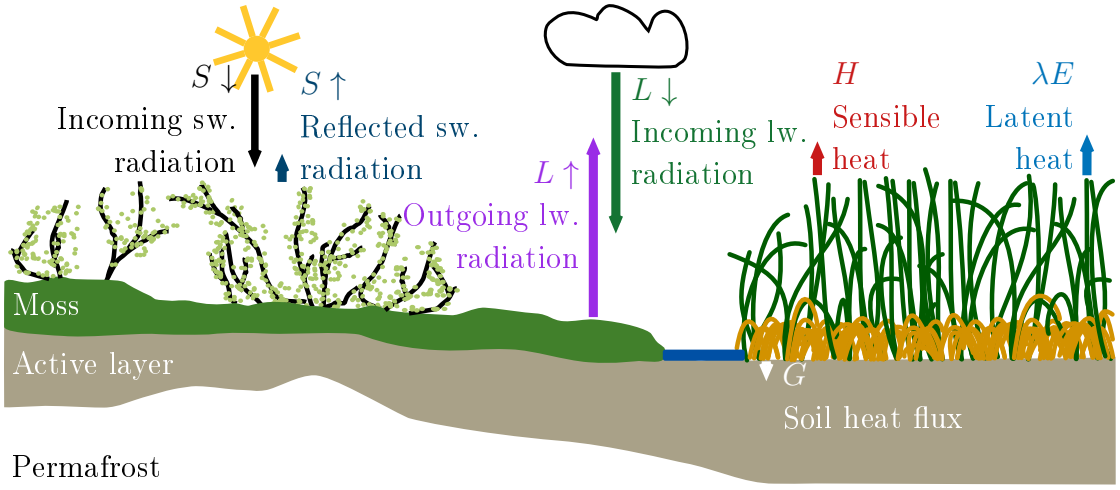

Figure 1.1: Schematic drawing of the landscape energy budget with shortwave ($S\downarrow$, $S\uparrow$) and longwave ($L\downarrow$, $L\uparrow$) radiation, turbulent heat fluxes (λE, H), and soil heat flux (G); the arrows are not associated with the different landcover types.

The right side of the energy budget equation (Equation 1.1) contains the turbulent heat fluxes (λE, H) and the soil heat flux (G). λE is the energy used for phase change of water, the latent heat. Evaporation from surfaces and transpiration by plants are the most important processes changing λE, but also dew and rime formation are part of the latent heat flux (*Oke*, 1987). Summer average λE in polygonal tundra can be around 40 W m^{-2} (*Langer et al.*, 2011b). The second turbulent flux is the sensible heat H, which is the warming of air. Mean summer values of about 20 W m^{-2} have been measured in Siberian polygonal tundra (*Langer et al.*, 2011b). The last term is the soil heat flux G. In permafrost regions, this energy is not only used to warm the soil, but also to thaw frozen ground. In autumn and winter, the

soil heat flux is mostly negative meaning that the soil releases energy to the atmosphere through cooling and freezing. In comparison with the radiation fluxes, the tundra soil heat flux is small, in the range of $10\,\mathrm{W\,m^{-2}}$ (Chapter 2).

The energy budget is always defined with respect to a reference surface. However, this concept becomes more complicated with vegetation as it separates the soil heat flux, which is per definition below the canopy, and the other fluxes, which are usually defined above the canopy (Figure 1.1). Most studies of the energy budget do not consider the energy stored in the canopy (*Chambers et al.*, 2005). This energy, which is used for photosynthesis and warming of the canopy, can be up to 10% of the daily net radiation (*Chapin et al.*, 2011).

However, even if energy storage in the canopy is neglected, vegetation strongly affects the energy budget in multiple ways. The most important effect is the reduction of **albedo** by tall and dense canopies. In general, forests have the lowest albedo, followed by tall shrubs, low shrubs and tundra without shrubs (*Thompson et al.*, 2004). However, wetlands can also have low albedo values (*Gamon et al.*, 2012) as water surfaces absorb most solar radiation, in particular at small sun zenith angles. At the large scale, already a small reduction in albedo, for example due to shrub expansion, can lead to substantial warming (*Lawrence and Swenson*, 2011).

The second feedback of vegetation on the amount of energy in the soil–plant–atmosphere system is by the **outgoing longwave radiation**, which is mainly controlled by surface temperature. The warmer the surface, the more longwave radiation is emitted (*Oke*, 1987). The soil surface temperature is related to vegetation cover indirectly, because vascular vegetation influences moss cover and soil moisture (*Westermann et al.*, 2011). Other factors such as soil shading also reduce soil surface temperature (*Briggs et al.*, 2014).

Other effects of vegetation on the energy budget do not affect the total amount of energy in the soil–plant–atmosphere system, but the partitioning of the available energy into turbulent fluxes or soil heat flux. Due to cold soil temperature and ice content, **soil heat flux** is usually a strong energy sink in the Arctic summer (*McFadden et al.*, 1998). Mosses decrease the ground heat flux through insulation (*Beringer et al.*, 2001; *O'Donnell et al.*, 2009; *Blok et al.*, 2011a). Furthermore, soil shading by vascular plants has been suggested as mechanism for reducing the soil heat flux (*Benninghoff*, 1952; *Briggs et al.*, 2014). If less shortwave radiation is transmitted through the canopy to the soil surface, less energy is directly available for warming and thawing the soil. Even though soil shading does not reduce the total amount of energy in the soil–plant system, it changes the energy partitioning so that more energy is used for turbulent heat fluxes instead of the soil heat flux.

Evapotranspiration is strongly affected by vegetation type and cover. Moss cover can have two opposing effects. On one hand, transpiration by mosses can be larger than by shrubs in tundra ecosystems (*McFadden et al.*, 1998; *Vourlitis and*

Oechel, 1999; *Beringer et al.*, 2001, 2005). As mosses cannot control transpiration by closing stomata, moss transpiration is very high as long as water is available. On the other hand, the strong moss transpiration can lead to drying of the moss layer, which reduces evapotranspiration as compared to bare soil (*Vourlitis and Oechel*, 1999; *Blok et al.*, 2011a). In case of a desiccated moss layer, vascular plants can maintain some transpiration if the roots reach below the moss layer. Otherwise, energy partitioning into transpiration is limited under dry conditions and proportionally more energy is converted into sensible heat flux (*Blok et al.*, 2011a).

In the Arctic summer, the **sensible heat flux** is usually smaller than the latent heat flux (*Beringer et al.*, 2005), in particular on wet sites (*Langer et al.*, 2011b). At some locations with little moss cover or permanently wet conditions, the sensible heat flux is smaller than the ground heat flux (*Beringer et al.*, 2001; *Langer et al.*, 2011b). As moss cover reduces the ground heat flux, it promotes energy partitioning into sensible heat (*Beringer et al.*, 2001).

1.5 The Kytalyk field site

So far, most tundra energy budget studies were carried out in Alaska (e.g. *Eugster et al.*, 2000; *Thompson et al.*, 2004). Vegetation–climate interaction has been studied only at a few locations in northern Siberia, such as the Lena delta (*Langer et al.*, 2011b). Large tundra areas remain poorly studied although it has been shown that large scale landscape change differs between Arctic Alaska and Arctic Siberia (*Wang and Key*, 2005b; *Wania et al.*, 2009; *Lin et al.*, 2012). While lakes are shrinking and the surface is drying in tundra regions in Alaska (*Oechel et al.*, 2000; *Jones et al.*, 2011; *Lin et al.*, 2012) and Canada (*Smol and Douglas*, 2007; *Carroll et al.*, 2011), surface wetting has been observed in Siberia (*Lin et al.*, 2012), at least in areas with continuous permafrost (*Smith et al.*, 2005). Alaska and north Siberia also show different magnitudes of changes in air and soil temperatures (IPCC, 2013). These differences in landscape and climate change indicate that more effort is needed to study the large tundra region of northern Siberia.

Currently, energy flux data are measured at three locations in the northeast Siberian tundra (*Kasurinen et al.*, 2014), on Samoylov Island in the Lena river delta (*Langer et al.*, 2011b; *Muster et al.*, 2012; *Boike et al.*, 2013), in the Kolyma river floodplain nearby Cherskii (*Corradi et al.*, 2005; *Merbold et al.*, 2009), and in Kytalyk in the Indigirka lowlands (*van Huissteden et al.*, 2005; *Parmentier et al.*, 2011b). The advantage of the Kytalyk site is that it is not located in a river floodplain. Therefore, it may be more representative of the vast Siberian lowlands. Furthermore, several vegetation types can be found within a small area.

The Kytalyk field site is located in a nature reserve in northeast Siberia (70.8 °N, 147.5 °E, Figure 1.2). Kytalyk is located in the low Arctic, about 170 km south

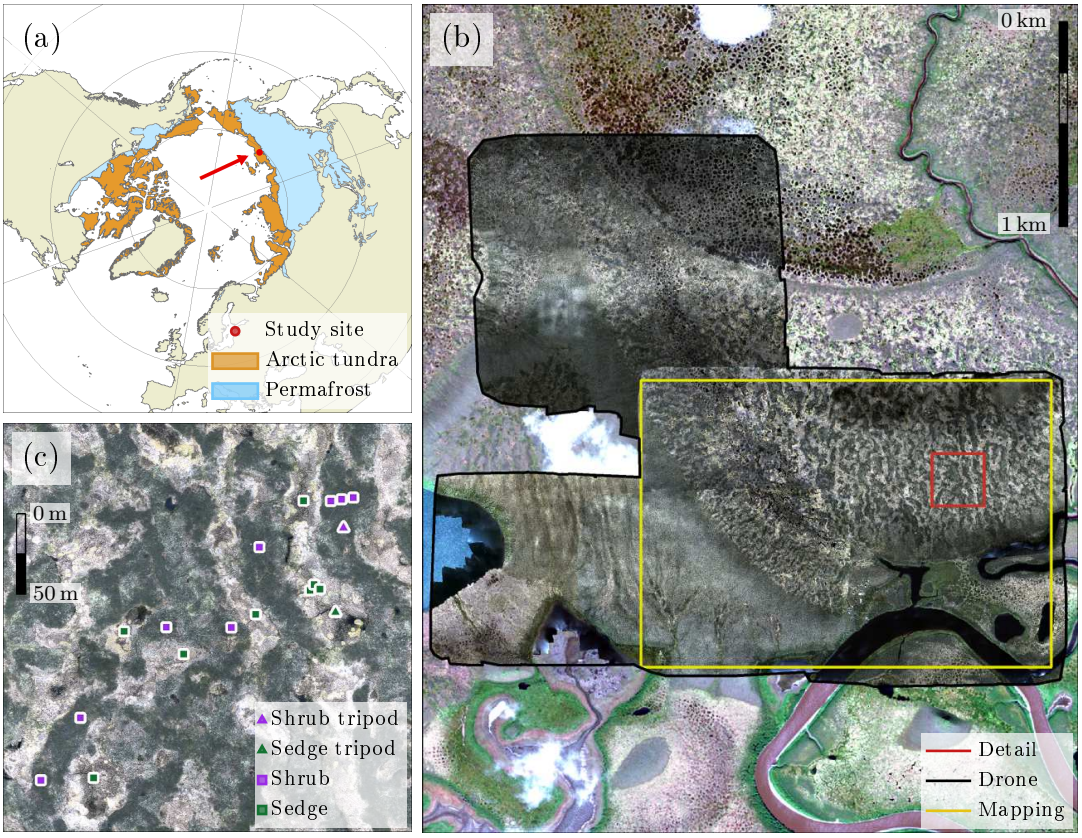

Figure 1.2: (a) Map of the study site location in northeast Siberia and the extents of Arctic tundra (orange, *Walker et al.* (2005)) and continuous permafrost (blue, *Brown et al.* (2000)), (b) satellite image (GeoEye-1) of the site including drone orthomosaics, the extent of the vegetation map (yellow), and the location of the detailed measurements (red), and (c) orthomosaic of the study site including measurement locations on dwarf shrubs (purple) and wet sedges (green); squares indicate spatially distributed measurements, triangles indicate automatic measurement stations.

of the coast of the East Siberian Sea. The site is located at the river Berelekh, a tributary of the Indigirka. By these rivers, the study site is accessible by boat, and snow scooter in winter, from the town of Chokurdakh, which is located about 27 km southeast of Kytalyk.

The lowland tundra is characterised by a drained thaw lake bed and a Pleistocene yedoma ridge (*Schirrmeister et al.*, 2012). Kytalyk is underlain by continuous, ice-rich permafrost (*Brown et al.*, 2002; *Iwahana et al.*, 2014) of several hundred meter depth (*Romanovskii et al.*, 2004). A soil layer of about 25–55 cm depth thaws every summer and refreezes in winter, the so-called active layer thickness (*van Huissteden et al.*, 2005). With about seven pingos per 100 km^2, the area has one of the highest densities of pingos of Siberia (*Grosse and Jones*, 2011). Six pingos within 5 km

radius of the study site are indicated on a local map (D-471 H-89-Hb, 1989).

The mean annual air temperature is −13 °C and the mean monthly temperature varies between −34.2 °C in January and 10.4 °C in July (*van der Molen et al.*, 2007). The snow cover lasts about 240 days each year (*van der Molen et al.*, 2007). During summer months, it rains on average 76 mm, 120 mm precipitation fall as snow every year (*Nauta et al.*, 2015). Snowmelt has been observed between 18 May and 10 June in a multi-year study by *Parmentier et al.* (2011b). The growing season starts about four weeks after snow melt and ends in early September in all years (*Parmentier et al.*, 2011b). As Kytalyk is located at 70.8 °N, polar night lasts about two months in winter and the sun does not set between 15 May and 29 July (Chapter 2). About 20% of the summer days can be defined as clear sky, 20% as cloudy and 60% as partly cloudy (Chapter 2). Incoming shortwave radiation is on average 190 W m^{-2} during the growing season and incoming longwave radiation 330 W m^{-2} (Chapter 2).

On the circumpolar Arctic vegetation map, the Kytalyk field site is located at the border between tussock sedge, dwarf shrub, moss tundra and low shrub tundra (*Walker et al.*, 2005). However, at small scale, six different tundra vegetation types as defined by *Walker et al.* (2005) can be found on the site (Table 1.1). These vegetation types occur close to each other in a fine-scale mosaic depending on soil moisture, pH, and nutrients.

As prostrate dwarf shrub tundra (classes P1 and P2) occurs only in small isolated patches, it is not considered further in this study. Low shrub tundra (S2) is mostly restricted to river and lake banks. Tussock tundra (G4) is widespread in the study region, in particular in elevated areas. Dwarf shrub tundra (S1) and sedge wetland (W2) are the two characteristic vegetation types of the drained thaw lake bed. Within these two vegetation types, different dominant species and canopy characteristics such as height and leaf area can be found. Thus, the classes S1 and W2 are subdivided into more detailed sub-classes for this study (Table 1.1, Figure 1.3). The vegetation height is generally less than 50 cm (*Blok et al.*, 2010; *Parmentier et al.*, 2011b), except for low shrub tundra, which can reach 2 m height.

1.6 In situ observational and modelling approaches

In situ observations and radiative transfer modelling were combined to quantify the effect of tundra vegetation on the radiation budget and permafrost thaw. Field measurements provided information on all three components, (I) the tundra vegetation distribution, composition, and structure, (II) the radiation budget above canopy and soil shading, and (III) the soil heat flux and permafrost thaw depth. The combination of vegetation observations and energy budget components did not only allow the direct comparison between vegetation types, but also served as input and validation data for the radiative transfer modelling.

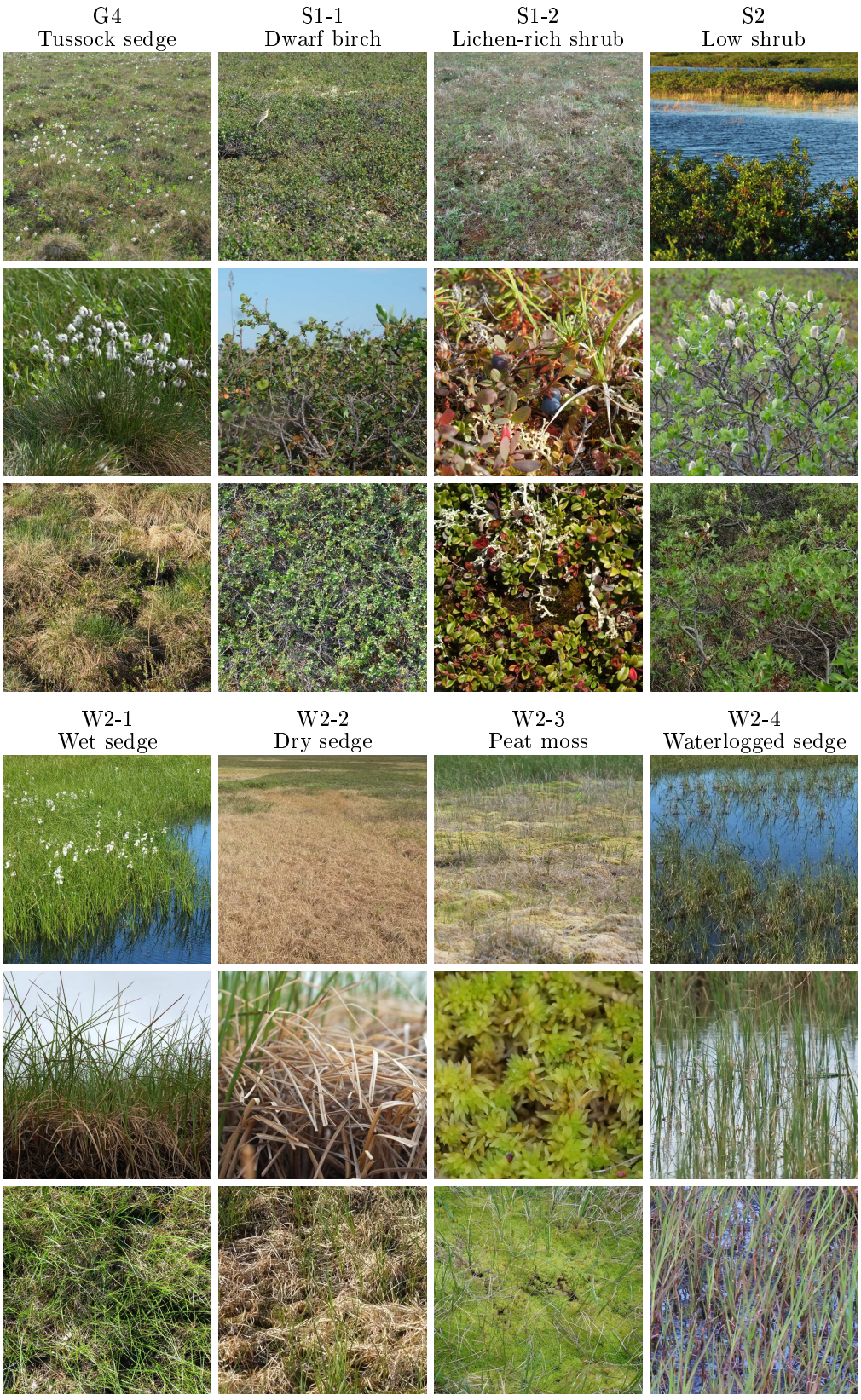

Figure 1.3: Photographs of eight tundra vegetation classes used in this study.

Table 1.1: Vegetation classes from the circumpolar Arctic vegetation map (*Walker et al.*, 2005) present at the study site; sub-classes were defined for this study based on differences in species composition and canopy properties.

Class	Sub-class	Description	Canopy height	Characteristic species
G4		Tussock sedge, dwarf shrub, moss tundra	<40 cm	*Eriophorum vaginatum, Vaccinium* sp.
P1		Prostrate dwarf shrub, herb tundra (<80% cover, dry)	<10 cm	*Dryas octopetala*
P2		Prostrate/hemiprostrate dwarf shrub tundra (40–100% cover)	<20 cm	*Cassiope tetragona*
S1		Erect dwarf shrub tundra	<40 cm	
	S1-1	- closed shrub canopy		*Betula nana, Salix pulchra*
	S1-2	- scattered shrubs, lichen-rich		*Vaccinium vitis-idaea*, mosses, lichen
S2		Low shrub tundra (moist)	>40 cm	*Salix pulchra*
W2		Sedge, moss, dwarf shrub wetland	<40 cm	
	W2-1	- wet, dense, green		*Eriophorum angustifolium*
	W2-2	- drier, more standing dead leaves		*Eriophorum angustifolium, Sphagnum* sp.
	W2-3	- mostly moss		*Sphagnum* sp.
	W2-4	- waterlogged, few standing dead leaves		*Carex* sp.

In my **in situ observations**, I set up two automatic measurement stations, carried out spatially distributed measurements on additional plots, did further auxiliary measurements, mapped vegetation reference points, and obtained orthophotos (Figure 1.4). An overview of all measured variables is presented in Table A.1 in the appendix.

Automatic stations were installed to measure time series of energy budget components, temperature and soil moisture. Using time series, I analysed the effects of cloud cover and solar zenith angle and I obtained estimates of seasonal averages. I installed two automatic measurement stations, one in the centre of a dwarf shrub and the second in the centre of a wet sedge patch (Figure 1.2c). These measurements included the above canopy radiation budget (Figure 1.4a,b), below canopy shortwave radiation (Figure 1.4c,d), air temperature at different heights above canopy (Figure 1.4f), soil temperature in different depths, soil heat flux at 10 cm depth (Figure 1.4s), and soil moisture. Radiation instruments were fixed to one tripod per patch at 1.5 m above the canopy. Additionally, two automatic cameras recorded snow melt timing and vegetation phenology at each location. Air temperature was measured 9 m away from the tripod at the datalogger locations. Soil temperature, moisture,

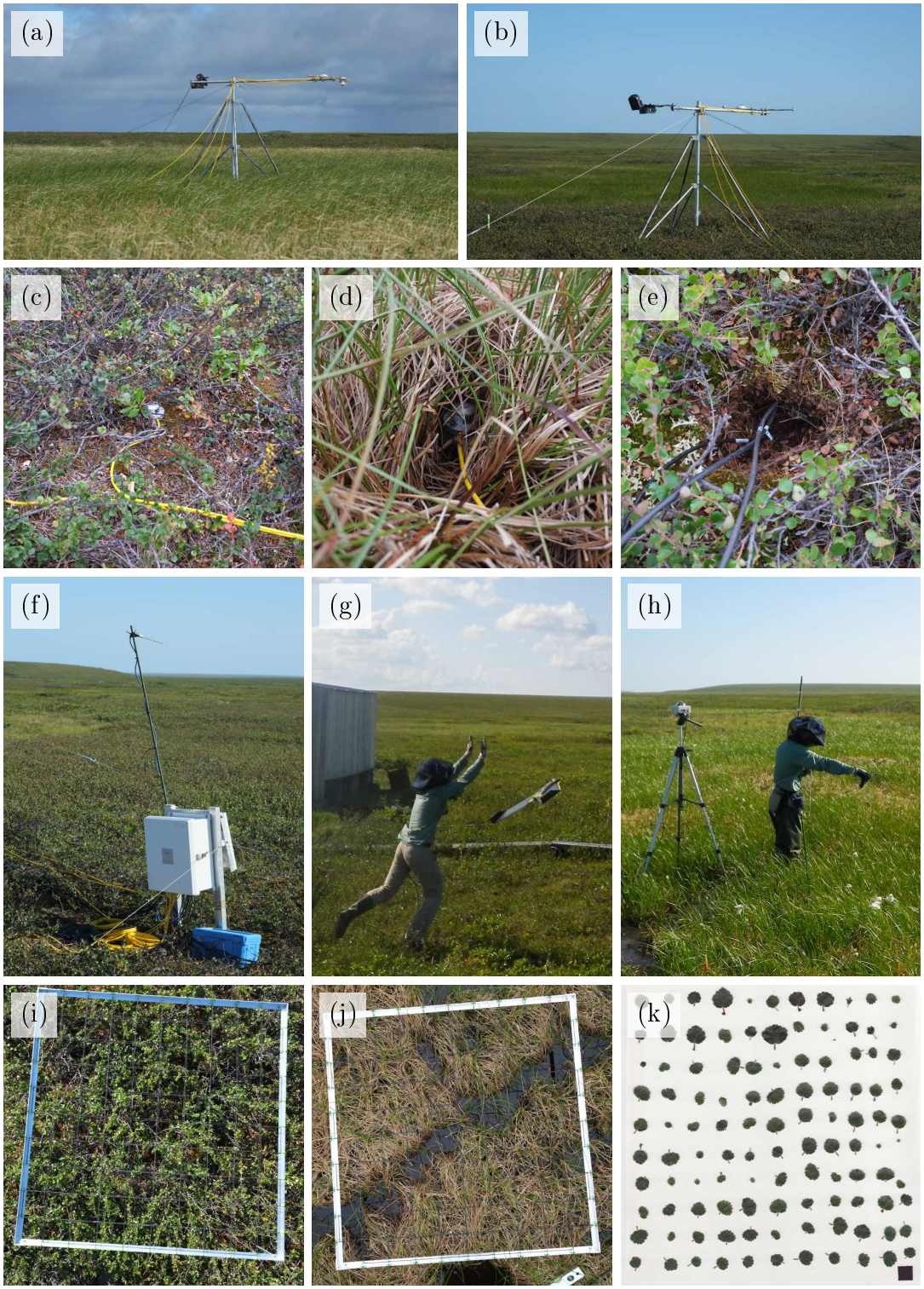

Figure 1.4: Photographs of field measurements: (a,b) above canopy radiation, (c,d) canopy transmittance, (e) soil heat flux and temperature, (f) air temperature and datalogger box, (g) orthophotos using a drone, (h) canopy spectral reflectance, (i,j) leaf area index using a point quadrat, and (k) destructive leaf area index using scanned leaves (pictures g,h by Bingxi Li).

and heat flux sensors were buried within 7 m from the datalogger locations. Nine below canopy shortwave radiation sensors were installed in the beginning of each growing season, four below wet sedges and five below dwarf shrubs. More details on the set up, including a schematic of the measurement locations (Figure A.2) and tables with detailed information on the sensors used (Tables A.2–A.4) can be found in the appendix.

The radiation data series covers 07 July – 31 August 2013, 11 May – 17 August 2014, and 25 April – 09 July 2015. The soil flux data begin ten days later in 2013 and span the same period as radiation measurements in 2014 and 2015.

Spatially distributed measurements were used to obtain canopy properties and to assess whether or not the automatic measurements were representative for the respective vegetation types at the automatic stations (Figure 1.2c). I measured multiple variables at eight plots of 1 m × 1 m per vegetation type. These measurements were repeated several times during the growing seasons of 2013 and 2014. The variables in question were leaf and wood area index (Figure 1.4i,j), fractional cover of background types below dwarf shrubs, Active Layer Thickness (ALT), canopy and standing dead leaf height, transmitted Photosynthetically Active Radiation (PAR) below canopy, and spectral reflectance (Figure 1.4h).

Auxiliary measurements were needed for more details on vegetation properties as input of radiative transfer modelling, for model validation, and for soil properties. As the auxiliary measurements involved removing vegetation, they were done nearby the permanent plots. I took six different kinds of auxiliary measurements, all for dwarf shrubs and wet sedges. (I) I took destructive measurements of leaf, wood, and standing dead leaf area to calibrate the spatially distributed measurements (Figure 1.4k). This involved cutting vegetation, separating the biomass by species and organ, scanning a subset, drying, and weighing. (II) I measured leaf, standing dead leaf, and wood optical properties. (III) I took levelled photographs of the canopy to estimate the leaf, standing dead leaf, and wood angle distributions. (IV) I measured canopy PAR transmittance and spectral reflectance depending on sun angle and fraction of diffuse light. (V) I measured canopy PAR transmittance and spectral reflectance depending on canopy density by sequentially removing parts of the biomass and taking measurements in between. (VI) I measured soil thermal properties at the locations of the soil heat flux measurements and in one soil pit per vegetation type (KD2 PRO, Decagon Devices).

Vegetation reference points were used for training and validating the vegetation map. Reference points of different vegetation types were taken within the

larger study area (Figure 1.3, Table 1.1). I recorded the GPS coordinate in the middle of representative vegetation patches and noted the vegetation type and the radius this type was covering around the point.

Orthophotos were used to compute a digital surface model, a NDVI (normalised difference vegetation index) map, and the spectral reflectance for vegetation mapping. The orthophotos were obtained with an eBee (senseFly) drone during the summer of 2014 (Figures 1.2b, 1.4g). 35 of 49 flights provided usable pictures with one of the three cameras, one 'normal' red-green-blue camera, a red edge camera, and a near infra-red camera. In total, I got 4611 usable red-green-blue pictures, 2536 red edge, and 480 near infra-red pictures. The spatial resolution was about $4\,\mathrm{cm\,pixel^{-1}}$.

In addition to my field measurements, I used field data conceived and collected by Angela M. Erb during the growing season 2012 (*Erb*, 2013). This data covered experimental treatments of dwarf shrub canopies with reduced shrub densities and heights. Furthermore, I analysed spectral canopy reflectance measured by Gabriela Schaepman-Strub in 2008. Maitane Iturrate-Garcia contributed leaf area, leaf angle, and leaf optical properties data of *Eriophorum vaginatum* and *Salix pulchra*.

I used the **3D radiative transfer model** DART to extend the results from the field to situations with different canopy properties and from two vegetation types to seven vegetation types and water (*Gastellu-Etchegorry et al.*, 2004). I parametrised and validated the model using the field data described above. Data analysis was performed using MATLAB (Version R2015a), R (*R Core Team*, 2015, Version 3.2.3), ArcGIS (Version 10.2), ENVI (Version 5.2), and PostflightTerra 3D (Version 4.0.83).

1.7 Research questions and outline

The data and analysis contributed to answering the four main research questions of this thesis leading to a better understanding of the radiation budget of tundra vegetation.

1. What is the difference between the solar radiation budget of two widespread tundra vegetation types, dwarf shrubs and wet sedges (Chapter 2)?
2. How does the solar radiation budget of tundra vegetation influence soil heat flux and permafrost thaw (Chapter 2)?
3. How do dwarf shrub canopy properties affect the shortwave radiation budget (Chapter 3)?
4. How does vegetation heterogeneity influence the shortwave radiation budget at the local and the landscape scale (Chapter 4)?

I address these four questions using a combination of field measurements and radiative transfer modelling. In Chapter 2, I present the result of radiation and soil heat flux time series on dwarf shrub (*Betula nana*) and wet sedge (*Eriophorum angustifolium*) canopies. I quantify the differences between the wet sedge and dwarf shrub radiation budget for the growing season and the snowmelt period and discuss the relative importance of differences in albedo, soil shading, and soil properties for permafrost thaw. In Chapter 3, I use field data from 2012 (*Erb*, 2013) for input and validation of a 3D radiative transfer model (DART). Using this model, I quantify the radiation budget of dwarf shrub (*Betula nana*) canopies with variable leaf and woody area. I analyse the importance of leaves and woody parts separately and test different model parametrisations. Chapter 4 broadens the focus from two vegetation types to all common types present at the study site. Based on detailed field measurements and orthophotos, I parametrise the DART radiative transfer model at the landscape scale. I quantify the spatial variability of the radiation budget for all vegetation types and evaluate which factors contribute most to the spatial variability of albedo, canopy transmittance and light absorbed by the canopy. I summarise my methods, results, and conclusions in the three main chapters of this thesis. Finally, I discuss the most important findings of all chapters and some additional observations in the synthesis (Chapter 5). The thesis is completed with Appendix A describing the in situ measurement set-up and data analysis in more detail and Appendix B on radiative transfer model validation.

2 Contrasting radiation and soil heat fluxes in Arctic shrub and wet sedge tundra

Inge Juszak[1], Werner Eugster[2], Monique M. P. D. Heijmans[3], and Gabriela Schaepman-Strub[1]

Abstract

Vegetation changes, such as shrub encroachment and wetland expansion, have been observed in many Arctic tundra regions. These changes feed back to permafrost and climate. Permafrost can be protected by soil shading through vegetation as it reduces the amount of solar energy available for thawing. Regional climate can be affected by a reduction in surface albedo as more energy is available for atmospheric and soil heating. Here, we compared the shortwave radiation budget of two common Arctic tundra vegetation types dominated by dwarf shrubs (*Betula nana*) and wet sedges (*Eriophorum angustifolium*) in North-East Siberia. We measured time series of the shortwave and longwave radiation budget above the canopy and transmitted radiation below the canopy. Additionally, we quantified soil temperature and heat flux as well as active layer thickness. The mean growing season albedo of dwarf shrubs was 0.15 ± 0.01, for sedges it was higher (0.17 ± 0.02). Dwarf shrub transmittance was 0.36 ± 0.07 on average, and sedge transmittance was 0.28 ± 0.08. The standing dead leaves contributed strongly to the soil shading of wet sedges. Despite a lower albedo and less soil shading, the soil below dwarf shrubs conducted less heat resulting in a 17 cm shallower active layer as compared to sedges. This result was supported by additional, spatially distributed measurements of both vegetation types. Clouds were a major influencing factor for albedo and transmittance, particularly in sedge vegetation. Cloud cover reduced the albedo by 0.01 in dwarf shrubs and by 0.03 in sedges, while transmittance was increased by 0.08 and 0.10 in dwarf shrubs and sedges, respectively. Our results suggest that the observed deeper active layer below wet sedges is not primarily a result of the summer canopy radiation budget. Soil properties, such as soil albedo, moisture, and thermal conductivity,

[1]Department of Evolutionary Biology and Environmental Studies, University of Zurich, Winterthurerstrasse 190, 8057 Zurich, Switzerland
[2]Institute of Agricultural Sciences, ETH Zurich, Universitätstrasse 2, 8092 Zurich, Switzerland
[3]Plant Ecology and Nature Conservation, Wageningen University, Droevendaalsesteeg 3, 6708 PB Wageningen, The Netherlands

may be more influential, at least in our comparison between dwarf shrub vegetation on relatively dry patches and sedge vegetation with higher soil moisture.

Reprinted as in **Biogeosciences Discussions** with references merged at the end of this thesis:
I. Juszak, W. Eugster, M. M. P. D. Heijmans and G. Schaepman-Strub, 2016, Contrasting radiation and soil heat fluxes in Arctic shrub and wet sedge tundra, *Biogeosciences Discussions*, 1–24, doi:10.5194/bg-2016-41
in review for **Biogeosciences**

The time series data and canopy structural and radiative properties used for this work are available at `https://doi.org/10.1594/PANGAEA.860561`.

I.J. participated in designing the study, planned and carried out field measurements, performed the data analysis, and wrote the manuscript. W.E. contributed to the data analysis and to the manuscript preparation. M.M.P.D.H. contributed to writing the manuscript and G.S.-S. conceived the study and provided input for the data analysis and the manuscript.

2.1 Introduction

Recent climate warming in the Arctic (*Stocker et al.*, 2013) is associated with increasing shrub abundance, cover, and biomass in many regions (*Tape et al.*, 2006; *Myers-Smith et al.*, 2011; *Sturm et al.*, 2001b; *McManus et al.*, 2012; *Lantz et al.*, 2013; *Frost and Epstein*, 2014). However, vegetation can change in multiple directions and at larger scales the dominance of shrub tundra or wet sedge tundra is controlled by soil moisture and surface hydrology. While permafrost collapse leads to wetland expansion in some continuous permafrost regions (*Smith et al.*, 2005; *Jorgenson et al.*, 2006; *Lin et al.*, 2012; *Schuur et al.*, 2015), drying has been observed in others (*Oechel et al.*, 2000; *Carroll et al.*, 2011; *Jones et al.*, 2011; *Lin et al.*, 2012). Shrub encroachment lowers the tundra albedo and thus positively feeds back to global warming (*Sturm et al.*, 2001b; *Lawrence and Swenson*, 2011; *Loranty and Goetz*, 2012). However, larger scale atmospheric effects do not explain variations of permafrost conditions at the local scale, where wetland vegetation is often associated with deeper active layers (*Anisimov et al.*, 2002; *Mi et al.*, 2014).

Dwarf birch (*Betula nana*) profits more than other species from warming (*Walker et al.*, 2003a) and fertilisation (*Bret-Harte et al.*, 2001; *Hobbie et al.*, 2005). It is a common species in many Arctic regions (*de Groot et al.*, 1997) and likely to be the primary driver of shrub expansion (*Sturm et al.*, 2001a). Common cottongrass (*Eriophorum angustifolium*) is a widespread wet sedge species (*Phillips*, 1954). In comparison with other sedges, *Eriophorum angustifolium* does not strongly profit from nutrient addition or warming (*Shaver et al.*, 1998). However, it can expand in disturbed areas (*Chapin and Shaver*, 1981; *Nauta et al.*, 2015) and where the surface gets wetter due to abrupt permafrost thaw (*Schuur et al.*, 2015).

Arctic tundra ecosystems commonly comprise small scale vegetation patterns of shrubs, graminoids, and cryptogams associated with soil pH and moisture variation (*Chapin et al.*, 2000a; *Gamon et al.*, 2012). This intra-ecosystem variability is relevant for the radiation budget as it can have stronger effects on the summer albedo than the difference among biomes, such as tundra and boreal forest (*Chapin et al.*, 2000a; *Eugster et al.*, 2000). Vegetation alters the radiation budget at the soil surface which is critical for the ground heat flux and thus for permafrost thaw (*Jacobsen and Hansen*, 1999; *Beringer et al.*, 2005). Shallower thaw depths have been observed below shrub canopies as compared to below other tundra vegetation (*Anisimov et al.*, 2002; *Walker et al.*, 2003b). *Blok et al.* (2010) suggested that the overall warming effect of Arctic shrub encroachment due to decreasing albedo can be mitigated by soil shading.

The surface radiation budget is strongly influenced by cloud cover, which reduces the amount of incoming shortwave radiation and increases the fraction of diffuse light. High cloud fractions between 65% and 90% have been reported over Arctic

land surfaces during the summer months (*Curry et al.*, 1996; *Wang and Key*, 2005b; *Dong et al.*, 2010). Recently, Arctic cloud cover has increased (*Wang and Key*, 2005a) and further increase is likely due to climate change (*Chapin et al.*, 2005; *Vavrus et al.*, 2009). Cloudy conditions reduce the albedo at solar zenith angles of 60° or more (*Yang et al.*, 2008) and increase the radiation fraction reaching the soil below the vegetation (at solar zenith angles above 50°, *Mahat and Tarboton*, 2012). Therefore, changes in cloud cover potentially impact the tundra surface radiation budget and interact with the predicted changes in tundra vegetation.

Furthermore, additional components of the plant–soil system are closely linked with the radiation budget. For example, it has been shown that canopy shading affects the abundance and richness of mosses and lichens, which are suppressed by well-growing deciduous shrubs (*van Wijk et al.*, 2003; *Walker et al.*, 2006). Moreover, the radiation budget is linked with the carbon cycle. CO_2 fluxes were found to be highly related to net radiation in an Arctic tussock tundra site (*Oechel et al.*, 2014).

Despite the importance of shading for the permafrost energy budget and plant species competition, it is rarely measured below different tundra vegetation types. While several studies assessed solar radiation transmittance below Arctic shrubs (*Bewley et al.*, 2007; *Chong et al.*, 2012; *Juszak et al.*, 2014; *Williams et al.*, 2014), this study compared shrub shading with shading by other vegetation types. Furthermore, the radiation and soil heat flux budget of Arctic tundra has been more extensively studied in Alaska, Canada, and Europe than in the vast Siberian lowlands.

The aim of our study was to quantify the above-canopy radiation budget, below-canopy transmitted shortwave radiation, and soil heat fluxes of two widespread tundra vegetation types, dwarf shrubs and wet sedges. We complemented time series measurements of these three components with spatially distributed measurements at the Kytalyk research site, North-East Siberia. In this way, we evaluated the importance of albedo and soil shading for permafrost thawing. Furthermore, we characterised the impact of weather conditions on radiative fluxes as cloud conditions are likely to change in the future. Our results will assist modelling attempts in providing details on local scale variability of albedo, soil shading, and soil heat flux in an Arctic tundra ecosystem.

2.2 Methods

2.2.1 Field site, vegetation, and soil

The study area is located in a drained thaw lake bed in the Kytalyk nature reserve, North-East Siberia (70.83 °N, 147.49 °E, Fig. 3.1a). It is characterised by continuous permafrost and an active layer thickness of 25–55 cm (*van Huissteden et al.*,

2005). The mean annual permafrost temperature at 15 m depth close to the site is −9.4 °C (*Romanovsky et al.*, 2010). The study region in lowland tundra is underlain by very ice-rich permafrost (*Iwahana et al.*, 2014), which makes it susceptible to rapid changes in case of warming (*Jorgenson et al.*, 2006). A multi-year study by *Parmentier et al.* (2011b) observed the snowmelt between 18 May and 10 June. The growing season started about four weeks after snowmelt and ended early September in all years (*Parmentier et al.*, 2011b).

The vegetation at the study site is classified as tussock sedge, dwarf shrub, and moss tundra in the Circumpolar Arctic vegetation map (*Walker et al.*, 2005). More specifically, in the drained thaw lake bed, elongated, well-drained patches of erect dwarf shrub tundra alternate with depressions of sedge, moss dwarf shrub wetland (Fig. 3.1b). Dwarf shrub and sedge patches are irregularly shaped and about 10–20 m wide and 70–150 m long (Fig. 3.1b). The surface elevation of dwarf shrub patches is 0.3–0.7 m higher than of wet sedge depressions. While dwarf shrub patches have an active layer thickness of 15–25 cm, it is 26–48 cm at wet sedges (*van Huissteden et al.*, 2005). In winter, snow accumulates in the wet sedge depressions and reaches a depth of about 25 cm at the dwarf shrub patches (*Nauta et al.*, 2015).

The centre of dwarf shrub patches is dominated by dwarf birch (*Betula nana*, Fig. 3.1e, f). Willows (e.g. *Salix pulchra*) complement the dwarf birches and dominate the canopies along the rivers. Communities of lingonberry (*Vaccinium vitis-idaea*), mosses, and lichen surround the dense dwarf birch vegetation. Towards the lower, wetter areas peat mosses and sedges border the dwarf shrub patches. Most commonly, the wet sedge community is comprised of common cottongrass (*Eriophorum angustifolium*, Fig. 3.1c, d), which does not form tussocks. Although dwarf birch dominated areas are usually separated from wet sedge areas by the described transition zones, in some places they can be found directly bordering each other. Sedges can invade drowning shrub-covered areas (*Myers-Smith et al.*, 2011), especially after disturbance (*Nauta et al.*, 2015), and shrubs can colonise peat moss covered areas, which in turn invade wet sedge depressions.

Blok et al. (2010) measured an average dwarf birch canopy height of 21 cm, dry above ground biomass of 400 g m^{-2} and a total shrub cover of about 70%. The wet sedge *Eriophorum angustifolium* can cover 50% of the surface in wet sedge locations (*Schirrmeister et al.*, 2012) and reach a maximum height of about 50 cm.

Below dwarf shrubs, the soil is mainly covered by mosses (about 38%, predominantly *Dicranum* sp., *Polytrichum* sp., and *Aulacomnium* sp.), shrub litter (about 56%), and some lichen (about 4%). The moss layer below dwarf shrubs is about 4–5 cm thick (*Blok et al.*, 2011a). Below 10–15 cm of highly organic soil (*Blok et al.*, 2010), mineral clay soil mixed with organic matter can be found. The soil moisture is usually below saturation and varies between 0.3 and 0.6 $m^3\,m^{-3}$ in the growing season, depending on weather conditions (see below for details on instruments and

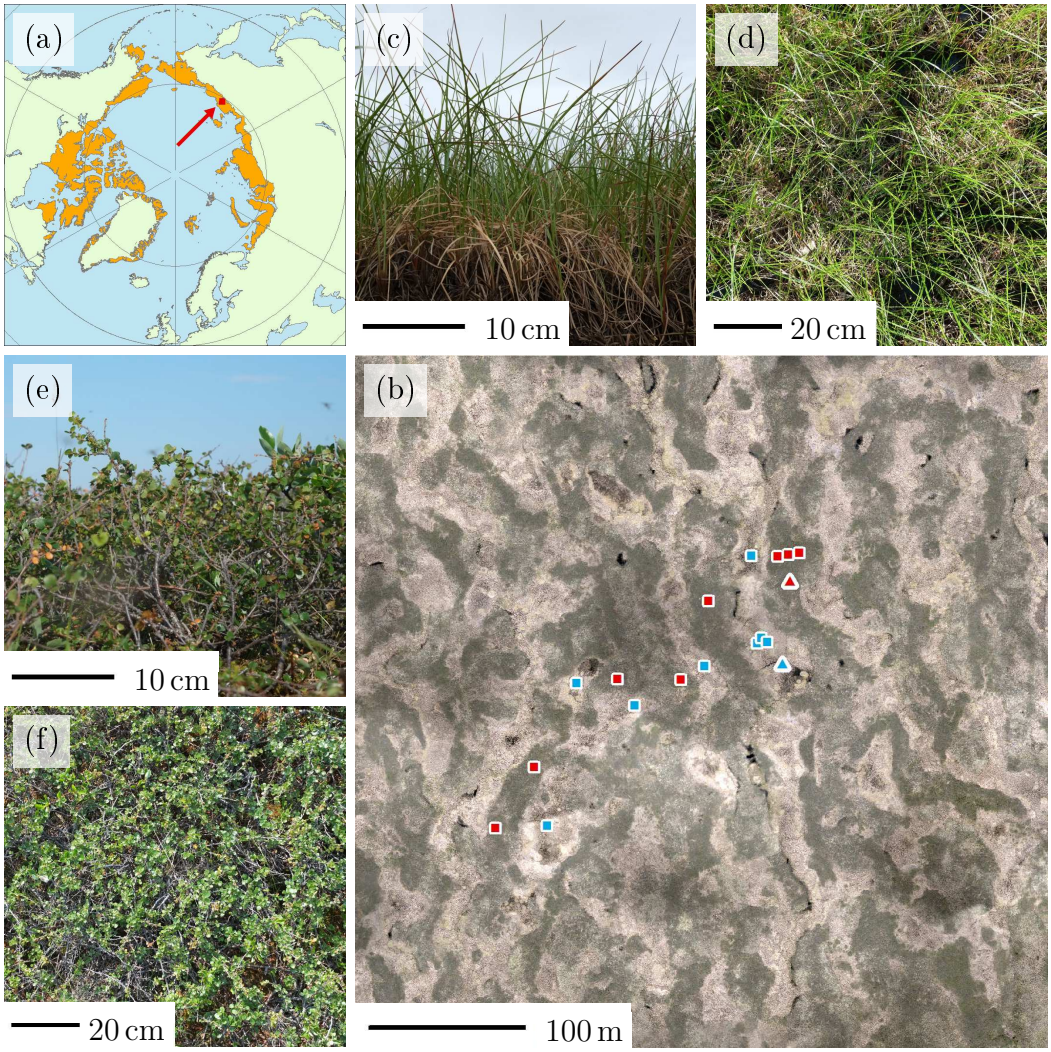

Figure 2.1: Location of the Kytalyk research station and Arctic tundra extent (a, data from *Walker et al.* (2005)), drone imagery (July 2014) of the site including time series measurement locations (b, triangles, red for dwarf shrubs and blue for sedges) and the distributed plot measurements (b, squares), sedge vegetation (c, d) and dwarf shrub vegetation (e, f).

measurements). With a thermal conductivity of $0.08\,\mathrm{W\,m^{-1}\,K^{-1}}$ the highly organic top soil below dwarf birch is strongly insulating. The heat capacity of this layer is about $0.5\,\mathrm{MJ\,m^{-3}\,K^{-1}}$. The deeper clay layer has a thermal conductivity of about $0.80\,\mathrm{W\,m^{-1}\,K^{-1}}$ and a heat capacity of $2.1\,\mathrm{MJ\,m^{-3}\,K^{-1}}$. Below the green sedge leaves, a 10–20 cm thick layer of dry, standing dead leaves covers the water or wet litter. In the dense sedge patches studied, there were almost no mosses or other species growing below the standing dead leaves. The uppermost 13–19 cm of the soil is water saturated, loose organic material (*Bartholomeus et al.*, 2012) with a water content of about $0.7\,\mathrm{m^3\,m^{-3}}$. Due to the water content, this layer has a high thermal conductivity ($0.44\,\mathrm{W\,m^{-1}\,K^{-1}}$) and heat capacity ($3.3\,\mathrm{MJ\,m^{-3}\,K^{-1}}$) (see below for details on instruments and measurements).

2.2.2 Measurements

We assessed the effect of wet sedge versus dwarf birch dominated vegetation on energy fluxes above canopy, below canopy, and in the top soil layer with field measurements. Time series of radiation and soil heat flux were acquired at a permanent location close to the centre of one patch per vegetation type. These measurements were complemented by sporadic measurements in eight spatially distributed plots per vegetation type to assess the spatial variation. For our below ground measurements in the sedge plot, we defined the top of the dark, wet, and cohesive litter as reference height. In the dwarf shrub plot, we used the top of the moss or litter as reference height (*Blok et al.*, 2011a).

The time series were recorded by two automatic measurement stations on a dwarf shrub and an adjacent sedge patch, located about 50 m apart (Fig. 3.1b, triangles). The instrument height was about 1.5 m above canopy to ensure that the instrument's footprint covered only one vegetation type. We used Kipp & Zonen CMP11 pyranometers (285–2800 nm) for incoming and reflected shortwave radiation, and an array of four (on sedge) and five (on dwarf shrub) Kipp & Zonen SPLITE2 silicon pyranometers (400–1100 nm) for below-canopy transmitted shortwave radiation. We installed the instruments on the moss or litter surface below dwarf shrubs and below some of the sedge standing dead leaves but above the early summer water level. We measured net longwave radiation with a Kipp & Zonen CNR2 net radiometer (300–2800 nm and 4.5–42 µm) in each plot. The two shortwave radiation flux components of the CNR2 also allowed for cross-validation with the CMP11 sensor data in our quality control procedure. Additionally, we cross-validated our incoming shortwave radiation measurements with one SPLITE2 pyranometer. Soil heat flux was measured in the organic top soil using three heat flux plates (HFP01, Hukseflux) per vegetation type at a depth of 10 cm below the reference height. Soil temperature data were acquired using three sensors (T107, Campbell Scientific) per vegetation

type at a depth of 4 cm below the reference height. We measured soil moisture with two sensors (ThetaProbe ML2x, Delta-T Devices) per vegetation type and converted the signal to volumetric water content using standard parameters for organic soil. The data from all sensors were recorded every 30 sec and averaged at 10 min intervals using a Campbell Scientific CR1000 datalogger. The radiation data series covers 07 July 2013 – 31 August 2013 and 11 May 2014 – 17 August 2014. The soil flux data begin ten days later in 2013 and span the same period as radiation measurements in 2014. We measured the soil thermal properties with a KD2 PRO, Decagon Devices, instrument on 04 and 05 August 2013. The measurements were done at all locations of soil heat flux measurements and in one soil pit per vegetation type to estimate soil properties below the highly organic horizon. The measurement date was after a dry summer period.

In order to assess the spatial variability of dwarf shrub and sedge vegetation and the spatial representativeness of the time series measurements, we additionally measured vegetation and radiation parameters in eight plots of 1 m^2 per vegetation type (Fig. 3.1b, squares). Three of the eight plots were located within the same vegetation patch as the time series measurements but outside of the footprint of the instruments. In the 16 plots we measured spectral exitance about 1 m above the canopy with an Ocean Optics Jaz spectrometer using a bare 100 µm fiber. Spectral irradiance was measured before and after the exitance measurements of each plot using the same spectrometer and an upwards pointing fiber equipped with a cosine corrector. From these two measurements we calculated the hemispherical-conical reflectance factor in nadir direction in the range of photosynthetically active radiation (PAR, 400–700 nm). We measured incident and transmitted PAR with a Delta-T Devices SunScan ceptometer. Below canopy, 64 sensors on a 1 m long probe recorded transmitted PAR simultaneously with the above-canopy BF3 sensor. Active layer thickness and canopy height were measured relative to the reference height by inserting a metal probe at 25 points of a regular grid in every plot. Canopy height was estimated as average height of the highest leaves within a 5 cm radius around the measurement point. Additionally, we measured maximum height at all plots. We measured projected dwarf shrub leaf and wood area using a 1 m^2 point quadrat and recording all contacts between a vertically inserted needle and the vegetation at 81 points (*Wilson*, 1959). The leaf area of other vascular plants on the dwarf shrub plots was negligible. In two destructive leaf area index (LAI) measurements we found that the point quadrat counts underestimated the shrub leaf area by 15% and 28%, which was 0.18 and 0.25 in absolute values.

To estimate sedge leaf area index non destructively, we used an empirical allometric approach,

$$\mathrm{LAI} = \frac{h_c}{h_r} \cdot \frac{1}{A} \cdot \sum_{i=1}^{m} n_i \cdot L_i$$

where h_c is the canopy height, A is the size of the investigation area (m^2), n is the number of tillers of size i, and L is the average leaf area (m^2) of tillers of size i. Tiller size is expressed by the number of leaves that a tiller has, so the smallest tiller with $i = 1$ has one leaf only and the largest tillers have $m = 7$ leaves. The allometric value L_i for each tiller size was determined via destructive sampling on a $50 \cdot 50\,cm^2$ plot with reference canopy height h_r from which 18 tillers out of 162 were randomly selected for analysis. We measured the length and width of all leaves and subsequently cut the leaves in segments to allow for accurate scanning of the one-sided leaf area. Thus, the empirical relationship of LAI as a function of n_i and h_c could be used on eight $1\,m^2$ plots for non destructive LAI estimation. Within each plot, we selected 16 subplots of $10 \cdot 10\,cm^2$ size. In each of them we counted the number of tillers of each tiller size class (n_i) and measured the canopy height h_c to estimate LAI. For validation, three destructive harvests were done to ascertain the quality of the non destructive LAI estimates. This indicated that LAI was accurate to within $\pm 0.4\,m^2\,m^{-2}$: tiller counting overestimated the LAI by 0.4 and 0.3 in two plots while LAI was underestimated by 0.4 on the third plot.

2.2.3 Data analysis

To quantify the effects of vegetation type on the radiation budget, we computed net radiation R_n,

$$R_n = K_\downarrow - K_\uparrow + L_\downarrow - L_\uparrow$$

with K and L being shortwave and longwave radiation fluxes, respectively. Arrows in the index show downward ($\downarrow$) and upward ($\uparrow$) directed radiation. The difference $K_\downarrow - K_\uparrow$ is the net shortwave radiation. Shortwave albedo α is derived as

$$\alpha = \frac{K_\uparrow}{K_\downarrow}$$

and transmittance T is the ratio between downwelling shortwave radiation measured below canopy (index *bc*) and the same measurement carried out above canopy (index *ac*),

$$T = \frac{K_{\downarrow,bc}}{K_{\downarrow,ac}}.$$

To assess transmittance of each vegetation type, we combined all data of the five (below dwarf shrubs) and four (below sedges) sensors.

The radiation budget is strongly influenced by weather conditions and the solar zenith angle. We estimated both in order to isolate the vegetation effects. We calculated the solar zenith angle of each measurement using a MATLAB® script by Vincent Roy following an algorithm by *Reda and Andreas* (2004). We binned all solar zenith angles into 2° bins and used 10 min averages for K and L to compute

R_n, α, and T. In order to reduce the solar angle influence, we took daily average fluxes of K and L to compute R_n, α, and T for the analysis of vegetation type and cloud cover effects. In this case, we computed mean and standard deviation per day or cloud condition. We use the term 'soil shading' as reduction of incoming shortwave radiation (1–transmittance). We define the peak growing season as 1 July – 15 August (Fig. 2.2).

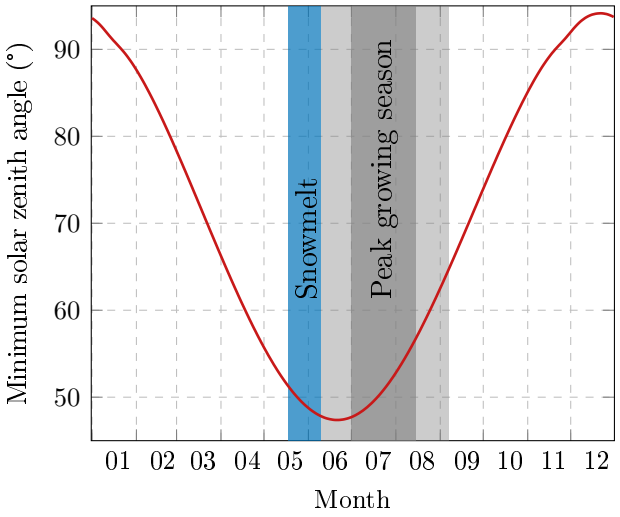

Figure 2.2: Variation of the solar zenith angle at solar noon (14:10 local time); snowmelt (blue) and growing season (light grey) in different years (dates from *Parmentier et al.*, 2011b) and peak growing season (1 July – 15 August).

In order to quantify the effects of clouds on the shortwave radiation budget, we classified the cloud cover into three categories, clear sky, partly cloudy, and cloudy. The classification was based on the cloud factor cf (*Tuller*, 1976; *Crawford and Duchon*, 1999)

$$cf = 1 - \frac{K_{\downarrow,measured}}{K_{\downarrow,potential}}$$

with measured ($K_{\downarrow,measured}$) and potential ($K_{\downarrow,potential}$) incoming shortwave radiation. We computed $K_{\downarrow,potential}$ for each 10 min interval using an atmospheric transfer model by *Corripio* (2003) on the basis of the *Iqbal* (1983) study on solar radiation transfer through the atmosphere. The most important model inputs were site location, measured air temperature, and measured surface albedo. Other parameters were ozone layer thickness (300 DU), visibility (180 km), and relative humidity (80%). Topographic shading was neglected because the research site is almost flat. We validated the model using observed clear-sky $K_{\downarrow,measured}$. As the relative error of $K_{\downarrow,measured}$ and $K_{\downarrow,potential}$ increases at low values in the morning and evening, we only computed cloud factors when $K_{\downarrow,potential} > 50\,\mathrm{W\,m^{-2}}$. We calculated the mean cloud factor, either within a day or of each time step. While we used the daily

classification to analyse vegetation and cloud impacts, the 10 min classification was needed for solar zenith angle effects. Each day with a mean cloud factor below 0.15 was classified as 'Clear sky', days above 0.55 were classified as 'Cloudy' while all other days were categorised as 'Partly cloudy'. We used the same thresholds as for daily values for the 10 min intervals but with the additional condition that clear-sky and cloudy intervals required a standard deviation < 0.1 determined from 1-hour centred at the 10 min interval of interest. Higher variation indicated partly cloudy conditions. We used MATLAB® for all computations.

We used t-tests to assess the difference between dwarf shrub and sedge characteristics, namely in canopy height, LAI, PAR reflectance, and PAR transmittance on the spatially distributed plots. Mean values are shown ± standard deviation to illustrate the spatial or temporal variability.

2.3 Results

2.3.1 Canopy structure

Dwarf shrub and sedge vegetation showed different canopy characteristics, radiation budgets, and soil heat fluxes. The sedge canopy was on average 48.0 ± 0.8 cm high, almost twice the height of the dwarf shrub canopy (Fig. 2.3a). The estimated sedge leaf area index was on average 1.4 ± 0.3 and the projected dwarf shrub leaf area index as estimated using point quadrats was 0.8 ± 0.1 (Fig. 2.3b). Apart from the green leaves, also wood and standing dead material can influence the radiation budget. The dwarf shrub wood area index was similar to the leaf area index. The sum of projected shrub leaf and wood area index was 1.5 ± 0.3, slightly higher than wet sedges leaf area index. Below dwarf shrubs, litter covered on average 56% of the surface. In all three destructive harvests of sedge leaf and standing dead leaf area we found that standing dead leaf area was 1.1 times green leaf area. Additionally, wet litter covered most of the surface below green and dead sedge leaves.

2.3.2 Above-canopy radiation budget

Dwarf shrub and wet sedge vegetation influence the radiation budget differently. While the dwarf shrub canopy reflected less shortwave radiation, it emitted more longwave radiation. The difference between both vegetation types in net radiation on average and at any solar zenith angle was very small (Table 2.1, Fig. 2.5a, b).

During the growing season, sedge albedo was consistently higher than dwarf shrub albedo (Fig. 2.4 and 2.5c, d). The growing season mean daily albedo was 0.15 for dwarf shrubs and 0.17 for sedges (Table 2.1). In absolute terms, the dwarf shrub vegetation–soil system absorbed on average $5\,\mathrm{W\,m^{-2}}$ more shortwave radiation than sedge vegetation during the 2013 and 2014 growing seasons. The growing season

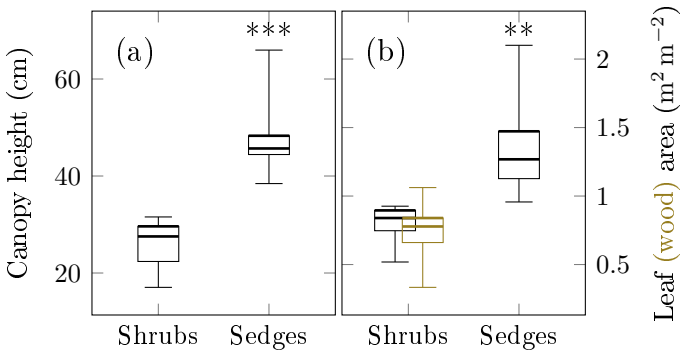

Figure 2.3: Spatial variability of canopy height (a) and leaf and wood area index (b) measured 28 – 30 July 2013, percentiles (25, 50, and 75), minimum and maximum values of eight plots per vegetation type; significant differences between vegetation types are shown with ** ($p \leq 0.01$) and *** ($p \leq 0.001$).

albedo differences between the vegetation types based on time series measurements are consistent with spatially replicated spectrometer measurements in the PAR region in eight plots per vegetation type (Fig. 2.6b). However, PAR reflectance was 0.024 ± 0.006 above dwarf shrubs and 0.034 ± 0.008 above sedges and thus much lower than shortwave albedo.

Additionally, the spring snow depth was 39 cm deeper in the sedge depression than on the elevated dwarf shrub patch (71 cm and 32 cm, respectively, 09 May 2014). Thus, the snow on the sedge patch melted about ten days later (03 June 2014) as compared to the dwarf shrub patch (24 May 2014). Due to the albedo difference between snow covered and snow free surfaces, the dwarf shrub patch absorbed 125 MJ m^{-2} (145 W m^{-2} on 10 days) shortwave radiation more than the sedge patch in this time (Fig. 2.6a).

Clouds reduced albedo and net radiation of both canopies throughout the summer (Fig. 2.5). The reduction in albedo was more pronounced for sedges than for dwarf shrubs (Table 2.1). While the clear-sky albedo of both vegetation types increased at higher solar zenith angles, the cloudy-sky albedo was similar to the clear-sky albedo at solar noon for all zenith angles (Fig. 2.5c, d). Due to the strong effect of zenith angle on clear-sky albedo, the cloud effects were strongest in August, when the minimum solar zenith angle was larger than in June or July (Fig. 2.2). In both summers 2013 and 2014 about 20% of the days were classified as clear sky and 20% as cloudy, the remaining as partly cloudy.

2.3.3 Soil shading

Canopy transmittance was on average 0.36 below dwarf shrubs and 0.28 below sedges during the growing season (Table 2.1, Fig. 2.7a, b). This difference implied that

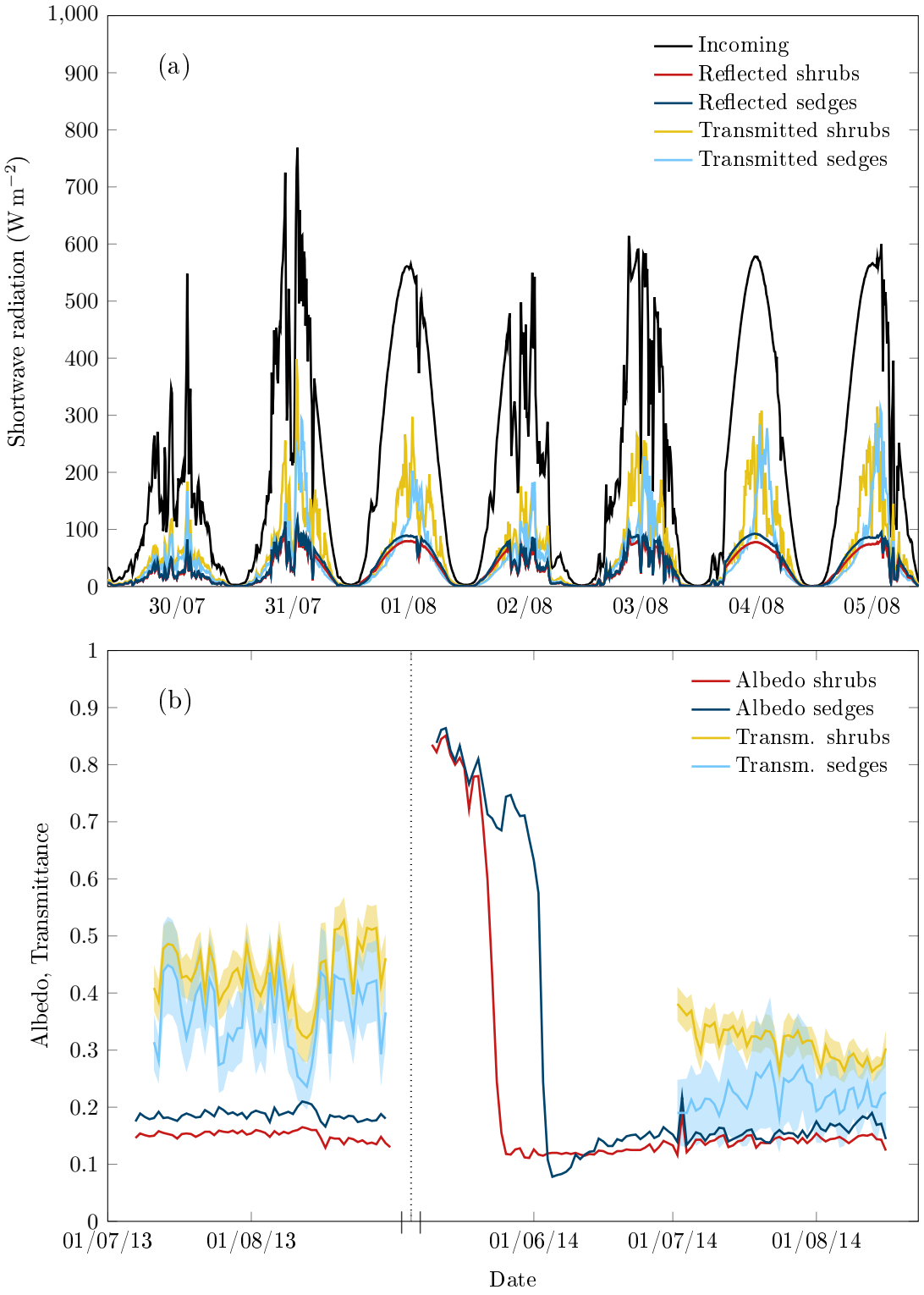

Figure 2.4: (a) Shortwave radiation fluxes, one week time series of 2014 and (b) daily albedo and transmittance time series; shaded area around transmittance represents ± standard error of the mean of the spatial replicates.

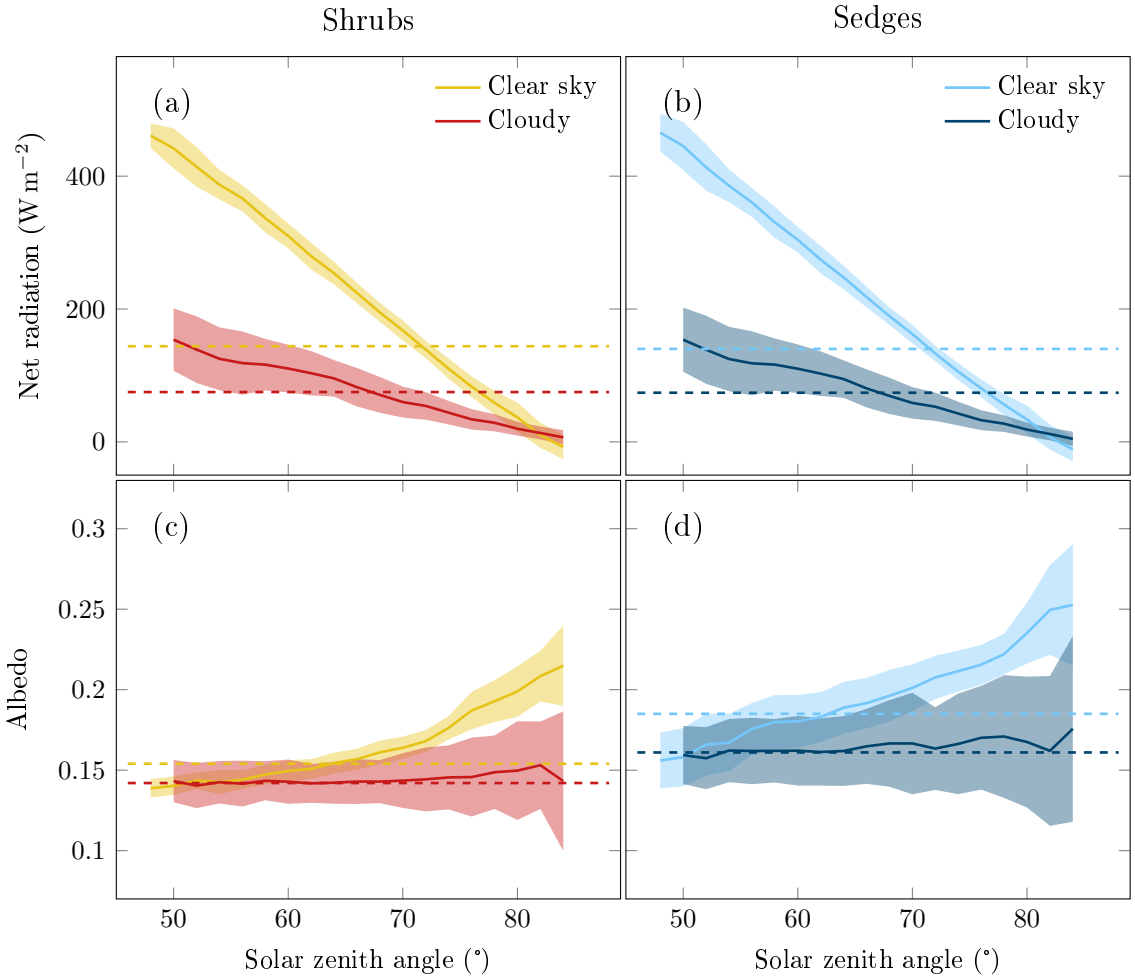

Figure 2.5: Dependence of net radiation (a, b) and albedo (c, d) on solar zenith angle and cloud cover for dwarf shrub (a, c) and sedge (b, d), growing season mean ± standard deviation values calculated for 2° intervals; the dashed lines represent the mean diel value under each condition.

Table 2.1: Energy fluxes and soil temperatures (mean ± standard deviation determined from daily averages) of dwarf shrub and sedge vegetation under varying cloud conditions in the peak growing season 2013 and 2014; sw. denotes shortwave.

Type	Condition	Albedo	Transmittance	Net radiation	Net sw. radiation	Soil temp. (−4 cm)	Soil heat flux (−10 cm)
				$W\,m^{-2}$	$W\,m^{-2}$	°C	$W\,m^{-2}$
Dwarf	All	0.15 ± 0.01	0.36 ± 0.07	116.0 ± 3.8	157.0 ± 5.4	5.9 ± 2.0	8.6 ± 3.2
shrubs	Clear sky	0.15 ± 0.01	0.32 ± 0.04	144.0 ± 3.4	215.0 ± 3.4	7.2 ± 2.0	10.6 ± 3.7
	Partly cloudy	0.15 ± 0.01	0.36 ± 0.06	123.0 ± 3.0	164.0 ± 3.6	6.1 ± 1.7	8.8 ± 2.9
	Cloudy	0.14 ± 0.02	0.40 ± 0.07	75.0 ± 2.7	89.0 ± 2.6	4.3 ± 1.6	6.1 ± 2.0
Sedges	All	0.17 ± 0.02	0.28 ± 0.08	114.0 ± 3.8	152.0 ± 5.2	5.8 ± 2.3	14.8 ± 5.2
	Clear sky	0.19 ± 0.02	0.23 ± 0.03	140.0 ± 3.4	207.0 ± 3.4	7.0 ± 2.6	16.9 ± 6.0
	Partly cloudy	0.17 ± 0.02	0.27 ± 0.07	121.0 ± 3.0	160.0 ± 3.6	5.8 ± 2.1	15.1 ± 5.0
	Cloudy	0.16 ± 0.02	0.33 ± 0.10	74.0 ± 2.7	87.0 ± 2.6	4.6 ± 1.8	11.9 ± 3.9

the surface below dwarf shrubs was exposed to $15\,W\,m^{-2}$ shortwave radiation in addition to what we observed below sedge vegetation. The spatially distributed measurements in the PAR range also showed a significant difference between the two vegetation types (Fig. 2.7c). However, the major effect could be attributed to the multi-year standing dead leaves below the green sedge leaves. The green leaves transmitted more light (0.62 ± 0.11) than dwarf shrubs (0.25 ± 0.07), but most light was reflected or absorbed by the standing dead layer (Fig. 2.7c).

Transmittance was strongly influenced by clouds (Fig. 2.7a, b). On average, clouds increased the transmittance by 25% below dwarf shrubs and by 43% below sedges (Table 2.1). However, for specific locations and sun angles the clear-sky transmittance exceeded the transmittance of cloudy times (Fig. 2.8). Transmittance was generally higher at small solar zenith angles, especially for sedges and at clear-sky conditions (Fig. 2.7a, b). Furthermore, soil shading was highly spatially and temporally variable, especially under clear-sky conditions (Fig. 2.7a, b and Fig. 2.8).

2.3.4 Soil heat flux and permafrost active layer

Except during the cold and snow-covered period, the soil heat flux at 10 cm depth was consistently higher below sedges than below dwarf shrubs (Fig. 2.9a). As soon as the dwarf shrub patch was partly snow free in May 2014, the soil heat flux at the sedges reached a peak of $30\,W\,m^{-2}$ while the heat flux below dwarf shrubs was less than $5\,W\,m^{-2}$. Afterwards, the sedge soil heat flux reduced to about 1.6 times the flux below dwarf shrubs by the end of July (Fig. 2.9). The mean growing season soil heat flux of 2013 and 2014 was $8.6\,W\,m^{-2}$ on the dwarf shrub and $14.8\,W\,m^{-2}$ on the sedge patch (Table 2.1). The 2014 growing season was wetter than 2013,

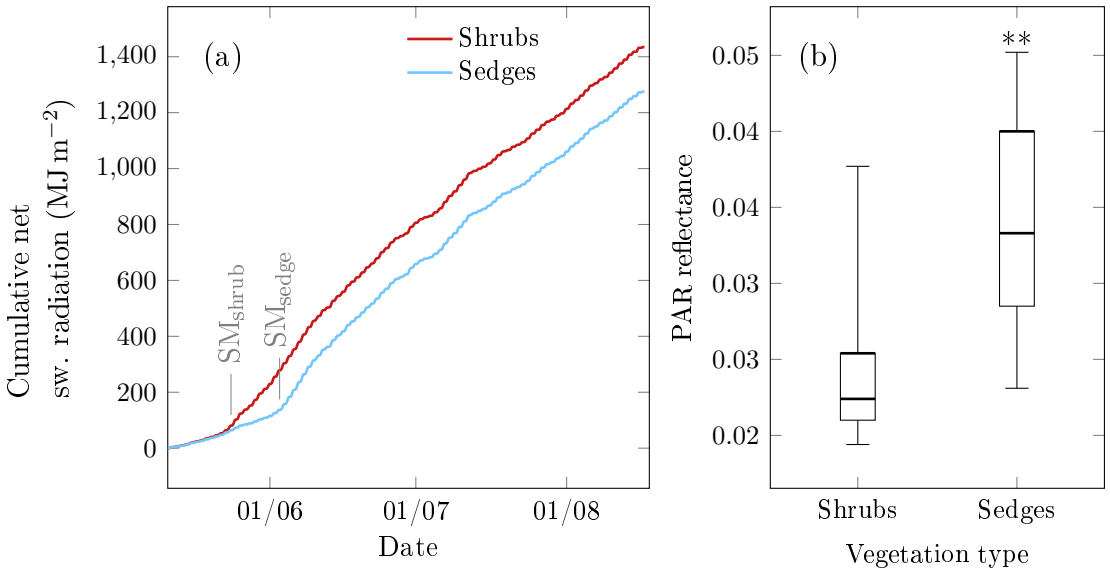

Figure 2.6: (a) Cumulative net shortwave (sw.) radiation 11 May – 16 August 2014, day of complete snowmelt (SM) indicated for dwarf shrubs and sedges and (b) spatial variability of PAR (400–700 nm) reflectance within vegetation type measured on 25 July 2013, percentiles (25, 50, and 75), minimum and maximum values of eight plots per vegetation type; significant differences between vegetation types are shown with ** ($p \leq 0.01$).

resulting in elevated soil moisture content below dwarf shrubs (0.52 $m^3\,m^{-3}$ and 0.37 $m^3\,m^{-3}$ in 2014 and 2013, respectively). The sedges soil was saturated at all times with a moisture content of about 0.7 $m^3\,m^{-3}$. However, we observed higher water levels at the sedges in 2014. The wetter conditions in 2014 fostered higher soil heat fluxes below both vegetation types. Top soil temperature below dwarf shrubs was on average 1.1 °C warmer in the dry growing season 2013, while it was 0.6 °C colder than below sedges in the wet growing season 2014. On average over both summer measurement periods, the top soil temperature was almost equal below both vegetation types (Table 2.1). The spatially distributed active layer thickness measurements were consistent with the soil heat flux measurements. On average, the active layer below sedges was 1.8 times deeper than below dwarf shrubs (Fig. 2.9b).

2.4 Discussion

We found that wet sedges shade the soil more efficiently than dwarf shrubs, which is in contrast to the higher soil heat flux below sedges. The considerable shading by wet sedges can partly be explained by the thick layer of standing dead leaves. The soil heat flux, on the other hand, depended strongly on soil properties. This is in contrast to the studies by *Blok et al.* (2010) and *Lawrence and Swenson* (2011), which

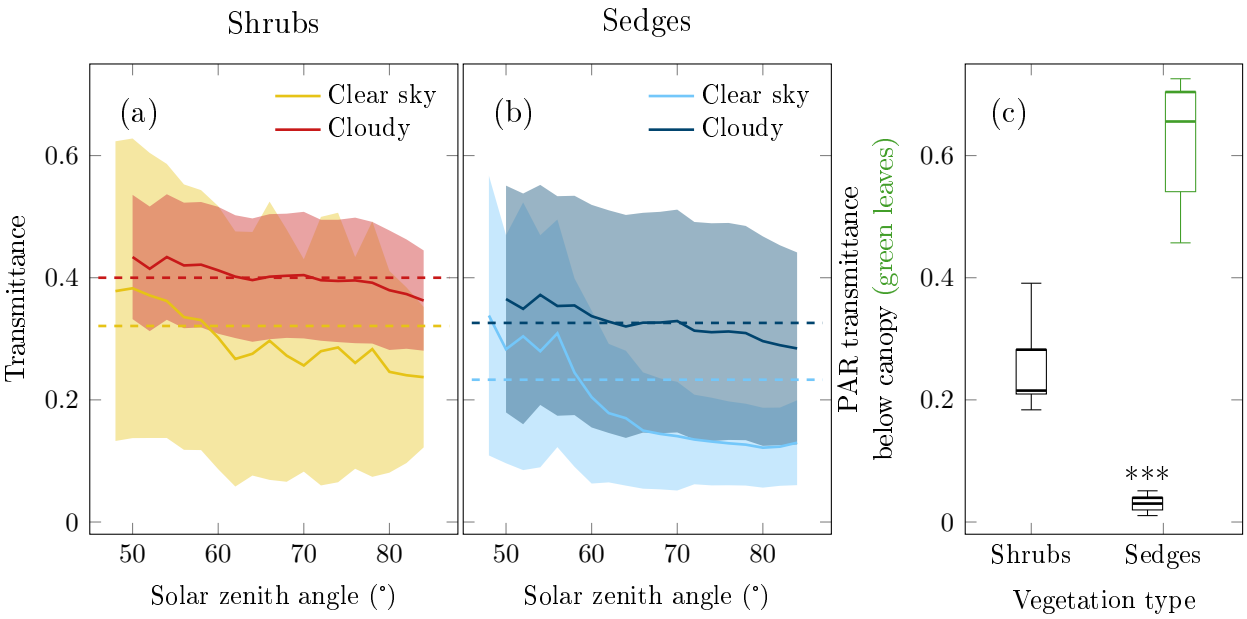

Figure 2.7: (a,b) Shortwave transmittance depending on solar zenith angle and cloud cover for dwarf shrub (a) and sedge (b), growing season mean ± standard deviation calculated for 2° intervals, the dashed lines represent the mean diel value under each condition and (c) spatial variability of PAR (400–700 nm) transmittance measured 03 August 2013, percentiles (25, 50, and 75), minimum and maximum values of eight plots per vegetation type; significant differences between vegetation types are shown with *** ($p \leq 0.001$).

identified soil shading as important control of local permafrost thaw. A schematic of the differences we found between key components of the dwarf shrub and wet sedge system can be found in Fig. 2.10. The different components are explained in more detail below.

2.4.1 Above-canopy radiation budget

Differences in surface albedo can affect air temperature and permafrost thaw (*Lawrence and Swenson*, 2011; *Bonfils et al.*, 2012). Numerous studies found that shrub tundra has a lower growing season albedo than no-shrub tundra (*Chapin et al.*, 2000b; *Thompson et al.*, 2004; *Beringer et al.*, 2005; *Ahrends et al.*, 2012). Our study agrees with this finding although the albedo difference between dwarf shrubs and wet sedges was small (Table 2.1). The mean growing season albedo of 0.15 for dwarf shrubs and 0.17 for sedges observed in our study agree well with literature values (*Chapin et al.*, 2000b; *Eugster et al.*, 2000; *Ahrends et al.*, 2012). The low values we measured for PAR reflectance (Fig. 2.6b) are in the same range as values measured by *Lloyd et al.* (2001) on an Arctic palsa mire. At our study site, the wet sedge

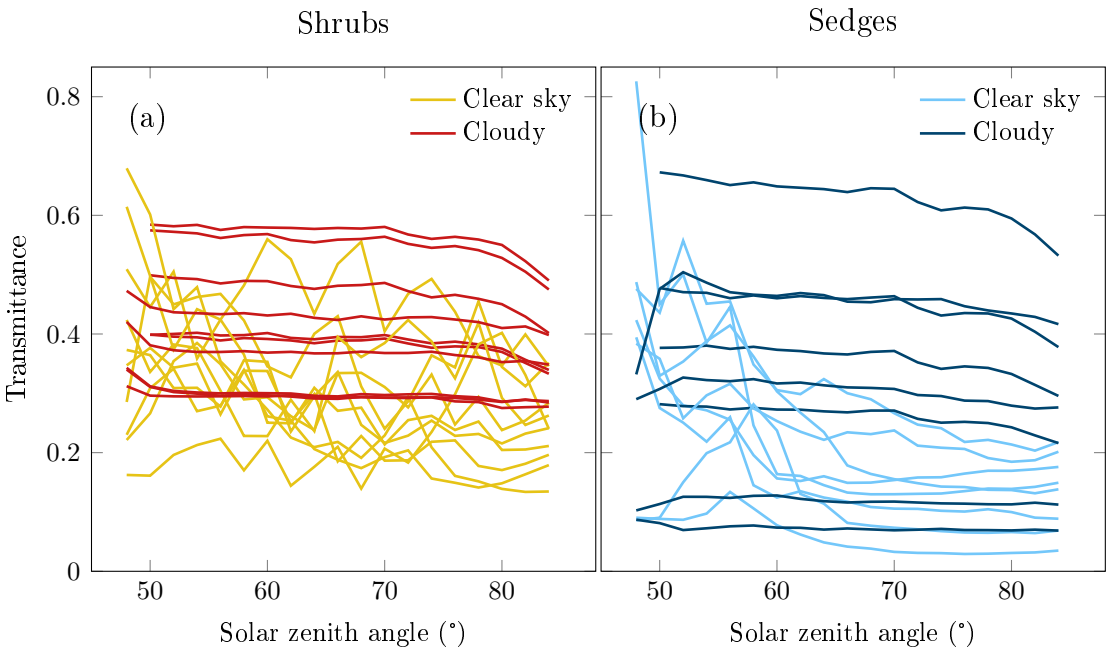

Figure 2.8: Transmittance depending on solar zenith angle and cloud cover; mean values per zenith angle for each single sensor location in each summer; dwarf shrubs (a) and sedges (b).

canopy was almost twice as tall as the dwarf shrub canopy (Fig. 2.3). In general, taller canopies trap light more efficiently and thus have a lower albedo (*Oke*, 1987). This is not the case in our comparison between dwarf shrubs and wet sedges, which may be due to two reasons. First, the wet sedge canopy comprises light-coloured standing dead leaves. Second, leaf and wood angle distributions are a dominant control of canopy reflectance (*Verstraete*, 1987; *Asner*, 1998). While dwarf shrubs may have a spherical leaf angle distribution (*Juszak et al.*, 2014), wet sedges likely have erectophil leaves. As compared to the dry summer of 2013, the albedo was lower by 0.01 on dwarf shrubs and by 0.03 on sedges during the wetter summer of 2014. In the wet year, standing water remained at the sedge patch throughout the growing season. Low albedo values on wet sedge locations, especially with standing water, have been reported in literature (*Lafleur et al.*, 1997; *Langer et al.*, 2011b; *Gamon et al.*, 2012).

Shrubs are associated with earlier snowmelt and thus decreased spring albedo (*Sturm et al.*, 2005; *Pomeroy et al.*, 2006). In spring 2014, the snow melted ten days earlier on the dwarf shrub patch as compared to the wet sedge patch. As found by *Chapin et al.* (2005) and *Sturm et al.* (2005), in our study snowmelt timing was far more important for the overall energy budget than the growing season albedo difference (Fig. 2.6a). Apart from the large albedo difference in this period, the

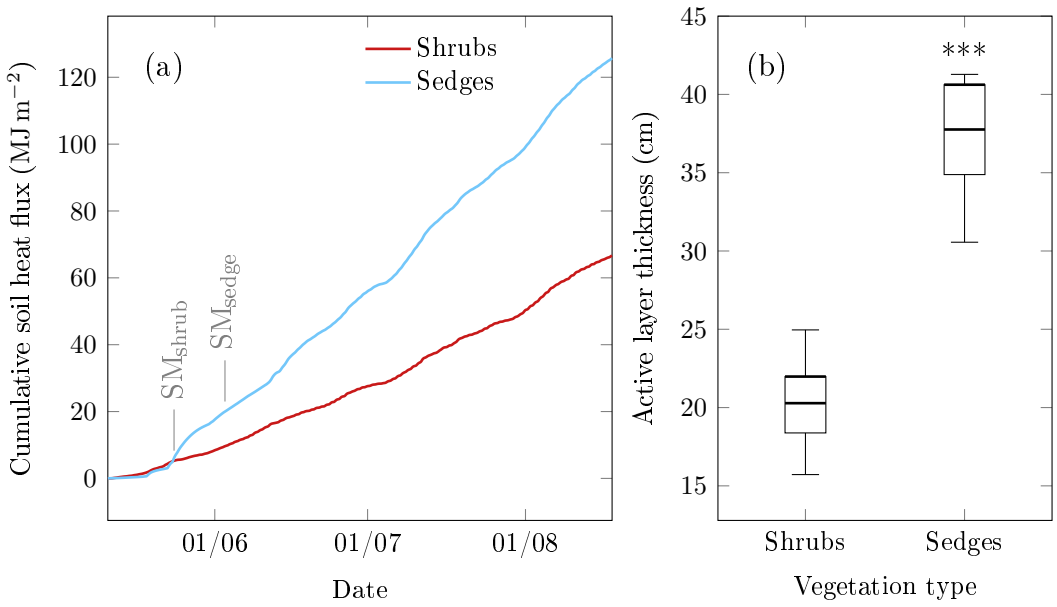

Figure 2.9: (a) Cumulative soil heat flux 2014 at −10 cm depth, day of complete snowmelt (SM) indicated for dwarf shrubs and sedges and (b) spatial variability of active layer thickness within vegetation type, measured 28 – 30 July 2013, percentiles (25, 50, and 75), minimum and maximum values of eight plots per vegetation type; significant differences between vegetation types are shown with *** ($p \leq 0.001$).

high values of incoming shortwave radiation end of May and beginning of June contributed to the effect. However, at our study site, the earlier snowmelt at the shrub location was not primarily due to branches exposed above the snow surface (*Sturm et al.*, 2005; *Pomeroy et al.*, 2006), but rather due to the thinner snow cover. The snow cover levelled out some of the micro-topography. Thus more snow accumulated in the sedge depression (71 cm) than on the elevated dwarf shrub patch (32 cm). This is in contrast to observation from study sites with taller shrubs which trap snow and thus lead to a deeper snow pack (*Sturm et al.*, 2001a; *Liston et al.*, 2002).

We found that clouds reduced the diel albedo by 0.01 (dwarf shrubs) to 0.03 (sedges). These values agree well with the value of 0.02 stated in *Eugster et al.* (2000) for vegetated and unvegetated tundra. As clear-sky and cloudy-sky albedo differ most at large solar zenith angles, cloud cover reduced the albedo most strongly in the late growing season. The average growing season albedo is likely to decrease in case of increased cloud cover in the future (*Chapin et al.*, 2005; *Wang and Key*, 2005a; *Vavrus et al.*, 2009). The strong cloud impact on albedo masked other temporal trends within the growing season that may be caused by soil moisture or vegetation phenology.

While dwarf shrubs and sedges differed in the shortwave radiation budget, the

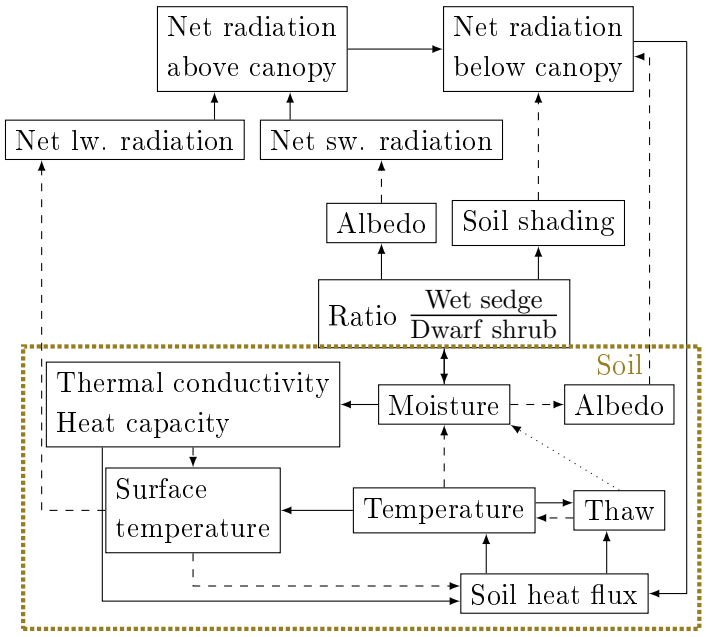

Figure 2.10: Different vegetation types are associated with soil properties and soil heat fluxes (brown box), the radiation budget above and below canopy. Latent and sensible heat fluxes are not included as they were not measured in this study and effect directions are unclear. Permafrost thaw can feed back to soil moisture, but the direction of the effect depends on ice content and drainage conditions. Solid arrows represent positive, dashed arrows negative, and dotted arrows unknown feedback; lw. and sw. denote longwave and shortwave, respectively.

growing season net radiation was similar (Table 2.1, Fig. 2.10). On one hand, the dwarf shrub canopy–soil system absorbed more shortwave radiation, on the other hand it emitted more longwave radiation as daily maximum soil temperatures were higher. However, in accordance with *Rouse* (2000) we found that during the snowmelt period net radiation strongly depended on the snow cover. The different snow melt dates of the vegetation types affected the growing season length locally which may influence the tundra carbon cycle, via respiration, primary production, and methane exchange.

2.4.2 Soil shading

Soil shading by shrubs has been suggested as major factor mitigating permafrost thaw at the local scale (*Blok et al.*, 2010). However, unlike for forests or crops, shading by tundra vegetation has rarely been measured. In the shortwave range, we found an average growing season transmittance of 0.36 below dwarf shrubs and 0.28 below sedges (Table 2.1). In the PAR range, dwarf shrubs transmitted on average 25% and sedges only 3% (Fig. 2.7c). The dwarf shrub PAR transmittance was in the

same range as values by *Juszak et al.* (2014) measured at the same field site. *Williams et al.* (2014) measured PAR transmittance below tundra shrubs of 70–100 cm height, two to three times taller than the dwarf shrubs in our study (Fig. 2.3a). They found a PAR transmittance of about 0.2, which is the lower boundary of the range of values we obtained. The extremely low values of PAR transmittance below sedges were partly due to the lower measurement height of PAR as compared to shortwave transmittance. The shortwave transmittance sensor of 34 mm height was placed above the early summer maximum water level. The PAR sensor of 16 mm height was inserted as low as possible above the current wet litter or water surface. The standing dead leaves are a major component of the sedge vegetation (Figure 3.1c) and account for most reflection or absorption (Fig. 2.7c).

The reference level at the dwarf shrub site is above the shrub litter, which forms a thin, compact layer on the ground with more heavily degraded litter at the bottom and more loose, recent litter towards the top. Unlike the shrub canopy, the sedge canopy includes lots of standing dead material. We defined the reference level for canopy transmittance and soil heat flux below this light-coloured layer but above the wet, dark-coloured, and compact litter. This distinction between standing dead leaves and wet litter is useful because of the different structure of both layers. Standing dead leaves form a 10–20 cm thick layer with arching dry leaves and large air spaces. Below this layer, more compacted, older, and usually water-saturated litter forms a continuous surface. In case of shrub or sedge litter on the ground, energy can be transferred from the litter to the soil through heat conduction. Therefore, the thermal properties of the litter can be treated similar to the thermal properties of the soil. For wet sedges, the thermal properties of the dry, standing dead leaves are less important as the leaves are surrounded by air and heat conduction will be dominated by the air. Thus heat conduction through the standing dead leaves may be limited and energy convection or radiation through the standing dead layer may be more important. Therefore we argue that for energy budget considerations shrub litter and wet litter of sedges can be treated analogously to soil, while sedge standing dead leaves resemble more green leaves and have to be treated as part of the above-ground canopy.

Clouds decreased soil shading of both vegetation types, especially at large solar zenith angles (Fig. 2.7a, b). The *Williams et al.* (2014) study on Arctic shrubs did not find a dependency of canopy transmittance on diffuse or direct radiation. However, we found that the effect was strongest for large solar zenith angles and *Williams et al.* (2014) measured at smaller solar zenith angles, around noon, and more than 2° lower latitude. The strong dependency of clear-sky sedge transmittance on sun angle can be attributed to the vertical orientation of the leaves. In general, direct radiation transmittance decreases for large solar zenith angles as the path through the vegetation lengthens. For both vegetation types, transmittance was more vari-

able under clear-sky conditions, which indicates an additional dependency on the solar azimuth angle for specific locations. The higher transmittance of diffuse light as compared to direct light at large solar zenith angles has been measured in a number of studies (e.g. *Eck and Deering*, 1992; *Promis et al.*, 2009; *Dengel et al.*, 2015). However, although the canopies shade less efficiently at cloudy conditions than during clear-sky hours, clouds reduce the absolute amount of transmitted shortwave radiation. Thus if the cloud cover increases, less shortwave radiation warms the soil directly.

2.4.3 Soil heat flux and permafrost active layer

Increasing active layer thickness can lead to substantial carbon emissions from permafrost soils (*Schuur et al.*, 2009) and thus positively feeds back to climate warming (*Field et al.*, 2007). We found a 17 cm shallower active layer and 6.2 $W\,m^{-2}$ lower soil heat flux at 10 cm depth below dwarf shrubs as compared to sedges (Fig. 2.9a, Table 2.1), which agrees well with other studies (*Anisimov et al.*, 2002; *Walker et al.*, 2003b; *Blok et al.*, 2010). We evaluated possible drivers of this difference between vegetation types. The dwarf shrub canopy reflected less shortwave radiation and transmitted more to the moss or soil surface below. Thus, if the shortwave radiation budget was the major driver, a higher soil heat flux could be expected below the dwarf shrubs. The outgoing longwave radiation was slightly higher at the dwarf shrub patch. Thus the above-canopy net-radiation was almost equal at both vegetation types (Table 2.1), and hence differences in resulting energy fluxes (sensible, latent, and ground heat flux) were purely internally controlled by the vegetation structure and activity or soil properties.

Several Arctic studies found similar or less evapotranspiration in low shrub tundra as compared to wetland tundra (*Eugster et al.*, 2000; *Rouse*, 2000; *Eaton et al.*, 2001; *McFadden et al.*, 2003). At our field site, dwarf shrub LAI was smaller than sedge LAI (Fig. 2.3b) and the shrub soil was much drier. Thus, we do not expect more energy loss due to evapotranspiration of the dwarf shrubs. The higher ground heat flux at the wet sedges may have lead to reduced sensible heat flux (*McFadden et al.*, 1998). Although the average top-soil temperatures were very similar below both vegetation types (Table 2.1), the heat flux towards the sedge soil was larger. The same gradient between cold soil and warm air temperature may lead to higher flux below sedges as the thermal conductivity of the waterlogged sedges soil was about five times higher than of the peaty dwarf shrub top soil (0.44 $W\,m^{-1}\,K^{-1}$ and 0.08 $W\,m^{-1}\,K^{-1}$, respectively). The heat capacity below wet sedges (3.3 $MJ\,m^{-3}\,K^{-1}$) was more than six times the value measured below dwarf shrubs (0.5 $MJ\,m^{-3}\,K^{-1}$). This stronger energy sink may have further enhanced the soil heat flux below sedges. *Williams and Quinton* (2013) also found that altered

moisture conditions were more important for permafrost thaw than the shortwave radiation budget along linear disturbances in a boreal forest. Another difference between the two vegetation types is the soil albedo. The wet litter surface below sedges had a low albedo, possibly less than the litter and moss surface below dwarf shrubs. Model results by *Juszak et al.* (2014) indicate a surface albedo below dwarf shrubs of 0.17 at our site. Given the average growing season transmittance of $64\,\mathrm{W\,m^{-2}}$, the dwarf shrub soil may absorb around $53\,\mathrm{W\,m^{-2}}$. With a low soil albedo, the sedge soil may have absorbed a greater fraction of the transmitted shortwave radiation ($49\,\mathrm{W\,m^{-2}}$ on average) than the dwarf shrub soil, an effect that may partly compensate the more efficient shading.

In summary, differences in net radiation are smaller than expected, and clearly additional driving forces besides canopy–radiation interactions must be considered for explaining soil heat flux and active layer thickness in future studies, namely soil albedo and soil thermal conductivity (Fig. 2.10).

2.5 Conclusions

Our field data show that permafrost thaw was lower below tundra dwarf shrubs as compared to sedges, but not as a result of increased soil shading. Neither the above-canopy radiation budget nor soil shading explained the spatial differences in active layer thickness. Despite lower shortwave reflectance and higher transmittance by the dwarf shrubs, the soil below dwarf shrubs showed a smaller heat flux and a shallower active layer than below sedges. We found that the differences in snow melt timing were more important for the shortwave radiation budget than growing season albedo differences between the two vegetation types. Cloud cover reduced albedo and soil shading of both vegetation types but more strongly so for sedges. Standing dead leaves accounted for most of the soil shading of the sedge canopy. Soil properties, such as soil albedo and thermal conductivity, appear to be more important than the direct effect of the above-ground vegetation layer. Our results highlight the complexity of the atmosphere–vegetation–permafrost interaction. Future studies will need to incorporate plant traits, such as green, woody, and dead biomass, soil properties, as well as spatial patterns of vegetation types. These variables may be key controls of the potential feedbacks between vegetation changes and permafrost thaw and deserve more attention to understand the complex interactions between tundra ecosystems and climate.

2.6 Acknowledgements

We thank T. Maximov and his group at the Siberian Branch of the Russian Academy of Science for supporting our field work. We thank Joseph P. McFadden, UC Santa

Barbara, and Luca Belelli Marchesini, VU Amsterdam, for fruitful discussions on earlier versions of this manuscript. This work was supported by the Swiss National Science Foundation through project grant 140631 and by the Netherlands Organisation for Scientific Research (NWO Vidi-grant 864.09.014). We were further supported by the University of Zurich through the University research priority programme on Global Change and Biodiversity (URPP GCB).

3 Arctic shrub effects on NDVI, summer albedo and soil shading

Inge Juszak[1], Angela M. Erb[1,2], Trofim C. Maximov[3], and Gabriela Schaepman-Strub[1]

Abstract

The influence of Arctic vegetation on albedo, latent and sensible heat fluxes, and active layer thickness is a crucial link between boundary layer climate and permafrost in the context of climate change. Shrubs have been observed to lower the albedo as compared to lichen or graminoid-tundra. Despite its importance, the quantification of the effect of shrubification on summer albedo has not been addressed in much detail. We manipulated shrub density and height in an Arctic dwarf birch (*Betula nana*) shrub canopy to test the effect on shortwave radiative fluxes and on the normalized difference vegetation index (NDVI), a proxy for vegetation productivity used in satellite-based studies. Additionally, we parametrised and validated the 3D radiative transfer model DART to simulate the amount of solar radiation reflected and transmitted by an Arctic shrub canopy. We compared results of model runs of different complexities to measured data from North-East Siberia. We achieved comparably good results with simple turbid medium approaches, including both leaf and branch optical property media, and detailed object based model parameterisations. It was important to explicitly parameterise branches as they accounted for up to 71% of the total canopy absorption and thus contributed significantly to soil shading. Increasing leaf biomass resulted in a significant increase of the NDVI, decrease of transmitted photosynthetically active radiation, and repartitioning of the absorption of shortwave radiation by the canopy components. However, experimental and modelling results show that canopy broadband nadir reflectance and albedo are not significantly decreasing with increasing shrub biomass. We conclude that the leaf to branch ratio, canopy background, and vegetation type replaced by

[1]Institute of Evolutionary Biology and Environmental Studies, University of Zurich, Winterthurerstrasse 190, 8057 Zurich, Switzerland

[2]now at: School for the Environment, University of Massachusetts Boston, 100 Morrisey Boulevard, Boston, MA 02125-3393, USA

[3]Biological Problems of the Cryolithozone, Russian Academy of Sciences, Siberian Division, 41 Lenin Prospekt, Yakutsk, Yakutia 677980, Russian Federation

shrubs need to be considered when predicting feedbacks of shrubification to summer albedo, permafrost thaw, and climate warming.

Reprinted as in **Remote Sensing of Environment** with references merged at the end of this thesis:
I. Juszak, A. M. Erb, T. C. Maximov and G. Schaepman-Strub, 2014, Arctic shrub effects on NDVI, summer albedo and soil shading, *Remote Sensing of Environment*, 153, 79–89, doi: 10.1016/j.rse.2014.07.021

I.J. performed the data analysis and the radiative transfer modelling and wrote the manuscript. A.M.E. conceived the study, carried out the field measurements, contributed to the data analysis and to the manuscript preparation. G.S.-S. conceived the study, carried out the field measurements, and provided input for the data analysis and the manuscript.

3.1 Introduction

Arctic ecosystems have been exposed to air temperature increases of almost double the global mean in the 20th century (*Chapin et al.*, 2000a; *Serreze et al.*, 2000; *Solomon et al.*, 2007; *Cowtan and Way*, 2014). Further increases in air temperature and precipitation, as projected for the north-eastern Siberian tundra (*Solomon et al.*, 2007), may cause further shifts in the vegetation distribution in the Arctic (*Pearson et al.*, 2013). Currently observed changes include northward movement of trees and shrubs, which increasingly dominate large areas of tundra (e.g. *Sturm et al.*, 2001b; *Tape et al.*, 2006; *Myers-Smith et al.*, 2011; *Miller and Smith*, 2012). Productivity estimates based on remote sensing, dendroecological, and plot data show an increasing trend with temperature, while the sensitivity of this effect is mediated by soil moisture, with productivity in wet areas responding stronger to temperature increase than in dry areas (*Forbes et al.*, 2010; *Huemmrich et al.*, 2010; *Blok et al.*, 2011b; *Elmendorf et al.*, 2012b; *Berner et al.*, 2013; *Kim et al.*, 2014).

Shrub cover and distribution is not only affected by climate, it also controls important components of the surface energy balance. Main observed and expected feedbacks of increasing shrub cover include a reduction of the albedo, an increase in evapotranspiration, and a local decrease in the permafrost active layer due to soil shading (*Pearson et al.*, 2013). Shrub cover reduces the surface albedo during the growing season (*Beringer et al.*, 2005; *Sturm et al.*, 2005; *Bonfils et al.*, 2012), but the effect is most pronounced during critical snow accumulation and snowmelt periods (*Sturm et al.*, 2005; *Loranty et al.*, 2011). The additional shortwave radiation absorbed by the canopy is partly partitioned into latent and sensible heat fluxes which are likely to increase with increasing shrub height and density (*Beringer et al.*, 2005; *Bonfils et al.*, 2012). Increasing shrub cover increases surface roughness and thus the coupling between the atmosphere and the surface (*Beringer et al.*, 2005). These fluxes are also modulated by other system properties including soil moisture and the presence of mosses (*Blok et al.*, 2011a).

Additionally, shrubs affect the amount of shortwave radiation transmitted to the soil surface, an important component of the soil surface energy balance (*Eugster et al.*, 2000). While shrubs increased the winter soil temperature, summer soil temperature was reduced through shading (*Myers-Smith and Hik*, 2013). At least at the local scale, shrub shading may offset air temperature warming and reduce active layer thickness (*Blok et al.*, 2010; *Jorgenson et al.*, 2010). These changes in the energy balance resulting from shrub expansion may in turn facilitate further shrub growth (*Chapin et al.*, 2005; *Swann et al.*, 2010).

The quantification of the effect of shrubification on summer albedo has not been addressed in much detail, apart from observations across a latitudinal gradient. It is hard to relate satellite based albedo data to shrub abundance in the Arctic as

the spatial resolution of operational satellite-derived albedo products is 0.5–1 km. As such, we are currently unable to effectively assess shrub cover and abundance at this scale. We therefore performed an experimental and radiative transfer modelling study to disentangle the effect of shrub density and height on reflected and transmitted shortwave radiation fluxes and NDVI, the proxy most often used to estimate long-term productivity at large spatial scale (e.g. *Hope et al.*, 2004; *Bhatt et al.*, 2010). Radiative transfer modelling can help to quantify reflected and transmitted shortwave radiation, including subdaily and seasonal variation (*Widlowski et al.*, 2011). It can be used to validate simpler approaches which are often used in large-scale modelling (*Pinty et al.*, 2006). Two studies on Arctic shrubs quantify the absorption of solar radiation of woody elements before leaf-out (*Bewley et al.*, 2007; *Reid et al.*, 2014), but, to our knowledge, no study so far has simulated the full radiative budget of Arctic dwarf shrub leaves and branches including spectral reflectance of the canopy and transmitted radiation.

We present results of modelling and experimental work on the effect of dwarf birch leaf and branch area on the radiative balance. Unlike most studies on the effect of vegetation on the energy balance of the Arctic (e.g. *Beringer et al.*, 2005; *Chapin et al.*, 2005; *Loranty et al.*, 2011), we did not compare different ecosystems but quantified the effects of varying biomass within one vegetation type. We ran the 3D radiative transfer model DART (*Gastellu-Etchegorry et al.*, 1996; *Grau and Gastellu-Etchegorry*, 2013) for shrub vegetation of different densities. The model was initialised with field data which included detailed information on vegetation structure and leaf and branch optical properties. We validated the model with canopy reflected and transmitted radiation measurements on natural canopies and vegetation with experimentally reduced density. We compared results from models with different levels of complexity to assess the importance of detailed shrub representation on shortwave radiation results.

3.2 Methods

3.2.1 Field site

The Kytalyk field site is located in the Indigirka lowlands, North-East Siberia (70.83 °N, 147.49 °E, Figure 3.1, a). The mean annual air temperature is −10.5 °C with a range of −32.5 °C in January and 10.4 °C in July (*van der Molen et al.*, 2007). The mean annual precipitation is 220 mm (*Parmentier et al.*, 2011a). Kytalyk is in the continuous permafrost zone with an average active-layer thickness (ALT) of 42 cm. Dry areas show a reduced ALT of 12–28 cm, while the ALT in wetter areas ranges from 22–50 cm (*Mi et al.*, 2014).

The Circumpolar Arctic Vegetation Map classifies the vegetation at the study

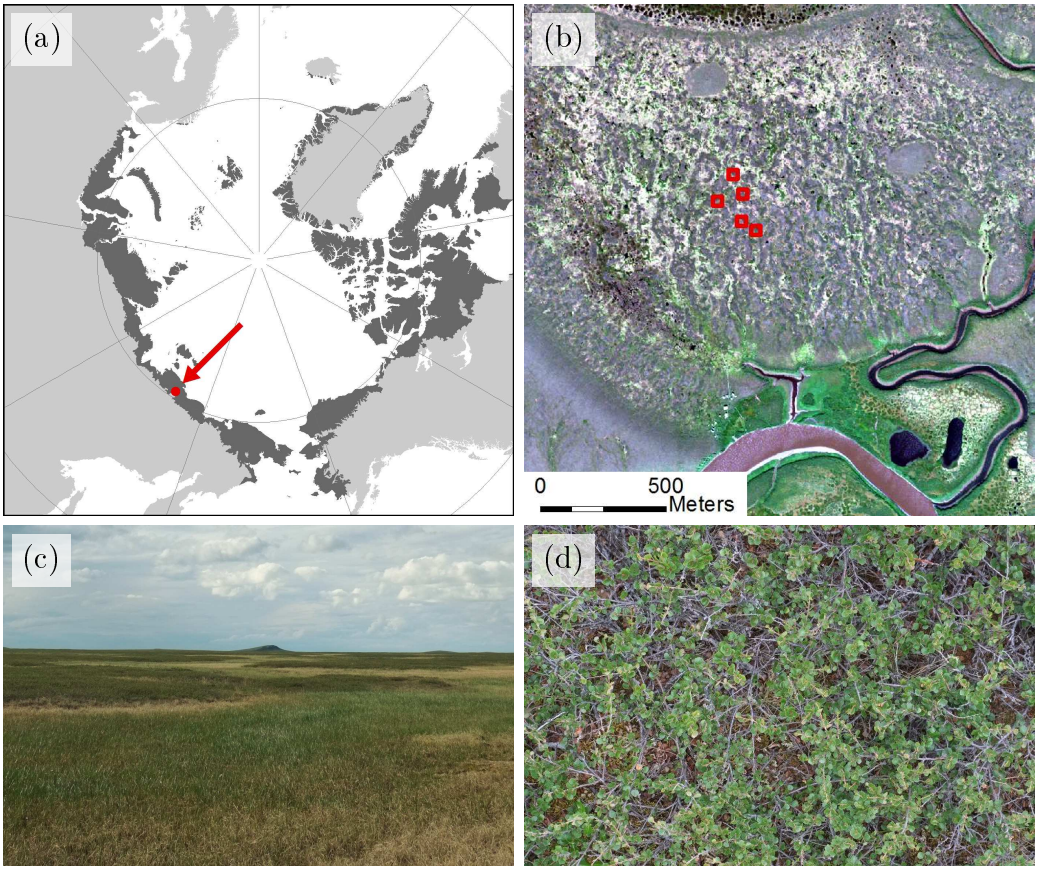

Figure 3.1: Overview of the stations location in north-east Siberia and the extent of Arctic tundra (a, dark grey, data from *Walker et al.* (2005)), satellite image (GeoEye-1) of the site with the location of the five plots (b, red squares), tundra landscape (c) and dwarf birch vegetation (d, detail of about 60·90 cm).

site as tussock-sedge, dwarf-shrub, moss tundra (*Walker et al.*, 2005). Dwarf birch (*Betula nana*) is the main shrub type (Figure 3.1, d). Shrubs and sedges are arranged alternately in small patches associated with micro topography and moisture on the scale of a few meters in the area of a drained thaw lake bed (Figure 3.1, b and c).

3.2.2 Field experiment and measurements

We conducted a field campaign in June and July 2012 and measured input and validation data to parameterise a radiative transfer model for dwarf birch canopies. We performed a manipulation experiment to increase the variability and range of plot characteristics. The experiment included five replicate plots on different dwarf birch patches, each with a control, height, and density treatment. For the height treatment we removed the top 5 cm of all dwarf birch branches. For the density treatment we removed roughly one third of the dwarf birch branches above the moss

layer. We use the term 'branch' for dwarf birch ramets, separate units that belong to a clonal population. The branches, or ramets, are not connected above-ground and have simple shapes with minimal off-shoots. Additionally, subplots of complete shrub removal were used for background optical properties and biomass estimations. The control, height, and density treatment plots were 2 m·2 m in size and the removal plots were 0.8 m · 0.8 m. The vegetation characteristics after treatment are shown in Table 3.2. We tested all variables of interest for preexisting biases due to plot selection and evaluated the treatment effects over time with statistical methods.

Detailed information on vegetation structure and properties were required to parameterise the radiative transfer model. For the dwarf birch canopy we used point-quadrat grids to measure the leaf area index (LAI in $m^2\,m^{-2}$) and the branch area index (BAI in $m^2\,m^{-2}$) as well as the canopy height at three timepoints in June and July on each subplot (dates in Table 3.1). We recorded all leaf and branch hits on a 0.5 m·0.5 m grid of 81 points. Plant area index (PAI in $m^2\,m^{-2}$) is the sum of LAI and BAI. We use LAI as abbreviation for total, one-sided leaf area per ground area. As branches are cylindrical, we use the product of branch diameter and branch length as proxy for branch area. We counted the number of shrub stems and leaves and estimated the shape of a typical branch from photographs and measurements from a removed branch. The 3D branch structure was then reconstructed using the graphics software blender^{TM}.

Additionally we measured leaf and bark optical properties (Figure 3.2) with an ASD spectrometer (Analytical Spectral Devices, Fieldspec4), high-intensity contact probe, and leaf clip. The ASD covers the spectral range of 350–2500 nm in 3 nm spectral resolution in the visible range and 10 nm spectral resolution in the NIR. We measured leaf top, leaf bottom, and bark spectral reflectance on a black background with a measurement spot size of 10 mm. We distinguished two types of dwarf birch branches, old branches with a grey colour (63% of the branches) and young branches, reddish in colour (37%). As we could not measure leaf transmittance (T) in the field, it was estimated from the measured leaf reflectance (R) and two other datasets which included reflectance and transmittance using equation 3.1.

$$T_{estimated}(\lambda) = \max\left(R_{measured}(\lambda) \cdot \left(\frac{T_{reference}(\lambda)}{R_{reference}(\lambda)}\right), 0\right) \tag{3.1}$$

In the range λ =400–1900 nm we took the reference data from integrating sphere measurements of a horticultural dwarf birch in Zurich. For the longer wavelengths (1900–2500 nm), the integrating sphere data was too noisy so we used data for the silver birch (*Betula pendula*) from the LOPEX database (*Hosgood et al.*, 1995, revised 2005) as a reference. This approach was used because, apart from the noise, the the ratio $\frac{T(\lambda)}{R(\lambda)}$ was similar for both reference data sets.

We used reflectance measurements of the removal plots as background property in

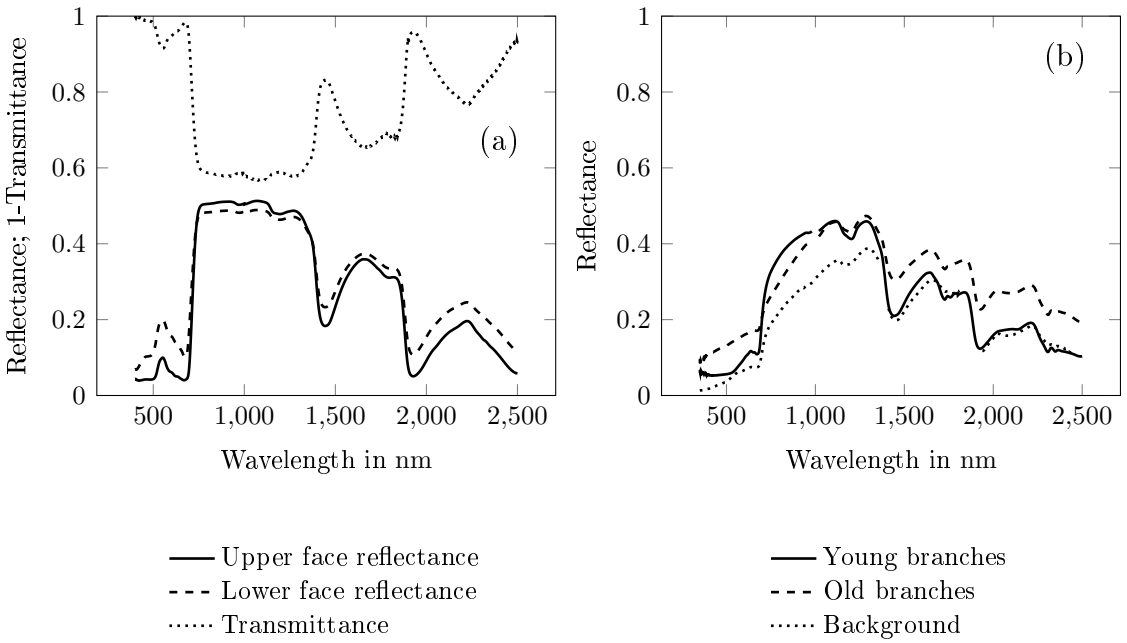

Figure 3.2: Mean dwarf birch leaf (a) and bark optical properties and background reflectance (b).

the DART simulations (Figure 3.2, b). The background below the shrubs on average consisted of 50% dwarf birch litter, 48% mosses and 2% lichen.

To validate the radiative transfer model we measured canopy hemispherical-directional spectral reflected radiation (λ =350–2500 nm) vertically ≈1 m above the soil surface using an ASD with a 5° field of view. 25 single exitance readings were averaged for each measurement and we took three such measurements on every subplot at each time point. We measured spectral irradiance from the reflectance of a spectralon® white panel. From exitance and irradiance we calculated spectral reflectance (R_{nadir}, Equation 3.2) and broadband reflectance (Rb_{nadir}, Equation 3.3).

Furthermore we calculated the NDVI (Normalized Difference Vegetation Index), which is often used as a proxy for vegetation productivity (e.g. *Beck and Goetz*, 2011; *Gamon et al.*, 2013). We calculated NDVI from the nadir spectral reflectance measurements using the red and NIR bands according to AVHRR (Advanced Very High Resolution Radiometer) specifications (Equation 3.4) as AVHRR data are often used in studies of Arctic vegetation (e.g. *Hope et al.*, 2004; *Bhatt et al.*, 2010).

$$R_{nadir}(\lambda) = \frac{\text{Exitance}(\lambda)}{\text{Irradiance}(\lambda)} \tag{3.2}$$

$$Rb_{nadir} = \frac{\sum_{\lambda=400\,nm}^{2500\,nm} \text{Exitance}(\lambda)}{\sum_{\lambda=400\,nm}^{2500\,nm} \text{Irradiance}(\lambda)} \tag{3.3}$$

$$NDVI = \frac{R_{nadir}(nir_{725-1000\,nm}) - R_{nadir}(red_{580-680\,nm})}{R_{nadir}(nir_{725-1000\,nm}) + R_{nadir}(red_{580-680\,nm})} \tag{3.4}$$

Table 3.1: Details on all measured variables and the model inputs; * indicates measurements on plot 5 only.

Variable	Method	Dates in 2012	Value
Measured model input			
Leaf area index of dwarf birch (LAI)	Point-quadrant grid	18 - 19/06, 23/06* & 25/06 & 14/07	
Branch area index of dwarf birch (BAI)	Point-quadrant grid	18 - 19/06, 23/06* & 25/06 & 14/07	
Canopy height	Point-quadrant grid	06/07	23 cm±5 cm
Number of dwarf birch stems	Count on removal plots	29/06 - 04/07	
Number of dwarf birch leaves	Count on removal plots	21 - 23/06	
Dwarf birch branch structure	Manual measurements, photos, 3D model using blender^{TM}	20 - 23/06 & 29/06 & 04/07 & 06/07	Branch length $\approx$ 41 cm, leaf diameter $\approx$ 1 cm
Leaf spectral reflectance	ASD (contact probe)	14/07	
Branch spectral reflectance	ASD (contact probe)	05/07	
Background reflectance	ASD (nadir, 1 m, 5° field of view)	08/07	
Measured model validation			
tPAR	Delta T SunScan	18/06, 23/06* & 28/06 & 03/07	
Canopy reflectance	ASD (nadir, 1 m, 5° field of view)	18/06, 23/06* & 08/07 & 11/07	
Irradiance	ASD (white panel)	18/06, 23/06* & 08/07 & 11/07	
Other input parameters			
Sun zenith angle	Geometric	30/06, 1 h from solar noon	49°
Atmosphere parameterisation	DART sub-arctic winter, aerosols rural (V=23 km), aerosol optical depth factor: 0.2	Validated with measured irradiance	Aerosol optical depth at 550 nm: 0.065
Leaf angle distribution (for turbid medium)	Estimated (photos)		Spherical
Branch angle distribution (for turbid medium)	Estimated (photos)		Erectophile
General model set-up			
Mode			Flux tracking
Scene size			0.5 m · 0.5 m
Cell size			2.5 cm
Wavelength range			400–2500 nm
Wavelength interval			10 nm

The Photosynthetically Active Radiation transmitted below the canopy (tPAR, 400–700 nm) was measured with a Delta-T Devices SunScan Canopy Analysis System. The system consists of two instruments with simultaneous recording: the SunScan Probe (SS1) is a one-meter long wand with 64 equally spaced sensors which is inserted below the canopy to measure the amount of transmitted PAR. The Sunshine Sensor (BF3) is mounted above the canopy and measures total incoming PAR and diffuse incoming PAR.

3.2.3 Modelling

The simulations were performed with the DART (Discrete Anisotropic Radiative Transfer) model (*Gastellu-Etchegorry et al.*, 1996, 2004; *Grau and Gastellu-Etchegorry*, 2013) version 5.4.6. (November 2013). DART enables 3D radiative transfer simulations through atmosphere and canopies in the wavelength range 0.3–120 µm. The general settings and all model inputs are summarized in Table 3.1. We parameterised the reflectance of soil and understory below the shrub layer with the mean reflectance spectra of the removal subplot measurements after the treatment (Figure 3.2). This background reflectance is assumed to be lambertian and the transmittance of the background was set to zero.

We used two representations of shrub canopy, voxels filled with turbid medium and objects composed of small triangular surfaces. Turbid medium calculations require inputs on vegetation height and leaf angles (Table 3.1). In the simulations with objects, leaves were arranged on the branches as observed on a sample branch. All branches were included in the scene at randomly generated azimuth and elevation angles and positions. Six model complexities (Figure 3.3) were tested:

I Turbid cells with the optical properties of leaves

II Two classes of turbid cells with optical properties of leaves or branches

III Branches as idealised vertical cones ('stems') and turbid cells with leaf optical properties

IV Branches as triangulated objects and turbid cells with leaf optical properties

V Branches and leaves as triangulated objects

VI Only leaves as triangulated objects

For all complexities we varied PAI between 0 and 4 in steps of 0.4. We used an equal contribution of leaves and branches assuming LAI = BAI = PAI/2, which agrees well with the point-quadrat measurements on control subplots (Figure 3.4

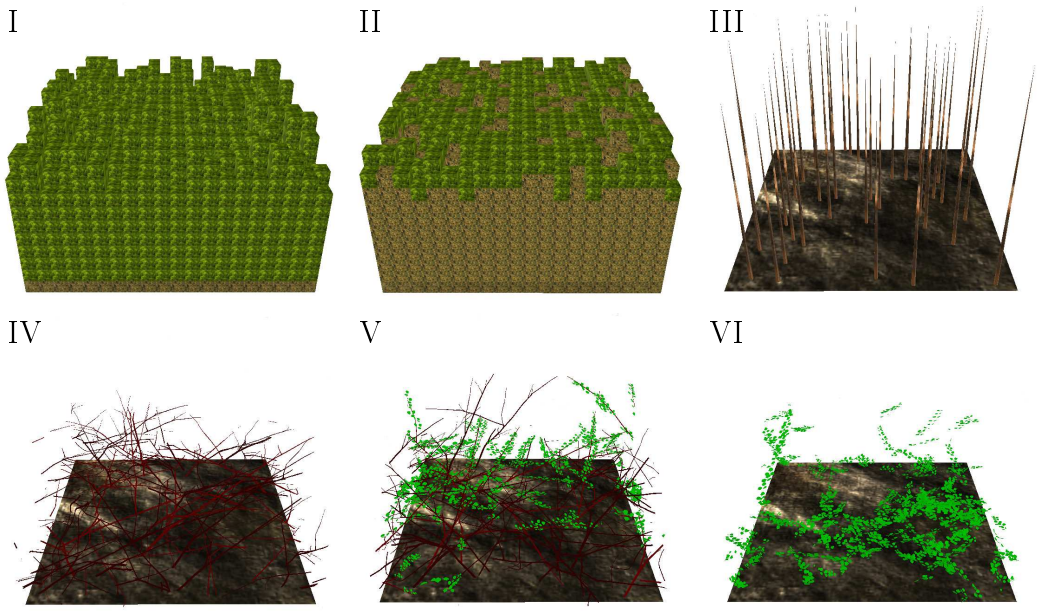

Figure 3.3: Visualisation of the six DART model complexities, each shown for LAI = BAI = 0.2; III and IV additionally contain leaves as turbid medium which would obstruct the branches in the visualisation.

a, b; Table 3.2). For the complexities which include branches, we additionally simulated the scene with a constant PAI of 2 and different contributions of leaves and branches (LAI between 0 and 2 and corresponding BAI between 2 and 0 in steps of 0.2).

For model validation we used four outputs which correspond to our field data, tPAR, nadir spectral (R_{nadir}, Equation 3.2) and broadband (Rb_{nadir}, Equation 3.3) reflectance, and NDVI (Equation 3.4). Further model outputs that cannot be validated with our field data are other components of the 3D radiative budget including the fraction of transmitted, absorbed, and reflected radiation and the reflectance in directions other than nadir.

3.3 Results

3.3.1 Treatment effects on the dwarf shrub canopy

We assessed the treatment effect by testing LAI, BAI, tPAR, Rb_{nadir}, and NDVI for pre-treatment biases (Figure 3.4). Before treatment none of the five variables was significantly different between either density or height subplots and control subplots. After the treatment LAI, tPAR, and NDVI were significantly different on both density and height subplots as compared to control subplots (Figure 3.4). The P-values of BAI and Rb_{nadir} were smaller after treatment than before treatment,

however, the differences between treatment subplots and control subplots were not statistically significant (Figure 3.4). In all cases the location of the subplots was not significant ($P > 0.01$, values not shown).

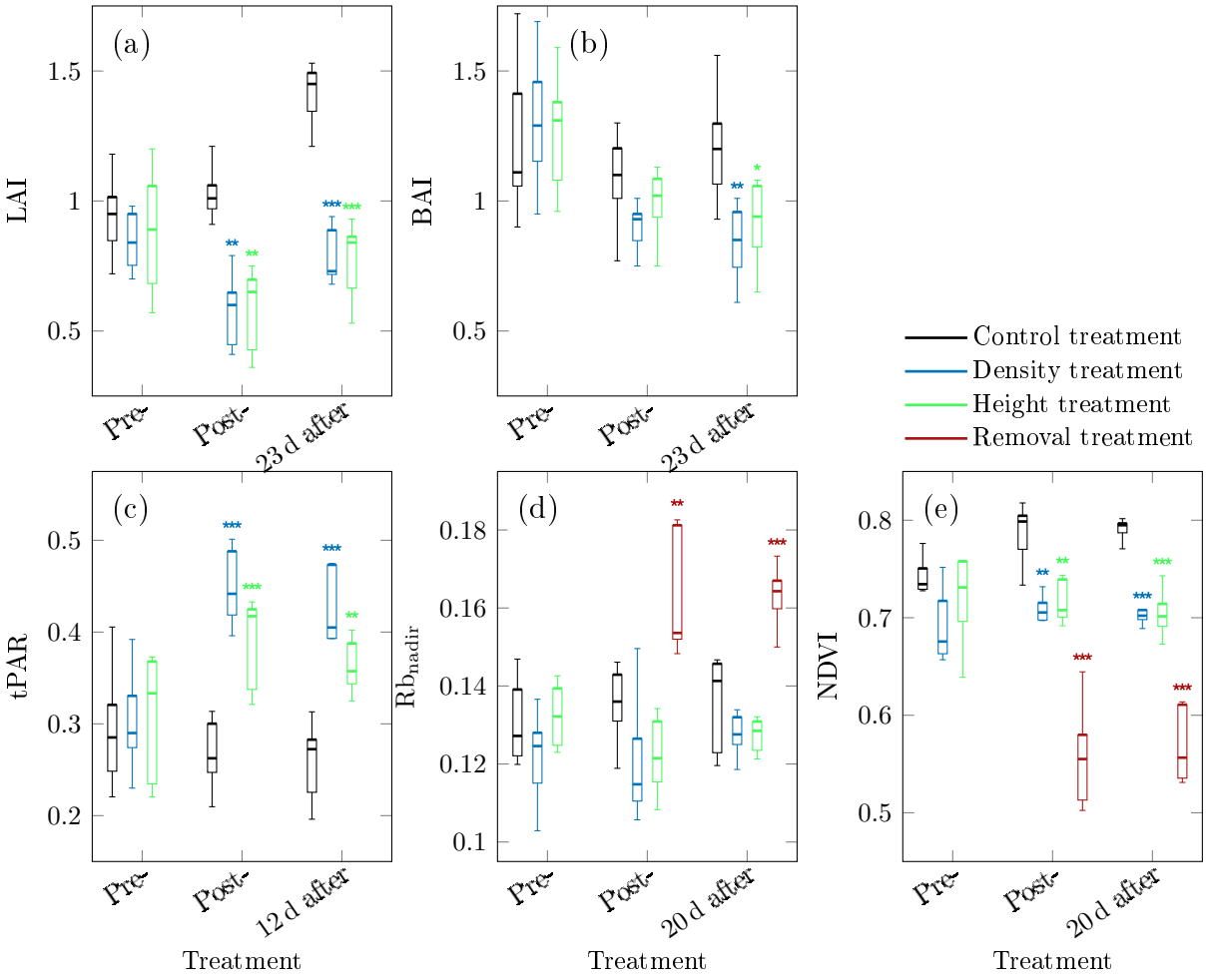

Figure 3.4: Effect of treatment and variation with time of LAI (a), BAI (b), tPAR (c), $\mathrm{Rb_{nadir}}$ (d), and NDVI (e); the central mark of the boxes is the median of five replicate plots, the edges are the 25th and 75th percentiles, and the whiskers denote the most extreme values; significance of the difference between control and other treatment subplots for each time step: $p < 0.001 :^{***}, p < 0.01 :^{**}, p < 0.05 :^{*}$; measurement dates in Table 3.1.

The magnitude and direction of the change induced by the treatments is shown in Table 3.2. As could be expected, tPAR increased on density and height subplots due to biomass removal. Broadband nadir reflectance ($\mathrm{Rb_{nadir}}$) was lower on density and height subplots as compared to control subplots while the total shrub removal increased the reflectance. In general, reflectance showed small differences between the treatments and over time. This can be attributed to the weak correlation be-

Table 3.2: Post-treatment measurements: mean and standard deviation of five replicate plots and mean difference between treatment and control subplots in percent of the control measurement; negative values show a reduction due to the treatment, positive values an increase.

	Control	Density		Height		Removal	
	Value	Value	Dif. (%)	Value	Dif. (%)	Value	Dif. (%)
Fresh biomass ($kg\,m^{-2}$)	1.54 ± 0.33	1.09 ± 0.28	-28.9	1.36 ± 0.31	-11.4	-	
Canopy height (cm)	23.3 ± 2.3	20.9 ± 3.7	-10.4	16.6 ± 1.0	-28.7	-	
Branches per m^2	107 ± 14	72 ± 11	-32.3	119 ± 20	11.5	-	
LAI	1.03 ± 0.11	0.57 ± 0.15	-44.2	0.58 ± 0.17	-43.7	-	
BAI	1.09 ± 0.20	0.90 ± 0.10	-17.1	0.99 ± 0.15	-8.5	-	
tPAR	0.27 ± 0.04	0.45 ± 0.04	67.7	0.39 ± 0.05	44.4	-	
Rb_{nadir}	0.14 ± 0.01	0.12 ± 0.02	-11.3	0.12 ± 0.01	-9.8	0.16 ± 0.02	20.8
NDVI	0.79 ± 0.03	0.71 ± 0.01	-9.9	0.72 ± 0.02	-8.8	0.56 ± 0.06	-29.4

tween the reflectance and LAI, BAI or PAI in the range of $1 < PAI < 3$ (Table 3.3). The biomass removal led to reduced NDVI values (Table 3.2). We observed a notable increase over time in LAI and NDVI on control subplots between the pre- and post-treatment measurements, indicating vegetation development (Figure 3.4, a, e). The treatment also changed the leaf to branch ratio of the shrub vegetation. While LAI/BAI increased strongly over time in the control subplots, the treatment subplots only showed an increase over time between the last two measurements and the ratios were generally lower, especially for the height treatment.

3.3.2 tPAR - data and model results

The amount of transmitted radiation below the canopy (tPAR) decreases with increasing plant area (Figure 3.5, a). The correlation coefficient between measured tPAR and PAI is -0.79, which is stronger than the correlation of tPAR with LAI or BAI (-0.65 and -0.62, respectively; Table 3.3). Thus for tPAR both leaves and branches have to be considered.

Table 3.3: Pearson's correlation coefficients of LAI, BAI, and PAI with tPAR, nadir broadband reflectance (Rb_{nadir}), and NDVI for all measurements except removal subplots.

	tPAR	Rb_{nadir}	NDVI
LAI	-0.65	0.37	0.73
BAI	-0.62	-0.08	0.09
PAI	-0.79	0.19	0.53

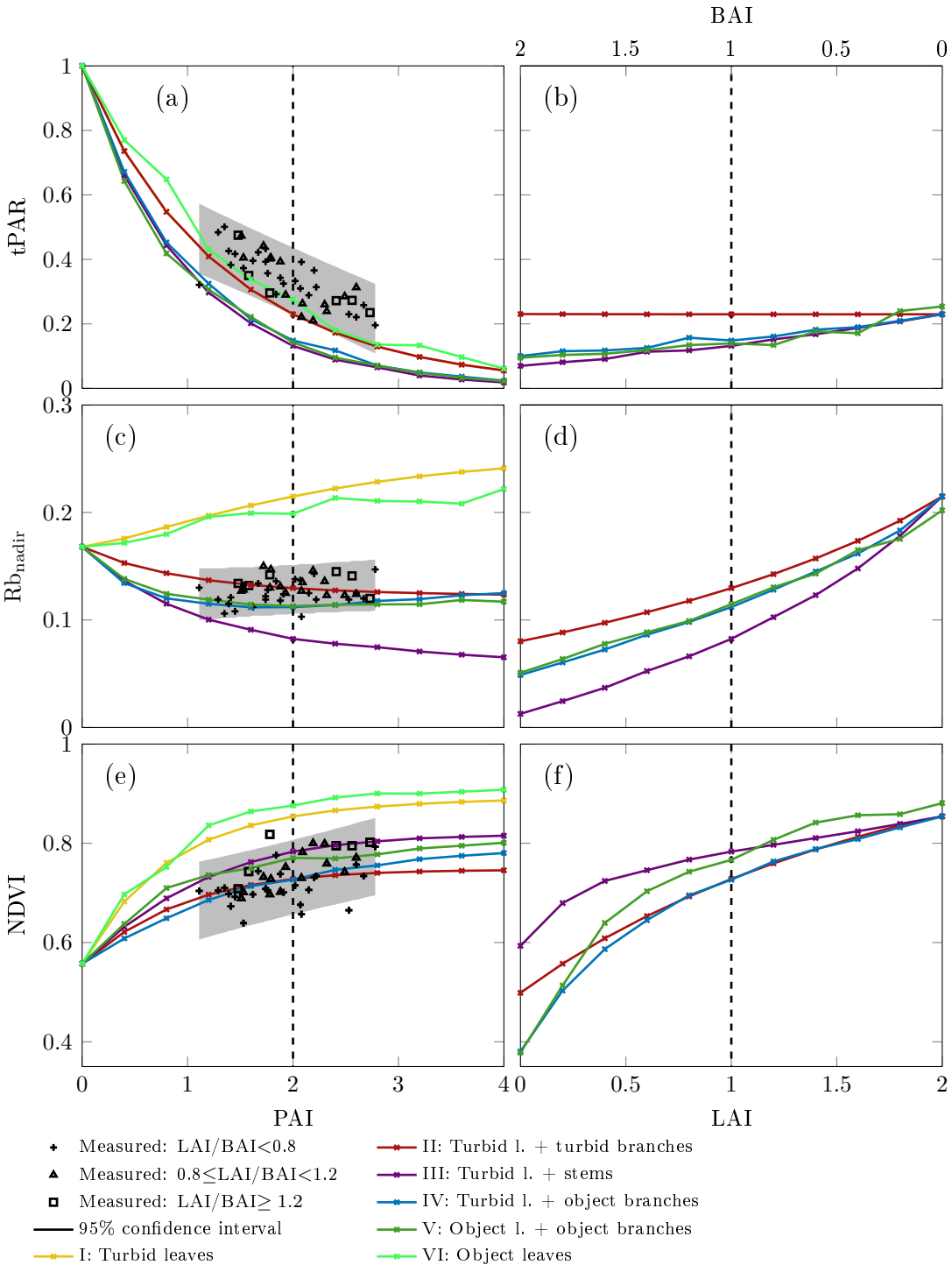

Figure 3.5: tPAR (top row), Rb_{nadir} (middle row), and NDVI (bottom row) with modelled data using LAI = BAI and measured data from all subplots (left column) and with modelled data using different leaf to branch ratios with PAI = 2 (right column); the different symbols of measured data show three categories of observed leaf / branch ratios; the grey area is the 95% confidence interval around a linear regressions of the data; the vertical dashed lines mark the input parameter set shown in all subplots.

All model simulations reproduce the observed decrease of tPAR with PAI (Figure 3.5, a). However, all model complexities also underestimate tPAR, especially those which include object branches or stems, which simulate values outside of the 95% confidence interval of the data (III-V, Figure 3.5, a). For the turbid medium approach the medium classification has a negligible influence on tPAR as the reflectance of branches and leaves is similar in the visible range and leaf transmittance is only 7.7%.

The ratio between leaves and branches influences tPAR less than total PAI (Figure 3.5, b). For II (turbid leaves and turbid branches), tPAR is almost identical for all ratios between leaves and branches, whereas all other complexities show between 2.3 and 3.3 times higher tPAR for simulations with only leaves as compared to only branches (Figure 3.5, b).

3.3.3 Reflectance - data and model results

The measured broadband nadir reflectance varies only slightly between 0.1 and 0.15 (Figure 3.4, d) and is weakly related to PAI (correlation coefficient of 0.19, Table 3.3). The correlation with LAI is 0.37, slightly stronger. Thus we observe that the amount of plant material does not have a strong effect on reflectance and possibly has a weak positive effect in the range of 1–3 PAI.

Unlike with tPAR, the simulation complexities reveal substantial differences in the relationship between PAI and reflectance. I and VI, which only consider leaves, clearly overestimate the reflectance which in simulations increases strongly with PAI (Figure 3.5, c). Without branches the simulated reflectance is higher than the background reflectance (shown at PAI = 0), due in part to the relatively dark background.

The simulation with stems (III) underestimates the amount of reflected solar radiation, as results show a strong decline in reflectance in the range of modelled PAI (Figure 3.5, c). Apparently the vertical orientation of the stems is not a good approximation of the dwarf birch shrubs and the effect of shading is overestimated. The differences between simulations which include turbid or object branches (II, IV, and V) are less pronounced and the modelled reflectance is within the 95% confidence interval of measured data. Complexities II, IV, and V show very little variation in reflectance when PAI is in the range of 1–3 PAI. This model result agrees well with our field measurements. If leaves and branches are simulated as turbid media, the reflectance decreases slightly with increasing PAI, a trend observed across the whole range (1–3 PAI). The simulation with turbid leaves and object branches (IV) and leaves and branches as objects (V) show a minimum reflectance at PAI = 1.6 and PAI = 2, respectively, and an increase in reflectance for denser canopies (Figure 3.5, c). A higher contribution of leaves to the PAI increases the

broadband reflectance for all model complexities (Figure 3.5, d). In general the ratio between leaves and branches has a stronger effect on the modelled reflectance than the total PAI with LAI = BAI.

Apart from broadband nadir reflectance, we also used the spectral reflectance for model validation (Figure 3.6). Two different spectral regions can be distinguished, the visible and the near infrared range.

In the visible range all model complexities show different results, especially at the green peak. The green peak (≈550 nm) is highest in model complexities which include only leaves (I, VI) and lowest with turbid leaves and stems (III) (Figure 3.6, a). Complexity V (object leaves and branches) also underestimates the green peak in simulations with LAI = BAI. The effect of total PAI on reflectance in the visible is small for PAI > 0.8 (Figure 3.6, b). However, the ratio between leaves and branches is very important for both the shape of the reflectance spectrum and the absolute values (Figure 3.6, c). The more leaves are simulated compared to branches, the more pronounced is the reflectance peak in the green and the minimum in the red. Additionally, more leaves result in higher total reflectance in the visible range. The results for LAI > BAI fit the measured data much better than simulations with less leaves.

In the near infrared the models with only leaves overestimate the reflected radiation drastically. Using LAI = BAI = 1 the model including the vertical stems (III) underestimates the reflectance and the other model complexities are within the range of the control subplot measurements (Figure 3.6, d). As in the visible part of the spectrum, total PAI is most important for reflectance in the near infrared for PAI < 0.8 (Figure 3.6, e). The leaf to branch ratio strongly influences the modelled reflectance (Figure 3.6, f), especially the absolute values.

3.3.4 NDVI - data and model results

As expected, we found a positive relationship between NDVI and PAI (Figure 3.5, e). However, NDVI is more strongly correlated with LAI than PAI and is not at all correlated with BAI (Table 3.3). In general the relationship between NDVI and LAI is much more pronounced than between reflectance and LAI. Our measurements of the background reveal an average NDVI of 0.56 (Figure 3.4, e), which agrees well with contact measurements of the mosses below the shrubs. The measured NDVIs of dwarf birch canopy range between 0.61 and 0.82 and the lowest NDVI values were measured on plots with lower leaf / branch ratios (Figure 3.5, e).

All model simulations show an increase of NDVI with PAI, but the complexities differ in the maximum NDVI returned for large PAIs (Figure 3.5, e). The simulations with only leaves (I and VI) overestimate NDVI strongly, while all simulations which include branch optical properties (II, III, IV, and V) simulate values in the range

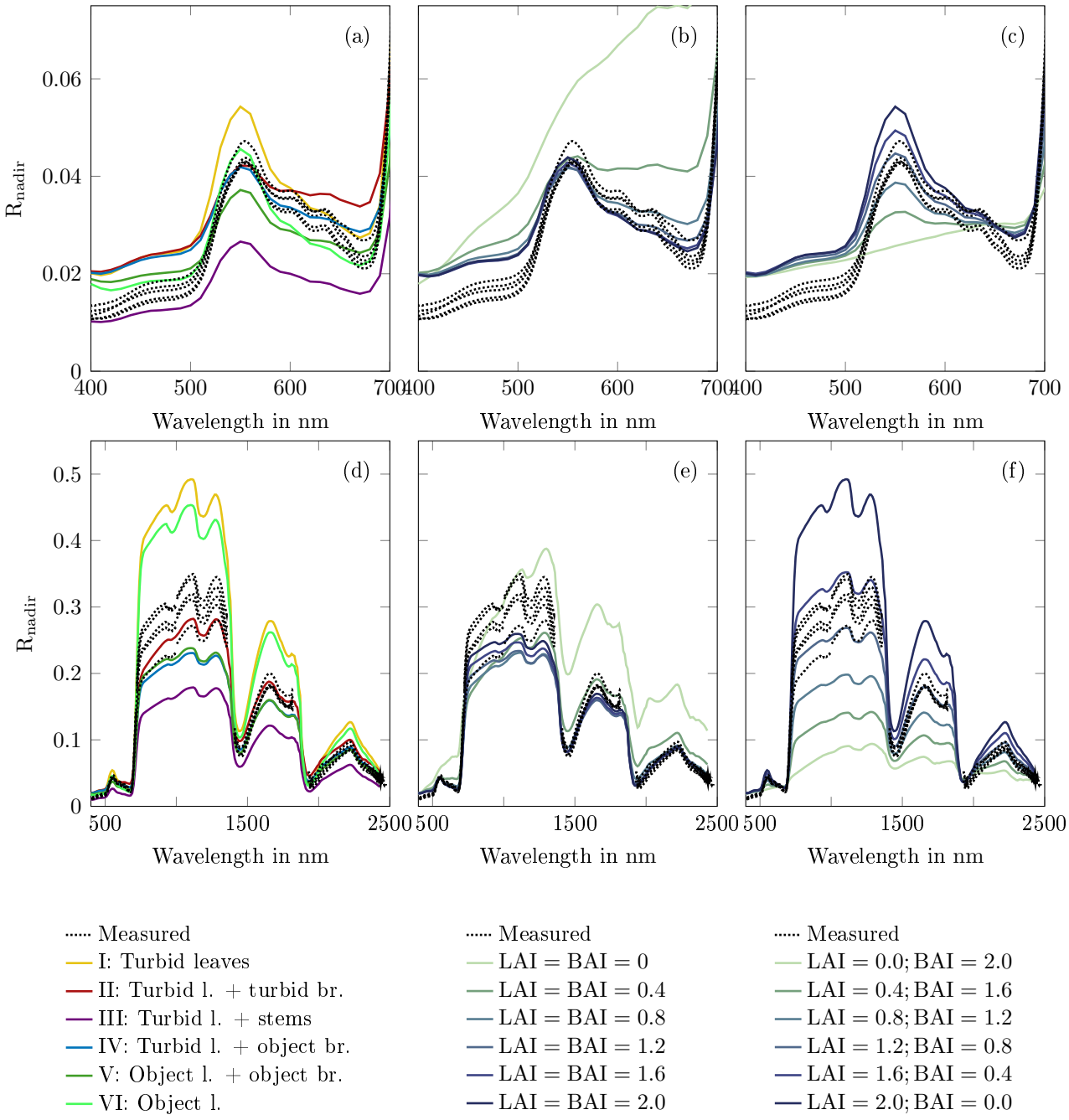

Figure 3.6: Reflectance in nadir direction (R_{nadir}) in the visible range (top row) and whole range (bottom row) measured on the five control plots 08/07/2013 (PAI between 1.78 and 2.3, Figure 3.4) in comparison with (a,d) model results for PAI = 2, LAI = BAI, (b,e) model results for different PAIs with turbid leaves and object branches (IV) and (c,f) model results with PAI = 2 and different ratios of LAI/BAI with turbid leaves and object branches (IV); one legend per column.

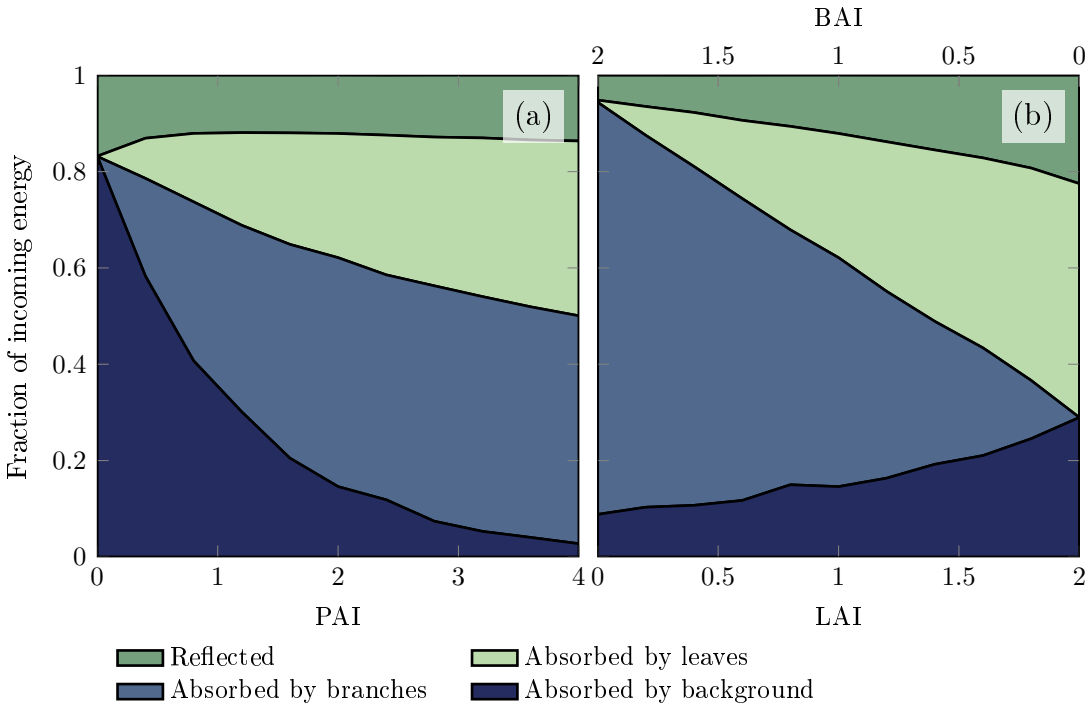

Figure 3.7: Energy balance as simulated with complexity IV (object branches and turbid leaves) (a) modelled data using LAI = BAI and (b) modelled data using different leaf to branch ratios with PAI = 2.

of the confidence interval. As we found in the model results for reflectance, NDVI simulations are very sensitive to the ratio of leaves to branches (Figure 3.5, f).

3.3.5 Energy balance - model results

We used the DART model output to estimate the importance of branches and leaves in the energy balance. Here we only show modelling results for IV (object branches and turbid leaves), however, the results are very similar for V (object branches and object leaves). As described above, the fraction of reflected energy is almost the same for different PAIs (Figure 3.7, a). The amount of absorbed radiation by the background decreases non-linearly with increasing PAI as leaves and branches provide more and more shading. For LAI = BAI branches contribute between 71% (low PAI) and 57% (high PAI) to the total absorption of the canopy.

The ratio between leaves and branches does not only change the partitioning of absorbed radiation within the vegetation layer, but also the amount of energy absorbed by the background (Figure 3.7, b). A higher fraction of leaves leads to greater reflection and higher absorption by the background layer.

3.4 Discussion

3.4.1 Field data

In our study the ratio between leaf and branch area changes during the season from 0.73 on average before treatment to 1.22 as the mean of the control subplots at the last measurement in mid-July. The early-season measurements correspond well to the ratio of 0.7 for tall Arctic shrubs measured by *Thompson et al.* (2004). It has to be noted that our measurements likely underestimate both LAI and BAI as we used point-quadrat grid measurements with vertical needle insertion.

Our treatments did not affect LAI and BAI equally but rather changed the ratio between the two. This is especially true for the height treatment which cannot be considered representative of a naturally shorter canopy. The treatment removed mostly young branch tips with many leaves while older, more woody parts of the canopy remained. This combination of changes in PAI and leaf / branch ratio between each treatment is a limitation when comparing the measurements to the model results and when drawing conclusions on natural changes.

Transmitted radiation was underestimated by the radiative transfer model in all complexities. We propose two main reasons. First, the measurements may overestimate tPAR as the sky was overcast on the second and third sampling date. Cloud cover can increase tPAR as diffuse light is expected to reduce shadows (*Eck and Deering*, 1992; *Reid et al.*, 2014). However, our data does not show a systematic difference between the clear-sky pre-treatment measurements and the two sets of overcast measurements. As such the measurement conditions do not completely explain the differences. The second reason for the differences could lie in the model parameterisation. We did not consider clumping in our model runs with turbid media, and in the object based complexities we may be underestimate leaf and branch clumping.

The values of nadir reflectance between 0.1 and 0.15 measured in our study (Figure 3.4) are slightly lower than the albedo values reported for dwarf birch dominated tundra in literature, which are 0.16 (*Eugster et al.*, 2000) and 0.17 (*Thompson et al.*, 2004; *Beringer et al.*, 2005). One reason may be that, as shown by our model results for local conditions, nadir reflectance is slightly lower than albedo. Another possibility is that our dataset only includes selected, clear-sky values collected around noon and is therefore not a complete data series. Furthermore we selected specifically dwarf birch patches with closed dwarf birch cover while other studies include larger fractions of other species. In the studies by *Thompson et al.* (2004) and *Beringer et al.* (2005) dwarf shrub tundra includes a mixture of vegetation containing dwarf birch as well as other deciduous and evergreen shrubs. The albedo value from *Eugster et al.* (2000) was measured on a plot with dwarf birch and willow species.

Blok et al. (2011c) found a negative relationship between shrub fractional cover and albedo at the Kytalyk research site on experimental plots in 2009. In contrast, our results show a weak positive correlation between nadir reflectance and PAI. One reason for this discrepancy might be that we compare different variables. Our study focused on nadir reflectance and LAI, while *Blok et al.* (2011c) measured albedo and fractional cover. However, our model results show a strong positive correlation between albedo and nadir reflectance and *Blok et al.* (2011c) report a positive relation between dwarf shrub fractional cover and LAI. Therefore, it is not expected that slightly different variables would lead to the observed change in relationship between plant area proxies and reflectance quantities. Another reason for the discrepancy between the studies may be the difference in observed LAI ranges. In our study LAI varied between 0.36 and 1.48 compared to a range of 0.2 to 1 in *Blok et al.* (2011c). Our model results show that the initial decrease of nadir reflectance seen with increasing PAI between 0 and 1, levels off for PAI > 1. These results also suggest that reflectance may increase at higher PAI values, especially if the number of leaves as compared to branches increases (IV, Figure 3.5 c, d). As such both our and *Blok et al.* (2011c) measurements may be showing different parts of the picture. It is important to note that both studies report a weak correlation with R^2 values of $0.37^2 = 0.14$ (Table 3.3) and 0.47, respectively. This may be in part due to the relatively few measurements included, especially in the LAI - albedo relationship of *Blok et al.* (2011c).

Several studies show a negative correlation between biomass or LAI and canopy reflectance across different ecosystem types in the Arctic (e.g. *Thompson et al.*, 2004; *Beringer et al.*, 2005). In contrast our measurements and model results show that for the given shrub vegetation increasing PAI does not significantly decrease the growing season albedo. Thus studies that relate Arctic greening to the radiation balance need to differentiate between greening through increased growth of the existing vegetation type and greening through replacement of one vegetation type with another. In addition, our study focused on the growing season while several studies suggest, that the most important effect of shrub presence and height on the radiation balance is in winter and spring when the shrubs mask the snow and enhance snowmelt (e.g. *Pomeroy et al.*, 2006; *Marsh et al.*, 2010; *Loranty et al.*, 2011).

Our NDVI measurements of dwarf birch canopy range from 0.6 to 0.8 (Figure 3.5, e). This range agrees well with other studies from shrub tundra (*Riedel et al.*, 2005; *Blok et al.*, 2011c) which also report a positive relationship between NDVI and shrub cover. However, our data and model results indicate a saturation of NDVI for PAIs starting between 2 and 3 (Figure 3.5, e). Thus NDVI might be less useful for relating further Arctic greening to biomass (*Rees et al.*, 1998), especially as it also relates to other factors like moisture conditions (*Gamon et al.*, 2013) and background type (*Hope et al.*, 1993; *Rocha and Shaver*, 2009). We found relatively

high background NDVI values due to mosses below the shrub canopy. This is consistent with the study by *Boelman et al.* (2011) which also reports higher NDVI values for vegetation prior to leaf out when woody branch coverage is sparse as compared to more dense branch coverage, which masks the background vegetation.

Our findings have important implications on the summer energy balance of the soil-plant system. Unlike previously thought, a denser shrub canopy may not increase the overall energy availability as the effect on canopy albedo is small and we observed a positive relationship between the two. The major effect of shrub density is on energy partitioning within the canopy-soil system. Denser canopies transmit less radiation to the soil and likely increase energy loss due to evapotranspiration (*Bonfils et al.*, 2012). Therefore, a dense shrub canopy may reduce the ALT and soil temperatures. Furthermore, soil shading influences the plant community below the shrubs as species richness has been found to decline with increasing shrub height and density (*Pajunen et al.*, 2011). More specifically, soil shading has been found to cause reduction in the moss layer below dense shrub canopies which has implications for soil temperatures, active layer depth, and the rate of soil decomposition (*Walker et al.*, 2006; *Blok et al.*, 2011a).

3.4.2 Simulations

In the past a variety of models, ranging from very simple to 3D Monte Carlo or flux tracking approaches, have been used for simulating radiative transfer in vegetation. We used the DART model to compare six different 3D approaches. DART proved to be an effective tool for studying the influence of leaf and branch parameterisation in radiative transfer modelling. Our results corroborate other studies which found DART to be a useful tool for modelling radiative transfer in vegetation (*Gastellu-Etchegorry et al.*, 1999, 2004; *Malenovský et al.*, 2008). However, the model had not yet been validated for dwarf-shrub tundra.

The main result of our modelling study is the importance of including branches as well as leaves in radiation balance calculations. The importance of branches, stems or woody elements in general has been stressed by other authors for forest canopies (*Malenovský et al.*, 2008; *Verrelst et al.*, 2010). However, few studies exist on the influence of woody elements on the radiative balance of Arctic shrubs. Two studies that measured transmitted radiation below deciduous Arctic tall-shrub vegetation did so in spring before leaf-out and found significantly reduced radiation compared to open locations (*Bewley et al.*, 2007; *Reid et al.*, 2014). Depending on solar angle and exact measurement location, both studies revealed absorption by the woody biomass of the shrubs to be as much as 60% in extreme cases (low solar angles or dense canopy) and 30 to 40% on average. Our model results suggest, that in dwarf birch vegetation branches are likely to contribute more to total radiation absorption than

leaves (Figure 3.7). As the partitioning changes nonlinearly with PAI, both elements should be included in radiation transfer or energy balance modelling. While PAI is clearly the most important driver for tPAR, the ratio between leaves and branches has a stronger influence on reflectance and NDVI (Figure 3.5). Thus we would like to emphasise the need for measurements of leaf to branch ratios of different vegetation types so that these ratios can be included in models of the energy or radiation balance.

Four of the six model complexities tested in our study included a parameterisation of branches (II-V). The implementation of branches as vertical stems (III) is not appropriate as it massively underestimates nadir reflectance and is less accurate than branches represented by turbid medium or objects. For the complexities with object branches the differences between leaves as turbid medium (IV) and as objects (V) are relatively small. These model complexities slightly underestimated nadir reflectance and strongly underestimated tPAR while NDVI is simulated well. The model run with turbid leaves and turbid branches (II) simulates all three variables best although the tPAR values are on the lower boundary of the measurements. It should be noted here, however, that leaf and branch angle distributions are influential parameters for turbid medium calculations and were not measured in the field. Furthermore, we assumed 'no clumping' in our simulations with turbid media because of the lack of input data. Including a clumping factor of 0.8 in the simulation with turbid leaves and branches (II) has a small effect on simulated Albedo and NDVI (less than 3% for all PAI), but increases tPAR significantly by 0.04 to 0.08 depending on the plant area (results not shown). Thus simulations with clumped turbid media match the measured tPAR data best while turbid media without clumping and object branches show strong discrepancies between model results and data. This suggests that also the object branches might be too uniformly distributed on the modelled scene.

It should be noted here that we simulated only one solar angle which corresponds to local conditions one hour before noon. Thus our results for the energy balance (Figure 3.7) show just a snap-shot and not average values for the whole season.

3.5 Conclusions

Our most important conclusions concerning Arctic dwarf-shrub vegetation are as follows:

- For plant areas between 1–3 $m^2\,m^{-2}$ nadir reflectance is very weakly correlated with dwarf birch PAI and the relationship is positive.

- Nadir reflectance and NDVI are mainly influenced by leaf area and leaf to branch ratio, less so by plant area.

- Woody biomass of dwarf birch shrubs accounts for 57% to 71% of the total canopy absorbed radiation for LAI = BAI in our model results.

- Energy partitioning between leaves and branches is non linear.

These findings have important implications for the impacts of increased Arctic shrub density. While increasing shrub biomass may not lead to significant albedo reduction under constant ecosystem type, the partitioning of the absorbed radiation between soil and canopy is likely to change. The changes in energy balance of the soil and thus the permafrost may not be easily observable from space as shrub plant area indices above 2 are not significantly related to NDVI or, in general, reflectance in any spectral region.

We demonstrated the importance of leaf to branch ratios for all parts of the shortwave radiation balance. Thus we suggest that more effort is needed to measure this ratio in the field and to explicitly include it in radiative transfer and energy balance models. Furthermore, canopy background and vegetation type replaced by shrubs need to be considered when predicting feedbacks of shrubification to summer albedo, permafrost thaw, and climate warming.

Acknowledgements

We acknowledge the support by ASD Goetz Instrument Support Program for providing a spectrometer for field measurements in the Siberian tundra. We would like to thank the Siberian Branch of the Russian Academy of Science for the support. This work was supported by the Swiss National Science Foundation through project grant 140631. We were further supported by the University of Zurich through the University research priority programme on Global Change and Biodiversity (URPP GCB). We like to thank the developers, especially J.-P. Gastellu-Etchegorry and CESBIO, for making the DART software freely available, and F. Schneider and M. Schaepman at the Remote Sensing Laboratories, University of Zurich, for discussions and comments.

4 Drivers of shortwave radiation fluxes in Arctic tundra across scales

Inge Juszak[1], Maitane Iturrate-Garcia[1], Jean-Philippe Gastellu-Etchegorry[2], Michael E. Schaepman[3], Trofim C. Maximov[4], and Gabriela Schaepman-Strub[1]

Abstract

Vegetation composition and water surface area are changing in many tundra regions due to climate warming, which is twice as strong in the Arctic as compared to the global mean. Such landcover changes feed back to climate and permafrost thaw through altering the surface energy budget. We quantified the influence of vegetation type, canopy characteristics, and patchiness on the tundra shortwave radiation budget. We used in situ measurements and vegetation mapping to parametrise a 3D radiative transfer model (DART) for summer conditions at the Kytalyk test site in northeast Siberia. We analysed model results assessing the most important drivers of canopy albedo, transmittance, and absorptance of photosynthetically active radiation (PAR). Tundra albedo was strongly influenced by the fractional cover of water surfaces. Unlike plant area index, shrub cover significantly decreased the albedo. Canopy transmittance and PAR absorptance (f_{APAR}) were almost entirely controlled by plant area index at the landscape scale. Only about one half of the total plant area index consisted of green leaves, while wood and standing dead leaves contributed equally to the other half. While the spatial arrangement and patch size of vegetation types and open water did not significantly influence the radiation budget at the landscape scale, it contributed to the large variability at the local scale. The variation of the radiation budget within single vegetation types potentially affects larger scale energy, water, and carbon fluxes as other studies showed that evapotranspiration and primary productivity are sensitive to local variability of shortwave radiation.

[1]Department of Evolutionary Biology and Environmental Studies, University of Zurich, Winterthurerstrasse 190, 8057 Zurich, Switzerland

[2]Centre d'Etudes Spatiales de la BIOsphère (CESBIO) - CNES, CNRS, IRD, Université de Toulouse, 31401 Toulouse cedex 9, France

[3]Remote Sensing Laboratories, University of Zurich, Winterthurerstrasse 190, 8057 Zurich, Switzerland

[4]Institute for Biological Problems of Cryolithozone, Siberian Branch of Russian Academy of Sciences, 41 Lenin Avenue, Yakutsk, Yakutia 677980, Russian Federation

Submitted to **Remote Sensing of Environment** with references merged at the end of this thesis.

I.J. conceived the study, carried out the field measurements, performed the data analysis and the radiative transfer modelling and wrote the manuscript. M.I.-G. carried out field measurements and contributed to the manuscript preparation. J.-P.G.-E. provided input on the radiative transfer modelling and on the manuscript. M.E.S. contributed to the data analysis and the writing of the manuscript. G.S.-S. conceived the study, carried out field measurements, and provided input for the data analysis and the manuscript.

4.1 Introduction

Vegetation is an important part of the climate system as it does not only react to climatic drivers but also influences climate through changing Earth's surface properties. Arctic greening, in particular the expansion of shrubs in tundra areas, is associated with recent climate warming (*Sturm et al.*, 2001b; *Myers-Smith et al.*, 2011; *Fraser et al.*, 2014). This greening directly affects the surface albedo, which feeds back to climate through large scale warming (*Chapin et al.*, 2005; *Loranty et al.*, 2011). Vegetation effects on permafrost thaw are more complex since increased vegetation density cannot only lead to atmospheric warming but also partly decouple permafrost from the atmosphere through insulation and soil shading (*Eugster et al.*, 2000; *Walker et al.*, 2003b; *Cannone and Guglielmin*, 2009; *Briggs et al.*, 2014).

Tundra landscapes typically show small scale patterns including water bodies and distinct vegetation patterns (*Walker et al.*, 2008). Landscape variation and associated differences in soil moisture, nutrients, and pH can lead to different vegetation composition within meters (*Walker et al.*, 2011; *Muster et al.*, 2012). These patterns can either remain stable over decades (*Gamon et al.*, 2012) or change rapidly for example due to permafrost degradation (*Schuur et al.*, 2015). Large scale vegetation dynamics are also affected by wetland area and the water budget. While an increase in lake and wetland area has been observed in the Siberian tundra (*Smith et al.*, 2005; *Lin et al.*, 2012), the American Arctic shows a drying trend (*Oechel et al.*, 2000; *Carroll et al.*, 2011; *Jones et al.*, 2011; *Lin et al.*, 2012). Shrubs such as dwarf birch (*Betula nana*) profit from warming and fertilisation and become increasingly dominant (*Bret-Harte et al.*, 2001). Changes in vegetation composition and climate have led to an increase in productivity (*de Jong et al.*, 2013) and a decrease in growing season length (*Sweet et al.*, 2015; *Garonna et al.*, 2016) in many tundra regions.

Vegetation feeds back to climate through the surface energy budget. Densification of tundra vegetation reduces the surface albedo and thus amplifies warming (*Beringer et al.*, 2005). As the top soil temperature is influenced by canopy shading, also the outgoing longwave radiation is affected by vegetation (*Westermann et al.*, 2011). Furthermore, vegetation alters surface roughness and evapotranspiration, which leads to changes of the turbulent heat fluxes (*Boudreau and Rouse*, 1995).

Permafrost is affected by vegetation cover in multiple ways. On one hand, vegetation shades the ground and thus reduces the amount of shortwave radiation that is absorbed by the soil (*Benninghoff*, 1952; *Briggs et al.*, 2014). On the other hand, vascular plants influence moss abundance through shading and litter production (*van Wijk et al.*, 2003). Mosses can strongly insulate the soil from air temperature (*Beringer et al.*, 2001; *Blok et al.*, 2011a). Additional processes, such as trapping of snow by vegetation (*Pomeroy et al.*, 2006), further influence the interaction between

vegetation and permafrost thaw.

Currently, little is known about the radiation budget of patterned tundra landscapes. While satellite observations are too coarse to resolve fine scale differences among vegetation types (*Muster et al.*, 2012), 3D radiative transfer models enable the quantification of shortwave radiation budget components in heterogeneous landscapes (*Schneider et al.*, 2014).

The aim of this study is to quantify the shortwave radiation budget of heterogeneous tundra. The focus is on increasing the understanding of drivers of canopy albedo, transmittance, and absorbed radiation from patch to landscape scale. Using a 3D radiative transfer model, we provide insights into typical length scales of horizontal interaction between vegetation types. We first assessed the current vegetation distribution and canopy properties at the Kytalyk research site in northeast Siberia. Secondly, we parametrised the DART 3D radiative transfer model (*Gastellu-Etchegorry et al.*, 2004; *Grau and Gastellu-Etchegorry*, 2013) for the major vegetation types present at the site and quantified the shortwave radiation budget for 21 transects ranging from dwarf birch vegetation to other vegetation types and water surfaces.

4.2 Methods

4.2.1 Field site

Our field site is the Kytalyk nature reserve located in the Indigirka lowlands, northeast Siberia (70.8 °N, 147.5 °E, Figure 4.1a). According to the circumpolar Arctic vegetation map, vegetation is classified as tussock sedge, dwarf shrub, moss tundra (*Walker et al.*, 2005). Low shrub tundra (mainly *Salix pulchra*) occurs along rivers and at lake shores. The area is dominated by continuous permafrost of several hundred meters depth (*Romanovskii et al.*, 2004) with an active layer thickness of 12 to 50 cm (*Mi et al.*, 2014). The Kytalyk field site is described in more detail in *van der Molen et al.* (2007); *Nauta et al.* (2015) and *Juszak et al.* (2016a). The size of our study area is 1.4 km × 2 km (Figure 4.1b).

4.2.2 Remote sensing data and products

We used a ground referenced orthomosaic from a UAV (unmanned aerial vehicle, eBee, senseFly), acquired with digital cameras in four spectral bands (red, green, blue, and near infra-red (NIR)) to generate a NDVI (Normalized Difference Vegetation Index) map, a DSM (digital surface model), and a landcover map of dominant vegetation types. The map products have a spatial resolution of 5 cm and an extent of 1.4 km × 2 km.

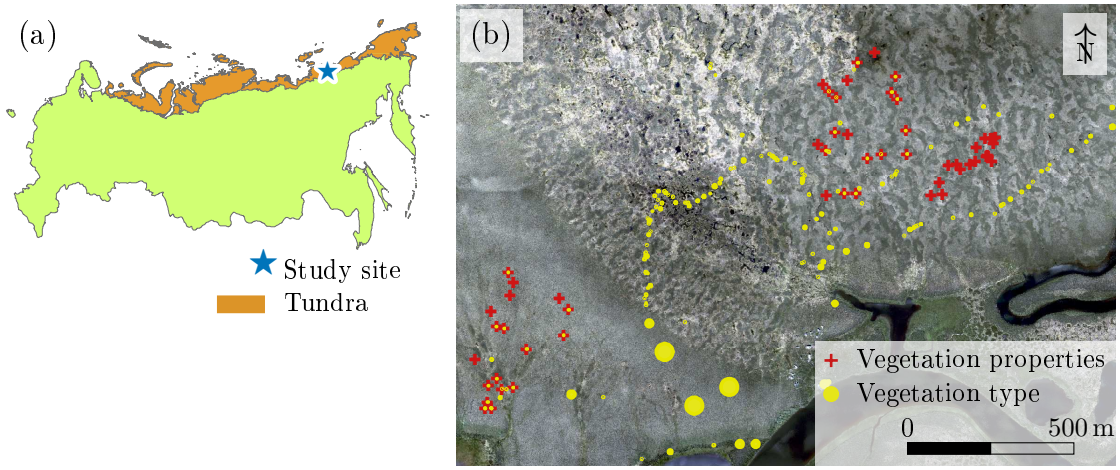

Figure 4.1: (a) Location of the study site in northeast Siberia and extent of Arctic tundra (orange, *Walker et al.*, 2005) and (b) orthomosaic of the study site including measurement locations of vegetation properties (red) and reference points for vegetation mapping (yellow, point size indicates represented area).

Orthomosaic, NDVI, and DSM

The orthomosaic, which we obtained from the drone flights, revealed some artefacts due to inhomogeneous illumination during and between flights (Figure 4.2a). These artefacts propagated to the NDVI map, spatial input variables, and the vegetation map (Figure 4.2b). We estimated the NDVI from the red (ρ_{red}) and NIR reflectance (ρ_{NIR}):

$$\mathrm{NDVI} = \frac{\rho_{\mathrm{NIR}} - \rho_{\mathrm{red}}}{\rho_{\mathrm{NIR}} + \rho_{\mathrm{red}}} \tag{4.1}$$

The DSM was generated from the point cloud which was created during the image matching. It uses noise filtering and surface smoothing to minimise the occurrence of artefacts in the model (Postflight Terra 3D, Version 4.0.83). The elevation difference between the river and the highest area of the ridge was about 23 m. Fine scale drainage patterns could be detected in the DSM, for example in the area of the drained thaw lake bed. The DSM showed small scale height differences between the elevated shrub patches and wet sedge depressions. The DSM represented a level between the top of canopy and the soil surface. Since the vegetation was low (< 0.8 m) and mostly sparse (average LAI of all vascular vegetation types < 1.5), some of the reference points for the DSM may have been mapped at the soil surface. Additionally, the DSM was smoothed by the filtering process. Thus we considered the DSM an appropriate approximation of the ground elevation and used it as topographic input for modelling.

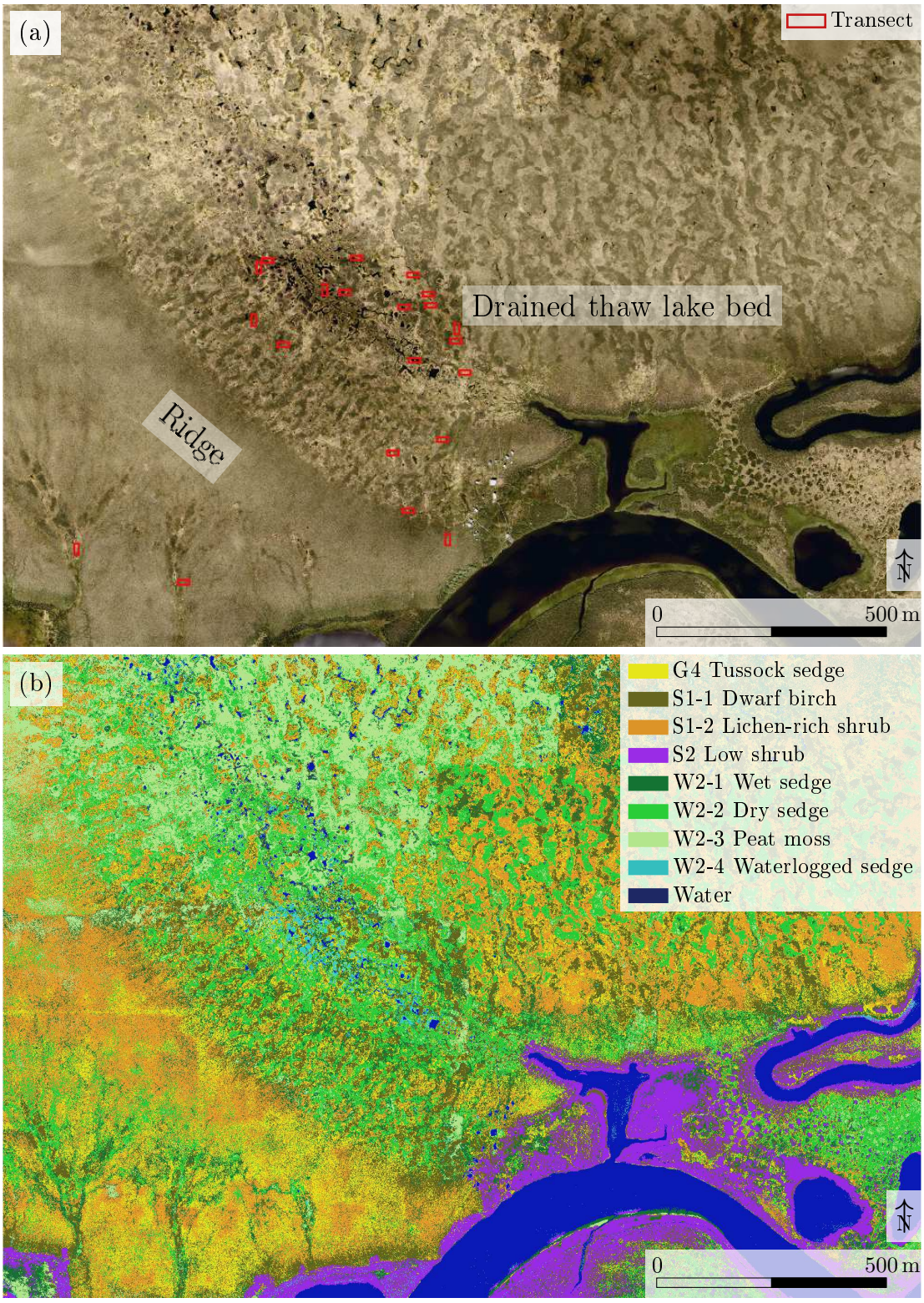

Figure 4.2: (a) Orthomosaic of the study area (1.4 km × 2 km) including the locations of 21 transects and (b) vegetation map.

Vegetation map

The reference points for training and validation of the vegetation map were acquired in the field (Figure 4.1b). We defined eight vegetation types based on the class definition in the circumpolar Arctic vegetation map (*Walker et al.*, 2005) which we split into sub-classes depending on species composition and canopy properties (Table 4.1). We performed supervised classification (ENVI, Version 5.2). To assess the classification accuracy, we took a random subset of the validation points with an equal amount of pixels per vegetation type (732 pixels). We computed the confusion matrix, user's accuracy, producer's accuracy, and the Kappa coefficient (*Strahler et al.*, 2006).

Table 4.1: Vegetation classes from the circumpolar Arctic vegetation map (*Walker et al.*, 2005) and sub-classes as defined for this study; the background colours indicate the colour used for this vegetation type in maps and graphs.

Class	Sub-class	Description
G4		Tussock sedge (*Eriophorum vaginatum*), dwarf shrub, moss tundra
S1		Erect dwarf shrub tundra (< 40 cm)
	S1-1	Dwarf birch (*Betula nana*) dominated
	S1-2	Lichen-rich shrub, *Vaccinium* spp. dominated
S2		Low shrub tundra (> 40 cm, *Salix pulchra*)
W2		Sedge, moss, dwarf shrub (< 40 cm) wetland
	W2-1	Wet sedge, *Eriophorum angustifolium* dominated, dense, green
	W2-2	Dry sedge, *Eriophorum angustifolium* and *Sphagnum* spp. dominated
	W2-3	Peat moss (*Sphagnum* spp.) dominated
	W2-4	Waterlogged sedge, *Carex* spp. dominated, few standing dead leaves
Water		Open water

Betula dwarf shrubs (S1-1) and *Salix* low shrubs (S2) covered about 20% of the landscape, another 39% was covered by densely vegetated wetlands (W2-1, W2-2, W2-3) and 8% by water bodies and waterlogged sedges (W2-4). The remaining area was classified as either tussock sedge (G4) or lichen-rich dwarf shrub tundra (S1-2). The Kappa coefficient of the vegetation classification was 0.44, the overall accuracy was 50%. The confusion matrix (Table 4.2) indicates that tussock tundra (G4) was similar to lichen-rich shrub tundra (S1-2). Therefore, large parts of the tussock tundra in the area of the ridge have been misclassified as S1-2 (Figure 4.2b). Furthermore, dry sedges (W2-2) and peat moss tundra (W2-3) resembled each other in appearance and (shallow) water was often classified as waterlogged sedges (W2-4).

Table 4.2: Confusion matrix of the vegetation map calculated from a random subset of the validation data with an equal number of validation pixels per class.

		Map									Producer's
		G4	S1-1	S1-2	S2	W2-1	W2-2	W2-3	W2-4	Water	accuracy (%)
Ground truth	G4	**160**	41	468	0	47	6	10	0	0	22
	S1-1	133	**297**	240	0	43	15	0	4	0	41
	S1-2	54	43	**483**	0	99	37	16	0	0	66
	S2	1	27	2	**652**	19	2	0	28	1	89
	W2-1	18	104	14	0	**338**	188	49	21	0	46
	W2-2	18	0	162	0	17	**407**	128	0	0	56
	W2-3	0	0	78	0	0	424	**230**	0	0	31
	W2-4	19	27	0	0	10	3	0	**654**	19	89
	Water	0	0	4	0	15	1	0	629	**83**	11
	User's accuracy (%)	40	55	33	100	57	38	53	49	81	Overall **50%**

4.2.3 Vegetation characteristics used as model input variables and parameters

The above vegetation classes were modelled in the 3D radiative transfer model DART based on vegetation type specific variables and parameters. We use the term 'variable' for spatially varying model input data and the term 'parameter' for spatially invariant model input within a given vegetation type. The variables are green and standing dead leaf, and wood area index as well as canopy and standing dead leaf height.

For each vegetation type, we either measured the variables in the field or compiled values from literature (see Appendix Section 4.A.1 for details). We computed spatially varying green leaf area index (LAI) from NDVI following *Street et al.* (2007); *Campioli et al.* (2009):

$$\mathrm{LAI} = a \cdot \exp\left(b \cdot \mathrm{NDVI}\right). \tag{4.2}$$

We obtained a and b by fitting the exponential relationship on five quantiles (0.05, 0.25, 0.50, 0.75, and 0.95) of the in situ LAI measurements and UAV-derived NDVI of all pixels within the vegetation type in question (see Appendix, Table 4.6).

We used linear regressions with observed LAI to spatially extrapolate wood and standing dead leaf area index as well as canopy and standing dead leaf height:

$$x = p \cdot \mathrm{LAI} + q \tag{4.3}$$

where x is the extrapolated variable and p and q represent vegetation type specific parameters (see Appendix, Table 4.6). The average and standard deviation of all variables for each vegetation type were computed for the entire transects (Table 4.3).

Table 4.3: Summary of canopy properties used as model input; for plant area index and canopy height mean ± standard deviation of all transects are provided; these values were also used for homogeneous cover types; the species column indicates which species was used for inclination angle and optical properties measurements.

Class	Description	Area index			Height (cm)		Species	Background
		Green leaf	Wood	Standing dead leaf	Canopy	Standing dead leaf		
G4	Tussock sedge	0.24±0.10	-	-	12.2±0.0	-	*E. vaginatum*	S1-2
S1-1	Dwarf birch	1.08±0.16	1.02±0.09	-	26.6±1.2	-	*B. nana*	S1-1, removal
S1-2	Lichen-rich shrub	-	-	-	-	-	-	S1-2
W2-1	Wet sedge	1.32±0.33	-	1.53±0.38	47.6±5.4	22.1±2.6	*E. angustifolium*	Water
W2-2	Dry sedge	0.55±0.23	-	0.64±0.26	24.4±1.9	15.8±1.8	*E. angustifolium*	W2-3
W2-3	Peat moss	-	-	-	-	-	-	W2-3
W2-4	Waterlogged sedge	0.46±0.12	-	-	33.2±2.0	-	*E. angustifolium*	Water
Water	Shallow water	-	-	-	-	-	-	Water

An example of all input variables for one transect is shown in Figure 4.3. The LAI included *Betula* and *Salix* shrubs as well as *Eriophorum* and *Carex* sedges but neither dwarf shrubs < 5 cm such as *Vaccinium* spp. and *Ledum palustre*, nor grasses nor forbs. The LAI only made up for about half of the total plant area index (PAI) with about one fourth being wood and one fourth standing dead leaves. The average canopy height was 25.3 cm in the study area.

Input parameters were the angle distribution and the optical properties of green leaves, standing dead leaves, and wood and the background reflectance. We measured the leaf angle distribution with the method by *Pisek et al.* (2011) and applied a correction for green and standing dead sedge leaves and wood (Appendix, Figure 4.A.2). The correction was necessary because it was not possible to identify wood or sedge leaves that were perpendicular to the image plane (see Appendix, Section 4.A.2 for details).

Optical properties of green and standing dead leaves and wood were measured in the field with a dual integrating sphere design for reflected and transmitted light in the spectral range from 400–950 nm (Jaz & SpectroClip, Ocean Optics). From 950–2500 nm, we used dwarf birch (*Betula nana*) optical properties measured at the same field site for leaves, standing dead leaves, and wood of all species (Fieldspec4, ASD Inc., *Juszak et al.*, 2014, Appendix, Figure 4.A.3a).

We measured spectral background reflectance on canopies lower than 5 cm and on shallow water (Fieldspec4, ASD Inc.). Reflectance measurements of *Vaccinium* dominated lichen-rich shrub communities (S1-2) were selected as background for

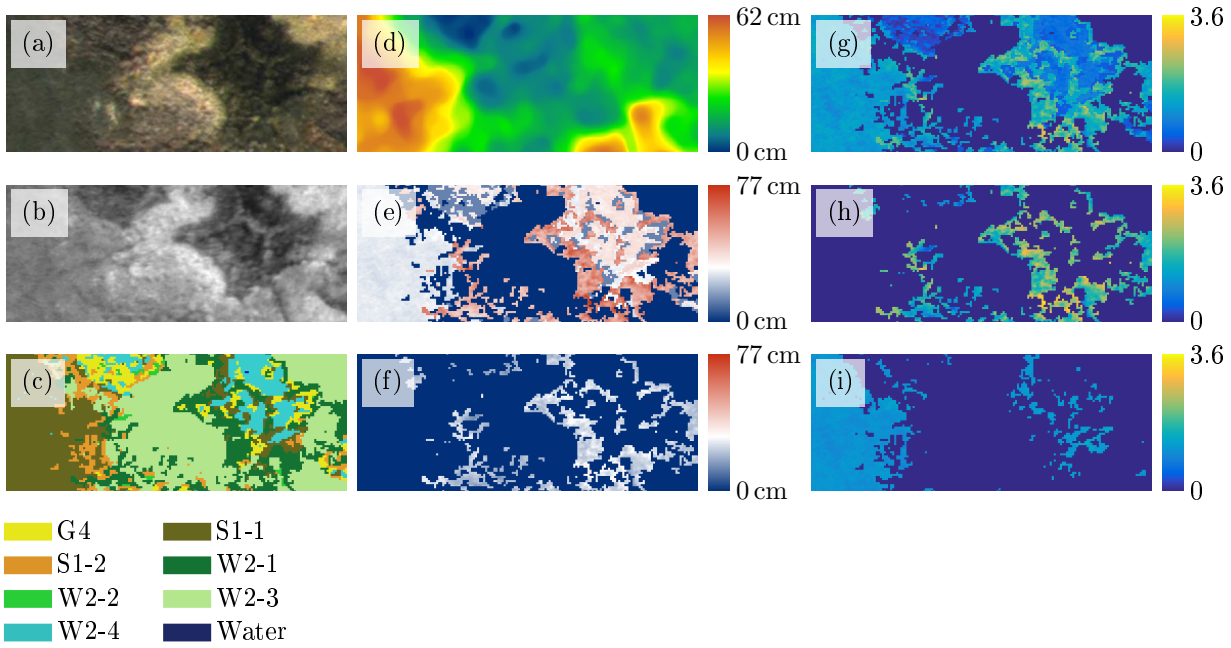

Figure 4.3: Input variables for one transect (10 m × 25 m) as an example; (a) RGB image, (b) near infra-red image, (c) vegetation map, (d) digital surface model, (e) canopy height, (f) standing dead leaf height, (g) green leaf area index, (h) standing dead leaf area index, and (i) wood area index.

tussock sedge tundra as the species composition was similar. Peat moss (W2-3) dominated below dry sedge vegetation and was thus used as background for modelling. For wet and waterlogged sedges we used measurements of shallow water as background (Table 4.3). Additionally, we used the background reflectance below dwarf birch (S1-1) after removing the shrubs (see *Juszak et al.*, 2014). At least four measurements were averaged per background type (Appendix, Figure 4.A.3b).

4.2.4 Selection of subsets for modelling

Model simulations were done with two different land cover complexities. First, we simulated homogeneous land cover types without topography and second, we simulated the radiation budget of 21 transects including heterogeneous tundra vegetation. For both complexities, we used the same average canopy properties (Table 4.3).

To quantify the shortwave radiation budget of heterogeneous tundra, we selected subsets of the study area on the vegetation map (Figure 4.2b). We chose transects within an area covered by a single flight because of artefacts due to inhomogeneous illumination (Figure 4.2a). Due to the low vegetation height of the tundra in our study area (Table 4.3) and the small scale spatial variability of vegetation type, we selected 21 transects of 10 m × 25 m representative of the landscape scale. Each

transect represented a transition between dwarf birch dominated vegetation (S1-1) and other vegetation types or water (Figure 4.4). As low shrub tundra (S2) was restricted to lake and river banks, we did not choose transects in this vegetation type. The remaining six vegetation types and water were each dominating three transects. Additionally, all vegetation types were represented in smaller fractions also in the other transects. The patch size distribution differed among the transects.

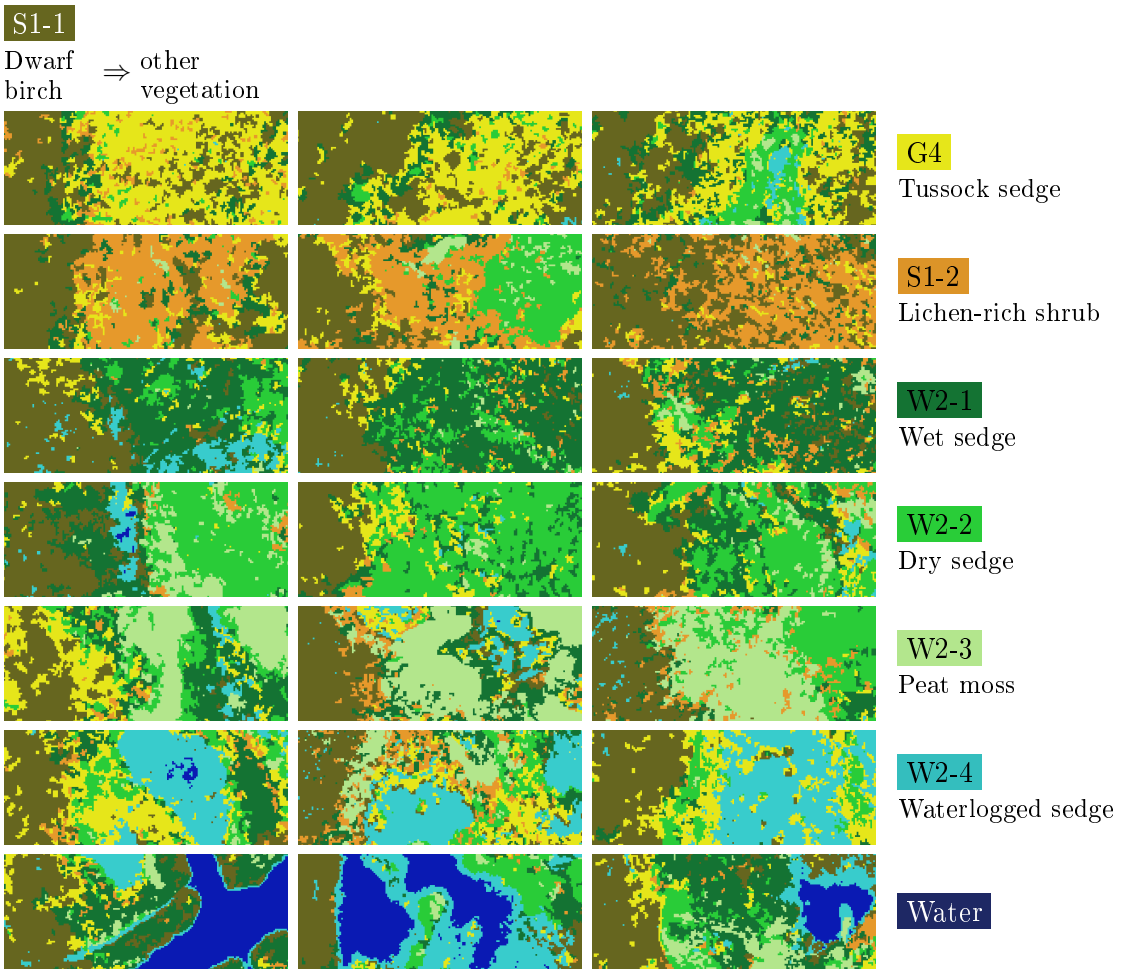

Figure 4.4: Vegetation maps of 21 transects (10 m × 25 m); the rows represent different major vegetation types sorted by the mean characteristic length of the major type with simple polygons on the left and more complex polygons on the right.

We computed explanatory variables at two different levels, for the whole transects and for each vegetation patch. For the transects, we used the explanatory variables (I) average Plant Area Index (PAI) including green leaves, standing dead leaves, and wood, (II) fractional cover of each vegetation type, and (III) mean characteristic length, which we defined as mean ratio of patch area to patch perimeter. The radiation budget of a single patch is influenced by its vegetation type, PAI, canopy

height, neighbouring vegetation, and topography. Topography influences the radiation budget more at the patch scale than at the transect scale, because the transects are mostly flat on average while mounds and tussocks influence local slope and exposition. We assessed the influence of local variability and boundary effects using the characteristic length of the single vegetation patches in relation with their radiation budget.

4.2.5 Radiation budget simulations with DART

We simulated the radiation budget using the DART 3D radiative transfer model (*Gastellu-Etchegorry et al.*, 1996; *Grau and Gastellu-Etchegorry*, 2013, Version 5.6.1). This model has been applied and validated extensively, for example for forest canopies (*Malenovský et al.*, 2008; *Schneider et al.*, 2014), crops (*Duthoit et al.*, 2008), and tundra dwarf shrubs (*Juszak et al.*, 2014). The DART model formed part of the radiation transfer model intercomparison (RAMI) (*Pinty et al.*, 2001; *Widlowski et al.*, 2015).

Model configuration

We parametrised the DART radiative transfer model for 21 transects and 9 homogeneous cover types. Vegetation was parametrised in a voxel grid filled with turbid media scatterers (*Schneider et al.*, 2014). Three types of turbid media were simultaneously considered: green leaves, dead leaves, and wood. Each turbid medium was simulated as vertically homogeneous column within its respective height. However, standing dead leaves of wet and dry sedges were implemented with a lower height than green leaves (Table 4.3). Thus, voxels at low height were dominated by standing dead leaves and higher voxels by green leaves in these two vegetation classes. For the transects, we used the DSM as topography while we simulated the homogeneous cover types without topography (Table 4.4a).

We simulated shortwave radiation fluxes in the MODIS bands 1 to 7 (Table 4.4b) and derived broadband shortwave quantities from a linear combination of bands with coefficients by *Liang et al.* (1999). Additionally, we simulated broadband photosynthetically active radiation (PAR) to assess canopy absorbed PAR (f_{APAR}) and to compare the results with the PAR conversion from three MODIS bands by *Liang et al.* (1999). In the simulations, the illumination was defined by the total irradiance and the fraction of diffuse light for each spectral band (Table 4.4). The spectral irradiance was defined as the reflectance of a Spectralon panel measured on 11/07/2012 using a spectrometer (Fieldspec4, ASD Inc.). All spectrometer measurements within a MODIS band width or the PAR range were convolved to the respective band width. The diffuse fraction in the PAR range was obtained from field measurements under clear sky conditions (Delta-T Devices, BF3). In other

wavebands, diffuse fractions were obtained with DART simulations of atmosphere radiative transfer for conditions at noon mid of July with a subarctic summer atmosphere. We adjusted the aerosol optical depth factor so that the simulated diffuse fraction in the PAR range matched the observations.

Table 4.4: (a) General model configuration and (b) spectral bands with respective irradiance and diffuse fraction (SKYL).

(a)		(b)			
Characteristic	Value	Wavelength (nm)	MODIS band	Irradiance ($W\,m^{-2}\,\mu m^{-1}$)	Diffuse fraction (%)
Mode	Flux-tracking	400–700	-	968	19.0
x, y, z resolution	5.0 cm	459–479	3	1079	25.4
(voxel grid)		545–565	4	1044	13.5
Scene size		620–670	1	930	13.2
- homogeneous cover type	1 m × 1 m	841–876	2	636	7.5
- transects	10 m × 25 m	1230–1250	5	310	3.6
Scene type	Repetitive	1628–1652	6	154	2.0
Topography		2105–2155	7	58	1.3
- homogeneous cover type	no				
- transects	yes				
Vegetation representation	Turbid media				
Sun position	15/07/2015, 1 hour before solar noon				
Atmosphere	Spectral SKYL (from DART)				
No. of directions	193				

Model outputs

We analysed three major model outputs. The first output was the albedo one metre above the soil surface, which we converted from spectral to shortwave albedo (*Liang et al.*, 1999). The second output was shortwave irradiance at the soil surface divided by above canopy irradiance. We call this variable 'transmittance', which equals to '1 - soil shading' (*Benninghoff*, 1952). Canopy transmittance is an important boundary condition for soil heat flux and permafrost thaw (*Briggs et al.*, 2014). We considered the fraction of photosynthetically active radiation absorbed by the canopy (f_{APAR}) as third output. We defined the canopy as vascular vegetation parametrised in the radiative transfer model. Therefore, mosses, lichen and vascular

plants lower than 5 cm, which we treated as background, were not included in our f_{APAR} calculation. Although f_{APAR} is closely linked to canopy transmittance, it provides additional information as it is associated with photosynthesis and thus the carbon cycle (*Ruimy et al.*, 1994; *Huemmrich et al.*, 2010). Before analysing the model output, we removed 2 m borders on all sides of the transects to eliminate edge effects. Thus the remaining transect size was 6 m × 21 m (120 × 420 pixels).

4.2.6 Weighted averages

In addition to the 3D radiative transfer simulations, we estimated the radiation budget of each transect using weighted averages. In a first step, we computed the radiation budget of homogeneous vegetation types with DART using the same mean vegetation type specific variables as for the transect simulations in a small and repetitive scene (Table 4.3). DART was configured in the same way as for the transects, but the scene was smaller and did not include topography (Table 4.4). In a second step, we computed the average albedo, transmittance, and f_{APAR} weighted by vegetation type fraction for each transect.

4.2.7 Statistical analysis

We estimated the importance of different transect characteristics on the mean radiation budget using an analysis of variance (ANOVA, f-test) (*R Core Team*, 2015, Version 3.2.3). The response variables were transect albedo, transmittance, and f_{APAR}. The explanatory variables were the fraction of shrub cover (S1-1), the combined fraction of water and waterlogged sedges (W2-4), mean transect plant area index, and mean transect patch characteristic length. We did a 4-way ANOVA per response variable without taking into account interactions between explanatory variables. Our model first accounted for the explanatory variable with the highest correlation coefficient with the response. We changed the order of the other three response variables in the model to assess the robustness of the model results and possible relationships among the explanatory variables. The radiation budget simulated with the 3D radiative transfer model was compared with the weighted averages using a paired t-test (*R Core Team*, 2015, Version 3.2.3).

4.3 Results

4.3.1 Drivers of the radiation budget at the landscape scale

We compared modelled radiation budgets of different transects to estimate the importance of different landscape elements. Transect albedo was strongly negatively related with water fractional cover (including waterlogged sedges (W2-4), Pearson

correlation $R = -0.91$, Figure 4.5b). Although the correlation between albedo and shrub cover was weak ($R = 0.19$, Figure 4.5a), shrub cover significantly affected the albedo if the statistical model accounted for the water effect first (Table 4.5a). After accounting for water cover, neither plant area index (PAI) nor the average patch characteristic length were significantly related to transect albedo, even if the model did not account for shrub cover first. The correlation between each pair of explanatory variables was less than $R^2 = 0.3$.

Table 4.5: The effect of transect characteristics on simulated (a) albedo and (b) transmittance expressed as ANOVA results; water cover includes waterlogged sedges (W2-4). Each characteristic takes one of 20 degrees of freedom (df); please note the different variable order; *** $P \leq 0.001$; ** $P \leq 0.01$; ns: not significant.

(a) Albedo

Explanatory variables	df	F	P
Water cover	1	277.90	***
Shrub cover	1	38.15	***
Plant area index	1	0.01	ns
Characteristic length	1	0.89	ns

(b) Transmittance

	df	F	P
Plant area index	1	617.38	***
Shrub cover	1	9.71	**
Water cover	1	2.13	ns
Characteristic length	1	0.91	ns

Modelled transect f_{APAR} and shortwave transmittance were strongly negatively correlated ($R = -0.99$). PAI strongly reduced canopy transmittance ($R = -0.98$, Figure 4.5g) and increased f_{APAR} ($R = 0.98$, Figure 4.5k). The second most important driver of both variables was shrub cover ($R = -0.34$ and $R = 0.28$ for transmittance and f_{APAR}, respectively, Figure 4.5e, i), which significantly influenced transmittance but not f_{APAR} when PAI was accounted for (Table 4.5b). Water cover and average patch characteristic length did not significantly affect transmittance and f_{APAR}.

4.3.2 Comparison of DART model results with weighted averages

We analysed results of 3D radiative transfer simulations as compared to a weighted average of the radiation budget with given fractional cover per vegetation type and average type properties. Using the 3D DART model, transect albedo values appeared to be significantly lower than the weighted average ($p < 0.001$, Figure 4.6a). On average, the albedo reduction when using the 3D approach was 0.004, corresponding to 3% of the average albedo, and the maximum absolute difference was 0.01.

Canopy transmittance was on average 3% higher in the 3D model results as compared to the weighted average (Figure 4.6b). However, this was not the case for all transects. For single transects, the absolute transmittance difference was between

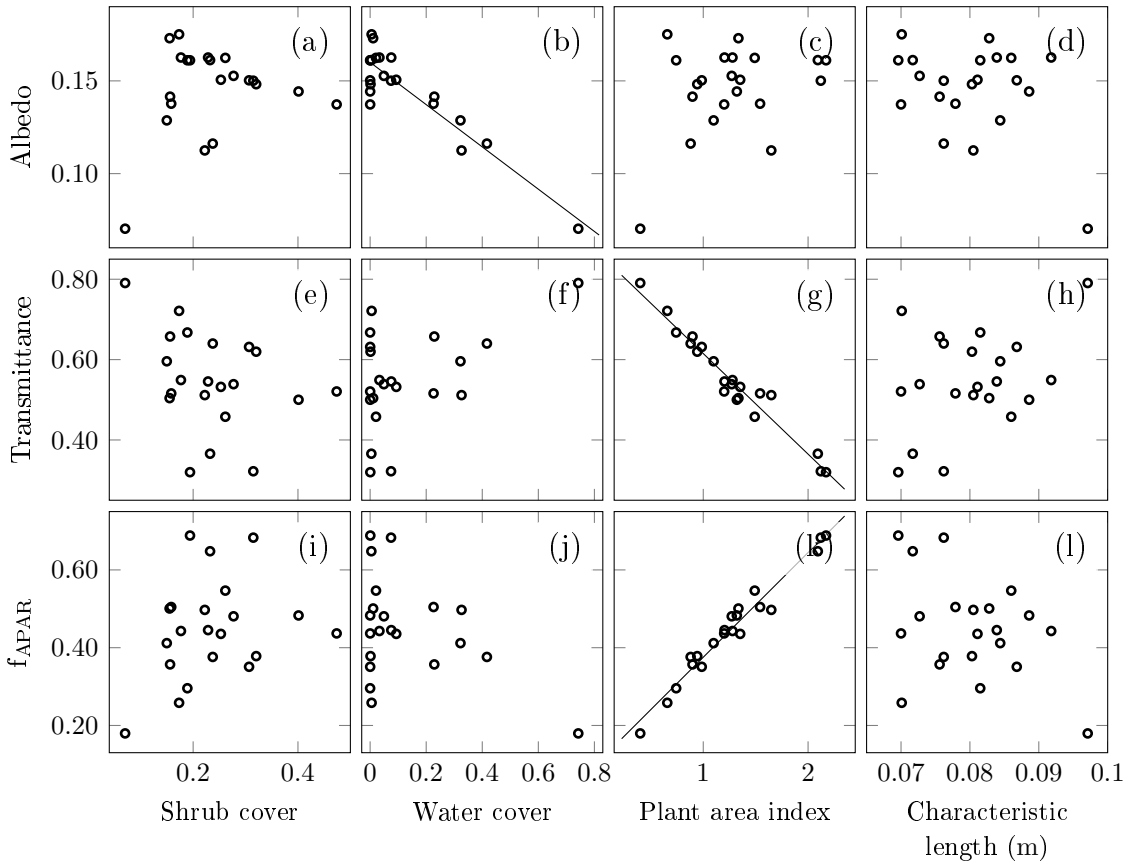

Figure 4.5: Modelled DART transect (a–d) albedo, (e–h) transmittance, and (i–l) f_{APAR} as a function of (a, e, i) transect shrub cover (S1-1), (b, f, j) combined cover of water and waterlogged sedges (W2-4), (c, g, k) plant area index, and (d, h, l) average characteristic length; regression lines are included for data with $R^2 > 0.25$.

-0.06 and 0.09. The 3D model results were significantly different from the weighted averages ($p < 0.05$). Transmittance modelled with the 3D approach was generally higher than with the weighted average for transects with low PAI and low shrub cover (results not shown).

As described above, f_{APAR} was strongly negatively related with transmittance. Consequently, f_{APAR} was slightly reduced when using the 3D radiative transfer model as compared to the weighted average (Figure 4.6c). The absolute difference varied between -0.10 and 0.06, on average 3% of the total f_{APAR}. However, the difference between f_{APAR} modelled with DART and f_{APAR} calculated from weighted averages was not significant ($p > 0.1$).

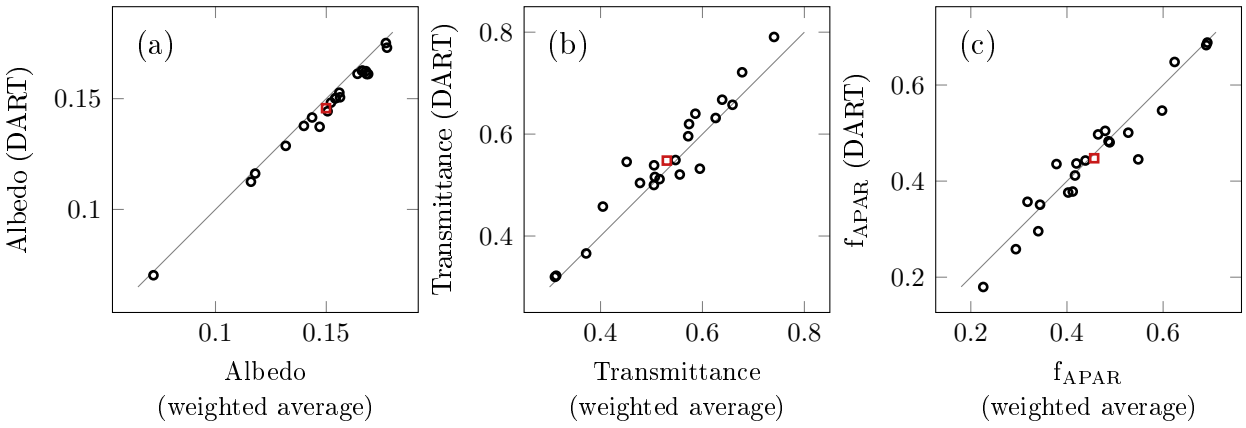

Figure 4.6: (a) Albedo, (b) transmittance, and (c) f_{APAR} modelled for each transect with DART and computed with weighted averages; each point represents one transect, the mean of all transects is the red square, the line represents a 1:1 relationship.

4.3.3 Small scale spatial variation in albedo, transmittance, and f_{APAR}

At the patch scale, variations in PAI, canopy height, topography, and neighbouring vegetation type led to considerable variations of albedo, transmittance, and f_{APAR} among cells of the same type (Figure 4.7). As observed for the whole transects (Figure 4.6a), albedo was on average lower in the 3D transect simulation as compared to the simulation of single vegetation types (Figure 4.7a). However, this was not the case for the vegetation types with relatively low albedo (dwarf birch (S1-1), waterlogged sedges (W2-4)) and water. While the transmittance of highly transmitting vegetation types was reduced due to boundary effects, it was increased in denser vegetation (Figure 4.7b). Boundary effects strongly increased f_{APAR}, especially for vegetation types with dense canopies that absorbed much radiation anyway (Figure 4.7c).

While transmittance and f_{APAR} were highly negatively correlated at the landscape scale, the negative correlation between them was only $R = -0.43$ at the patch scale. Patch f_{APAR} remained highly positively correlated with PAI ($R = 0.96$). However, the correlation between patch transmittance and PAI was less strongly negative ($R = -0.57$) than at the landscape scale.

The larger the patch area was in relation to its perimeter, the smaller was the influence of bordering vegetation, LAI variation, and topography on the patch average albedo, canopy transmittance, and f_{APAR} (Figure 4.8). The characteristic length at which a radiation budget component is independent of boundary effects can be estimated from the convergence of an upper and a lower hull curve. Depending on the vegetation type, variation in patch albedo and f_{APAR} was small for patches with characteristic lengths above 0.5 m on average, while patch transmittance was variable until 0.7 m. However, the variability among vegetation types was large (Fig-

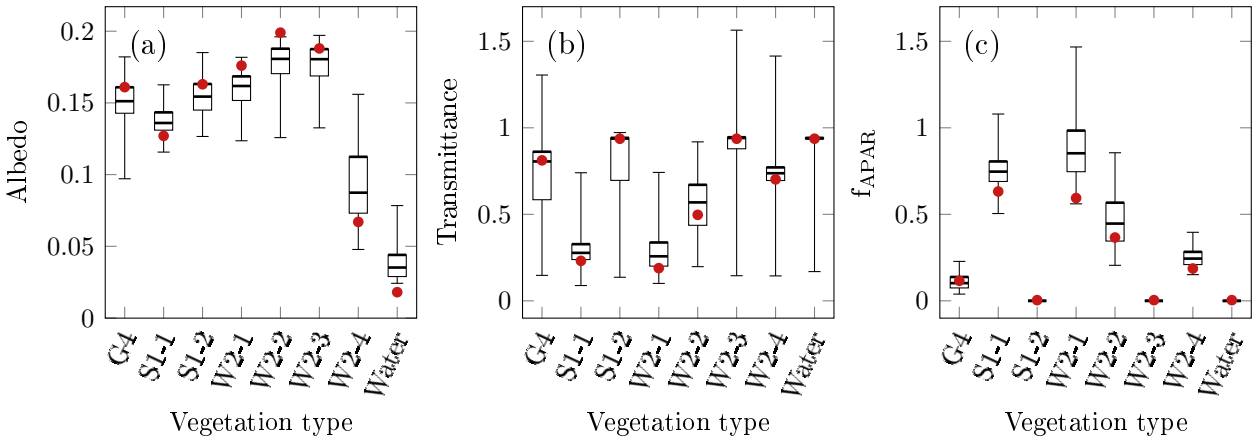

Figure 4.7: Modelled radiation budget for all cells of all transects, (a) albedo, (b) transmittance, and (c) fraction of PAR absorbed by the canopy (f_{APAR}); the boxes indicate the 0.25, 0.5, and 0.75 quantiles, the whiskers are the 0.02 and 0.98 quantiles; red dots indicate the modelling results using homogeneous cover types.

ure 4.8). Thus, the characteristic length scale depended on the radiation quantity in question and on vegetation type. In terms of patch area, converging hull functions indicated small boundary effects for patches of 7 m^2 or more for albedo and f_{APAR} and 10 m^2 area for transmittance, respectively. Although only 2% of the patches were larger than 7 m^2, such large patches represented 65% of the total area in the modelled transects.

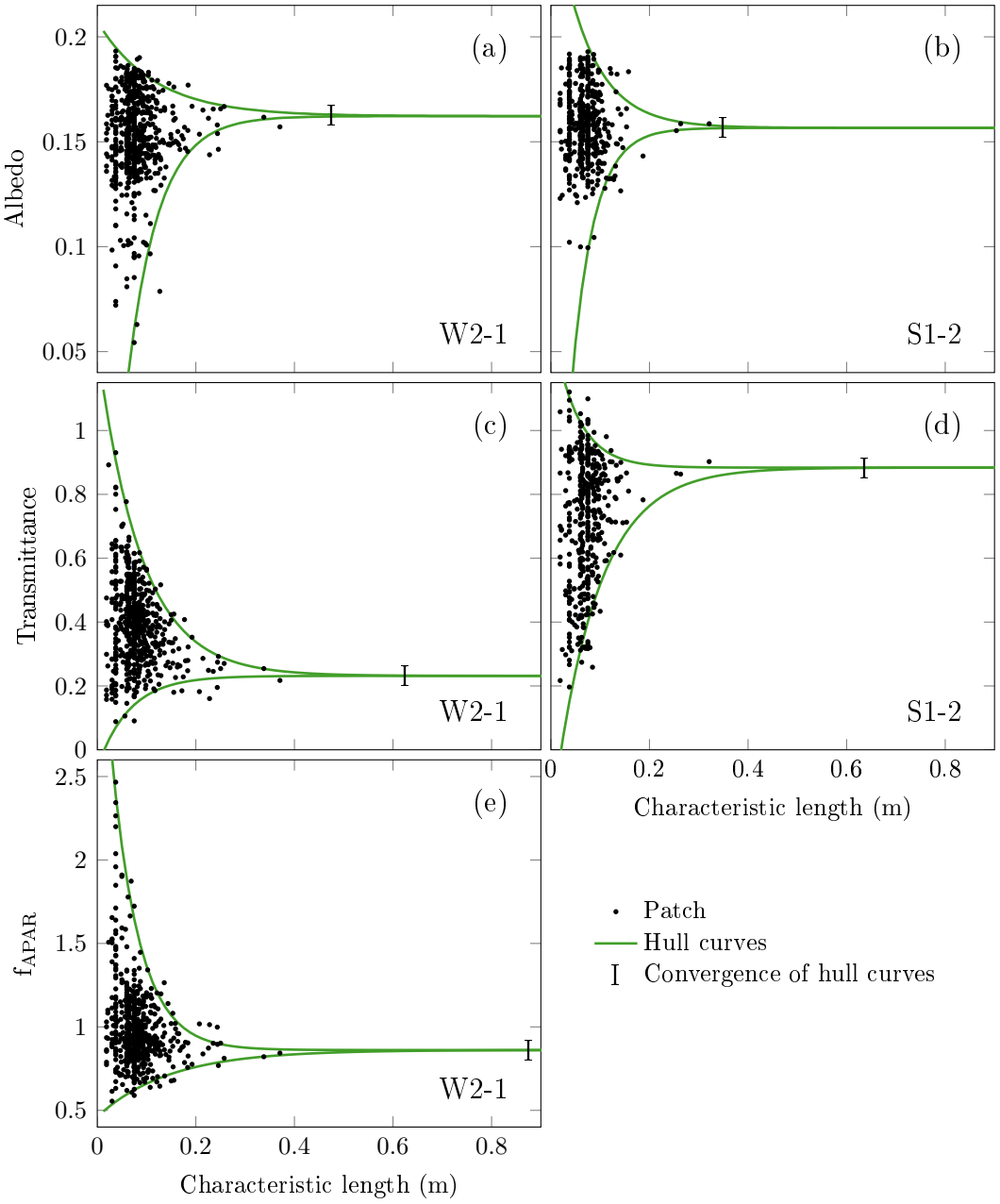

Figure 4.8: Mean patch (a,b) albedo, (c,d) transmittance, and (e) PAR absorbed by the canopy (f_{APAR}) as a function of characteristic length (patch area to perimeter ratio) for wet sedges (W2-1) and lichen-rich shrubs (S1-2); one point per patch; the green lines represent exponential curves fitted to the outer points as hull curves and converging at the indicated point (threshold = 0.001).

4.4 Discussion

We identified the most important drivers of the radiation budget at the landscape scale, quantified the differences between 3D modelling and simple weighted averages, and assessed the local scale variability of radiation fluxes.

4.4.1 Vegetation map and canopy characteristics

Our vegetation map had a Kappa coefficient of 0.44 with the original nine land cover classes. The achieved accuracy was lower than in other studies classifying tundra vegetation using orthomosaics (*Lantz et al.*, 2010; *Muster et al.*, 2012) or high resolution satellite imagery (*Atkinson and Treitz*, 2012; *Virtanen and Ek*, 2014; *Siewert et al.*, 2015). The difficulties of our classification were mostly due to similar reflectance properties of several classes.

The vegetation classification accuracy and the 3D modelling (Figure 4.7a) indicate that several of the pre-defined vegetation classes have similar reflectance properties. This functional similarity is in contrast to the differences among vegetation types in terms of species composition and canopy properties such as height or plant area index (PAI). As these canopy properties translate into specific radiation transmittance and absorptance characteristics, they play an important part in the radiation budget at the landscape scale and are thus included in the 3D radiative transfer modelling.

We used field observations of spatial leaf area index (LAI) variability within vegetation classes and an NDVI map to extrapolate LAI over the whole study region. Several studies showed strong relationships between NDVI and LAI in Arctic tundra (*Shippert et al.*, 1995; *Riedel et al.*, 2005; *Campioli et al.*, 2009), especially if each vegetation type was treated separately (*Street et al.*, 2007). *Williams et al.* (2001) estimated a mean error of prediction of around 16% when extrapolating tundra LAI based on NDVI. However, we were not able to validate the spatial LAI distribution due to a lack of observations in the same time period as the orthophotos. All other input variables, namely wood area index, standing dead leaf area index, canopy height, and standing dead leaf height, were extrapolated based on linear relationships with LAI. We are not aware of any other study which spatially extrapolated these canopy characteristics in a tundra ecosystem.

We found that green leaves only contributed about one half to the total PAI. The importance of wood for Arctic shrub canopies has been highlighted by *Thompson et al.* (2004) who measured larger wood area indices than leaf area indices in tundra shrubs. *Juszak et al.* (2014) emphasised the role of wood for the radiation absorption of tundra dwarf shrubs. The large area of standing dead sedge leaves found at our study site is relevant for the radiation budget, as dead leaves can contribute significantly to canopy reflectance (*Chapin et al.*, 2000b) and shading (*Caldwell et al.*, 1974).

4.4.2 Drivers of the radiation budget at the landscape scale

We found that the fraction of standing water was by far the most important driver of landscape albedo (Table 4.5). The importance of standing water for spatial and temporal tundra albedo variations has been highlighted in several studies (*Lafleur et al.*, 1997; *Gamon et al.*, 2012) and has been acknowledged by defining lake area as essential climate variable (*Bojinski et al.*, 2014). Arctic tundra often comprises small scale water bodies which cannot be detected based on medium resolution satellite imagery such as Landsat-7 (*Muster et al.*, 2012; *Virtanen and Ek*, 2014). In polygonal tundra, this can lead to a 35% lower estimate of water surface area and translate into high uncertainties in energy fluxes, especially evapotranspiration (*Muster et al.*, 2012). While small water bodies are included in the satellite albedo estimates, they are neglected in medium and large scale landcover maps (such as *Gould et al.*, 2003; *Walker et al.*, 2005). Simplified landcover maps and underestimation of the water surface area can affect large scale modelling results, especially in wetlands. Our results showed that wetlands with high cover of peat mosses or dry sedges had the highest albedo within the tundra landscape at our site, while water bodies and waterlogged sedges had the lowest albedo (Figure 4.7).

The second significant driver of landscape albedo was shrub cover, which was more important than PAI. The importance of shrub cover is well known, as shrub expansion is associated with a positive feedback to global warming (*Chapin et al.*, 2005; *Blok et al.*, 2011c; *Lawrence and Swenson*, 2011). However, at the larger scales shrub cover and PAI are linked (*Thompson et al.*, 2004; *Beringer et al.*, 2005) and their relative importance for growing season albedo cannot easily be disentangled in modelling studies that increase both values simultaneously (such as in *Lawrence and Swenson*, 2011; *Bonfils et al.*, 2012).

PAI explained almost all variability of transmittance and f_{APAR} among the transects. The importance of PAI for f_{APAR} (*Myneni et al.*, 1997; *Asner et al.*, 1998; *Shabanov et al.*, 2000) and transmittance has been highlighted in other studies (*Flerchinger et al.*, 2009; *Juszak et al.*, 2014). At the landscape scale, average patch characteristic length (the ratio of patch area and perimeter) did not significantly influence the radiative budget (Table 4.5).

4.4.3 Comparison of DART model results with weighted averages

Our simulations indicated that weighted averages overestimate the albedo of complex landscapes as compared to 3D radiative transfer modelling. This finding is consistent with studies of the forest and the global radiation budget (*Rowe*, 1993; *Yuan et al.*, 2014). However, in our study, the difference was only about 3% (Figure 4.6). The small effect may be due to low canopy height in our simulations (*Dickinson et al.*, 2008).

Simulations with the 3D approach on average increased canopy transmittance by only 3% as compared to the simple approach. The underestimation of transmittance by simple models is consistent with *Knyazikhin et al.* (1997), who found that 1D simulations overestimate the decline of solar radiation in a canopy with depth.

In line with albedo and transmittance, the f_{APAR} results revealed little differences between the 3D model and a weighted average, while other studies report significant underestimation of f_{APAR} using 1D models (*Kobayashi et al.*, 2014; *Loew et al.*, 2014; *Yuan et al.*, 2014). *Kobayashi et al.* (2014) show that 1D simulations in boreal forests underestimate the fraction of light absorbed by the canopy (f_{APAR}) by about 50%. As for albedo and transmittance, the small effect that we found is most likely due to the low vegetation at our study site. The tundra canopy in our model is less than 80 cm tall. Additionally, we explicitly include canopy gaps as independent vegetation types in both simulations, 3D and weighted averages.

Overall, we find that tundra albedo, transmittance, and f_{APAR} are less sensitive to model complexity than to landcover type and canopy characteristics at the landscape scale. As the effect of different model complexities is much smaller than the variability among the transects, we suggest that more effort should be made to estimate water cover, shrub cover, and PAI than to more physically based modelling at the landscape scale. However, the 3D model results depend on the model parametrisation and may differ more strongly from weighted averages when plants are simulated as objects instead of turbid media, or when the turbid media include vertical gradients. Furthermore, we find that at the small scale the heterogeneity of the radiation budget can be substantial and may require 3D modelling in case of non-linear feedbacks.

4.4.4 Small scale spatial variation in albedo, transmittance, and f_{APAR}

In agreement with *Oliphant et al.* (2006), we found that at the 5 cm pixel and the patch scale albedo, transmittance, and f_{APAR} can be substantially different from mean values of the respective vegetation types. While transmittance variability may influence permafrost thaw locally (*Briggs et al.*, 2014), the importance of f_{APAR} for the canopy energy, water, and carbon budget has been shown in several studies of tundra ecosystems (*Caldwell et al.*, 1974; *Huemmrich et al.*, 2010; *Tagesson et al.*, 2012). For example, evapotranspiration is sensitive to spatial heterogeneity of radiation (*Song et al.*, 2009; *He et al.*, 2014). *He et al.* (2014) simulated lower water stress in a forest with a model that included 3D radiative fluxes and canopy structure as compared to a homogeneous case due to the light limited vegetation in shaded areas. *Sprintsin et al.* (2012) showed strong effects of the radiation scheme on modelled gross primary production.

Boundary effects extended to larger patches for canopy transmittance as compared

to albedo and f_{APAR}. This may be a consequence of the different relevant levels. While albedo and f_{APAR} are determined by the mean scattering centre of the canopy, transmittance is defined below canopy. Thus lateral shading may affect the radiation at soil level further away from the tall elements. The characteristic length scale differed between vegetation types, which indicates complex interaction between the spatial vegetation distribution and the radiation budget.

Although our landscape scale simulations revealed little differences between the radiation budget of the 3D model and weighted averages, we find that at the small scale, heterogeneity can be substantial. As tundra landscapes typically comprise small scale vegetation patterns (*Gamon et al.*, 2013; *Virtanen and Ek*, 2014), local variability of the shortwave radiation budget may influence larger scale energy, water, and carbon fluxes in case of non-linear responses.

4.5 Conclusions

Our modelling results show that the surface area of water bodies and waterlogged sedges is the most important driver of tundra albedo in summer. Shrub cover is the second most important control and explains more of the spatial albedo variations than plant area index. Canopy transmittance and absorbed PAR are almost entirely controlled by plant area index at the landscape scale. At the landscape scale, 3D radiative transfer modelling results in about 3% lower albedo and canopy absorbed PAR and 3% higher canopy transmittance as compared to a weighted average of the radiation budget of the vegetation types contributing to the landscape. Thus, the effect of different model complexities is much smaller than the variability depending on the cover type and canopy plant area. However, using the 3D radiative transfer model we found considerable variability of albedo, transmittance, and canopy absorbed PAR at the local scale. This local scale radiation variability may influence photosynthesis and evapotranspiration. Our results highlight that large scale modelling studies need to thoroughly parametrise the local scale water cover and the plant area index, which does not only include green leaves but also standing dead leaves and wood.

Acknowledgements

We thank Tim Grünberg, Institute of Fluid Dynamics, ETH Zurich, for helping with the projection of leaf angles, raster calculations, and computational resources. This work is supported by the Swiss National Science Foundation through project grant 140631 and by the University of Zurich research priority program on Global Change and Biodiversity (URPP GCB).

4.A Detailed description of the methods

4.A.1 Input variables for radiative transfer modelling

Plant area index We used different methods to measure green leaf area index (LAI) for shrubs and graminoids in the field. *Betula nana* (S1-1) projected LAI and wood area index were measured non-destructively using 1 m × 1 m point quadrat grids where we vertically lowered a needle at 81 points and recorded all contacts with leaves or wood. We did in total 25 measurements on 10 plots within two growing seasons. We computed LAI by dividing projected LAI by the average point quadrat efficiency. The point quadrat efficiency was estimated in two destructive harvests to be 0.78 for *B. nana* leaves and 0.76 for *B. nana* wood.

For estimating *Eriophorum angustifolium* (W2-1 and W2-2) LAI, we used an allometric approach, which involved counting leaves and destructively measuring single leaf areas. For sub-class W2-1, we measured canopy height and counted all tillers and the number of green leaves per tiller on 16 squares of 100 cm^2 on 1 m^2. We did in total 30 measurements on eleven plots within two growing seasons. For sub-class W2-2, we measured canopy height, counted tillers and leaves on four plots of 50 cm × 50 cm. We combined the information of both *E. angustifolium* sub-classes with destructively measured leaf sizes as in *Juszak et al.* (2016a). We measured the total standing dead leaf area of *E. angustifolium* on three destructive plots of wet sedge tundra (W2-1) by weighing all standing dead leaves and scanning a subset.

Eriophorum vaginatum (G4) LAI was estimated on seven plots of 50 cm × 50 cm. We counted the number of leaves per plot and multiplied it by the average area of single leaves that was obtained from scanning.

We extrapolated the LAI spatially using the NDVI and an exponential function (Equation 4.2). To avoid unrealistically large LAI values, we reduced all LAI which were more than 1.5 times higher than the maximum observation to the maximum observed LAI. The parameters a and b are shown in Table 4.6 and the statistics of the modelled LAI per vegetation type in the transects in Table 4.3. We used literature values of LAI for low shrub tundra (S2) and waterlogged sedge tundra (W2-4). For low shrub tundra we took the minimum (LAI=0.77) and maximum (LAI=1.95) values from Imnavait creek water tracks, Alaska by *Williams et al.* (2006) and fitted them to the 0.05 and 0.95 quantiles of the NDVI data. The literature LAI values were consistent with other sources (*Beringer et al.*, 2005). For *Carex* spp. dominated waterlogged sedge tundra we used LAI=0.4 (*Carex* spp. dominated wetland near Toolik, Alaska, *Shaver and Chapin* (1991); *McFadden et al.* (2003)) as median and took the maximum value of LAI=0.65 (wet sedges without shrubs, S3, Imnavait creek, Alaska, *Williams et al.* (2006)) to fit to the 0.95 quantile.

We used linear regressions with observed LAI to spatially extrapolate the other input variables (Equation 4.3, Table 4.6). Due to the lack of observations for low

Table 4.6: Parameters a and b for computing LAI from NDVI with an exponential equation (Equation 4.2) and parameters p and q for for computing other variables from LAI with a linear equation (Equation 4.3) for each vegetation type; canopy and standing dead leaf height in mm.

Variable \ Type		G4	S1-1	S2	W2-1	W2-2	W2-4
LAI	a	0.00002976	0.02618681	0.05929370	0.01425009	0.00202313	0.01523543
	b	12.6308	4.8927	4.4051	6.1931	8.8501	4.7804
Wood area index	p	0	0.536	0.536	0	0	0
	q	0	0.439	0.439	0	0	0
Standing dead	p	0	0	0	1.16	1.16	0
leaf area index	q	0	0	0	0	0	0
Canopy height	p	0	7.21	80	16.7	8.51	16.7
	q	12.2	18.8	40	25.5	19.7	25.5
Standing dead	p	0	0	0	8.13	8.13	0
leaf height	q	0	0	0	11.3	11.3	0

shrub tundra wood area index, we used the same parameters that we obtained from the fit of dwarf birch leaf and wood area index (Table 4.6). We estimated standing dead leaf area and green leaf area index destructively at three plots of wet sedges (*E. angustifolium*, W2-1). Due to the limited number of observations, we forced the regression through zero assuming that standing dead leaves are always associated with plants which also have green leaves. We used the same parameters also for dry sedges (*E. angustifolium*, W2-2).

Canopy and standing dead leaf height We used two different approaches to measure canopy height. For dwarf birch (*B. nana*, S1-1) and wet sedges (*E. angustifolium*, W2-1) we measured canopy height at 25 points of a 1 m × 1 m point quadrat grid at the same time and plots as our LAI estimate. At the *E. angustifolium* plots, we also measured standing dead leaf height above the water or wet litter surface. On the other hand, we measured canopy height of single individuals on six tussock sedge plots (*E. vaginatum*, G4) and five dry sedge plots (*E. angustifolium*, W2-2).

We extrapolated canopy height spatially for each type using a linear regression between canopy height and LAI measured at the same plots at the same time (Equation 4.3). For tussock tundra, the linear fit showed a negative relationship between LAI and canopy height for the six observations. Instead of a negative slope, we used a constant canopy height independent of the leaf area. For low shrub tundra we adjusted the parameters p and q in a way that the final canopy height varied between 1 and 2 m (Table 4.3), a range that we observed in the field. We used the parameters of *E. angustifolium* dominated wet sedge tundra (W2-1) also for *Carex*

ssp. dominated waterlogged sedge tundra (W2-4, Table 4.6). We only observed a layer of standing dead leaves below *E. angustifolium*, in the vegetation types W2-1 and W2-2. Standing dead leaf height was related to LAI using the same parameters for both types although our field measurements covered only type W2-1.

4.A.2 Input parameters for radiative transfer modelling

Leaf and wood angle distribution We measured the leaf angle distribution in three different ways depending on species and organ. For *B. nana* leaves, we used the method by *Pisek et al.* (2011). This method employs carefully levelled photography of the vegetation taken from all cardinal directions. In each image, we identified leaves which were perpendicular to the image plane. We marked these leaves in the image and calculated the leaf inclination angle (Leaf normal – nadir, Figure 4.A.1a). In total, we measured 1294 *B. nana* leaves. We fitted a beta function to the data to reduce the scatter (Figure 4.A.2a). Beta functions are commonly used for leaf inclination angle distributions (e.g. *Goel and Strebel*, 1984; *Strebel et al.*, 1985; *Wang et al.*, 2007).

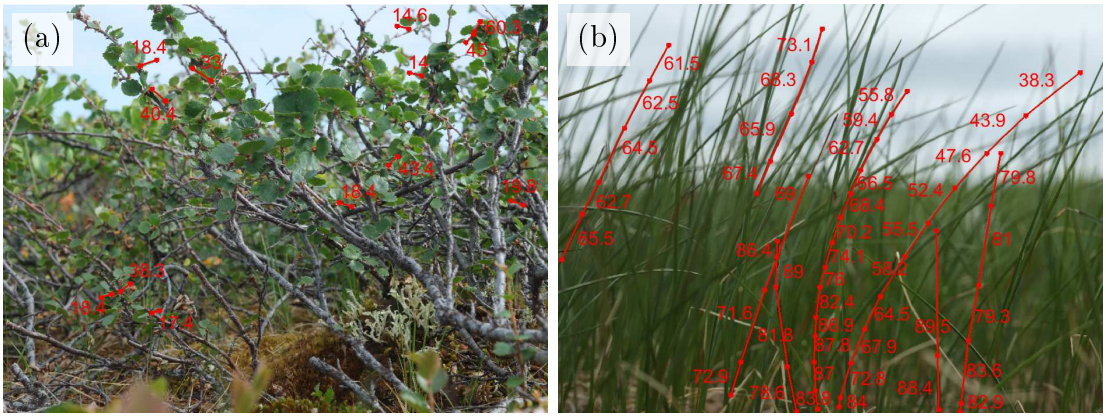

Figure 4.A.1: Sample pictures used for measuring leaf angle distribution of (a) *B. nana* and (b) *E. angustifolium*; red numbers indicate the leaf inclination angle of a leaf or leaf segment.

We had to modify the method by *Pisek et al.* (2011) for *B. nana* wood and *E. angustifolium* green and standing dead leaves as it was not possible to identify cylindrical or triangular objects perpendicular to the image plane. In this case, we marked all segments of green leaves, standing dead leaves, and wood that were visible on the images, even the segments pointing towards or away from the camera, in total more than 8000 per organ (Figure 4.A.1b). For leaves that were inclined towards or away from the camera, this raw data overestimated the leaf inclination angle. We corrected for this effect in three steps. First, we weighted the histograms

of measured inclination angles by the length of each identified segment. We did that for each azimuth view direction separately and then took the mean of all probability distributions as we did not identify an equal amount of segments in each view direction. Second, we converted the observed, projected leaf inclination angle distribution to the real inclination angle distribution assuming a random distribution of leaf azimuth angles. This step involved binning the leaf inclination angles and computing weights for each bin which describe, how much of which original leaf angle has contributed to this bin given random azimuth angles. The real leaf angle distribution was computed by solving a linear system of equations with the projected leaf angle distribution and the weights of all bins. Third, we corrected for the fact that leaves appeared shorter on the images if they were not perpendicular to the image plane. Finally, we fitted a beta function to the data (Figure 4.A.2b–d) in the same way as for *B. nana* leaves.

For *E. vaginatum* and *Salix pulchra*, we manually measured the leaf inclination angles of 21 and 39 leaves, respectively. As the number of measured leaves was small, we did not fit a beta function to the data but selected the best fitting standard leaf angle distributions, 'erectophil' for *E. vaginatum* and 'uniform' for *S. pulchra* (Figure 4.A.2e, f) (*de Wit*, 1965).

Leaf and wood optical properties We measured optical properties of plant organs in the field using an Ocean Optics SpectroClip probe (Figure 4.A.3). The probe features two integrating spheres of about 3.5 cm diameter, one for the reflectance and the second for the transmittance of the sample. The sample is fitted between the two spheres with a measurement area of 5 mm diameter. In addition to our measurements of samples, we regularly took reference measurements with a 99% and a 50% reflectance standard and without sample. The integrating spheres were too small in comparison to the sample size to provide data without correction for multiple interactions between light and sample (*Jacquez and Kuppenheim*, 1955). Thus we did a first-order correction of the raw reflectance and transmittance measurements. We estimated the fraction of light that interacted twice with the sample before being recorded using a comparison between the readings of the 99% standard and the 50% standard. Although we could only calibrate this fraction for non-transmitting samples, we used the same value also for the correction of the transmittance signal. The correction of the samples transmittance involved assuming equal reflectance and transmittance of both leaf sides. We tested the correction for leaves which we measured with the standard procedure, including transmittance, and on a black background.

E. vaginatum leaves were too thin to be measured with the SpectroClip probe in the standard procedure. Therefore, we fixed multiple leaves next to each other on a sample holder. As all leaves together covered the measurement area, we could use the

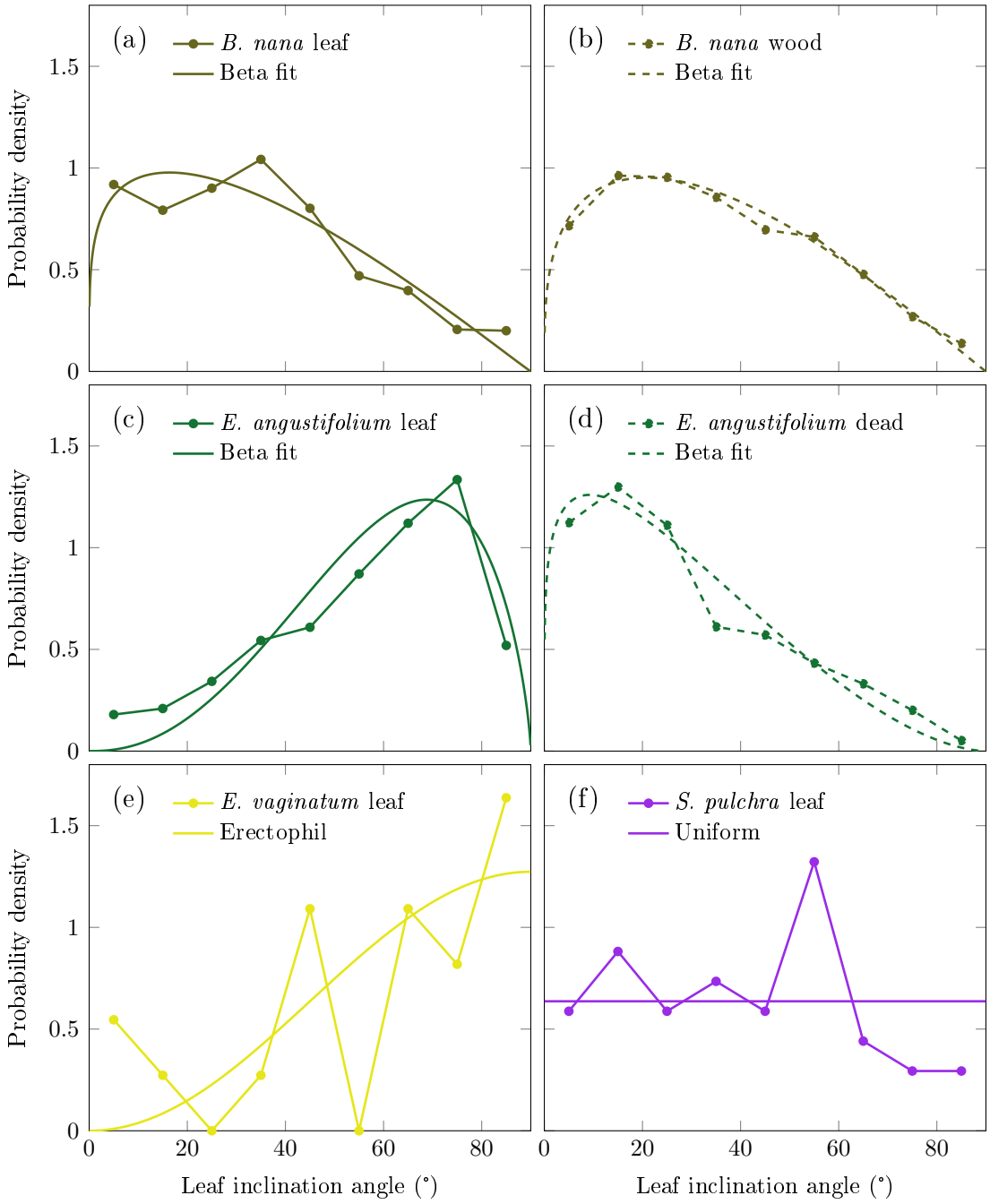

Figure 4.A.2: Probability density (bin width: 1 rad = 57.3°) of measured green leaf, standing dead leaf, and wood inclination angle distributions and fitted functions of (a) *Betula nana* leaves, (b) *B. nana* wood, (c) *Eriophorum angustifolium* green leaves, (d) *E. angustifolium* standing dead leaves, (e) *Eriophorum vaginatum* leaves, and (f) *Salix pulchra* leaves.

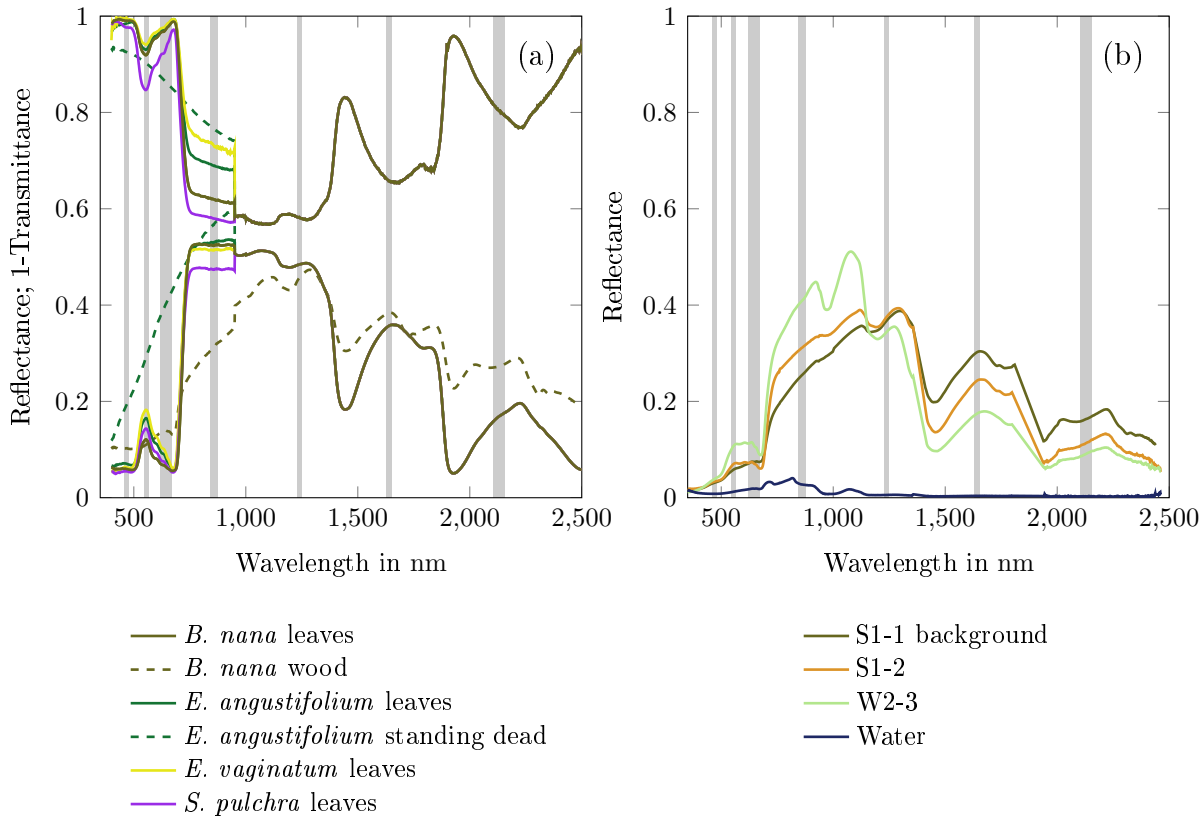

Figure 4.A.3: (a) Upper face reflectance (bottom half) and transmittance (top half) of the major species (bottom face reflectance not shown for clarity) and (b) background reflectance; the grey lines indicate the MODIS bands 1–7 used for modelling.

reflectance measurement without further correction. However, for the transmittance measurement, we had to adjust for the reduced transmittance due to the holder. We estimated the *E. vaginatum* leaf transmittance (T) from the corrected transmittance measurement ($T_{measured}$) and the transmittance of the empty holder ($T_{empty\ holder}$):

$$T = \frac{T_{measured}}{T^2_{empty\ holder}} \tag{4.4}$$

5 General discussion

In this thesis, I used a combination of field measurements and 3D radiative transfer modelling to quantify the effect of tundra vegetation on the radiation budget and to link it to permafrost thaw.

Field data indicated that the canopy albedo of dwarf shrubs (*Betula nana*) was lower than the albedo of wet sedges (*Eriophorum angustifolium*). However, the absolute albedo difference was small and the net radiation above canopy was almost equal for both vegetation types (Research question 1, Chapter 2). Wet sedges shaded the soil more efficiently than dwarf shrubs, mainly because of the standing dead leaves. Thus, more energy for warming and thawing the soil was available below dwarf shrubs. In contrast, we observed a deeper active layer and higher soil heat flux below wet sedges as compared to below dwarf shrubs (Research question 2, Chapter 2). The difference in soil heat flux was mainly attributed to soil properties, in particular the thermal conductivity which was about five times higher in the waterlogged sedge soil as compared to the peat layer below dwarf shrubs.

While field observations are mostly restricted to current canopy properties, radiative transfer modelling can extend the analysis to possible future states of the vegetation. Additionally, modelling can help to understand which of the canopy components influence the radiation budget most. We found that for dwarf shrubs the proportion of wood as compared to leaves was an important driver of canopy albedo and the amount of radiation absorbed by the canopy (Research question 3, Chapter 3). On the other hand, canopy albedo was quite insensitive to total plant area at a constant leaf to wood ratio. Chapter 3 also served as a proof of concept for modelling tundra vegetation as turbid media using the DART 3D radiative transfer model.

Although dwarf shrubs and wet sedges were two important components of the tundra vegetation, they only covered about 25% of the landscape at the Kytalyk research site and other types influenced the radiation budget significantly at the landscape scale (Research question 4, Chapter 4). In particular, the fraction of open water and waterlogged sedges (*Carex* spp.) was an important driver of landscape albedo. Furthermore, the plant area index strongly affected canopy absorptance and transmittance. While patch size and spatial distribution did not significantly influence the radiation budget at the landscape scale, they contributed to local variability and thus may affect other energy fluxes such as evapotranspiration.

In Sections 5.1 to 5.4, I discuss in more detail the key results of all three chapters

including some results that have not been presented yet. In particular, all chapters show how vegetation controls the radiation budget (Section 5.1), an effect that may be altered by vegetation diversity at the landscape scale (Section 5.2). All chapters stress the importance of expanding the focus from green leaves to wood and standing dead plant material (Section 5.3). Additionally, I show in more detail how much radiation is absorbed by the background below all major vegetation types (Section 5.4).

5.1 The role of vegetation in the radiation budget

In this thesis, I quantified the influence of vegetation on the radiation budget. Two major factors can be distinguished. The first factor is vegetation composition, either at the species level or based on functional types. The second factor are canopy characteristics such as leaf area index and canopy height. While I concentrated on the difference among species in Chapter 2 and on canopy properties of a single species in Chapter 3, Chapter 4 includes both, different vegetation types and spatial variability of canopy properties.

Effects of vegetation type

Albedo differences among Arctic tundra vegetation types have been observed at many tundra locations (*Eugster et al.*, 2000; *Beringer et al.*, 2005; *Gamon et al.*, 2012). In a detailed comparison between Arctic dwarf shrubs and wet sedges I found that wet sedges had a 0.02 higher growing season albedo (Figure 2.4). Additionally, I observed the largest difference between shrubs and sedges in the snowmelt period when the albedo decreased ten days earlier at the dwarf shrub vegetation because the snow melted earlier. Differences in snowmelt timing are common between shrub and graminoid tundra (*Sturm et al.*, 2005; *Pomeroy et al.*, 2006) and act as a major positive feedback between shrub cover and air temperature (*Chapin et al.*, 2005). I found larger differences in growing season albedo between dry and waterlogged wetland vegetation than between dwarf shrubs and wet sedges (Figures 4.7a, 5.1). Thus, the fractions of open water and waterlogged sedges (W2-4) are the most important drivers of albedo in patterned tundra and need to be estimated carefully.

As most vegetation types have a relatively low leaf area, the background below the canopy also influences the albedo. For example, waterlogged litter and shallow water have a much lower albedo than dry mosses or lichen (Figure 4.A.3b). The background albedo changes depending on soil moisture or water level. Therefore, I observed a higher albedo of dwarf shrubs and especially of wet sedges in the drier growing season of 2013 as compared to 2014 (Figure 2.4).

While several studies measured or modelled the canopy transmittance of Arctic shrubs (*Chong et al.*, 2012; *Williams et al.*, 2014), I presented data and model results

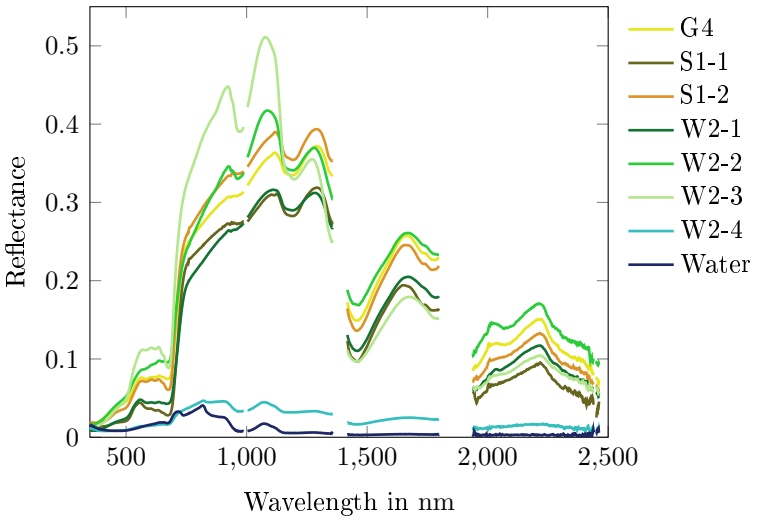

Figure 5.1: Mean measured canopy nadir reflectance of all major vegetation types and water; the tundra vegetation types are tussock sedges (G4), dwarf shrubs (S1-1), lichen-rich dwarf shrubs (S1-2), wet sedges (W2-1), dry sedges (W2-2), peat mosses (W2-3), and waterlogged sedges (W2-4) (see Figure 1.3).

including several types of graminoid tundra. I found that wet sedge tundra shaded the soil more efficiently than dwarf shrubs, especially due to standing dead leaves (Figure 2.7). However, the plant area index and thus the canopy structure was more important for landscape scale transmittance and canopy absorptance than the vegetation type (Figure 4.5).

Effect of canopy structure

Large-scale comparisons most often attribute albedo differences to leaf area index (LAI, *Thompson et al.*, 2004; *Beringer et al.*, 2005) or canopy height (*Oke*, 1987). I did not find a relationship between canopy reflectance and LAI of dwarf shrubs and wet sedges in the field (Figure 5.2a). The wet sedges even had a taller canopy and higher albedo than the dwarf shrubs (Figure 5.2b). Except for very low shrub densities, simulations showed that dwarf shrub albedo was relatively insensitive to plant area index (Figure 3.7a). However, I found that for shrubs the ratio between wood and leaf area was more important for the albedo than the total leaf area (Figure 3.7b). Wet sedge albedo, on the other hand, strongly depended on the amount of open water and bright litter (see the difference among wet (W2-1), dry (W2-2) and waterlogged sedges (W2-4) in Figures 4.7a, 5.1). Thus, for low tundra vegetation other drivers influence canopy reflectance more than canopy LAI or height, namely non-green plant material and background albedo (Section 5.3).

On the other hand, I found that transmittance was strongly influenced by leaf and plant area index (Figures 4.5g, 5.2c). This was also observed for the amount

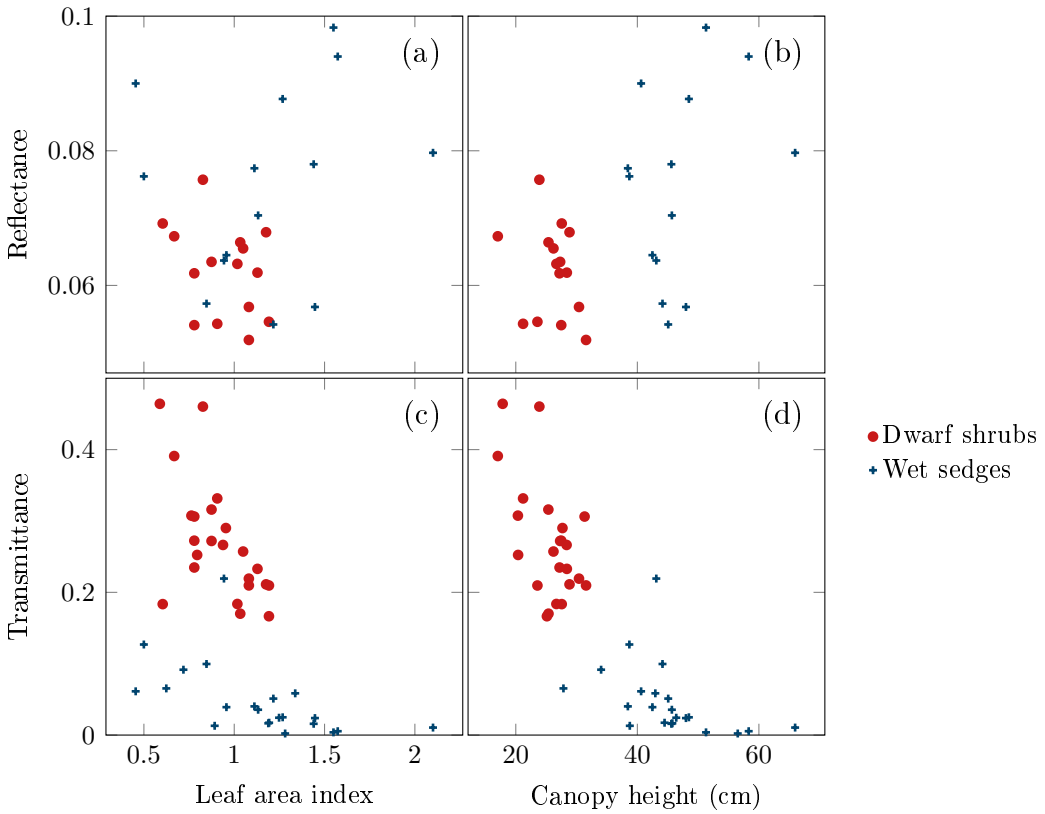

Figure 5.2: (a,b) Canopy nadir reflectance (400–950 nm) and (c,d) transmittance (400–700 nm) as a function of leaf area index and canopy height of dwarf shrubs and wet sedges.

of radiation absorbed by the canopy (Figures 3.7a, 4.5k), which agrees well with previous studies (*Asrar et al.*, 1992; *Myneni et al.*, 1997; *Huemmrich et al.*, 2010).

In summary, I found that albedo is more sensitive to vegetation type, which includes the type-specific background. On the other hand, canopy transmittance and absorptance depend strongly on the canopy structure, mainly the plant area index.

5.2 Vegetation diversity and the radiation budget

If different vegetation types deploy different light use strategies, it can be expected that vegetation in more diverse landscapes absorbs more and thus reflects less light than in uniform landscapes. This relationship has been shown in forests (*Hardiman et al.*, 2011; *Jucker et al.*, 2014) and grasslands (*Spehn et al.*, 2000; *Vojtech et al.*, 2008) with varying species diversity. To test the effect of landscape diversity on the radiation budget, I calculated the Shannon diversity (*Shannon*, 1948; *Hill*, 1973) of the transects which were used for the landscape radiation budget calculations in

Chapter 4. The Shannon diversity H describes the entropy of fractional covers p for n vegetation types (Equation 5.1).

$$H = -\sum_{i=1}^{n} (p_i \cdot \ln(p_i)) \tag{5.1}$$

The mean transect albedo and canopy light absorption (F_{APAR}) were not related with vegetation type diversity. I found Pearson's correlation coefficients of $R = -0.06$ between diversity and albedo and $R = -0.03$ between diversity and F_{APAR} (Figure 5.3). I also assessed possible relationships statistically by including diversity in the model described in Section 4.2.7 and found that the effect of vegetation type diversity on albedo, transmittance, and F_{APAR} was insignificant.

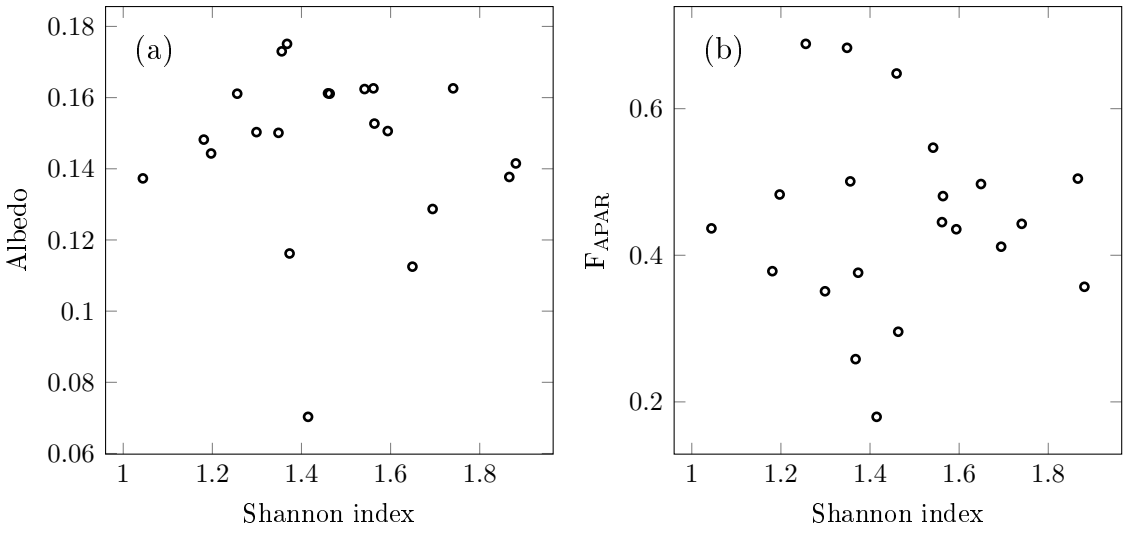

Figure 5.3: Modelled transect average radiation budget, (a) albedo and (b) canopy absorbed photosynthetically active radiation (F_{APAR}) as a function of vegetation type diversity (expressed as Shannon index) within the transects.

Thus I assume that effects of landscape structure or diversity on the radiation budget are small at the landscape scale in low tundra vegetation. However, in my simulations, the diversity was only among patches, while each patch had only one vegetation type with a single species. Several species with different light use strategies at the same location can potentially have a stronger effect on albedo, transmittance, and F_{APAR}.

5.3 Wood and litter are important canopy components

Climate influences vegetation composition and canopy structure, which in turn feed back to climate. Plants growing in Arctic environments have to withstand not only

cold soil and air temperatures (*Billings and Mooney*, 1968; *Nemani et al.*, 2003), but also strong nutrient limitation (*Shaver and Chapin*, 1995) and short growing seasons (*Barichivich et al.*, 2013). Furthermore, competition for light is reduced as compared to other biomes (*Billings and Mooney*, 1968). These conditions foster lower leaf areas indices (LAI, *Ganguly et al.*, 2014) and canopy heights (*Walker et al.*, 2005; *Simard et al.*, 2011) as compared to more favourable conditions. LAI has been defined as essential climate variable (*Bojinski et al.*, 2014) and global LAI estimates have been derived from satellite products (*Camacho et al.*, 2013; *Ganguly et al.*, 2014). However, as I show in all three Chapters, the LAI does not fully characterise the radiative transfer in tundra vegetation. Two other canopy properties are very important for the canopy–radiation interaction in Arctic tundra, namely wood and standing dead plant material.

Wood

Wood area index (synonymous with stem and branch area index, in $m^2\,m^{-2}$) is not commonly estimated in tundra areas. *Thompson et al.* (2004) measured it for forest (0.94), woodland (2.82) and tall shrub tundra (3.22) but not for low shrubs or dwarf shrubs at an Alaskan study site. Except for forest, they found higher wood area indices than LAI. Ecologically motivated studies often measure biomass instead of plant area. *Shaver et al.* (2001) measured dwarf birch (*Betula nana*) above ground wood biomass of $54\,g\,m^{-2}$, which was 79% of the total biomass. Not only the total biomass was larger for stems than for leaves, also the annual wood biomass production was 30% higher than the annual leaf production (*Shaver*, 1986).

Typical examples of dwarf shrubs at the Kytalyk study site are shown in Figure 5.4. Wood area indices were in the same range as LAI for dwarf shrubs (Figures 2.3, 5.5). However, the correlation was not very strong ($R = 0.49$, Figure 5.5) and thus the accuracy of wood area extrapolation based on leaf area is limited (Chapter 4).

In addition to plant area, I measured leaf and wood biomass on two plots of $1\,m^2$ destructively by clipping all ramets at the moss or litter surface, separating leaves from wood and air drying the biomass for about one week before weighing. Wood biomass also included dead branches. The first plot had in total $1115\,g\,m^{-2}$ dry wood mass, mostly *Betula nana* and 1.6% *Salix pulchra*. The total dwarf shrub dry leaf mass was $99\,g\,m^{-2}$. The second plot had a dry wood mass of $1251\,g\,m^{-2}$ (0.6% of it *Salix pulchra*) and $73\,g\,m^{-2}$ dried leaves. Thus, I found that green leaves made up for only 6–8% of the dry biomass, less than in the study by *Shaver et al.* (2001).

However, the importance of wood for the radiative budget is not only based on the large wood area and mass of tundra dwarf shrubs, but also on the radiative properties of the bark. As wood reflects a similar amount of radiation as leaves and does not transmit any radiation (Figures 3.2, 4.A.3), it is a better absorber.

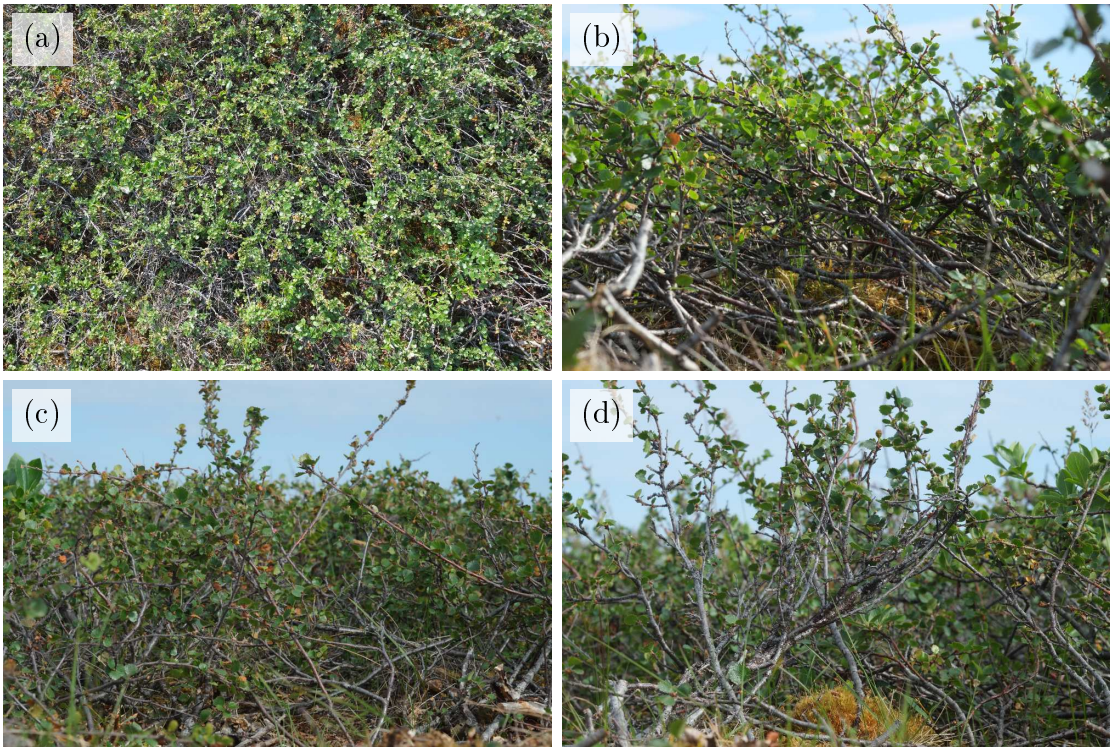

Figure 5.4: Dwarf birch (*Betula nana*) canopy, (a) topview of about $1 \times 1.5\,\mathrm{m}$ and (b–d) profiles; note the large amount of wood as compared to leaves.

In Chapter 3, I simulated the importance of wood for the radiation budget. In case of equal leaf and wood area index, wood contributed 71% to the total canopy absorptance in a loose canopy and 57% in a very dense canopy (Figures 3.7, 5.6a).

The importance of wood for the radiation budget has also been stressed by other authors for different environments. For example, *Kobayashi et al.* (2012) found that wood absorbed 12–39% of the PAR (photosynthetically active radiation) irradiance and 20–52% of the near infra-red irradiance in an oak woodland with an LAI of 0.77. *Asner et al.* (1998) and *Asner* (1998) stress the important contribution of wood to the total canopy absorptance for shrublands and other vegetation with low plant area indices.

Despite the importance of wood for the radiation budget, little field data are available that could help to accurately parametrise climate and land surface models. Currently, wood is treated very roughly in large scale models. Three different approaches are commonly used. The first example is the study on vegetation composition modelling using remotely sensed data of a treeline environment in Canada by *Olthof and Pouliot* (2010). The authors use a fixed wood area index of 0.17 for boreal shrubs (LAI=1.7) without indicating where this value was measured or how it was estimated. In comparison with my study, this wood area index seems to be

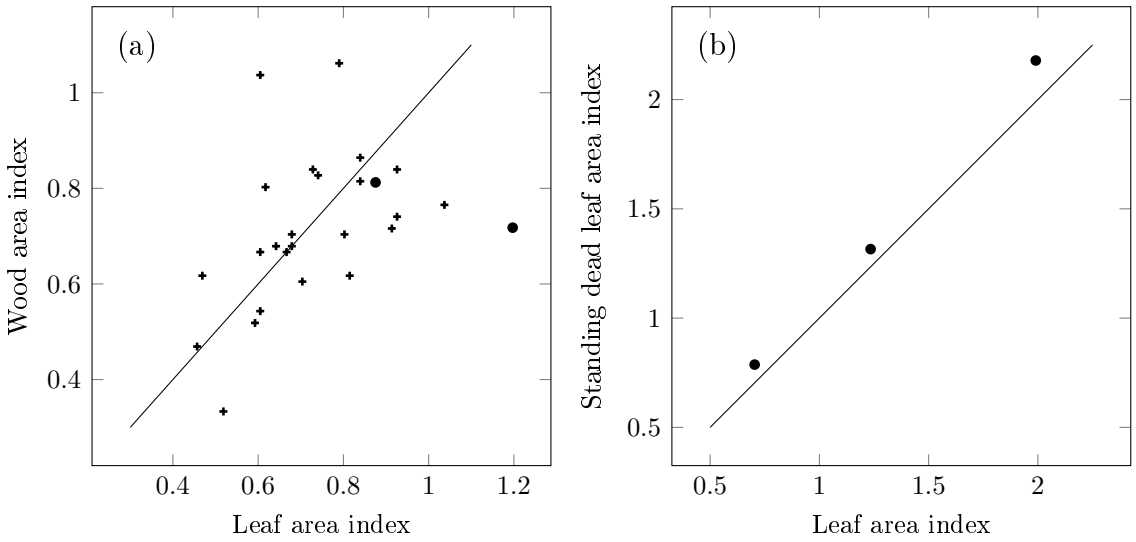

Figure 5.5: (a) Projected leaf and wood area index measured with point quadrat grids (plus) and destructively (circle) on dwarf shrub plots (*Betula nana*) and (b) destructively measured green leaf and standing dead leaf area index on wet sedge plots (*Eriophorum angustifolium*); the lines indicate 1:1 relationships.

very low. I measured an LAI of around 0.9 and a wood area index of 1.1 at dwarf shrub canopies (Figure 2.3). At the landscape scale, the spatially extrapolated wood area index was about 44% of LAI in the Kytalyk study region.

The second example are extensively used global models that compute wood area index from LAI using a constant fraction of 5% for non-forested areas (*Sellers et al.*, 1996; *Myneni et al.*, 1997).

The third example is the Common Land Model (CLM) which uses 17 different landcover types to describe all vegetation on earth (*Zeng et al.*, 2002). In this model, wood and dead leaves are combined to a single variable. The two shrubland types as well as permanent wetlands share common parameters for wood and dead leaf area index, which is a minimum of 1 and a seasonal cycle which adds new dead leaves and removes 50% of the dead leaves that died in the month before (*Zeng et al.*, 2002). This method has been used in other studies (e.g. in *Lawrence and Chase*, 2007). *Lawrence and Swenson* (2011) applied the same method but adjusted the maximal wood area index to 1.5 for Arctic areas. In the notation of *Lawrence and Swenson* (2011) the measure stem area index (SAI) only includes wood, no dead material. However, in that case the steep increase of stem area between August and October in their study is surprising. Several modelling studies, such as *Yi et al.* (2007), use a similar approach as in the CLM. *Yi et al.* (2007) take wood area values from *Bonan* (1996) which is based on the global study by *Dorman and Sellers* (1989). The primary origin of the wood data is probably a study by *Klink and Willmott*

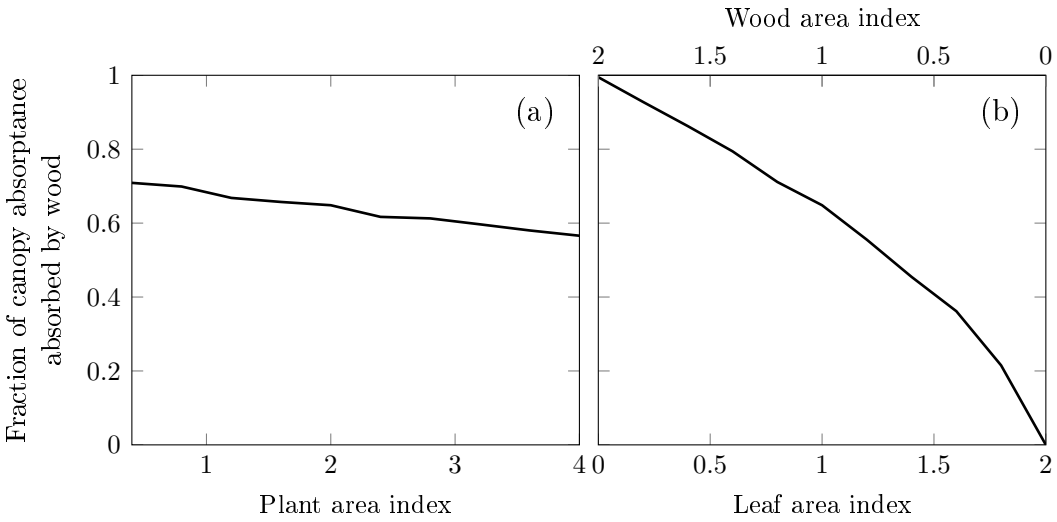

Figure 5.6: Partitioning of the shortwave radiation which is absorbed by the canopy as simulated in Chapter 3 with complexity IV (object branches and turbid leaves), see Figure 3.7, (a) modelled data using leaf area index = wood area index and (b) modelled data using different leaf to wood ratios with plant area index = 2.

(1985), which is not available. While *Dorman and Sellers* (1989) used the terms total LAI versus green LAI, the difference between the two was named stem area index in *Bonan* (1996) and subsequent studies.

Standing dead leaves

In Arctic tundra, decomposition of dead plant material is limited by cold temperature and frozen conditions during most of the year (*Jonasson et al.*, 2004; *Xue et al.*, 2016). The slow decomposition leads to an accumulation of litter on the soil surface. However, unlike shrub litter, dead graminoid leaves of the last growing season do not lie flat on the ground. At the Kytalyk site, dead wet sedge (*Eriophorum angustifolium*) leaves build a 10–20 cm thick layer above the water or wet litter surface (Figure 5.7). I measured *E. angustifolium* green and standing dead leaf area and biomass destructively at three plots, one of 0.25 m^2 in 2013 and two of 1 m^2 in 2014. In all harvests, I found that standing dead leaf area index was about 1.1 times green leaf area index (Table 5.1, Figure 5.5b). While standing dead leaves had a larger area index than green leaves, the dry biomass was roughly 10% lower (Table 5.1).

Standing dead leaves are not only important because of their large area in wet sedge canopies, but also because they have very different properties as compared to green leaves. Dead leaves reflect more light than green leaves (Figure 4.A.3). Additionally, the leaf angle distribution is different. While green *E. angustifolium* leaves are preferentially oriented vertically (erectophil), dead leaves are mostly horizontal (planophil, Figure 4.A.2). Thus dead leaves are effective in shading the soil (Figure 2.7c).

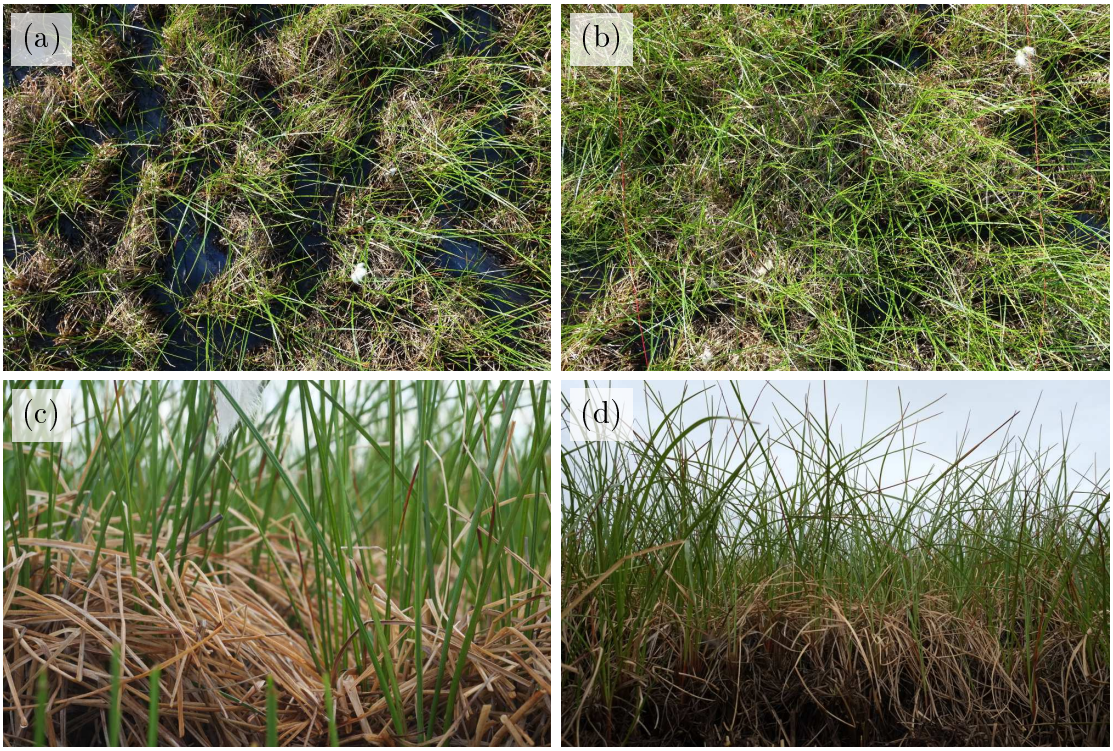

Figure 5.7: Wet sedge (*Eriophorum angustifolium*) canopy, (a,b) topviews of about 1 × 1.5 m and (c,d) profiles; note the amount of standing dead leaves.

The importance of standing dead leaves (synonymous with standing litter) for the tundra radiation budget has been highlighted by *Chapin et al.* (2000b), who found that dead sedge leaves increased the albedo of wet tundra in Alaska. Furthermore, *Caldwell et al.* (1974) showed that particularly at an alpine sedge community dead leaves contributed significantly to the shading of the whole canopy. *Asner et al.* (1998) and *Asner* (1998) stress the importance of standing dead leaves in graminoid communities, where they can significantly contribute to canopy absorptance and reflectance. Additionally, the layer of standing dead leaves may impact the turbulent transfer of heat and moisture between the saturated cold soil and the atmosphere.

In large scale modelling, dead leaves are often combined with wood in a single variable of 'not-photosynthetically active plant area' (e.g. *Bonan*, 1996). This is a strong simplification given the high reflectance and transmittance (especially in the near infra-red) of dead sedge leaves as compared to wood of shrubs or trees (Figure 4.A.3). *Sellers et al.* (1996) considered dead leaves separately. However, in their model, dead leaves were included only after peak LAI and not during the whole year. This is in contrast to my observations in low-arctic tundra. I found that standing dead leaves increased the albedo strongly in the beginning of the growing season before the green sedge leaves were fully developed.

Table 5.1: Results of three destructive green and standing dead leaf area index and leaf biomass measurements of *Eriophorum angustifolium*; the biomass was weighted after air drying the leaves for about one week; green leaves include culms.

Plot	Biomass ($g\,m^{-2}$)		Area index ($m^2\,m^{-2}$)	
	Green leaves	Dead leaves	Green leaves	Dead leaves
1	275	247	2.0	2.2
2	97	89	0.7	0.8
3	170	149	1.2	1.3

In summary, wood and standing dead leaves are important components of tundra canopies and should receive more attention. Currently, field observations of these two variables are very scarce. Additionally, the parametrisations in land surface and climate models often use very rough estimates of wood and standing dead leaf area, which partly were not updated since the 1980s.

5.4 Effect of the radiation budget on permafrost thaw

As vegetation type and structure influence the radiation budget, it can be expected that vegetation also influences the amount of energy which is warming and thawing the soil. It has been shown in a number of studies that the active layer thickness (ALT) differs among vegetation types (*Shiklomanov and Nelson*, 1999; *Anisimov et al.*, 2002). Furthermore, vegetation density and leaf area index (LAI) influence the ALT (*Benninghoff*, 1952; *Fisher et al.*, 2016). Although a number of studies suggest soil shading by vegetation as important factor for soil temperature and ALT (*Benninghoff*, 1952; *Blok et al.*, 2010; *Briggs et al.*, 2014), most studies on ALT distribution either use vegetation type as a proxy (*Shiklomanov and Nelson*, 1999; *Anisimov et al.*, 2002; *Walker et al.*, 2003b; *Fisher et al.*, 2016), or do not consider shading at all (*Hinkel and Nelson*, 2003; *Guan et al.*, 2010).

Dwarf shrubs and wet sedges

In this study, I measured soil temperature, soil heat flux, and ALT in the field below two contrasting vegetation types, dwarf shrubs and wet sedges (Chapter 2). While average growing season soil temperature at 4 cm depth was almost identical, the diel cycle was less pronounced below wet sedges as compared to dwarf shrubs (Figure 5.8a). The damped diel cycle below wet sedges can be explained by the different soil properties. The soil thermal conductivity was five times higher in the waterlogged sedge soil as compared to the peat top-soil below dwarf shrubs (Page 23). Thus the energy was transported downwards faster below wet sedges. Additionally, the heat capacity was more than six times higher below wet sedges than below dwarf shrubs, meaning that it took more energy to heat the sedge soil.

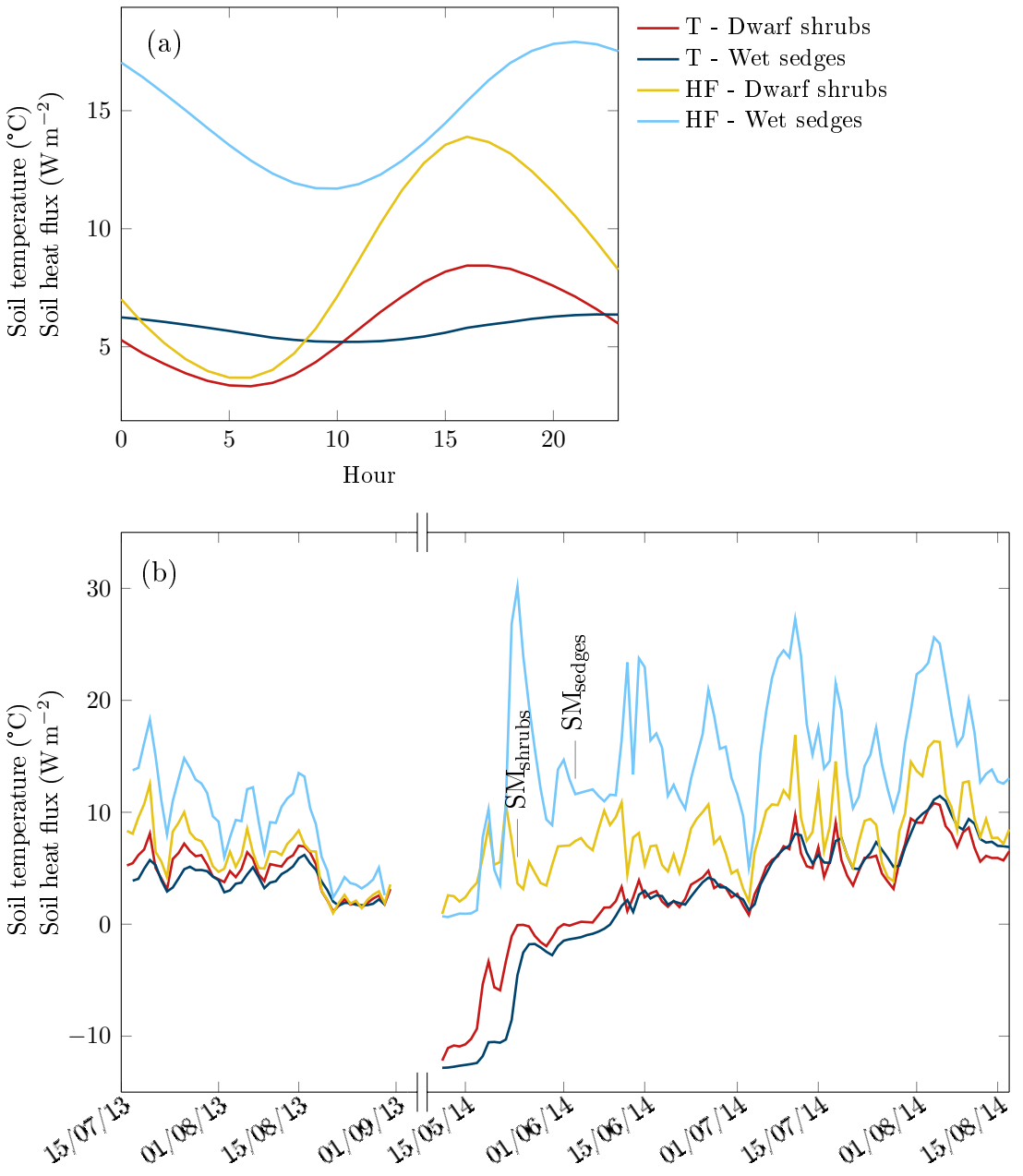

Figure 5.8: (a) Hourly mean values of growing season soil temperature (T) at 4 cm depth and soil heat flux (HF) at 10 cm depth below dwarf shrubs (*Betula nana*) and wet sedges (*Eriophorum angustifolium*); solar noon is at 14:00 local time and (b) diel mean values over the whole measurement period; date of snowmelt (SM) in 2014 indicated for both vegetation types.

Although the average top-soil temperature was similar for dwarf shrubs and wet sedges, the soil heat flux was consistently higher below wet sedges (Figure 5.8b). Therefore, the observed difference in soil heat flux could not be explained by the albedo or transmittance of the two vegetation types (Chapter 2).

As soil properties dominate soil heat flux and ALT differences between dwarf shrubs and wet sedges, it may be more promising to study the radiation budget influence based on variation within vegetation type. Within one type, the soil is less variable than between types. However, also within type, the ALT was not reduced below tall and dense vegetation (Figure 5.9a,b). Neither canopy transmittance, nor reflectance were related to ALT among plots of dwarf shrubs or wet sedges at the end of the growing season (Figure 5.9c,d). Thus I concluded that for dwarf shrubs and wet sedges, soil moisture and soil properties are more important drivers of permafrost thaw than canopy properties, albedo, and transmittance.

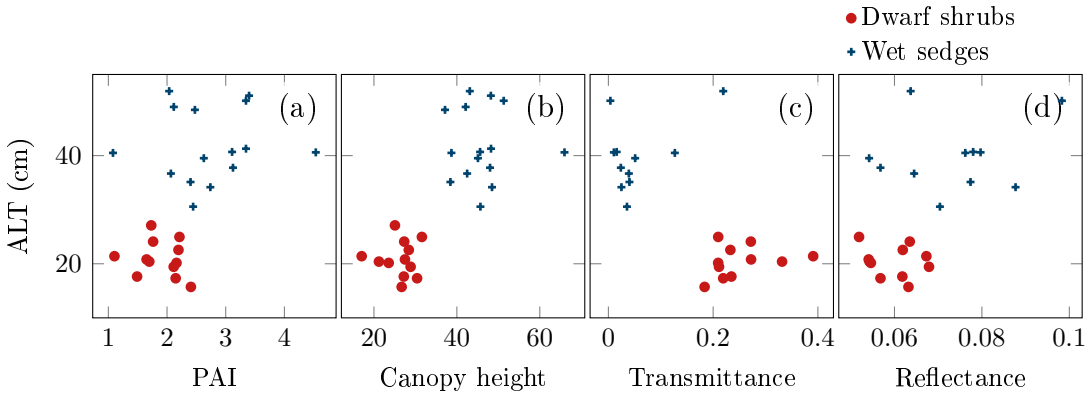

Figure 5.9: End of growing season active layer thickness (ALT) as a function of (a) plant area index (PAI), (b) canopy height in cm, (c) transmittance (400–700 nm) and (d) nadir reflectance (400–950 nm) of dwarf shrubs and wet sedges.

All major vegetation types

The analysis of two vegetation types was extended to all major vegetation types using the data and modelling described in Chapter 4. Furthermore, radiative transfer modelling enabled me to include background albedo and compute the total amount of solar energy absorbed by the background. I found that plant area index and water cover significantly influenced the average amount of solar radiation which was absorbed by the background (Table 5.2, method as in Section 4.2.7). The influence of the plant area index can be explained by soil shading as discussed in Chapter 4. The water cover additionally played a role because water surfaces and waterlogged sedges had a very low background albedo. Thus, the background absorbed a greater fraction of the transmitted radiation. Potential effects of shrub cover or the average patch characteristic length were not significant (Table 5.2, Figure 5.10).

Table 5.2: Simulated effect of transect characteristics on shortwave radiation absorbed by the background expressed as ANOVA results; water cover includes waterlogged sedges (W2-4). Each characteristic takes one of 20 degrees of freedom (df); *** $P \leq 0.001$; ns: not significant.

Explanatory variables	df	F	P
Plant area index	1	515.59	***
Water cover	1	67.34	***
Shrub cover	1	2.10	ns
Characteristic length	1	0.39	ns

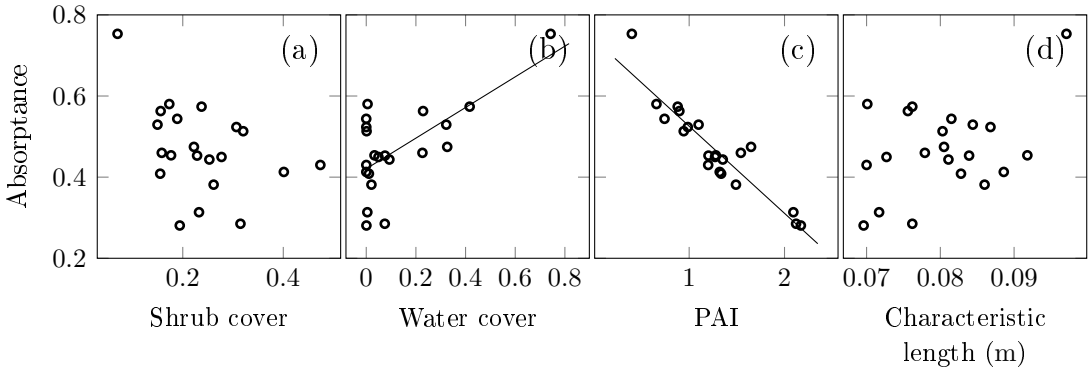

Figure 5.10: Modelled fraction of shortwave radiation absorbed by the background depending on transect (a) shrub cover (S1-1), (b) combined cover of water and waterlogged sedges (W2-4), (c) plant area index (PAI), and (d) average characteristic length; regression lines are included for data with $R^2 > 0.25$.

Even through canopy structure and background were very different for dwarf birch (S1-1) and wet sedges (W2-1), the amount of energy absorbed by the background was similar (Figure 5.11). Thus, the model results agreed well with the observations in the field (Chapter 2). However, other vegetation types showed very different values. While dwarf shrubs and wet sedges were the two types with the lowest amount of radiation absorbed by the background because of the high plant area index, vegetation types with less dense canopies fostered a higher energy flux to the background (Figure 5.11). Below the three types which have been simulated without canopy (lichen-rich shrubs S1-2, peat moss W2-3, and water), the background absorbed everything that was not reflected.

The background in the DART simulations included not only soil but also cryptogams and plants of < 5 cm height. Thus, the radiation that was absorbed by the background did not necessarily reach the soil. Cryptogams can insulate the soil and reduce the soil heat flux (*Beringer et al.*, 2001; *Blok et al.*, 2011a). Further-

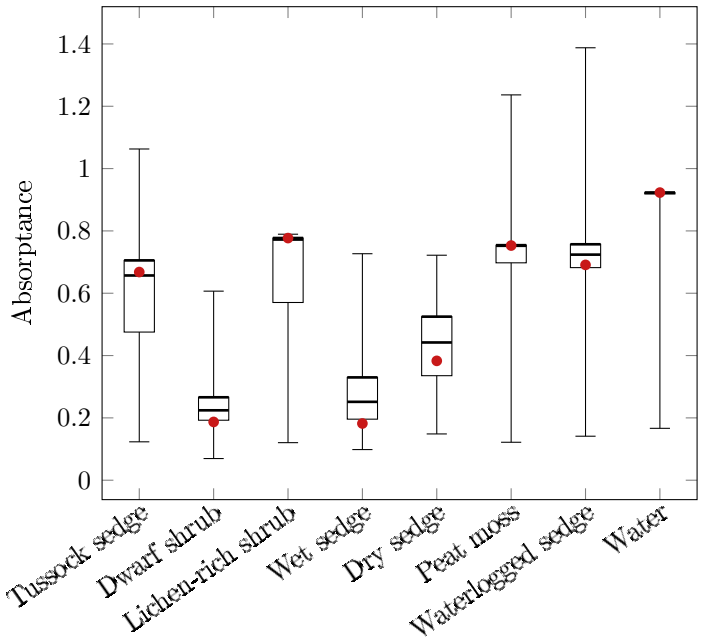

Figure 5.11: Modelled fraction of shortwave radiation absorbed by the background for all cells of all transects (compare Figure 4.7).

more, specific soil thermal properties are associated with each vegetation type and strongly affect the soil heat flux (Chapter 2). However, the amount of shortwave radiation absorbed by the background differs substantially among the vegetation types. Therefore, it is likely that the active layer thickness is affected by the shortwave radiation budget.

5.5 Outlook and implications

In chapters 2–5 of this thesis, I quantified the influence of vegetation composition and canopy properties on the tundra radiation budget. The range of factors studied in the single chapters led to the identification of important drivers and limitations of the current understanding, thereby expanding the focus from vegetation to surface water and soil.

Limitations and suggestions for further research

In this thesis, I presented extensive field data of the radiation budget of dwarf shrubs and wet sedges. These two vegetation types are important as they can be found in many Arctic areas and may expand in the future due to climate warming and changes in the water cycle. However, dwarf shrubs and wet sedges currently cover only about 25% of the Kytalyk research site. Furthermore, albedo, transmittance, and net radiation of these two vegetation types are rather similar, while other vegetation types such as peat moss (*Sphagnum* spp.) have substantially different canopy albedo

values. Thus my research question 1 should be extended to all major vegetation types to answer the question of how vegetation influences the radiation budget. While I included all major vegetation types in my study of the landscape scale radiation budget, detailed field data are currently lacking which could shed light on the temporal variation of the radiation budget and the snowmelt timing of all vegetation types. Furthermore, longer time series would be more informative as I found differences between the dry growing season 2013 and the wetter growing season 2014. As long-term changes in the surface moisture are likely due to climate change, the question arises, how soil moisture and water level influence the radiation budget.

I found that different soil thermal properties associated with the vegetation types played a major part in the soil heat flux. Soil properties concealed the effect of the canopy radiation budget on the soil heat flux. Field measurements on more vegetation types including a range of soil moisture conditions for each type could help to better answer the question of how the radiation budget influences permafrost thaw. These measurements should also include the temporal variation of soil thermal properties as these are a critical link between surface fluxes and permafrost conditions. Additionally, measurements of the turbulent heat fluxes would be beneficial because the energy partitioning into evapotranspiration and sensible heat may change in a future climate, especially if the soil moisture changes.

Canopy properties, in particular the woody parts, strongly affect the shortwave radiation budget of dwarf shrub canopies. Thus, an important research goal for further studies would be to determine the spatial distribution of wood area index in addition to leaf area index in Arctic tundra. Furthermore, it should be investigated if the currently observed shrub proliferation is associated with changes in the leaf to wood ratio.

Vegetation and water fractional cover significantly influence the shortwave radiation budget. My results on the radiation budget of single vegetation types and the most influential canopy characteristics could be extended to larger scale extrapolations of energy fluxes based on vegetation mapping. While I suggested a comprehensive set of eight vegetation types based on species composition and canopy structure, not all of them could be mapped with sufficient accuracy. Thus more accurate mapping should be included in future work. Such landcover maps combined with data on each vegetation type would enable an estimation of the radiation fluxes at the landscape scale. This would reduce the uncertainties in how much albedo, soil shading, and net radiation may change in response to vegetation change in a warmer Arctic.

Implications for studies of large scale fluxes

In this study, I stress different aspects of the diverse interactions among tundra vegetation, the radiation budget, and permafrost thaw. Thus, the most important implication of my work is the need to quantify the details and stop treating tundra as a single, homogeneous landcover class. This is particularly important for global land surface and climate modelling, which currently often do not consider the vegetation variability of tundra areas. In this respect, my work emphasises the need to incorporate three main attributes into models of tundra energy fluxes, (I) the fractional cover of water, (II) the total plant area including wood and standing dead leaves as separate components, and (III) the soil water content and soil properties which play a critical role in permafrost thaw. As large scale estimates of these three attributes are not currently available, more effort is needed to combine field data and high resolution satellite imagery to obtain spatially resolved data. Additionally, water cover, plant area index, and soil properties vary temporally during the summer and between different years. Thus, a multi-temporal data set is needed to adequately describe these drivers of the energy budget.

While the tundra radiation budget at the landscape scale is most sensitive to land cover and plant area index, 3D radiative transfer modelling indicates substantial local variability due to variations in canopy properties and boundary effects. Thus models which resolve non-linear coupling between radiation and other processes such as evapotranspiration or photosynthesis need to include a 3D radiation scheme.

5.6 Conclusions

My field data and modelling results show the high spatial variability of radiation and soil heat flux at a lowland tundra site as a result of vegetation composition and canopy properties. Within a couple of meters, the albedo can change between 0.03 of open water and 0.18 of peat moss dominated wetland. While dense wet sedge vegetation absorbs about 85% of the sunlight, the soil absorbs most energy on less densely vegetated patches. However, even within a single vegetation type, the radiation budgets can vary substantially at the small scale. As tundra dwarf shrubs have a high wood area, the wood is even more important than green leaves for soil shading. Similarly, for wet sedges I found that the standing dead leaves shade the soil very efficiently and thus are an important part of the canopy. Not only the radiation fluxes are highly variable in space but also the soil heat flux and the active layer thickness. However, even when net-radiation and canopy transmittance are similar, like for dwarf shrubs and wet sedges, the soil heat flux can differ strongly depending on the soil moisture and thermal properties.

References

Ahrends, H. E., S. F. Oberbauer, and W. Eugster (2012), Small-scale albedo-temperature relationship contrast with large-scale relations in Alaskan acidic tussock tundra, in *Proc. SPIE 8531, Remote Sensing for Agriculture, Ecosystems, and Hydrology XIV*, vol. 8531, p. 853113, doi:10.1117/12.974381.

Anisimov, O. A., N. I. Shiklomanov, and F. E. Nelson (2002), Variability of seasonal thaw depth in permafrost regions: a stochastic modeling approach, *Ecological Modelling*, *153*(3), 217–227, doi:10.1016/S0304-3800(02)00016-9.

Asner, G. P. (1998), Biophysical and biochemical sources of variability in canopy reflectance, *Remote Sensing of Environment*, *64*(3), 234–253, doi:10.1016/S0034-4257(98)00014-5.

Asner, G. P., C. A. Wessman, and S. Archer (1998), Scale dependence of absorption of photosynthetically active radiation in terrestrial ecosystems, *Ecological Applications*, *8*(4), 1003–1021, doi:10.1890/1051-0761(1998)008[1003:SDOAOP]2.0.CO;2.

Asrar, G., R. B. Myneni, and B. J. Choudhury (1992), Spatial heterogeneity in vegetation canopies and remote sensing of absorbed photosynthetically active radiation: A modeling study, *Remote Sensing of Environment*, *41*(2–3), 85–103, doi:10.1016/0034-4257(92)90070-Z.

Atkinson, D. M., and P. Treitz (2012), Arctic ecological classifications derived from vegetation community and satellite spectral data, *Remote Sensing*, *4*(12), 3948–3971, doi:10.3390/rs4123948.

Barichivich, J., K. R. Briffa, R. B. Myneni, T. J. Osborn, T. M. Melvin, P. Ciais, S. Piao, and C. Tucker (2013), Large-scale variations in the vegetation growing season and annual cycle of atmospheric CO_2 at high northern latitudes from 1950 to 2011, *Global Change Biology*, *19*(10), 3167–3183, doi:10.1111/gcb.12283.

Bartholomeus, H., G. Schaepman-Strub, D. Blok, R. Sofronov, and S. Udaltsov (2012), Spectral estimation of soil properties in Siberian tundra soils and relations with plant species composition, *Applied and Environmental Soil Science*, *2012*, 241,535, doi:10.1155/2012/241535.

Beck, P. S. A., and S. J. Goetz (2011), Satellite observations of high northern latitude vegetation productivity changes between 1982 and 2008: ecological variability and regional differences, *Environmental Research Letters*, *6*(4), 045,501, doi:10.1088/1748-9326/6/4/045501.

Benninghoff, W. S. (1952), Interaction of vegetation and soil frost phenomena, *Arctic*, *5*(1), 34–44.

Beringer, J., A. H. Lynch, F. S. Chapin, III, M. Mack, and G. B. Bonan (2001), The representation of Arctic soils in the land surface model: The importance of mosses, *Journal of Climate*, *14*(15), 3324–3335, doi:10.1175/1520-0442(2001)014<3324:TROASI>2.0.CO;2.

Beringer, J., F. S. Chapin, III, C. C. Thompson, and A. D. McGuire (2005), Surface energy exchanges along a tundra-forest transition and feedbacks to climate, *Agricultural and Forest Meteorology*, *131*(3–4), 143–161, doi:10.1016/j.agrformet.2005.05.006.

Berner, L. T., P. S. A. Beck, A. G. Bunn, and S. J. Goetz (2013), Plant response to climate change along the forest-tundra ecotone in northeastern Siberia, *Global Change Biology*, *19*(11), 3449–3462, doi:10.1111/gcb.12304.

Bewley, D., J. W. Pomeroy, and R. L. H. Essery (2007), Solar radiation transfer through a subarctic shrub canopy, *Arctic, Antarctic, and Alpine Research*, *39*(3), 365–374, doi:10.1657/1523-0430(06-023)[BEWLEY]2.0.CO;2.

Bhatt, U. S., et al. (2010), Circumpolar Arctic tundra vegetation change is linked to sea ice decline, *Earth Interactions*, *14*(8), 1–20, doi:10.1175/2010EI315.1.

Billings, W. D., and H. A. Mooney (1968), The ecology of arctic and alpine plants, *Biological Reviews*, *43*(4), 481–529, doi:10.1111/j.1469-185X.1968.tb00968.x.

Blok, D., M. M. P. D. Heijmans, G. Schaepman-Strub, A. V. Kononov, T. C. Maximov, and F. Berendse (2010), Shrub expansion may reduce summer permafrost thaw in Siberian tundra, *Global Change Biology*, *16*(4), 1296–1305, doi:10.1111/j.1365-2486.2009.02110.x.

Blok, D., M. M. P. D. Heijmans, G. Schaepman-Strub, J. van Ruijven, F. J. W. Parmentier, T. C. Maximov, and F. Berendse (2011a), The cooling capacity of mosses: Controls on water and energy fluxes in a Siberian tundra site, *Ecosystems*, *14*(7), 1055–1065, doi:10.1007/s10021-011-9463-5.

Blok, D., U. Sass-Klaassen, G. Schaepman-Strub, M. M. P. D. Heijmans, P. Sauren, and F. Berendse (2011b), What are the main climate drivers for shrub growth in Northeastern Siberian tundra?, *Biogeosciences*, *8*(5), 1169–1179, doi:10.5194/bg-8-1169-2011.

Blok, D., G. Schaepman-Strub, H. Bartholomeus, M. M. P. D. Heijmans, T. C. Maximov, and F. Berendse (2011c), The response of Arctic vegetation to the summer climate: relation between shrub cover, NDVI, surface albedo and temperature, *Environmental Research Letters*, *6*(3), 035,502, doi:10.1088/1748-9326/6/3/035502.

Boelman, N. T., L. Gough, J. R. McLaren, and H. Greaves (2011), Does NDVI reflect variation in the structural attributes associated with increasing shrub dominance in arctic tundra?, *Environmental Research Letters*, *6*(3), 035,501, doi:10.1088/1748-9326/6/3/035501.

Boike, J., et al. (2013), Baseline characteristics of climate, permafrost and land cover from a new permafrost observatory in the Lena River Delta, Siberia (1998 – 2011), *Biogeosciences*, *10*(3), 2105–2128, doi:10.5194/bg-10-2105-2013.

Bojinski, S., M. Verstraete, T. C. Peterson, C. Richter, A. Simmons, and M. Zemp (2014), The concept of essential climate variables in support of climate research, *Bulletin of the American Meteorological Society*, *95*(9), 1431–1443, doi:10.1175/BAMS-D-13-00047.1.

Bonan, G. B. (1996), A land surface model (LSM version 1.0) for ecological, hydrological, and atmospheric studies: technical description and user's guide, *Tech. Rep. NCAR/TN-417+STR*, Climate and Global Dynamics Division, National Center for Atmospheric Research (NCAR).

Bonfils, C. J. W., T. J. Phillips, D. M. Lawrence, P. Cameron-Smith, W. J. Riley, and M. Subin (2012), On the influence of shrub height and expansion on northern high latitude climate, *Environmental Research Letters*, *7*(1), 15,503–15,511, doi:10.1088/1748-9326/7/1/015503.

Boudreau, L. D., and W. R. Rouse (1995), The role of individual terrain units in the water balance of wetland tundra, *Climate Research*, *5*(1), 31–47, doi:10.3354/cr005031.

Bret-Harte, M. S., G. R. Shaver, J. P. Zoerner, J. F. Johnstone, J. L. Wagner, A. S. Chavez, R. F. Gunkelman, IV, S. C. Lippert, and J. A. Laundre (2001), Developmental plasticity allows *Betula nana* to dominate tundra subjected to an altered environment, *Ecology*, *82*(1), 18–32, doi:10.1890/0012-9658(2001)082[0018:DPABNT]2.0.CO;2.

Briggs, M. A., M. A. Walvoord, J. M. McKenzie, C. I. Voss, F. D. Day-Lewis, and J. W. Lane (2014), New permafrost is forming around shrinking Arctic lakes, but will it last?, *Geophysical Research Letters*, *41*(5), 1585–1592, doi:10.1002/2014GL059251.

Brown, J., K. M. Hinkel, and F. E. Nelson (2000), The circumpolar active layer monitoring (CALM) program: research designs and initial results, *Polar Geography*, *24*(3), 165–258, doi:10.1080/10889370009377698.

Brown, J., O. J. Ferrians, Jr., J. A. Heginbottom, and E. S. Melnikov (2002), Circum-Arctic map of permafrost and ground ice conditions, Version 2, NSIDC: National Snow and Ice Data Center, digital media.

Budishchev, A., et al. (2014), Evaluation of a plot-scale methane emission model using eddy covariance observations and footprint modelling, *Biogeosciences*, *11*(17), 4651–4664, doi:10.5194/bg-11-4651-2014.

Cahoon, S. M. P., P. F. Sullivan, G. R. Shaver, J. M. Welker, and E. Post (2012), Interactions among shrub cover and the soil microclimate may determine future Arctic carbon budgets, *Ecology Letters*, *15*(12), 1415–1422, doi:10.1111/j.1461-0248.2012.01865.x.

Caldwell, M. M., L. L. Tieszen, and M. Fareed (1974), The canopy structure of tundra plant communities at Barrow, Alaska, and Niwot Ridge, Colorado, *Arctic and Alpine Research*, *6*(2), 151–159, doi:10.2307/1550083.

Camacho, F., J. Cernicharo, R. Lacaze, F. Baret, and M. Weiss (2013), GEOV1: LAI, FAPAR essential climate variables and FCOVER global time series capitalizing over existing products. Part 2: Validation and intercomparison with reference products, *Remote Sensing of Environment*, *137*, 310–329, doi:10.1016/j.rse.2013.02.030.

Campioli, M., L. E. Street, A. Michelsen, G. R. Shaver, T. Maere, R. Samson, and R. Lemeur (2009), Determination of leaf area index, total foliar N, and normalized difference vegetation index for arctic ecosystems dominated by *Cassiope tetragona*, *Arctic, Antarctic, and Alpine Research*, *41*(4), 426–433, doi:10.1657/1938-4246-41.4.426.

Cannone, N., and M. Guglielmin (2009), Influence of vegetation on the ground thermal regime in continental Antarctica, *Geoderma*, *151*(3–4), 215–223, doi:10.1016/j.geoderma.2009.04.007.

Carroll, M. L., J. R. G. Townshend, C. M. DiMiceli, T. Loboda, and R. A. Sohlberg (2011), Shrinking lakes of the Arctic: Spatial relationships and trajectory of change, *Geophysical Research Letters*, *38*(20), L20,406, doi:10.1029/2011GL049427.

Chambers, S. D., J. Beringer, J. T. Randerson, and F. S. Chapin, III (2005), Fire effects on net

radiation and energy partitioning: Contrasting responses of tundra and boreal forest ecosystems, *Journal of Geophysical Research: Atmospheres*, *110*(D9), D09,106, doi:10.1029/2004JD005299, d09106.

Chapin, F. S., III, and G. R. Shaver (1981), Changes in soil properties and vegetation following disturbance of Alaskan Arctic tundra, *Journal of Applied Ecology*, *18*(2), 605–617.

Chapin, F. S., III, G. R. Shaver, A. E. Giblin, K. J. Nadelhoffer, and J. A. Laundre (1995), Responses of arctic tundra to experimental and observed changes in climate, *Ecology*, *76*(3), 694–711.

Chapin, F. S., III, et al. (2000a), Arctic and boreal ecosystems of western North America as components of the climate system, *Global Change Biology*, *6*(S1), 211–223, doi:10.1046/j.1365-2486.2000.06022.x.

Chapin, F. S., III, W. Eugster, J. P. McFadden, A. H. Lynch, and D. A. Walker (2000b), Summer differences among Arctic ecosystems in regional climate forcing, *Journal of Climate*, *13*(12), 2002–2010, doi:10.1175/1520-0442(2000)013<2002:SDAAEI>2.0.CO;2.

Chapin, F. S., III, et al. (2005), Role of land-surface changes in Arctic summer warming, *Science*, *310*(5748), 657–660, doi:10.1126/science.1117368.

Chapin, F. S., III, P. A. Matson, and P. Vitousek (2011), *Principles of Terrestrial Ecosystem Ecology*, Springer-Verlag New York, doi:10.1007/978-1-4419-9504-9.

Chong, M., E. Humphreys, and T. R. Moore (2012), Microclimatic response to increasing shrub cover and its effect on *Sphagnum* CO_2 exchange in a bog, *Ecoscience*, *19*(1), 89–97, doi:10.2980/19-1-3489.

Convey, P., et al. (2012), The impacts of climate change on circumpolar biodiversity, *Biodiversity*, *13*(3–4), 134–143, doi:10.1080/14888386.2012.732556.

Corradi, C., O. Kolle, K. Walter, S. A. Zimov, and E.-D. Schulze (2005), Carbon dioxide and methane exchange of a north-east Siberian tussock tundra, *Global Change Biology*, *11*(11), 1910–1925, doi:10.1111/j.1365-2486.2005.01023.x.

Corripio, J. G. (2003), Vectorial algebra algorithms for calculating terrain parameters from DEMs and solar radiation modelling in mountainous terrain, *International Journal of Geographical Information Science*, *17*(1), 1–23, doi:10.1080/713811744.

Cowtan, K., and R. G. Way (2014), Coverage bias in the HadCRUT4 temperature series and its impact on recent temperature trends, *Quarterly Journal of the Royal Meteorological Society*, *140*(683), 1935–1944, doi:10.1002/qj.2297, accepted Article.

Crawford, T. M., and C. E. Duchon (1999), An improved parameterization for estimating effective atmospheric emissivity for use in calculating daytime downwelling longwave radiation, *Journal of Applied Meteorology*, *38*(4), 474–480, doi:10.1175/1520-0450(1999)038<0474:AIPFEE>2.0.CO;2.

Curry, J. A., W. B. Rossow, D. Randall, and J. L. Schramm (1996), Overview of Arctic cloud and radiation characteristics, *Journal of Climate*, *9*(8), 1731–1764, doi:10.1175/1520-0442(1996)009<1731:OOACAR>2.0.CO;2.

de Groot, W. J., P. A. Thomas, and R. W. Wein (1997), *Betula nana* L. and *Betula glandulosa* Michx., *Journal of Ecology*, *85*(2), pp. 241–264, doi:10.2307/2960655.

de Jong, R., M. E. Schaepman, R. Furrer, S. de Bruin, and P. H. Verburg (2013), Spatial relationship between climatologies and changes in global vegetation activity, *Global Change Biology*, *19*(6), 1953–1964, doi:10.1111/gcb.12193.

de Wit, C. T. (1965), Photosynthesis of leaf canopies, in *Agricultural Research Reports no. 663*, Centre for Agricultural Publications and Documentation Wageningen.

DeMarco, J., M. C. Mack, and M. S. Bret-Harte (2014), Effects of arctic shrub expansion on biophysical vs. biogeochemical drivers of litter decomposition, *Ecology*, *95*(7), 1861–1875, doi:10.1890/13-2221.1.

Dengel, S., J. Grace, and A. MacArthur (2015), Transmissivity of solar radiation within a *Picea sitchensis* stand under various sky conditions, *Biogeosciences*, *12*(14), 4195–4207, doi:10.5194/bg-12-4195-2015.

Dickinson, R. E., L. Zhou, Y. Tian, Q. Liu, T. Lavergne, B. Pinty, C. B. Schaaf, and Y. Knyazikhin (2008), A three-dimensional analytic model for the scattering of a spherical bush, *Journal of Geophysical Research: Atmospheres*, *113*(D20), D20,113, doi:10.1029/2007JD009564.

Dong, X., B. Xi, K. Crosby, C. N. Long, R. S. Stone, and M. D. Shupe (2010), A 10 year climatology of Arctic cloud fraction and radiative forcing at Barrow, Alaska, *Journal of Geophysical Research: Atmospheres*, *115*(D17), D17,212, doi:10.1029/2009JD013489.

Dorman, J. L., and P. J. Sellers (1989), A global climatology of albedo, roughness length and stomatal resistance for atmospheric general circulation models as represented by the Simple Biosphere Model (SiB), *Journal of Applied Meteorology*, *28*(9), 833–855.

Duthoit, S., V. Demarez, J.-P. Gastellu-Etchegorry, E. Martin, and J.-L. Roujean (2008), Assessing the effects of the clumping phenomenon on BRDF of a maize crop based on 3D numerical scenes using DART model, *Agricultural and Forest Meteorology*, *148*(8–9), 1341–1352, doi:10.1016/j.agrformet.2008.03.011.

Eaton, A. K., W. R. Rouse, P. M. Lafleur, P. Marsh, and P. D. Blanken (2001), Surface energy balance of the western and central Canadian subarctic: Variations in the energy balance among five major terrain types, *Journal of Climate*, *14*(17), 3692–3703, doi:10.1175/1520-0442(2001)014<3692:SEBOTW>2.0.CO;2.

Eck, T. F., and D. W. Deering (1992), Canopy albedo and transmittance in a spruce-hemlock forest in mid-September, *Agricultural and Forest Meteorology*, *59*(3–4), 237–248, doi:10.1016/0168-1923(92)90095-L.

Elmendorf, S. C., et al. (2012a), Global assessment of experimental climate warming on tundra vegetation: heterogeneity over space and time, *Ecology Letters*, *15*(2), 164–175, doi:10.1111/j.1461-0248.2011.01716.x.

Elmendorf, S. C., et al. (2012b), Plot-scale evidence of tundra vegetation change and links to recent summer warming, *Nature Climate Change*, *2*(6), 453–457, doi:10.1038/nclimate1465.

Erb, A. M. (2013), Impact of changing shrub cover in the Arctic on the shortwave reflected and transmitted radiation, Master's thesis, University of Zurich.

Eugster, W., et al. (2000), Land–atmosphere energy exchange in Arctic tundra and boreal forest: available data and feedbacks to climate, *Global Change Biology*, *6*(S1), 84–115, doi:10.1046/j.1365-2486.2000.06015.x.

Field, C. B., D. B. Lobell, H. A. Peters, and N. R. Chiariello (2007), Feedbacks of terrestrial ecosystems to climate change, *Annual Review of Environment and Resources*, *32*(1), 1–29, doi:10.1146/annurev.energy.32.053006.141119.

Fisher, J. P., C. Estop-Aragonés, A. Thierry, D. J. Charman, S. A. Wolfe, I. P. Hartley, J. B. Murton, M. Williams, and G. K. Phoenix (2016), The influence of vegetation and soil characteristics on active-layer thickness of permafrost soils in boreal forest, *Global Change Biology*, doi:10.1111/gcb.13248.

Flerchinger, G. N., W. Xiao, T. J. Sauer, and Q. Yu (2009), Simulation of within-canopy radiation exchange, *Wageningen Journal of Life Sciences*, *57*(1), 5–15, doi:10.1016/j.njas.2009.07.004.

Forbes, B. C., M. M. Fauria, and P. Zetterberg (2010), Russian Arctic warming and 'greening' are closely tracked by tundra shrub willows, *Global Change Biology*, *16*(5), 1542–1554, doi:10.1111/j.1365-2486.2009.02047.x.

Fraser, R. H., T. C. Lantz, I. Olthof, S. V. Kokelj, and R. A. Sims (2014), Warming-induced shrub expansion and lichen decline in the Western Canadian Arctic, *Ecosystems*, *17*(7), 1151–1168, doi:10.1007/s10021-014-9783-3.

Frost, G. V., and H. E. Epstein (2014), Tall shrub and tree expansion in Siberian tundra ecotones since the 1960s, *Global Change Biology*, *20*(4), 1264–1277, doi:10.1111/gcb.12406.

Gamon, J. A., G. P. Kershaw, S. Williamson, and D. S. Hik (2012), Microtopographic patterns in an arctic baydjarakh field: do fine-grain patterns enforce landscape stability?, *Environmental Research Letters*, *7*(1), 015,502, doi:10.1088/1748-9326/7/1/015502.

Gamon, J. A., K. F. Huemmrich, R. S. Stone, and C. E. Tweedie (2013), Spatial and temporal variation in primary productivity (NDVI) of coastal Alaskan tundra: Decreased vegetation growth following earlier snowmelt, *Remote Sensing of Environment*, *129*, 144–153, doi:10.1016/j.rse.2012.10.030.

Ganguly, S., et al. (2014), *Biophysical Applications of Satellite Remote Sensing*, chap. Green Leaf Area and Fraction of Photosynthetically Active Radiation Absorbed by Vegetation, pp. 43–61, Springer Berlin Heidelberg, Berlin, Heidelberg, doi:10.1007/978-3-642-25047-7_2.

Garonna, I., R. de Jong, and M. E. Schaepman (2016), Variability and evolution of global land surface phenology over the past three decades (1982–2012), *Global Change Biology*, *22*(4), 1456–1468, doi:10.1111/gcb.13168.

Gastellu-Etchegorry, J.-P., V. Demarez, V. Pinel, and F. Zagolski (1996), Modeling radiative transfer in heterogeneous 3-D vegetation canopies, *Remote Sensing of Environment*, *58*(2), 131–156, doi:10.1016/0034-4257(95)00253-7.

Gastellu-Etchegorry, J.-P., P. Guillevic, F. Zagolski, V. Demarez, V. Trichon, D. Deering, and M. Leroy (1999), Modeling BRF and radiation regime of boreal and tropical forests - I. BRF, *Remote Sensing of Environment*, *68*(3), 281–316, doi:10.1016/S0034-4257(98)00119-9.

Gastellu-Etchegorry, J.-P., E. Martin, and F. Gascon (2004), DART: a 3D model for simulating satellite images and studying surface radiation budget, *International Journal of Remote Sensing*, *25*(1), 73–96, doi:10.1080/0143116031000115166.

Goel, N. S., and D. E. Strebel (1984), Simple beta distribution representation of leaf orientation in vegetation canopies, *Agronomy Journal*, *76*(5), 800–802, doi:10.2134/agronj1984.00021962007600050021x.

Gornall, J., I. Jónsdóttir, S. Woodin, and R. Wal (2007), Arctic mosses govern below-ground environment and ecosystem processes, *Oecologia*, *153*(4), 931–941, doi:10.1007/s00442-007-0785-0.

Gould, W. A., M. Raynolds, and D. A. Walker (2003), Vegetation, plant biomass, and net primary productivity patterns in the Canadian Arctic, *Journal of Geophysical Research: Atmospheres*, *108*(D2), 8167, doi:10.1029/2001JD000948.

Grau, E., and J.-P. Gastellu-Etchegorry (2013), Radiative transfer modeling in the Earth–Atmosphere system with DART model, *Remote Sensing of Environment*, *139*, 149–170, doi:10.1016/j.rse.2013.07.019.

Grosse, G., and B. M. Jones (2011), Spatial distribution of pingos in northern Asia, *The Cryosphere*, *5*(1), 13–33, doi:10.5194/tc-5-13-2011.

Guan, X. J., C. J. Westbrook, and C. Spence (2010), Shallow soil moisture – ground thaw interactions and controls – Part 1: Spatiotemporal patterns and correlations over a subarctic landscape, *Hydrology and Earth System Sciences*, *14*(7), 1375–1386, doi:10.5194/hess-14-1375-2010.

Hardiman, B. S., G. Bohrer, C. M. Gough, C. S. Vogel, and P. S. Curtis (2011), The role of canopy structural complexity in wood net primary production of a maturing northern deciduous forest, *Ecology*, *92*(9), 1818–1827, doi:10.1890/10-2192.1.

He, L., V. Y. Ivanov, G. Bohrer, K. D. Maurer, C. S. Vogel, and M. Moghaddam (2014), Effects of fine-scale soil moisture and canopy heterogeneity on energy and water fluxes in a northern temperate mixed forest, *Agricultural and Forest Meteorology*, *184*, 243–256, doi:10.1016/j.agrformet.2013.10.006.

Hill, M. O. (1973), Diversity and evenness: A unifying notation and its consequences, *Ecology*, *54*(2), 427–432.

Hinkel, K. M., and F. E. Nelson (2003), Spatial and temporal patterns of active layer thickness at Circumpolar Active Layer Monitoring (CALM) sites in northern Alaska, 1995–2000, *Journal of Geophysical Research: Atmospheres*, *108*(D2), 8168, doi:10.1029/2001JD000927.

Hinzman, L., et al. (2005), Evidence and implications of recent climate change in Northern Alaska and other Arctic regions, *Climatic Change*, *72*(3), 251–298, doi:doi:10.1007/s10584-005-5352-2.

Hinzman, L. D., C. J. Deal, A. D. McGuire, S. H. Mernild, I. V. Polyakov, and J. E. Walsh (2013), Trajectory of the Arctic as an integrated system, *Ecological Applications*, *23*(8), 1837–1868, doi:10.1890/11-1498.1.

Hobbie, S. E., L. Gough, and G. R. Shaver (2005), Species compositional differences on different-aged glacial landscapes drive contrasting responses of tundra to nutrient addition, *Journal of Ecology*, *93*(4), 770–782, doi:10.1111/j.1365-2745.2005.01006.x.

Hope, A. S., J. S. Kimball, and D. A. Stow (1993), The relationship between tussock tundra spectral reflectance properties and biomass and vegetation composition, *International Journal of Remote Sensing*, *14*(10), 1861–1874, doi:10.1080/01431169308954008.

Hope, A. S., K. R. Pence, and D. A. Stow (2004), NDVI from low altitude aircraft and composited NOAA AVHRR data for scaling Arctic ecosystem fluxes, *International Journal of Remote Sensing*, *25*(20), 4237–4250, doi:10.1080/01431160310001632710.

Hosgood, B., S. Jacquemoud, G. Andreoli, J. Verdebout, A. Pedrini, and G. Schmuck (1995, revised 2005), Leaf Optical Properties EXperiment 93 (LOPEX93), *Tech. rep.*, ECSC-EC-EAEC Brussels, Luxembourg, EUR 16095 EN.

Hudson, J. M. G., G. H. R. Henry, and W. K. Cornwell (2011), Taller and larger: shifts in Arctic tundra leaf traits after 16 years of experimental warming, *Global Change Biology*, *17*(2), 1013–1021, doi:10.1111/j.1365-2486.2010.02294.x.

Huemmrich, K. F., et al. (2010), Remote sensing of tundra gross ecosystem productivity and light use efficiency under varying temperature and moisture conditions, *Remote Sensing of Environment*, *114*(3), 481–489, doi:10.1016/j.rse.2009.10.003.

Hugelius, G., et al. (2014), Estimated stocks of circumpolar permafrost carbon with quantified uncertainty ranges and identified data gaps, *Biogeosciences*, *11*(23), 6573–6593, doi:10.5194/bg-11-6573-2014.

Iqbal, M. (1983), *An introduction to solar radiation*, Academic Press, New York - London.

Iwahana, G., et al. (2014), Geocryological characteristics of the upper permafrost in a tundra–forest transition of the Indigirka River Valley, Russia, *Polar Science*, *8*(2), 96–113, doi:10.1016/j.polar.2014.01.005.

Jacobsen, A., and B. U. Hansen (1999), Estimation of the soil heat flux/net radiation ratio based on spectral vegetation indexes in high-latitude Arctic areas, *International Journal of Remote Sensing*, *20*(2), 445–461, doi:10.1080/014311699213532.

Jacquez, J. A., and H. F. Kuppenheim (1955), Theory of the integrating sphere, *Journal of the Optical Society of America*, *45*(6), 460–466, doi:10.1364/JOSA.45.000460.

Jonasson, S., J. Castro, and A. Michelsen (2004), Litter, warming and plants affect respiration and allocation of soil microbial and plant C, N and P in arctic mesocosms, *Soil Biology and Biochemistry*, *36*(7), 1129–1139, doi:10.1016/j.soilbio.2004.02.023.

Jones, B. M., G. Grosse, C. D. Arp, M. C. Jones, K. M. Walter Anthony, and V. E. Romanovsky (2011), Modern thermokarst lake dynamics in the continuous permafrost zone, northern Seward Peninsula, Alaska, *Journal of Geophysical Research: Biogeosciences*, *116*(G2), G00M03, doi:10.1029/2011JG001666.

Jorgenson, M. T., Y. L. Shur, and E. R. Pullman (2006), Abrupt increase in permafrost degradation in Arctic Alaska, *Geophysical Research Letters*, *33*(2), L02,503, doi:10.1029/2005GL024960.

Jorgenson, M. T., V. Romanovsky, J. Harden, Y. Shur, J. O'Donnell, E. A. G. Schuur, M. Kanevskiy, and S. Marchenko (2010), Resilience and vulnerability of permafrost to climate change, *Canadian Journal of Forest Research*, *40*(7), 1219–1236, doi:10.1139/X10-060.

Jucker, T., O. Bouriaud, D. Avacaritei, I. Dănilă, G. Duduman, F. Valladares, and D. A. Coomes (2014), Competition for light and water play contrasting roles in driving diversity–productivity relationships in Iberian forests, *Journal of Ecology*, *102*(5), 1202–1213, doi:10.1111/1365-2745.12276.

Juszak, I., and F. Pellicciotti (2013), A comparison of parameterizations of incoming longwave radiation over melting glaciers: Model robustness and seasonal variability, *Journal of Geophysical Research: Atmospheres*, *118*(8), 3066–3084, doi:10.1002/jgrd.50277.

Juszak, I., A. M. Erb, T. C. Maximov, and G. Schaepman-Strub (2014), Arctic shrub effects on NDVI, summer albedo and soil shading, *Remote Sensing of Environment*, *153*, 79–89, doi:10.1016/j.rse.2014.07.021.

Juszak, I., W. Eugster, M. M. P. D. Heijmans, and G. Schaepman-Strub (2016a), Contrasting radiation and soil heat fluxes in Arctic shrub and wet sedge tundra, *Biogeosciences*, *13*, 4049–4064, doi:10.5194/bg-13-4049-2016.

Juszak, I., M. Iturrate-Garcia, J.-P. Gastellu-Etchegorry, M. E. Schaepman, T. C. Maximov, and G. Schaepman-Strub (2016b), Drivers of shortwave radiation fluxes in Arctic tundra across scales, *Remote Sensing of Environment*, under Review.

Kasurinen, V., et al. (2014), Latent heat exchange in the boreal and arctic biomes, *Global Change Biology*, *20*(11), 3439–3456, doi:10.1111/gcb.12640.

Kim, Y., J. S. Kimball, K. Zhang, K. Didan, I. Velicogna, and K. C. McDonald (2014), Attribution of divergent northern vegetation growth responses to lengthening non-frozen seasons using satellite optical-NIR and microwave remote sensing, *International Journal of Remote Sensing*, *35*(10), 3700–3721, doi:10.1080/01431161.2014.915595.

King, F. (2003), 11 – Transforming density functions, University of Cambridge Computer Laboratory, Lecture notes.

Klink, K., and C. J. Willmott (1985), Notes on a global vegetation data set for use in GCMs, Dept. of Geography, Univ. of Delaware, Newark, Delaware.

Knyazikhin, Y., G. Mießen, O. Panfyorov, and G. Gravenhorst (1997), Small-scale study of three-dimensional distribution of photosynthetically active radiation in a forest, *Agricultural and Forest Meteorology*, *88*(1–4), 215–239, doi:10.1016/S0168-1923(97)00036-1.

Kobayashi, H., D. D. Baldocchi, Y. Ryu, Q. Chen, S. Ma, J. L. Osuna, and S. L. Ustin (2012), Modeling energy and carbon fluxes in a heterogeneous oak woodland: A three-dimensional approach, *Agricultural and Forest Meteorology*, *152*, 83–100, doi:10.1016/j.agrformet.2011.09.008.

Kobayashi, H., R. Suzuki, S. Nagai, T. Nakai, and Y. Kim (2014), Spatial scale and landscape heterogeneity effects on FAPAR in an open-canopy black spruce forest in interior Alaska, *Geoscience and Remote Sensing Letters, IEEE*, *11*(2), 564–568, doi:10.1109/LGRS.2013.2278426.

Lafleur, P. M., and E. R. Humphreys (2008), Spring warming and carbon dioxide exchange over low Arctic tundra in central Canada, *Global Change Biology*, *14*(4), 740–756, doi:10.1111/j.1365-2486.2007.01529.x.

Lafleur, P. M., A. B. Wurtele, and C. R. Duguay (1997), Spatial and temporal variations in surface albedo of a subarctic landscape using surface-based measurements and remote sensing, *Arctic and Alpine Research*, *29*(3), 261–269, doi:10.2307/1552140.

Langer, M., S. Westermann, S. Muster, K. Piel, and J. Boike (2011a), The surface energy balance of a polygonal tundra site in northern Siberia – Part 2: Winter, *The Cryosphere*, *5*(2), 509–524, doi:10.5194/tc-5-509-2011.

Langer, M., S. Westermann, S. Muster, K. Piel, and J. Boike (2011b), The surface energy balance of a polygonal tundra site in northern Siberia – Part 1: Spring to fall, *The Cryosphere*, *5*(1), 151–171, doi:10.5194/tc-5-151-2011.

Lantz, T. C., S. E. Gergel, and S. V. Kokelj (2010), Spatial heterogeneity in the shrub tundra ecotone in the Mackenzie delta region, Northwest Territories: Implications for Arctic environmental change, *Ecosystems*, *13*(2), 194–204, doi:10.1007/s10021-009-9310-0.

Lantz, T. C., P. Marsh, and S. V. Kokelj (2013), Recent shrub proliferation in the Mackenzie Delta uplands and microclimatic implications, *Ecosystems*, *16*(1), 47–59, doi:10.1007/s10021-012-9595-2.

Lawrence, D. M., and S. C. Swenson (2011), Permafrost response to increasing Arctic shrub abundance depends on the relative influence of shrubs on local soil cooling versus large-scale climate warming, *Environmental Research Letters*, *6*(4), 045,504, doi:10.1088/1748-9326/6/4/045504.

Lawrence, P. J., and T. N. Chase (2007), Representing a new MODIS consistent land surface in the Community Land Model (CLM 3.0), *Journal of Geophysical Research: Biogeosciences*, *112*(G1), doi:10.1029/2006JG000168, g01023.

Liang, S., A. H. Strahler, and C. Walthall (1999), Retrieval of land surface albedo from satellite observations: A simulation study, *Journal of Applied Meteorology*, *38*(6), 712–725, doi:10.1175/1520-0450(1999)038<0712:ROLSAF>2.0.CO;2.

Liang, S., K. Wang, X. Zhang, and M. Wild (2010), Review on estimation of land surface radiation and energy budgets from ground measurement. remote sensing and model simulations, *Selected Topics in Applied Earth Observations and Remote Sensing, IEEE Journal of*, *3*(3), 225–240, doi:10.1109/JSTARS.2010.2048556.

Lin, D. H., D. R. Johnson, C. Andresen, and C. E. Tweedie (2012), High spatial resolution decade-time scale land cover change at multiple locations in the Beringian Arctic (1948–2000s), *Environmental Research Letters*, *7*(2), 025,502, doi:10.1088/1748-9326/7/2/025502.

Liston, G. E., J. P. McFadden, M. Sturm, and R. A. Pielke (2002), Modelled changes in arctic tundra snow, energy and moisture fluxes due to increased shrubs, *Global Change Biology*, *8*(1), 17–32, doi:10.1046/j.1354-1013.2001.00416.x.

Lloyd, C. R., R. J. Harding, T. Friborg, and M. Aurela (2001), Surface fluxes of heat and water vapour from sites in the European Arctic, *Theoretical and Applied Climatology*, *70*(1–4), 19–33, doi:10.1007/s007040170003.

Loew, A., P. M. van Bodegom, J.-L. Widlowski, J. Otto, T. Quaife, B. Pinty, and T. Raddatz (2014), Do we (need to) care about canopy radiation schemes in DGVMs? Caveats and potential impacts, *Biogeosciences*, *11*(7), 1873–1897, doi:10.5194/bg-11-1873-2014.

Loranty, M. M., and S. J. Goetz (2012), Shrub expansion and climate feedbacks in Arctic tundra, *Environmental Research Letters*, *7*(1), 011,005, doi:10.1088/1748-9326/7/1/011005.

Loranty, M. M., S. J. Goetz, and P. S. A. Beck (2011), Tundra vegetation effects on pan-Arctic albedo, *Environmental Research Letters*, *6*(2), 024,014, doi:10.1088/1748-9326/6/2/024014.

Mack, M. C., E. A. G. Schuur, M. S. Bret-Harte, G. R. Shaver, and F. S. Chapin, III (2004), Ecosystem carbon storage in arctic tundra reduced by long-term nutrient fertilization, *Nature*, *431*, 440–443, doi:10.1038/nature02887.

Mahat, V., and D. G. Tarboton (2012), Canopy radiation transmission for an energy balance snowmelt model, *Water Resources Research*, *48*(1), 1534, doi:10.1029/2011WR010438.

Malenovský, Z., E. Martin, L. Homolová, J.-P. Gastellu-Etchegorry, R. Zurita-Milla, M. E. Schaepman, R. Pokorný, J. G. P. W. Clevers, and P. Cudlín (2008), Influence of woody elements of a Norway spruce canopy on nadir reflectance simulated by the DART model at very high spatial resolution, *Remote Sensing of Environment*, *112*(1), 1–18, doi:10.1016/j.rse.2006.02.028.

Marsh, P., P. Bartlett, M. MacKay, S. Pohl, and T. Lantz (2010), Snowmelt energetics at a shrub tundra site in the western Canadian Arctic, *Hydrological Processes*, *24*(25), 3603–3620, doi:10.1002/hyp.7786.

McFadden, J. P., F. S. Chapin, III, and D. Y. Hollinger (1998), Subgrid-scale variability in the surface energy balance of Arctic tundra, *Journal of Geophysical Research: Atmospheres*, *103*(D22), 28,947–28,961, doi:10.1029/98JD02400.

McFadden, J. P., W. Eugster, and F. S. Chapin, III (2003), A regional study of the controls on water vapor and CO_2 exchange in Arctic tundra, *Ecology*, *84*(10), 2762–2776, doi:10.1890/01-0444.

McGuire, A. D., et al. (2009), Sensitivity of the carbon cycle in the Arctic to climate change, *Ecological Monographs*, *79*(4), 523–555, doi:10.1890/08-2025.1.

McManus, K. M., D. C. Morton, J. G. Masek, D. Wang, J. O. Sexton, J. R. Nagol, P. Ropars, and S. Boudreau (2012), Satellite-based evidence for shrub and graminoid tundra expansion in northern Quebec from 1986 to 2010, *Global Change Biology*, *18*(7), 2313–2323, doi:10.1111/j.1365-2486.2012.02708.x.

Merbold, L., W. L. Kutsch, C. Corradi, O. Kolle, C. Rebmann, P. C. Stoy, S. A. Zimov, and E.-D. Schulze (2009), Artificial drainage and associated carbon fluxes (CO_2/CH_4) in a tundra ecosystem, *Global Change Biology*, *15*(11), 2599–2614, doi:10.1111/j.1365-2486.2009.01962.x.

Mi, Y., J. van Huissteden, F. J. W. Parmentier, A. Gallagher, A. Budishchev, C. T. Berridge, and A. J. Dolman (2014), Improving a plot-scale methane emission model and its performance at a northeastern Siberian tundra site, *Biogeosciences*, *11*(14), 3985–3999, doi:10.5194/bg-11-3985-2014.

Miller, P. A., and B. Smith (2012), Modelling tundra vegetation response to recent Arctic warming, *AMBIO*, *41*(3), 281–291, doi:10.1007/s13280-012-0306-1.

Molau, U., and J. M. Alatalo (1998), Responses of subarctic-alpine plant communities to simulated environmental change: Biodiversity of bryophytes, lichens, and vascular plants, *Ambio*, *27*(4), 322–329.

Muster, S., M. Langer, B. Heim, S. Westermann, and J. Boike (2012), Subpixel heterogeneity of ice-wedge polygonal tundra: a multi-scale analysis of land cover and evapotranspiration in the Lena River Delta, Siberia, *Tellus B*, *64*, 17,301, doi:10.3402/tellusb.v64i0.17301.

Myers-Smith, I. H., and D. S. Hik (2013), Shrub canopies influence soil temperatures but not nutrient dynamics: An experimental test of tundra snow–shrub interactions, *Ecology and Evolution*, *3*(11), 3683–3700, doi:10.1002/ece3.710.

Myers-Smith, I. H., et al. (2011), Shrub expansion in tundra ecosystems: dynamics, impacts and research priorities, *Environmental Research Letters*, *6*(4), 045,509, doi:10.1088/1748-9326/6/4/045509.

Myers-Smith, I. H., et al. (2015), Climate sensitivity of shrub growth across the tundra biome, *Nature Climate Change*, *5*, 887–891, doi:10.1038/nclimate2697.

Myneni, R. B., R. Ramakrishna, R. Nemani, and S. W. Running (1997), Estimation of global leaf area index and absorbed par using radiative transfer models, *Geoscience and Remote Sensing, IEEE Transactions on*, *35*(6), 1380–1393, doi:10.1109/36.649788.

Nauta, A. L., et al. (2015), Permafrost collapse after shrub removal shifts tundra ecosystem to a methane source, *Nature Climate Change*, *5*(1), 67–70, doi:10.1038/nclimate2446.

Nemani, R. R., C. D. Keeling, H. Hashimoto, W. M. Jolly, S. C. Piper, C. J. Tucker, R. B. Myneni, and S. W. Running (2003), Climate-driven increases in global terrestrial net primary production from 1982 to 1999, *Science*, *300*(5625), 1560–1563, doi:10.1126/science.1082750.

O'Donnell, J. A., V. E. Romanovsky, J. W. Harden, and A. D. McGuire (2009), The effect of moisture content on the thermal conductivity of moss and organic soil horizons from black spruce ecosystems in interior Alaska, *Soil Science*, *174*(12), 646–651, doi:10.1097/SS.0b013e3181c4a7f8.

Oechel, W. C., G. L. Vourlitis, S. J. Hastings, R. C. Zulueta, L. Hinzman, and D. Kane (2000), Acclimation of ecosystem CO_2 exchange in the Alaskan Arctic in response to decadal climate warming, *Nature*, *406*, 978–981, doi:10.1038/35023137.

Oechel, W. C., C. A. Laskowski, G. Burba, B. Gioli, and A. A. M. Kalhori (2014), Annual patterns and budget of CO_2 flux in an Arctic tussock tundra ecosystem, *Journal of Geophysical Research: Biogeosciences*, *119*(3), 323–339, doi:10.1002/2013JG002431.

Ohlson, M., R. H. Økland, J.-F. Nordbakken, and B. Dahlberg (2001), Fatal interactions between scots pine and *Sphagnum* mosses in bog ecosystems, *Oikos*, *94*(3), 425–432.

Ohmura, A. (2001), Physical basis for the temperature-based melt-index method, *Journal of Applied Meteorology*, *40*(4), 753–761, doi:10.1175/1520-0450(2001)040<0753:PBFTTB>2.0.CO;2.

Oke, T. R. (1987), *Boundary layer climates*, 2 ed., Methuen & Co.

Oliphant, A., C. Susan, B. Grimmond, H.-P. Schmid, and C. A. Wayson (2006), Local-scale heterogeneity of photosynthetically active radiation (PAR), absorbed PAR and net radiation as a function of topography, sky conditions and leaf area index, *Remote Sensing of Environment*, *103*(3), 324–337, doi:10.1016/j.rse.2005.09.021.

Olofsson, J., L. Oksanen, T. Callaghan, P. E. Hulme, T. Oksanen, and O. Suominen (2009),

Herbivores inhibit climate-driven shrub expansion on the tundra, *Global Change Biology*, *15*(11), 2681–2693, doi:10.1111/j.1365-2486.2009.01935.x.

Olthof, I., and D. Pouliot (2010), Treeline vegetation composition and change in Canada's western Subarctic from AVHRR and canopy reflectance modeling, *Remote Sensing of Environment*, *114*(4), 805–815, doi:10.1016/j.rse.2009.11.017.

Pajunen, A. M., J. Oksanen, and R. Virtanen (2011), Impact of shrub canopies on understorey vegetation in western Eurasian tundra, *Journal of Vegetation Science*, *22*(5), 837–846, doi:10.1111/j.1654-1103.2011.01285.x.

Parmentier, F. J. W., J. van Huissteden, M. K. van der Molen, G. Schaepman-Strub, S. A. Karsanaev, T. C. Maximov, and A. J. Dolman (2011a), Spatial and temporal dynamics in eddy covariance observations of methane fluxes at a tundra site in northeastern Siberia, *Journal of Geophysical Research: Biogeosciences*, *116*(G15), G03016, doi:10.1029/2010JG001637.

Parmentier, F. J. W., M. K. van der Molen, J. van Huissteden, S. A. Karsanaev, A. V. Kononov, D. A. Suzdalov, T. C. Maximov, and A. J. Dolman (2011b), Longer growing seasons do not increase net carbon uptake in the northeastern Siberian tundra, *Journal of Geophysical Research: Biogeosciences*, *116*(G15), G04013, doi:10.1029/2011JG001653.

Pearson, R. G., S. J. Phillips, M. M. Loranty, P. S. A. Beck, T. Damoulas, S. J. Knight, and S. J. Goetz (2013), Shifts in Arctic vegetation and associated feedbacks under climate change, *Nature Climate Change*, *3*(7), 673–677, doi:10.1038/nclimate1858.

Phillips, M. E. (1954), *Eriophorum angustifolium* Roth, *Journal of Ecology*, *42*(2), 612–622.

Pinty, B., et al. (2001), Radiation transfer model intercomparison (RAMI) exercise, *Journal of Geophysical Research: Atmospheres*, *106*(D11), 11,937–11,956, doi:10.1029/2000JD900493.

Pinty, B., T. Lavergne, R. E. Dickinson, J.-L. Widlowski, N. Gobron, and M. M. Verstraete (2006), Simplifying the interaction of land surfaces with radiation for relating remote sensing products to climate models, *Journal of Geophysical Research: Atmospheres*, *111*(D2), D02,116, doi:10.1029/2005JD005952.

Pisek, J., Y. Ryu, and K. Alikas (2011), Estimating leaf inclination and G-function from leveled digital camera photography in broadleaf canopies, *Trees*, *25*(5), 919–924, doi:10.1007/s00468-011-0566-6.

Pomeroy, J. W., D. S. Bewley, R. L. H. Essery, N. R. Hedstrom, T. Link, R. J. Granger, J. E. Sicart, C. R. Ellis, and J. R. Janowicz (2006), Shrub tundra snowmelt, *Hydrological Processes*, *20*(4), 923–941, doi:10.1002/hyp.6124.

Promis, A., D. Schindler, A. Reif, and G. Cruz (2009), Solar radiation transmission in and around canopy gaps in an uneven-aged *Nothofagus betuloides* forest, *International Journal of Biometeorology*, *53*(4), 355–367, doi:10.1007/s00484-009-0222-7.

R Core Team (2015), *R: A Language and Environment for Statistical Computing*, R Foundation for Statistical Computing, Vienna, Austria.

Reda, I., and A. Andreas (2004), Solar position algorithm for solar radiation applications, *Solar Energy*, *76*(5), 577–589, doi:10.1016/j.solener.2003.12.003.

Rees, W. G., E. I. Golubeva, and M. Williams (1998), Are vegetation indices useful in the Arctic?, *Polar Record*, *34*(191), 333–336, doi:10.1017/S0032247400026036.

Rees, W. G., M. Williams, and P. Vitebsky (2003), Mapping land cover change in a reindeer herding area of the Russian Arctic using Landsat TM and ETM+ imagery and indigenous knowledge, *Remote Sensing of Environment*, *85*(4), 441–452, doi:10.1016/S0034-4257(03)00037-3.

Reid, T. D., R. L. H. Essery, N. Rutter, and M. King (2014), Data-driven modelling of shortwave radiation transfer to snow through boreal birch and conifer canopies, *Hydrological Processes*, *28*(6), 2987–3007, doi:10.1002/hyp.9849.

Riedel, S. M., H. E. Epstein, and D. A. Walker (2005), Biotic controls over spectral reflectance of Arctic tundra vegetation, *International Journal of Remote Sensing*, *26*(11), 2391–2405, doi:10.1080/01431160512331337754.

Rocha, A. V., and G. R. Shaver (2009), Advantages of a two band EVI calculated from solar and photosynthetically active radiation fluxes, *Agricultural and Forest Meteorology*, *149*(9), 1560–1563, doi:10.1016/j.agrformet.2009.03.016.

Romanovskii, N. N., H.-W. Hubberten, A. V. Gavrilov, V. E. Tumskoy, and A. L. Kholodov (2004), Permafrost of the east Siberian Arctic shelf and coastal lowlands, *Quaternary Science Reviews*, *23*(11–13), 1359–1369, doi:10.1016/j.quascirev.2003.12.014.

Romanovsky, V. E., et al. (2010), Thermal state of permafrost in Russia, *Permafrost and Periglacial Processes*, *21*(2), 136–155, doi:10.1002/ppp.683.

Rouse, W. R. (2000), The energy and water balance of high-latitude wetlands: controls and extrapolation, *Global Change Biology*, *6*(S1), 59–68, doi:10.1046/j.1365-2486.2000.06013.x.

Rowe, C. M. (1993), Incorporating landscape heterogeneity in land surface albedo models, *Journal of Geophysical Research: Atmospheres*, *98*(D3), 5037–5043, doi:10.1029/92JD02886.

Ruimy, A., B. Saugier, and G. Dedieu (1994), Methodology for the estimation of terrestrial net primary production from remotely sensed data, *Journal of Geophysical Research: Atmospheres*, *99*(D3), 5263–5283, doi:10.1029/93JD03221.

Russell, S. (1990), Bryophyte production and decomposition in tundra ecosystems, *Botanical Journal of the Linnean Society*, *104*(1–3), 3–22, doi:10.1111/j.1095-8339.1990.tb02208.x.

Schirrmeister, L., L. Pestryakova, S. Wetterich, and V. Tumskoy (2012), Joint Russian-German polygon project east Siberia 2011 – 2014: The expedition Kytalyk 2011, *Tech. Rep. 653*, Alfred Wegener Institute for Polar and Marine Research, Bremerhaven.

Schneider, F. D., R. Leiterer, F. Morsdorf, J.-P. Gastellu-Etchegorry, N. Lauret, N. Pfeifer, and M. E. Schaepman (2014), Simulating imaging spectrometer data: 3D forest modeling based on LiDAR and in situ data, *Remote Sensing of Environment*, *152*(0), 235–250, doi:10.1016/j.rse.2014.06.015.

Schneider, J., G. Grosse, and D. Wagner (2009), Land cover classification of tundra environments in the Arctic Lena Delta based on Landsat 7 ETM+ data and its application for upscaling of methane emissions, *Remote Sensing of Environment*, *113*(2), 380–391, doi:10.1016/j.rse.2008.10.013.

Schuur, E. A. G., K. G. Crummer, J. G. Vogel, and M. C. Mack (2007), Plant species composition and productivity following permafrost thaw and thermokarst in Alaskan tundra, *Ecosystems*, *10*(2), 280–292, doi:10.1007/s10021-007-9024-0.

Schuur, E. A. G., J. G. Vogel, K. G. Crummer, H. Lee, J. O. Sickman, and T. E. Osterkamp (2009), The effect of permafrost thaw on old carbon release and net carbon exchange from tundra, *Nature*, *459*(7246), 556–559, doi:10.1038/nature08031.

Schuur, E. A. G., et al. (2015), Climate change and the permafrost carbon feedback, *Nature*, *520*, 171–179, doi:10.1038/nature14338.

Sellers, P. J., C. J. Tucker, G. J. Collatz, S. O. Los, C. O. Justice, D. A. Dazlich, and D. A. Randall (1996), A revised land surface parameterization (SiB2) for atmospheric GCMS. Part II: The generation of global fields of terrestrial biophysical parameters from satellite data, *Journal of Climate*, *9*, 706–737, doi:10.1175/1520-0442(1996)009<0706:ARLSPF>2.0.CO;2.

Serreze, M. C., et al. (2000), Observational evidence of recent change in the northern high-latitude environment, *Climatic Change*, *46*(1-2), 159–207, doi:10.1023/A:1005504031923.

Shabanov, N. V., Y. Knyazikhin, F. Baret, and R. B. Myneni (2000), Stochastic modeling of radiation regime in discontinuous vegetation canopies, *Remote Sensing of Environment*, *74*(1), 125–144, doi:10.1016/S0034-4257(00)00128-0.

Shannon, C. E. (1948), A mathematical theory of communication, *The Bell System Technical Journal*, *27*(3), 379–423, doi:10.1002/j.1538-7305.1948.tb01338.x.

Shaver, G. R. (1986), Woody stem production in Alaskan tundra shrubs, *Ecology*, *67*(3), 660–669.

Shaver, G. R., and F. S. Chapin, III (1991), Production: Biomass relationships and element cycling in contrasting arctic vegetation types, *Ecological Monographs*, *61*(1), 1–31.

Shaver, G. R., and F. S. Chapin, III (1995), Long-term responses to factorial, NPK fertilizer treatment by Alaskan wet and moist tundra sedge species, *Ecography*, *18*(3), 259–275, doi:10.1111/j.1600-0587.1995.tb00129.x.

Shaver, G. R., L. C. Johnson, D. H. Cades, G. Murray, J. A. Laundre, E. B. Rastetter, K. J. Nadelhoffer, and A. E. Giblin (1998), Biomass and CO_2 flux in wet sedge tundras: Responses to nutrients, temperature, and light, *Ecological Monographs*, *68*(1), 75–97, doi:10.1890/0012-9615(1998)068[0075:BACFIW]2.0.CO;2.

Shaver, G. R., S. M. Bret-Harte, M. H. Jones, J. Johnstone, L. Gough, J. Laundre, and F. S. Chapin, III (2001), Species composition interacts with fertilizer to control long-term change in tundra productivity, *Ecology*, *82*(11), 3163–3181, doi:10.1890/0012-9658(2001)082[3163:SCIWFT]2.0.CO;2.

Shiklomanov, N. I., and F. E. Nelson (1999), Analytic representation of the active layer thickness field, Kuparuk River Basin, Alaska, *Ecological Modelling*, *123*(2–3), 105–125, doi:10.1016/S0304-3800(99)00127-1.

Shippert, M. M., D. A. Walker, N. A. Auerbach, and B. E. Lewis (1995), Biomass and leaf-area index maps derived from SPOT images for Toolik Lake and Imnavait Creek areas, Alaska, *Polar Record*, *31*, 147–154, doi:10.1017/S0032247400013644.

Sicart, J. E., J. W. Pomeroy, R. L. H. Essery, and D. Bewley (2006), Incoming longwave radiation to melting snow: observations, sensitivity and estimation in Northern environments, *Hydrological Processes*, *20*(17), 3697–3708, doi:10.1002/hyp.6383.

Siewert, M. B., J. Hanisch, N. Weiss, P. Kuhry, T. C. Maximov, and G. Hugelius (2015), Comparing carbon storage of Siberian tundra and taiga permafrost ecosystems at very high spatial resolution, *Journal of Geophysical Research: Biogeosciences*, *120*(10), 1973–1994, doi:10.1002/2015JG002999.

Simard, M., N. Pinto, J. B. Fisher, and A. Baccini (2011), Mapping forest canopy height globally with spaceborne lidar, *Journal of Geophysical Research: Biogeosciences*, *116*(G4), G04,021, doi:10.1029/2011JG001708.

Smith, L. C., Y. Sheng, G. M. MacDonald, and L. D. Hinzman (2005), Disappearing Arctic lakes, *Science*, *308*(5727), 1429, doi:10.1126/science.1108142.

Smol, J. P., and M. S. V. Douglas (2007), Crossing the final ecological threshold in high Arctic ponds, *Proceedings of the National Academy of Sciences*, *104*(30), 12,395–12,397, doi:10.1073/pnas.0702777104.

Solomon, S., D. Qin, M. Manning, Z. Chen, M. Marquis, K. B. Averyt, M. Tignor, and H. L. Miller (Eds.) (2007), *Climate Change 2007: The Physical Science Basis*, Cambridge University Press, IPCC, 2007.

Sonesson, M., and H. Bergman (1980), Area-harvesting as a method of estimating phytomass changes in a tundra mire, *Ecological Bulletins*, *30*, 127–137.

Song, C., G. Katul, R. Oren, L. E. Band, C. L. Tague, P. C. Stoy, and H. R. McCarthy (2009), Energy, water, and carbon fluxes in a loblolly pine stand: Results from uniform and gappy canopy models with comparisons to eddy flux data, *Journal of Geophysical Research: Biogeosciences*, *114*(G4), doi:10.1029/2009JG000951, g04021.

Spehn, E. M., J. Joshi, B. Schmid, M. Diemer, and C. Körner (2000), Above-ground resource use increases with plant species richness in experimental grassland ecosystems, *Functional Ecology*, *14*(3), 326–337.

Sprintsin, M., J. M. Chen, A. Desai, and C. M. Gough (2012), Evaluation of leaf-to-canopy upscaling methodologies against carbon flux data in North America, *Journal of Geophysical Research: Biogeosciences*, *117*(G1), doi:10.1029/2010JG001407, g01023.

Stocker, T. F., et al. (Eds.) (2013), *Climate Change 2013: The Physical Science Basis*, Cambridge University Press, IPCC, 2013.

Strahler, A. H., et al. (2006), *Global land cover validation: Recommendations for evaluation and accuracy assessment of global land cover maps*, Luxembourg: Office for Official Publications of the European Communities.

Strebel, D. E., N. S. Goel, and K. J. Ranson (1985), Two-dimensional leaf orientation distributions, *Geoscience and Remote Sensing, IEEE Transactions on*, *GE-23*(5), 640–647, doi:10.1109/TGRS.1985.289382.

Street, L. E., G. R. Shaver, M. Williams, and M. T. van Wijk (2007), What is the relationship between changes in canopy leaf area and changes in photosynthetic CO_2 flux in arctic ecosystems?, *Journal of Ecology*, *95*(1), 139–150, doi:10.1111/j.1365-2745.2006.01187.x.

Stuiver, B. M., D. A. Wardle, M. J. Gundale, and M.-C. Nilsson (2014), The impact of moss species and biomass on the growth of *Pinus sylvestris* tree seedlings at different precipitation frequencies, *Forests*, *5*(8), 1931, doi:10.3390/f5081931.

Sturm, M., J. P. McFadden, G. E. Liston, F. S. Chapin, III, C. H. Racine, and J. Holmgren (2001a), Snow-shrub interactions in Arctic tundra: A hypothesis with climatic implications, *Journal of Climate*, *14*(3), 336–344, doi:10.1175/1520-0442(2001)014<0336:SSIIAT>2.0.CO;2.

Sturm, M., C. Racine, and K. Tape (2001b), Increasing shrub abundance in the Arctic, *Nature*, *411*(6837), 546–547, doi:10.1038/35079180.

Sturm, M., T. Douglas, C. Racine, and G. E. Liston (2005), Changing snow and shrub conditions affect albedo with global implications, *Journal of Geophysical Research: Biogeosciences*, *110*(G1), G01,004, doi:10.1029/2005JG000013.

Swann, A. L., I. Y. Fung, S. Levis, G. B. Bonan, and S. C. Doney (2010), Changes in Arctic vegetation amplify high-latitude warming through the greenhouse effect, *Proceedings of the National Academy of Sciences*, *107*(4), 1295–1300, doi:10.1073/pnas.0913846107.

Sweet, S. K., K. L. Griffin, H. Steltzer, L. Gough, and N. T. Boelman (2015), Greater deciduous shrub abundance extends tundra peak season and increases modeled net CO_2 uptake, *Global Change Biology*, *21*(6), 2394–2409, doi:10.1111/gcb.12852.

Tagesson, T., M. Mastepanov, M. P. Tamstorf, L. Eklundh, P. Schubert, A. Ekberg, C. Sigsgaard, T. R. Christensen, and L. Ström (2012), High-resolution satellite data reveal an increase in peak growing season gross primary production in a high-Arctic wet tundra ecosystem 1992–2008, *International Journal of Applied Earth Observation and Geoinformation*, *18*, 407–416, doi:10.1016/j.jag.2012.03.016.

Tape, K., M. Sturm, and C. Racine (2006), The evidence for shrub expansion in Northern Alaska and the Pan-Arctic, *Global Change Biology*, *12*(4), 686–702, doi:10.1111/j.1365-2486.2006.01128.x.

Thompson, C., J. Beringer, F. S. Chapin, III, and A. D. McGuire (2004), Structural complexity and land-surface energy exchange along a gradient from arctic tundra to boreal forest, *Journal of Vegetation Science*, *15*(3), 397–406, doi:10.1111/j.1654-1103.2004.tb02277.x.

Tuller, S. E. (1976), The relationship between diffuse, total and extra terrestrial solar radiation, *Solar Energy*, *18*(3), 259–263, doi:10.1016/0038-092X(76)90025-6.

van der Molen, M. K., J. van Huissteden, F. J. W. Parmentier, A. M. R. Petrescu, A. J. Dolman, T. C. Maximov, A. V. Kononov, S. V. Karsanaev, and D. A. Suzdalov (2007), The growing season greenhouse gas balance of a continental tundra site in the Indigirka lowlands, NE Siberia, *Biogeosciences*, *4*(6), 985–1003, doi:10.5194/bg-4-985-2007.

van Huissteden, J., T. C. Maximov, and A. J. Dolman (2005), High methane flux from an arctic floodplain (Indigirka lowlands, eastern Siberia), *Journal of Geophysical Research: Biogeosciences*, *110*(G2), G02,002, doi:10.1029/2005JG000010.

van Wijk, M. T., et al. (2003), Long-term ecosystem level experiments at Toolik Lake, Alaska, and at Abisko, Northern Sweden: generalizations and differences in ecosystem and plant type responses to global change, *Global Change Biology*, *10*(1), 105–123, doi:10.1111/j.1365-2486.2003.00719.x.

Vavrus, S., D. Waliser, A. Schweiger, and J. Francis (2009), Simulations of 20th and 21st century Arctic cloud amount in the global climate models assessed in the IPCC AR4, *Climate Dynamics*, *33*(7–8), 1099–1115, doi:10.1007/s00382-008-0475-6.

Verrelst, J., M. E. Schaepman, Z. Malenovský, and J. G. P. W. Clevers (2010), Effects of woody elements on simulated canopy reflectance: Implications for forest chlorophyll content retrieval, *Remote Sensing of Environment*, *114*(3), 647–656, doi:10.1016/j.rse.2009.11.004.

Verstraete, M. M. (1987), Radiation transfer in plant canopies: Transmission of direct solar radiation and the role of leaf orientation, *Journal of Geophysical Research: Atmospheres*, *92*(D9), 10,985–10,995, doi:10.1029/JD092iD09p10985.

Virtanen, T., and M. Ek (2014), The fragmented nature of tundra landscape, *International Journal of Applied Earth Observation and Geoinformation*, *27*(Part A), 4–12, doi:10.1016/j.jag.2013.05.010.

Vojtech, E., M. Loreau, S. Yachi, E. M. Spehn, and A. Hector (2008), Light partitioning in experimental grass communities, *Oikos*, *117*(9), 1351–1361, doi:10.1111/j.0030-1299.2008.16700.x.

Vourlitis, G. L., and W. C. Oechel (1999), Eddy covariance measurements of CO_2 and energy fluxes of an Alaskan tussock tundra ecosystem, *Ecology*, *80*(2), 686–701, doi:10.1890/0012-9658(1999)080[0686:ECMOCA]2.0.CO;2.

Wahren, C.-H. A., M. D. Walker, and M. S. Bret-Harte (2005), Vegetation responses in Alaskan arctic tundra after 8 years of a summer warming and winter snow manipulation experiment, *Global Change Biology*, *11*(4), 537–552, doi:10.1111/j.1365-2486.2005.00927.x.

Walker, D. A., et al. (1998), Energy and trace-gas fluxes across a soil pH boundary in the Arctic, *Nature*, *394*(6692), 469–472, doi:10.1038/28839.

Walker, D. A., et al. (2003a), Phytomass, LAI, and NDVI in northern Alaska: Relationships to summer warmth, soil pH, plant functional types, and extrapolation to the circumpolar Arctic, *Journal of Geophysical Research: Atmospheres*, *108*(D2), 8169, doi:10.1029/2001JD000986.

Walker, D. A., et al. (2003b), Vegetation–soil-thaw-depth relationships along a low-arctic bioclimate gradient, Alaska: synthesis of information from the ATLAS studies, *Permafrost and Periglacial Processes*, *14*(2), 103–123, doi:10.1002/ppp.452.

Walker, D. A., et al. (2005), The Circumpolar Arctic vegetation map, *Journal of Vegetation Science*, *16*(3), 267–282, doi:10.1111/j.1654-1103.2005.tb02365.x.

Walker, D. A., et al. (2008), Arctic patterned-ground ecosystems: A synthesis of field studies and models along a North American Arctic transect, *Journal of Geophysical Research: Biogeosciences*, *113*(G3), G03S01, doi:10.1029/2007JG000504.

Walker, D. A., P. Kuss, H. E. Epstein, A. N. Kade, C. M. Vonlanthen, M. K. Raynolds,

and F. J. A. Daniëls (2011), Vegetation of zonal patterned-ground ecosystems along the North America Arctic bioclimate gradient, *Applied Vegetation Science*, *14*(4), 440–463, doi: 10.1111/j.1654-109X.2011.01149.x.

Walker, M. D., et al. (2006), Plant community responses to experimental warming across the tundra biome, *Proceedings of the National Academy of Sciences*, *103*(5), 1342–1346, doi:10.1073/pnas. 0503198103.

Wang, W.-M., Z.-L. Li, and H.-B. Su (2007), Comparison of leaf angle distribution functions: Effects on extinction coefficient and fraction of sunlit foliage, *Agricultural and Forest Meteorology*, *143*(1–2), 106–122, doi:10.1016/j.agrformet.2006.12.003.

Wang, X., and J. R. Key (2005a), Arctic surface, cloud, and radiation properties based on the AVHRR polar pathfinder dataset. Part II: Recent trends., *Journal of Climate*, *18*(14), 2575–2593, doi:10.1175/JCLI3439.1.

Wang, X., and J. R. Key (2005b), Arctic surface, cloud, and radiation properties based on the AVHRR polar pathfinder dataset. Part I: Spatial and temporal characteristics., *Journal of Climate*, *18*(14), 2558–2574, doi:10.1175/JCLI3438.1.

Wania, R., I. Ross, and I. C. Prentice (2009), Integrating peatlands and permafrost into a dynamic global vegetation model: 1. Evaluation and sensitivity of physical land surface processes, *Global Biogeochemical Cycles*, *23*(3), GB3014, doi:10.1029/2008GB003412.

Westermann, S., M. Langer, and J. Boike (2011), Spatial and temporal variations of summer surface temperatures of high-arctic tundra on Svalbard – Implications for MODIS LST based permafrost monitoring, *Remote Sensing of Environment*, *115*(3), 908–922, doi:10.1016/j.rse.2010.11.018.

Widlowski, J.-L., et al. (2011), RAMI4PILPS: An intercomparison of formulations for the partitioning of solar radiation in land surface models, *Journal of Geophysical Research: Biogeosciences*, *116*(G2), G02,019, doi:10.1029/2010JG001511.

Widlowski, J.-L., et al. (2015), The fourth phase of the radiative transfer model intercomparison (RAMI) exercise: Actual canopy scenarios and conformity testing, *Remote Sensing of Environment*, *169*, 418–437, doi:10.1016/j.rse.2015.08.016.

Williams, M., E. B. Rastetter, G. R. Shaver, J. E. Hobbie, E. Carpino, and B. L. Kwiatkowski (2001), Primary production of an arctic watershed: An uncertainty analysis, *Ecological Applications*, *11*(6), 1800–1816, doi:10.1890/1051-0761(2001)011[1800:PPOAAW]2.0.CO;2.

Williams, M., L. E. Street, M. T. van Wijk, and G. R. Shaver (2006), Identifying differences in carbon exchange among arctic ecosystem types, *Ecosystems*, *9*(2), 288–304, doi:10.1007/ s10021-005-0146-y.

Williams, M., E. B. Rastetter, L. Van der Pol, and G. R. Shaver (2014), Arctic canopy photosynthetic efficiency enhanced under diffuse light, linked to a reduction in the fraction of the canopy in deep shade, *New Phytologist*, *202*(4), 1267–1276, doi:10.1111/nph.12750.

Williams, T. J., and W. L. Quinton (2013), Modelling incoming radiation on a linear disturbance and its impact on the ground thermal regime in discontinuous permafrost, *Hydrological Processes*, *27*(13), 1854–1865, doi:10.1002/hyp.9792.

Wilson, J. W. (1959), Analysis of the spatial distribution of foliage by two-dimensional point quadrats, *New Phytologist*, *58*(1), 92–99, doi:10.1111/j.1469-8137.1959.tb05340.x.

Xue, K., et al. (2016), Tundra soil carbon is vulnerable to rapid microbial decomposition under climate warming, *Nature Climate Change*, doi:10.1038/nclimate2940.

Yang, F., K. Mitchell, Y.-T. Hou, Y. Dai, X. Zeng, Z. Wang, and X.-Z. Liang (2008), Dependence of land surface albedo on solar zenith angle: Observations and model parameterization, *Journal of Applied Meteorology and Climatology*, *47*(11), 2963–2982, doi:10.1175/2008JAMC1843.1.

Yi, S., M.-K. Woo, and M. A. Arain (2007), Impacts of peat and vegetation on permafrost degradation under climate warming, *Geophysical Research Letters*, *34*(16), L16,504, doi:10.1029/2007GL030550.

Yuan, H., R. E. Dickinson, Y. Dai, M. J. Shaikh, L. Zhou, W. Shangguan, and D. Ji (2014), A 3D canopy radiative transfer model for global climate modeling: Description, validation, and application, *Journal of Climate*, *27*(3), 1168–1192, doi:10.1175/JCLI-D-13-00155.1.

Zeng, X., M. Shaikh, Y. Dai, R. E. Dickinson, and R. Myneni (2002), Coupling of the Common Land Model to the NCAR Community Climate Model, *Journal of Climate*, *15*, 1832–1854, doi:10.1175/1520-0442(2002)015<1832:COTCLM>2.0.CO;2.

Zhang, X., F. W. Zwiers, G. C. Hegerl, F. H. Lambert, N. P. Gillett, S. Solomon, P. A. Stott, and T. Nozawa (2007), Detection of human influence on twentieth-century precipitation trends, *Nature*, *448*, 461–465, doi:10.1038/nature06025.

Acknowledgements

First of all I thank Gabriela Schaepman-Strub for giving me the opportunity to do research at a most fascinating place and for always being available for questions. I also thank the three members of my committee, Michael Schaepman, Werner Eugster, and Bernhard Schmid for our discussions and (also financial) support of my ideas. I am grateful to have been part of the University of Zurich URPP Global Change and Biodiversity as I enjoyed the numerous interdisciplinary activities and discussions.

I thank Angela Erb for conceiving and collecting the field data for Chapter 3 and Egor Starostin and Rachel Simeon for helping in the field. Many thanks to Monique M. P. D. Heijmans for providing soil sensors and helpful suggestions for Chapter 2. I am grateful for the amazing group of researchers sharing and improving my Kytalyk fieldwork experience. Further, I would like to thank Tatiana Strukova from the nature protection agency in Chokurdakh and Trofim C. Maximov, Alexander V. Kononov, and the other members of the IBPC Yakutsk for the logistic and administrative support of the field work. Thanks to the Pangaea platform for hosting my field data and to Jean-Philippe Gastellu-Etchegorry and his team for constantly improving the DART model.

I thank my colleagues and friends at the university for making work and breaks so enjoyable, for motivating me and listening to me whenever needed. Although it is really the group as a whole who makes the difference, I mention especially my friends Saeed Karbin who shared office and thoughts with me for three years, Irene Garonna who shared my whole PhD process with its ups and downs and Maitane Iturrate-Garcia who did not only share the field experience but also all worries and achievements. Last and most cordially I thank Tim Grünberg and my family for being there for me at all times.

Curriculum vitae

JUSZAK, Inge

Date of birth: 28 November 1986
Nationality: German

Education

09/2012 – 06/2016	**University of Zurich**, Switzerland PhD student in the Department of Evolutionary Biology and Environmental Studies
10/2006 – 10/2011	**Technische Universität Dresden**, Germany Graduated with *Diplom* in Hydrology, final grade 1.0
04/2011 – 09/2011	**ETH Zürich**, Switzerland Diploma thesis on the characterisation of the hydrological components in an alpine glacierised catchment; written at the Institute of Environmental Engineering
09/2009 – 06/2010	**ETH Zürich**, Switzerland Exchange student at the Institute of Environmental Engineering
08/1997 – 06/2006	**Gymnasium der Mariannhiller Missionare**, Maria Veen, Germany Graduated with *Abitur* (Allgemeine Hochschulreife), final grade 1.3
09/2003 – 08/2004	Student exchange year in the X Liceum Ogólnokształcące, Toruń, Poland

Awards and scholarship

Lohrmann-Medaille, Best graduate of the Faculty of Environmental Sciences, TU Dresden in the year 2011/2012

Outstanding student poster, EGU General Assembly 2015

Studienstiftung des Deutschen Volkes

Publications

Juszak and Pellicciotti (2013) A comparison of parameterizations of incoming longwave radiation over melting glaciers: Model robustness and seasonal variability,

Journal of Geophysical Research, 118 (8), 3066–3084

Juszak et al. (2014) Arctic shrub effects on NDVI, summer albedo and soil shading, *Remote Sensing of Environment*, 153, 79–89

Juszak et al. (2016a) Contrasting radiation and soil heat fluxes in Arctic shrub and wet sedge tundra, *Biogeosciences*, 13, 4049–4064

Juszak et al. (2016b) Drivers of shortwave radiation fluxes in Arctic tundra across scales, *Remote Sensing of Environment*, in review

Conference contributions

I. Juszak

A comparison of parameterisations of incoming longwave radiation over melting glaciers: model robustness and seasonal variability, *16th Alpine Glaciology Meeting*, Zürich, 2012 (poster presentation)

I. Juszak, A. Erb and G. Schaepman-Strub

Effect of shrubs on shortwave surface energy fluxes in the Arctic tundra – 3D radiative transfer modelling and model validation, *Patterns in Soil-Vegetation-Atmosphere-Systems: Monitoring, Modelling & Data Assimilation*, Bonn, 2013 (oral presentation)

I. Juszak, A. Erb, M. Iturrate and G. Schaepman-Strub

Effect of shrubification on shortwave radiation fluxes in the Siberian Arctic – Parameterisation and validation of a 3D radiative transfer model for dwarf shrubs using experimental data, *Global Vegetation Monitoring & Modeling*, Avignon, 2014 (oral presentation)

I. Juszak, M. Iturrate, T. C. Maximov and G. Schaepman-Strub

Effects of Arctic tundra vegetation types on the shortwave radiation balance, *8th annual international symposium on C/ H_2O/Energy balance and climate over boreal and arctic regions with special emphasis on eastern Eurasia*, Wageningen, 2014 (oral presentation)

I. Juszak and G. Schaepman-Strub

The impact of vegetation type on the shortwave radiation balance of the Arctic tundra, *EGU General Assembly 2015*, Vienna, 2015 (poster presentation)

I. Juszak, M. Iturrate-Garcia, and G. Schaepman-Strub

Influence of Arctic tundra vegetation on radiation and soil fluxes, *13th Swiss Geoscience Meeting*, Basel, 2015 (oral presentation)

I. Juszak, M. Iturrate Garcia, J.-P. Gastellu-Etchegorry, M. E. Schaepman, and G. Schaepman-Strub

Radiation budget and soil heat fluxes in different Arctic tundra vegetation types, *EGU General Assembly 2016*, Vienna, 2016 (oral presentation)

Appendices

A Measurement set-up and data analysis

A.1 In situ observations

The data collection at the Kytalyk field site included a number of different approaches to assess vegetation distribution, canopy properties, and energy budget components (Section 1.6). An overview of all variables measured in at least one of the four field campaigns between July 2013 and July 2015 is presented in Table A.1.

Table A.1: List of all in situ observations between July 2013 and July 2015 at the Kytalyk field site; all time series, spatially distributed, and auxiliary measurements were carried out at dwarf shrubs (*Betula nana*) and wet sedges (*Eriophorum angustifolium*); the plant organs studied were green leaves, standing dead leaves, and wood.

Time series	Spatially distributed measurements	Auxiliary measurements	Measurements in the larger study region
Incoming shortwave radiation	Plant organ area index	Plant organ biomass	Vegetation type reference points
Reflected shortwave radiation	Fractional cover of background types	Plant organ mass per area	Orthophotos
Below canopy transmitted shortwave radiation	Active layer thickness	Destructive plant organ area	Snowdepth
Incoming longwave radiation	Canopy and standing dead leaf height	Plant organ optical properties	Active layer thickness transects next to & in water bodies
Emitted longwave radiation	Canopy transmittance of photosynthetically active radiation (tPAR)	Plant organ angle distributions	
Air temperature	Canopy spectral reflectance	tPAR depending on sun angle and fraction of diffuse light	
Soil temperature		Canopy spectral reflectance depending on sun angle and fraction of diffuse light	
Soil heat flux at 10 cm depth		tPAR depending on canopy density	
Soil moisture		Canopy spectral reflectance depending on canopy density	
Snow melt timing and vegetation phenology		Soil thermal properties	

A.2 Design and instruments of automatic measurements

The experimental set-up consisted of two automatic stations for measuring the above canopy radiation budget, below canopy transmitted shortwave radiation, air temperature, soil temperature, soil moisture, and soil heat flux. All data were recorded by one datalogger per station with a measurement frequency of 30 seconds and

storage of averages and standard deviations every 10 minutes. The locations of the stations were 70°49'59.0" N, 147°30'17.1" E on dwarf shrubs (*Betula nana*) and 70°49'57.3" N, 147°30'16.6" E on wet sedges (*Eriophorum angustifolium*). More details on the location of the sensors are shown in Figure A.2. The sensor description and measurements are summarised in Table A.2 with some more details in Table A.3. Table A.4 includes the serial numbers of the specific sensors used for this work. One automatic camera per plot was looking vertically down and one was mounted as shown in Figure A.1.

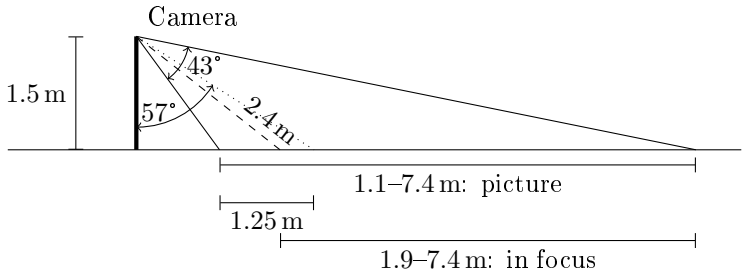

Figure A.1: Schematic drawing of the set-up and field of view of the cameras.

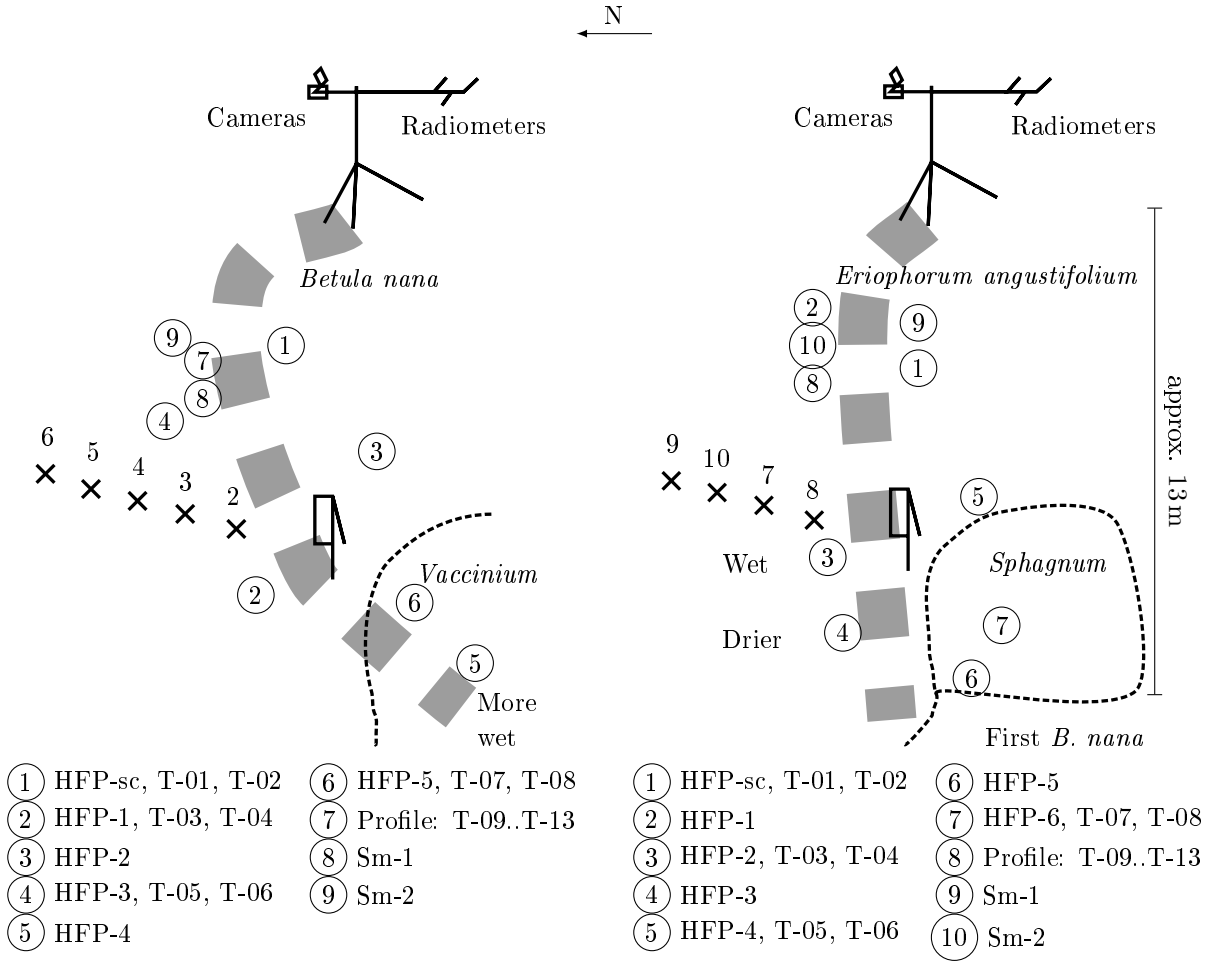

Figure A.2: Location of the soil measurements in both plots (o); x indicate SPLITE2; all SPLITE2 sensors are in one line with about 2 m between them; HFP denotes heat flux plate, T denotes soil temperature and Sm soil moisture sensors; the tripods were located at 70.8330°N, 147.5047°E on dwarf shrubs (*Betula nana*) and 70.8326°N, 147.5046°E on wet sedges (*Eriophorum angustifolium*).

Table A.2: Overview of the properties of sensors and loggers used in this study, part 1: General description.

Name	Model	Manufacturer	Short description
Data logger	CR1000	Campbell Scientific	Data logger to collect all automatic data, OS 22 or higher
Flash Memory Drive	SC115	Campbell Scientific	External storage for data logger
Multiplex	AM16/32B	Campbell Scientific	Multiplex for data logger
Albedometer	CMA11	Kipp& Zonen	Albedo
Pyranometer	CMP11	Kipp& Zonen	Reflected solar radiation
Pyrgeometer	CGR3	Kipp& Zonen	Incoming thermal radiation
Pyranometer	SPLITE2	Kipp& Zonen	Solar radiation below canopy
Net-radiometer	CNR2	Kipp& Zonen	Thermal and solar radiation budget
Thermocouple	Type E	VU	Air temperature
Thermistor	T107 (NTC / 100K6A)	Campbell Scientific (BetaTHERM)	Soil temperature
Self calibrating heat flux plate	HFP01SC	Hukseflux	Soil heat flux
Heat flux plate	HFP01	Hukseflux	Soil heat flux
Frequency domain soil moisture sensor	ML2x	Delta-T Devices	Soil moisture
Time lapse camera	TimelapseCam 8.0	Wingscapes	Automatic camera, snowmelt patterns, phenology
Spectrometer	Jaz-SpectroClip-TR	Ocean Optics	Portable spectrometer, leaf and canopy optical properties
Ceptometer	SunScan, SS1	Delta-T Devices	Ceptometer, transmitted photosynthetically active radiation (below canopy)

Table A.3: Overview of the properties of sensors and loggers used in this study, part 2: More details; sensitivity and accuracy values from the manuals.

Name	Sensitivity	Accuracy	Power supply	Output	Memory
Data logger	250Hz	0.12% of reading + offset	12 Vdc	±5 Vdc	2 MB Flash (OS), 4 MB SRAM (CPU, program & data)
Flash Memory Drive	-	-	5 Vdc	-	2 GB
Multiplex	-	-	12 Vdc	-	-
Albedometer	285–2800 nm	±2% (daily value)	-	0–15 mV	-
Pyranometer	285–2800 nm	±2% (daily value)	-	0–15 mV	-
Pyrgeometer	4.5–42 µm	±10% (daily value)	-	−4–4 mV	-
Pyranometer	400–1100 nm		-	0–120 mV	-
Net-radiometer	310–2800 nm, 4.5–42 µm	±4%	-	0–50 mV	-
Thermocouple	-		-	-	-
Thermistor	-	± 0.4 °C	-	-	-
Self calibrating heat flux plate	-	±3%	12 V	−10–20 mV	-
Heat flux plate	-	-15% to +5%	-	−10–20 mV	-
Frequency domain soil moisture sensor	-	±1%	12 V	0–1 V	-
Time lapse camera	RGB, Field of view 43°, Figure A.1	2592 x 1944 pixel	12 V	-	16 GB Flash
Spectrometer	350–1000 nm		Rechargeable Lithium-Ion (5 V)	-	2 GB Flash
Ceptometer	400–700 nm	±10%	10 AA Alkaline batteries	-	128 MB Flash

Table A.4: Specific sensors and loggers used in this study; WUR: Wageningen UR (Monique Heijmans).

Name	Number	Owner	Serial number
Data logger	2	UZH, WUR	E10510/E5686 (UZH), 8088/8313 (WUR)
Flash Memory Drive	2	UZH	2079, 2322
Multiplex	2	UZH, WUR	E8298 (UZH), 3223 (WUR)
Albedometer	1	UZH	120081
Pyranometer	1	UZH	127579
Pyrgeometer	1	UZH	100251
Pyranometer	10	UZH	125965, 125966, 125967, 125968, 125969, 125970, 125971, 125972, 125973, 125974
Net-radiometer	2	WUR	070014, 070015
Thermocouple	9 (4 broken)	WUR	-
Thermistor	26	WUR	07326/9 (left in the field), 07326/11 (left in the field), 15377/6, 07361/10, 07326/7, 17914/25, 17914/16, 17914/23, 07361/4, 07361/16, 17914/21, 15212/3, 17914/18, 07361/11, 15212/1, 15212/14, 17914/9, 07326/14, 07326/20, 07361/8, 17914/14, 07361/13, 07326/6, 17914/26, 07361/6, 07361/17
Self calibrating heat flux plate	2	WUR	001372, 001373
Heat flux plate	14	WUR	002097 (broken), 002098, 002099, 002100, 002779, 002780, 002781, 002782, 00794, 00791, 00790, 00789, 00795, 00788
Frequency domain soil moisture sensor	4	WUR	-
Time lapse camera	4	UZH	GC20600046, GC20602287, GC20602288, GC20801622
Spectrometer	1	UZH	08517
Ceptometer	1	UZH	-

A.3 Leaf optical properties measurements

I measured leaf optical properties with an Ocean optics Jaz spectrometer and a leaf-clip consisting of two small integrating spheres (Section 4.A.2, page 89). However, raw measurements of the leaf optical properties could not be used directly, as the sum of reflectance and transmittance was > 1 for many measurements in the near infra-red.

No transmittance: Upper sphere

The first order correction was based on an estimation of the fraction of light interacting with the sample twice (x). I did regular test measurements with two reflectance standards, one about 100% reflecting, the other 50% with the exact spectral reflectance known from the calibration certificates.

First order approximation:

$$1 = a + r \tag{A.1}$$

$$A = I \cdot a + x(I \cdot r \cdot a) \tag{A.2}$$

$$\begin{aligned} D_1 &= I - A \\ &= I - I \cdot (a + x \cdot r \cdot a) \\ &= I \cdot (1 - (1 - r + x \cdot r(1 - r))) \\ &= I \cdot (r - x \cdot r + x \cdot r^2) \end{aligned} \tag{A.3}$$

$$\frac{D_1}{I} = (1 - x) \cdot r + x \cdot r^2$$

$$0 = -\frac{D_1}{In \cdot x} + \frac{1 - x}{x} r + r^2$$

$$r = -\frac{1 - x}{2x} \pm \sqrt{\left(\frac{1 - x}{2x}\right)^2 + \frac{D_1}{I \cdot x}} \tag{A.4}$$

$$x = \frac{\frac{D_1}{I} - r}{r^2 - r} \tag{A.5}$$

All interactions are diffuse, however, in the sketch just one possibility is illustrated.

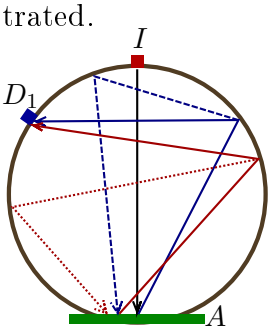

blue: first interaction, red: second interaction; dotted line and further interactions were not considered.

Including transmittance: Both spheres

A proper calibration of the transmittance readings was not possible. Thus, I used the fraction of light interacting with the sample twice (x) from the 'only reflectance' case (Equation A.5). Equations A.9 and A.10 were solved iteratively. As independent tests, I compared corrected leaf reflectance spectra of the same leaf measured twice, first normally and second on a non-transmitting black background. These tests were done for all leaves and showed good agreement.

First order approximation:

All interactions diffuse.

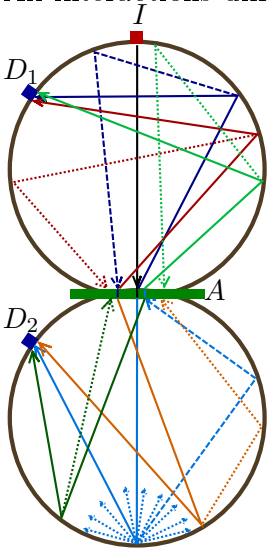

$$1 = a + r + t \tag{A.6}$$

$$A = I \cdot a + x \cdot I \cdot r_1 \cdot a + x \cdot I \cdot t_1 \cdot a$$

$$D_1 = I \cdot r_1(1-x) + I \cdot x \cdot r_1^2 + I \cdot t_1 \cdot x \cdot t_2 \tag{A.7}$$

$$D_2 = I \cdot t_1(1-x) + I \cdot x \cdot r_1 \cdot t_1 + I \cdot t_1 \cdot x \cdot r_2 \tag{A.8}$$

$$0 = I - A - D_1 - D_2 \qquad \text{tested, OK}$$

Solved for $r_1 = r_2$ & $t_1 = t_2$

$$0 = t^2 - \frac{D_1}{I \cdot x} + \frac{1-x}{x} r + r^2$$

$$r = -\frac{1-x}{2x} \pm \sqrt{\left(\frac{1-x}{2x}\right)^2 + \frac{D_1}{I \cdot x} - t^2} \tag{A.9}$$

$$t = \frac{D_2}{I\,(1 - x + 2x \cdot r)} \tag{A.10}$$

I	Incoming light from the lamp
A	Light absorbed by the sample
D_1, D_2	Light detected by sensor 1 or 2
r_1, r_2	Fraction of light reflected by sample side 1 or 2
t_1, t_2	Fraction of light transmitted by sample side 1 or 2
a	Fraction of light absorbed by sample
x	$0 < x < 1$ Fraction interacting with the sample again

A.4 Transformation of projected to effective leaf angle distribution

I estimated the leaf angle distribution of dwarf shrub leaves following *Pisek et al.* (2011). This method uses levelled photographs in all azimuth directions and visual identification of leaves that are perpendicular to the image plane. However, for dwarf birch wood and wet sedge green leaves and standing dead leaves I had to adapt this method because it was not possible to judge whether wood and leaves were perpendicular to the image plane. Thus, I identified all objects in the photographs and transformed the resulting distribution of projected angles back to 'real' angles assuming a random distribution of leaf azimuth angles (see also Section 4.A.2, Page 88).

The geometrical basis of the transformation is illustrated in Figure A.3 with:

a, b, c	Leaf extent in image plane and perpendicular
L	Leaf length
L'	Projected leaf length in view plane as identified from pictures
γ	Leaf azimuth angle (0° and 180° are in the image plane)
φ	Leaf zenith angle
φ'	Projected leaf zenith angle as identified from pictures

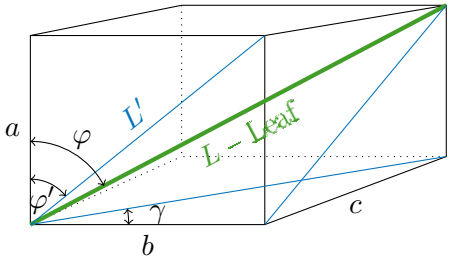

Figure A.3: Schematic of the effective φ and projected φ' leaf zenith angle.

Geometrical rules:

$$\tan(\varphi') = \frac{\sin(\varphi)\cos(\gamma)}{\cos(\varphi)} = \tan(\varphi)\cos(\gamma) \tag{A.11}$$

$$\Rightarrow \varphi' = \left|\tan^{-1}\left(\tan(\varphi)\cos(\gamma)\right)\right| \tag{A.12}$$

$$\Rightarrow \gamma = \cos^{-1}\left(\frac{\tan(\varphi')}{\tan(\varphi)}\right) \tag{A.13}$$

$$\Leftrightarrow \frac{\mathrm{d}\gamma}{\mathrm{d}\varphi'} = -\frac{\cot(\varphi)\sec^2(\varphi')}{\sqrt{1-\cot^2(\varphi)\tan^2(\varphi')}} \tag{A.14}$$

$$L' = L\frac{\cos(\varphi)}{\cos(\varphi')} \tag{A.15}$$

$$= L\frac{\cos(\varphi)}{\cos\left(\left|\tan^{-1}\left(\tan(\varphi)\cos(\gamma)\right)\right|\right)} \tag{A.16}$$

$$= L\cos(\varphi)\sqrt{\tan^2(\varphi)\cos^2(\gamma)+1} \tag{A.17}$$

Leaves that point away or towards the viewer appear shorter on the images, depending on their inclination angle. Thus, I estimated the reduction in visible leaf length (L') due to the azimuth angle for zenith angle φ_i and random azimuth angles from Equation A.17:

$$L'_i = L\frac{\sum_{\gamma=0}^{90}\cos(\varphi_i)\sqrt{\tan^2(\varphi_i)\cos^2(\gamma)+1}}{n} \tag{A.18}$$

using n steps between 0 and 90°

Numerical estimation of the weight w in the system of equation to solve to convert the projected angle distribution to the effective angle distribution for zenith angle class φ_i (with bin width d) from Equation A.14:

$$v_i = \mathrm{real}\left(\frac{\cot(\varphi_{i+d})\sec^2(\varphi)}{\sqrt{1-\cot^2(\varphi_{i+d})\tan^2(\varphi)}}\right) \tag{A.19}$$

$$w_i = \frac{v_i}{\sum v_i} \tag{A.20}$$

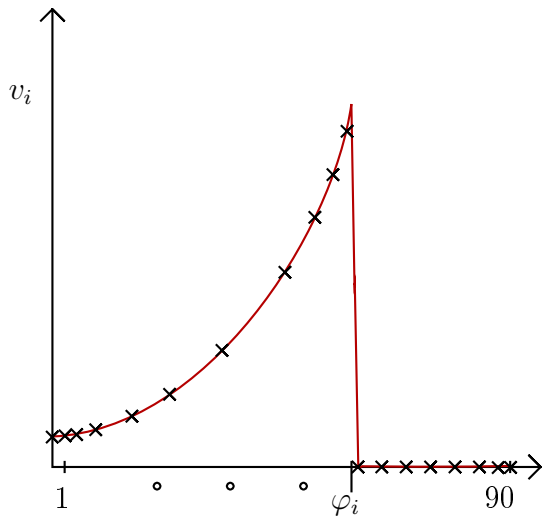

Figure A.4: Schematic of the weights of effective angles φ_i which contribute to the projected angle φ'_i.

System of equations of the distribution of φ from the known distribution of φ' using the weight w (one value per zenith angle) from Equation A.20:

$$P(\varphi') = wP_1(\varphi) \tag{A.21}$$

Solved in MATLAB with the backslash operator $P_{f_{orig}} = w \backslash P_{f_{proj}}$. As a last step, the new distribution is adjusted for the reduced visible length depending on the zenith angle and normalised:

$$P_2(\varphi_i) = \frac{P_1(\varphi_i)}{L'_i} \tag{A.22}$$

$$P(\varphi_i) = \frac{P_2(\varphi_i)}{\sum P_2} \tag{A.23}$$

The transformation of the density function is based on lecture notes by *King* (2003). Thanks to Tim Grünberg for helping with the concept and the numerical implementation.

A.5 NDVI, surface model, and vegetation map of the study area

The derivation of the remote sensing data and products is only described briefly in Section 4.2.2. Below are some more details on the field method and the data analysis.

I did 25 drone flights of four overlapping sub-areas with more than 5000 photos by three different Canon S110 cameras, one with standard red-green-blue (RGB) bands,

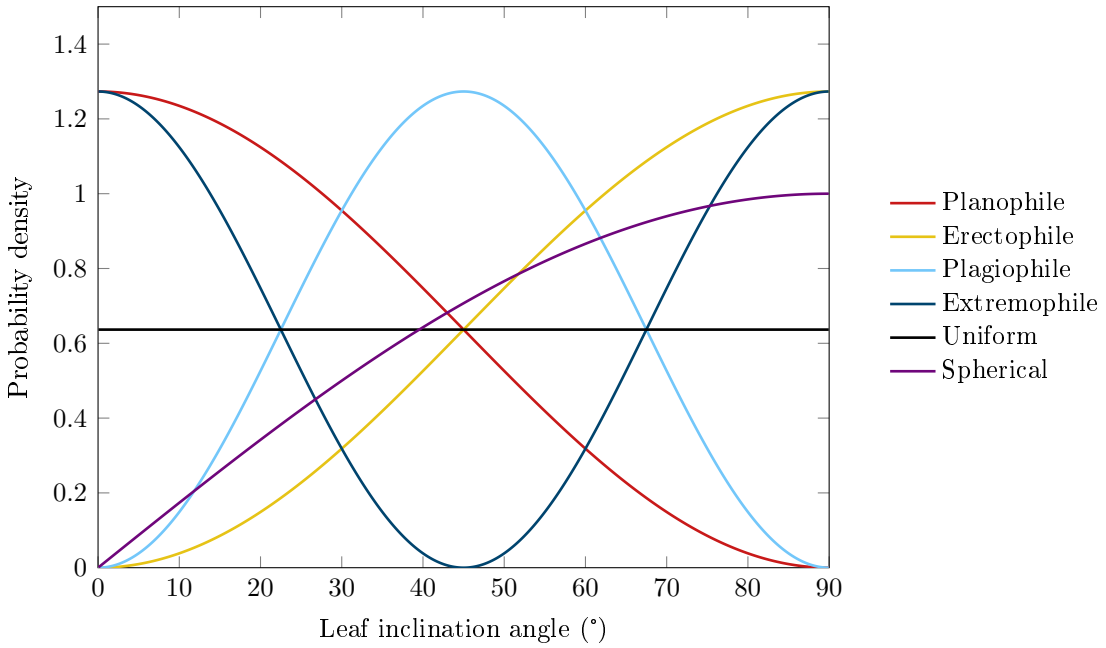

Figure A.5: Probability density (bin width: 1 rad = 57.3°) of often used standard leaf inclination angle distributions (*Goel and Strebel*, 1984).

one with a red edge (RE) band and one with a near infra-red (NIR) band. The pictures of each sub-area were merged to orthomosaics and calibrated reflectance maps (PostflightTerra 3D, Version 4.0.83) using a standard calibration for each camera. I reduced the resolution of the rasters from originally 4.1–4.4 cm to 5 cm per pixel and merged the four overlapping sub-areas (ENVI, Version 5.2). The RGB orthomosaic covered the entire study area (2.8 km^2) and the RE orthomosaic covered 96% of the study area. The remaining area was interpolated from the NIR orthomosaic, which covered this area and additionally an overlapping area with the RE orthomosaic of about 0.3 km^2. From this overlapping area, I also computed the conversion from RE to NIR to compute the NDVI.

The DSMs of the four sub-areas were created during the mosaicking. Before joining the sub-areas, I removed the offset among them (MATLAB, Version R2015a, Figure A.6).

To train and validate the vegetation map, I visually selected 187 points in the study area which were clearly within one vegetation type and estimated the radius for which each point was representative (Table A.5, point size in Figure 4.1b). As I was using a hand-held GPS with ±3 m accuracy, I needed to validate the point locations in comparison with the orthomosaic. I removed points that lay outside the vegetation type in question (22 points) and shifted points which lay on the border of a vegetation patch (32 points). For 40 points, I reduced the size of the estimated radius because they intersected with other vegetation types on the orthomosaic.

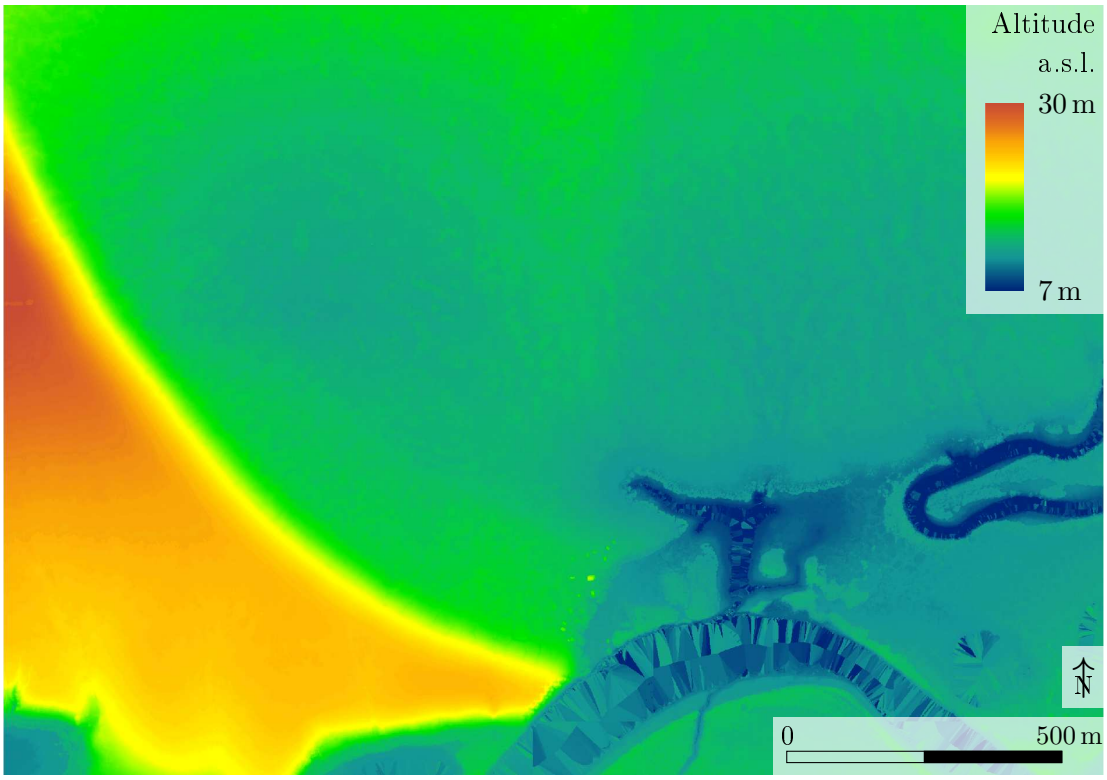

Figure A.6: Digital surface model of the study area (1.4 km × 2 km).

Half of the points were used for training of the vegetation classifier, the other half for validating the final map. I chose additional water training points based on the orthomosaic as they were difficult to access in the field.

I classified the vegetation based on the four image bands (RGB and RE) as well as hue and saturation, which I calculated from the RGB image. I additionally used the entropy of the hue image as seventh input channel. For more robust mapping results, I reduced the image resolution to 15 cm. The supervised classification was done with a maximum likelihood classifier (ENVI, Version 5.2). In the post-processing, I restricted low shrubs (S2) to areas close to rivers and floodplains. In order to reduce the number of patches smaller than 4 pixels, I sequentially assigned those pixels to classes with a similar likelihood if that increased the patch size.

For comparison with other tundra maps, I aggregated the nine original classes to four classes as defined by the circumpolar Arctic vegetation map (*Walker et al.*, 2005). These are tussock- sedge, dwarf shrub, moss tundra (G4), erect dwarf shrub tundra (S1-1, S1-2), low shrub tundra (S2), and sedge, moss, dwarf shrub wetland (W2-1, W2-2, W2-3, W2-4, and shallow water). For these four classes I obtained an overall accuracy of 65% and a Kappa coefficient of 0.53 using an equal amount of validation pixels per class. The best accuracy was achieved by including the lichen-

Table A.5: Vegetation classes from the circumpolar Arctic vegetation map (*Walker et al.*, 2005) and sub-classes as defined for this study based on differences in species composition and canopy properties; number of reference points in the field and area for which the points are representative.

Class	Sub-class	Description	Reference points	Area (m^2)
G4		Tussock-sedge (*Eriophorum vaginatum*), dwarf shrub, moss tundra	20	6785
S1		Erect dwarf shrub tundra (< 40 cm)		
	S1-1	Dwarf birch (*Betula nana*) dominated	34	600
	S1-2	Lichen-rich shrub, *Vaccinium* spp. dominated	27	99
S2		Low shrub tundra (> 40 cm, *Salix pulchra*)	7	1169
W2		Sedge, moss, dwarf shrub (< 40 cm) wetland		
	W2-1	Wet sedge, *Eriophorum angustifolium* dominated, dense, green	16	55
	W2-2	Dry sedge, *Eriophorum angustifolium* and *Sphagnum* spp. dominated	26	120
	W2-3	Peat moss (*Sphagnum* spp.) dominated	21	73
	W2-4	Waterlogged sedge, *Carex* spp. dominated, few standing dead leaves	9	101
		Open water	5	32
		TOTAL	165	9035

rich shrub tundra (S1-2) in the tussock tundra class (G4). The map with four classes aggregated in this way had an overall accuracy of 74% and a Kappa coefficient of 0.65 (Table A.6).

The classification accuracy was lower than in other studies classifying tundra vegetation using orthomosaics (*Lantz et al.*, 2010; *Muster et al.*, 2012) or high resolution satellite imagery (*Atkinson and Treitz*, 2012; *Virtanen and Ek*, 2014; *Siewert et al.*, 2015). The classification difficulties were due to three main reasons. First, I was not able to collect water reference points in deep ponds or the river. I added additional points representing deep water to the training data based on visual inspection of the orthomosaic. Thus, the classifier was trained on points which included deep water bodies in the water class. Shallow water was mostly classified as waterlogged sedges (W2-4). As I did not add additional points to the validation data, the classification accuracy of water was only computed for shallow ponds which I was able to access in the field. Given the typically low vegetation density of waterlogged sedges and the strong background effects in both, waterlogged sedges and shallow water,

Table A.6: Confusion matrix of the vegetation map with aggregated vegetation classes, random subset of the validation data with an equal number of validation pixels per class; (a) for vegetation sub-class S1-2 included in S1 and (b) for S1-2 included in G4.

(a) S1-2 included in S1

		Map				Producer's
		G4	S1	S2	W2	accuracy (%)
Ground truth	G4	**1780**	7105	0	924	18
	S1	1907	**7009**	0	893	72
	S2	23	599	**8420**	767	86
	W2	211	1274	0	**8324**	85
	User's accuracy (%)	45	44	100	76	Overall **65%**

(b) S1-2 included in G4

		Map				Producer's
		G4	S1	S2	W2	accuracy (%)
Ground truth	G4	**7072**	542	0	812	84
	S1	4348	**3446**	0	632	41
	S2	26	488	**7224**	688	86
	W2	983	281	0	**7162**	85
	User's accuracy (%)	57	72	100	77	Overall **74%**

this classification imprecision is not problematic and mainly due to suboptimal field sampling of reference points.

Second, the sub-classes dry sedges (W2-2) and peat moss (W2-3) were often misclassified because they appeared very similar on the orthomosaic. While peat moss occurred in both classes, the classes could be distinguished in the field based on the cover of sedges. However, dry sedges have a high cover of light-coloured standing dead leaves, which have a similar reflectance as peat moss areas. The albedo of W2-2 and W2-3 was almost identical (Figure 4.7). These two sub-classes were mainly distinguished for modelling canopy transmittance and absorptance and should be merged in a vegetation map.

Third and most importantly, erect dwarf shrub tundra (S1-1 and S1-2) cannot be clearly distinguished from tussock sedge tundra (G4) by the classifier. This difficulty has been pointed out by *Siewert et al.* (2015) in a classification of a GeoEye-1 satellite image of the same field site. Several other studies do not distinguish, or do not have, tussock tundra (*Lantz et al.*, 2010; *Atkinson and Treitz*, 2012; *Muster et al.*, 2012; *Virtanen and Ek*, 2014). *Schneider et al.* (2009) included tussock sedges in their vegetation map, but not in the accuracy assessment which assessed only seven of nine classes. The similarity between lichen-rich shrubs and tussock tundra is a consequence of the similarity of the two classes in terms of species composition. The major difference is the presence of *Eriophorum vaginatum*, a tussock forming sedge. However, this sedge has a low leaf area and canopy height at the site (Table 4.3) and thus does not dominate the surface reflectance. As I modelled very similar albedo values for S1-2 and G4, landscape scale albedo is insensitive to misclassification between these classes.

The classification accuracy could potentially be improved by including the NDVI.

However, I used the NDVI to spatially extrapolate model input variables and thus avoided circular reasoning by not including NDVI in the vegetation classification. A second potential classification input is microtopography. However, I used topography as input for the radiative transfer model and thus wanted to keep the vegetation classification independent of the topography. Spectrally similar vegetation classes could also have been avoided using an unsupervised classification approach (*Atkinson and Treitz*, 2012). However, unsupervised classification of tundra areas does not necessarily yield homogeneous vegetation classes (*Schneider et al.*, 2009). Furthermore, I collected input data for the radiative transfer model for specific vegetation classes in the field and thus was restricted to those for the modelling.

B Radiative transfer modelling

B.1 DART validation for all vegetation types

Canopy reflectance

For validation of the radiative transfer model, we measured canopy reflectance of all vegetation classes which we simulated with turbid media vegetation (Figure B.1). The measurements were done in the field with a spectrometer (Fieldspec4, ASD Inc.) in the same way as the measurements of background optical properties (Section 4.2.3, Page 72).

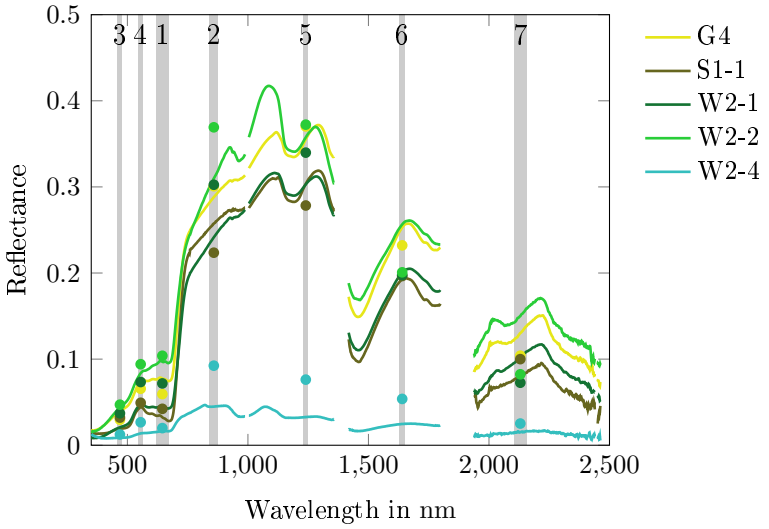

Figure B.1: Mean measured canopy reflectance; the dots indicate DART simulation results for MODIS bands 1–7 (grey).

The strongest deviation was between simulations and observations of waterlogged sedges (W2-4). However, we did not have good estimates of the leaf area index for this class, especially not at the locations where the reflectance spectra were measured. Furthermore, the canopy reflectance at higher wavelengths (especially MODIS bands 6 and 7) are underestimated by the DART model for dry sedges (W2-2) and tussock sedges (G4). This is most likely due to wrong leaf optical properties. In the range above 950 nm, I used the optical properties of dwarf shrub leaves for all green and dead leaves, as no other field data were available.

Canopy PAR transmittance

We measured canopy transmittance using a ceptometer (Sunscan, Delta-T Devices). The set-up consisted of a 1 m long probe with 64 PAR (photosynthetically active radiation, 400–700 nm) sensors that is inserted below canopy. The second part is an above canopy light sensor which takes readings of total and direct PAR simultaneously with the below canopy probe. We used the distribution of all single readings of 10 plots for dwarf shrubs (S1-1, *Betula nana*), 11 plots for wet sedges (W2-1, *Eriophorum angustifolium*), and 5 plots for tussock sedges (G4, *Eriophorum vaginatum*) (Figure B.2). For dry sedges (W2-2) and waterlogged sedges (W2-4) we did not have transmittance validation data.

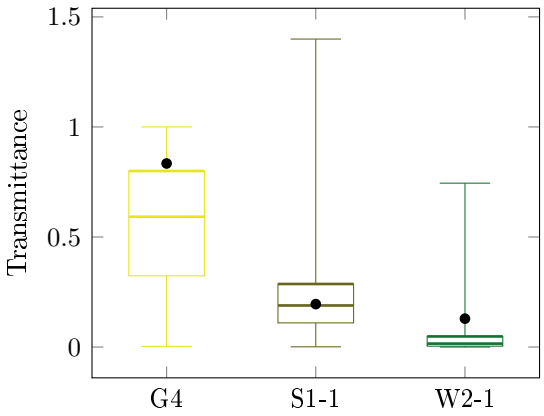

Figure B.2: Measured below canopy transmittance (400–700 nm); black dots indicate the average modelling results of the homogeneous cover types; see Figure 4.7b for modelled (shortwave) transmittance variability.